Deformations of Skeletal Structures

Finite Auxetic Mechanisms in Periodic Tessellations

Diplomarbeit
von
Holger Mitschke

Friedrich-Alexander-Universität zu Erlangen-Nürnberg
Institut für Theoretische Physik
Prof. Dr. Klaus Mecke

August 2009

Deformations of Skeletal Structures

Finite Auxetic Mechanisms in Periodic Tessellations

Diplomarbeit
von
Holger Mitschke

Friedrich-Alexander-Universität zu Erlangen-Nürnberg
Institut für Theoretische Physik
Prof. Dr. Klaus Mecke

August 2009

Zusammenfassung

Die vorliegende Diplomarbeit beschäftigt sich mit endlichen Deformationen von ebenen, periodischen, symmetrischen Gelenkstrukturen, die aus starren Stäben bestehen. Die Stäbe sind miteinander an Gelenken verbunden, wo sie reibungsfrei um diese rotieren können. Insbesondere werden Gelenkstrukturen, die Parkettierungen der Ebene mit Polygonen als Kacheln darstellen, betrachtet. Die Deformationen werden mit Hilfe eines numerischen Ansatzes ermittelt, der explizit Symmetrien einer Parkettierung erhält. Dies wird mit dem Ziel durchgeführt nach *auxetischen* Mechanismen in den betrachteten Parkettierungen zu suchen. Auxetische Mechanismen sind Deformationen mit einer negativen Querdehnungszahl (Poisson Zahl), d.h. sie expandieren in die transversale Richtung bei einer Dehnung in longitudinaler Richtung. Demgegenüber bedeutet eine positive Poisson Zahl die entgegengesetzte Reaktion, nämlich aufgrund der in einer Richtung aufgezwungenen Verlängerung kontrahiert die Struktur in die dazu senkrechte Richtung.

Deformationen von periodischen Gelenkstrukturen werden durch eine erzwungene Dehnung in eine gegebene Richtung untersucht, indem die Positionen der Gelenke als Lösung des Systems der Stabgleichungen, die die Unveränderlichkeit der Stablängen gewährleisten, ermittelt werden. Eine Gelenkstruktur ist starr, falls das System nur diskrete Lösungen besitzt. Sie ist eindeutig deformierbar, falls es einen stetigen 1-dimensionalen Lösungsraum gibt. Jedoch erhält man oft einen mehrdimensionalen Lösungsraum und damit keine eindeutige Deformation. Es gibt verschiedene Möglichkeiten für die Struktur sich aufgrund der aufgezwungenen Deformation zu verändern.

Für die Erörterung des Deformationsverhalten, insbesondere der Poisson Zahl, wird die Untersuchung auf eindeutige Deformationen beschränkt. Für den mehrdimensionalen Fall werden weitere Bedingungen eingeführt, um einen Pfad aus dem Kontinuum an möglichen auszuwählen. Translationsperiodische Systeme können weitere Symmetrien besitzen, wie zum Beispiel Spiegelachsen. Alle Symmetrien einer Struktur bilden eine mathematische Gruppe, wovon es in der Ebene genau 17 verschiedene gibt, den 17 kristallographischen Ebenengruppen. Die Gruppe beschreibt alle Symmetrien eines Systems ausgedrückt durch Symmetrieoperationen, die symmetrisch äquivalente Punkte aufeinander abbilden. Die Implementation ermöglicht es aus der Menge der Gelenkkoordinaten und der Paarmenge der Verstrebungen des Fundamentalbereichs der Einheitszelle alle Stabgleichungen und die Symmetrierelationen zwischen symmetrisch äquivalenten Punkten in allen gewünschten Gruppen zu erzeugen. Ihre Lösung wird mit Hilfe des Newton-Verfahrens bestimmt. Da das System von quadratischen Gleichungen nicht wie in der *rigidity theory* linearisiert wird, können endliche Dehnungen untersucht werden.

Die so ermittelten endlichen Deformationen der Gelenkstrukturen und die zugehörige Poisson Zahl als Funktion der momentanen Dehnung oder Kontraktion zeigen, dass auxetische Mechanismen für große Deformationen und aufrecht erhaltenen Symmetrien unter den Archimedischen, den 2-uniformen und uniformen Parkettierungen aus regelmäßigen Polygonen und sternförmigen Polygonen häufig sind. Zudem konnten zwei bislang unbekannte

Beispiele mit infinitesimaler negativer Poisson Zahl ohne zusätzlichen Symmetrieeinschränkungen identifiziert werden.

Die vorgestellte Methode zur numerischen Ermittlung von endlichen Deformationen von Gelenkstrukturen stellt die Basis für einen zukünftigen Zugang mit Methoden der statistischen Mechanik dar, um den allgemeinen hochdimensionalen Lösungsraum zu behandeln. Dieser Zugang kann auch dazu verwendet werden, um Deformationsmechanismen in ungeordneten Netzwerken zu verstehen und um systematisch nach morphologischen Charakteristiken, die zum Deformationsverhalten in Beziehung stehen, zu suchen.

Abstract

This thesis addresses finite deformations of plane, periodic, symmetric skeletal structures, consisting of rigid bars linked at joints where they can pivot freely. In particular skeletal structures based on tessellations of the plane by polygons are considered. Deformations are computed by a numerical approach that explicitly maintains symmetries of the tessellation. This method is applied to search for *auxetic* mechanisms in catalogues of tessellations. Auxetic mechanisms are deformations with a negative Poisson's ratio, i.e. they expand in the transversal directions when stretched in longitudinal direction. In contrast a positive Poisson's ratio stands for the opposite reaction of an imposed elongation in one direction, namely a contraction in the perpendicular direction.

A deformation of a periodic skeletal structure is studied by imposing an elongation in a given direction, and determining all joint positions as the solution of the system of bar equations, stating that all bar lengths remain unchanged. A skeletal structure is rigid if this system has only discrete solutions; it has a unique deformation if there is a 1-dimensional solution space. Often the solution space is multidimensional.

A numerical solution of this system of quadratic equations is obtained using the Newton-Raphson method. The Newton-steps are solved using the singular value decomposition to get the one with the smallest coordinate deviation in under-determinate situations. In contrast to rigidity theory the problem will not be linearised and the study of deformations with finite elongations is possible.

For the discussion of deformation behaviour, in particular Poisson's ratios, the analysis will be restricted to unique deformations. For the multidimensional cases, symmetry constraints are imposed to select one path of the continuum of possible deformations. Translational periodic systems can have further symmetries. All symmetries of one structure build a group. In the plane there are exact 17 different groups, called crystallographic plane groups. The group describes all symmetries of a system expressed by symmetry operations. They contain at least the translational operations, but can have more. The requirement that under deformation symmetries remain provides the possibility to reduce the dimension of the solution space. The symmetries of the full group or of possible subgroups are retained. The implementation offers the generation of the system of bar equations and the symmetry relationships between symmetric equivalent joints in the desired group from the list of joint coordinates and the set of linked pairs of joints in the asymmetric unit.

Finite deformations of the skeletal structures and their Poisson's ratio as a function of the elongation are determined for a number of classes of known tessellations. The main result is that a large number of the Archimedean, 2-uniform and uniform tessellations by regular polygons and star polygons have auxetic mechanisms for large deformations when constraining symmetries. Two as yet unknown examples of auxetic mechanisms at infinitesimal deformations without the additional symmetry constraints could also be identified.

The presented program to numerically calculate finite deformations of skeletal structures provides the basis for a future statistical mechanics approach to the generally multi-dimensional deformation space. The approach can also be used to understand deformation mechanisms of disordered networks, and to search systematically for structural characteristics that correlate to the deformation behaviour.

Contents

1 Introduction

Deformation of matter is usually considered as a macroscopic physical process and the bodies represent subspaces of the continuous D-dimensional Euclidean space [6, 31]. This continuum-mechanical description neglects the atomistic character of matter. There is no correspondence between the continuum *material points* and the distribution of atoms.

The measure for deformation is the *strain*. The strain describes the change in length per unit with respect to its prior length [6]. For homogeneous materials it is possible to introduce moduli which describe the complete linear elastic deformation behaviour of a macroscopic material. The strain tensor can be derived from these moduli which characterises the local strain at every point. In the most general anisotropic case there are 21 of such moduli. In the easiest case of isotropic homogeneous materials there are only two independent moduli which are sufficient [19].

For instance these are *Young's modulus* and *Poisson's ratio*[1] which quantify, how much stress must be applied to get length change by one unit length and how much the body expands or contracts in the perpendicular direction to the imposed axial strain [16]. Note the negative sign in the definition; a material that contracts vertically when stretched longitudinally has positive Poisson's ratio.

Auxetic[2] materials are those with a negative Poisson's ratio. If you squeeze a cube of auxetic, isotropic material, it will shrink in the perpendicular directions as shown in the images of Figure 1.1.

Figure 1.1: *A cube made of auxetic material shrinks in all direction when squeezed in only one direction.*

Auxetic behaviour is not the typical property of materials. Nearly all materials have a positive Poisson's ratio and the existence of auxetic materials has become well-known only in recent times. For instance, some older standard physics textbooks (Landau et al. [31] p. 16, Feynman et al. [16] Volume II p. 38-2) note that materials with a negative sign of Poisson's ratio are not known[3].

Another effect which leads also to a perpendicular expansion or contraction is *positive* or *negative normal stress*. Instead of a uniaxial longitudinal deformation an applied shear

[1] Siméon Denis Poisson (1781-1840), French mathematician, geometer and physicist. Also named after him are e.g. Poisson Distribution and Poisson Equation.

[2] This term was introduced in [15] as shorter notation of "negative Poisson's ratio material" and is borrowed from Greek: *auxetos* that may be increased, "referring to the width and volume increase when stretched", Synonyms after Yang et al. [46]: anti-rubber, dilatational

[3] But the possibility is not excluded. Thermodynamic considerations does not limit Poisson's ratio to only positive values. This has already been known over 150 years [32]

leads to this change. For instance a shear can be imposed by a contrary movement of two parallel plates fixed on the top and on the bottom side of a block of matter. In the cases of negative normal stress both plates move toward each other and reduce the distance between them. This has been found in matter of networks of semiflexible biopolymers [28].

Since Lakes presented in 1987 an auxetic, isotropic polymer foam, great interest in auxetic materials has evolved. The right image of Figure 1.3 shows as a stereo photograph of the auxetic foam from Lakes as published in [29]. Many other materials have been found like metallic foams, composites, micro porous polymers, ... Also natural occurring auxetic materials have been identified in skin/bones, cubic metals, α-cristobalite.

"An example of the practical application of a particular value of Poisson's ratio is the cork in a wine bottle. The cork must be easily inserted and removed, yet it also must withstand the pressure from within the bottle. Rubber, with a Poisson's ratio of 0.5, could not be used for this purpose because it would expand when compressed into the neck of the bottle and would jam. Cork, by contrast, with a Poisson's ratio of nearly zero, is ideal in this application" (extracted from [29]).

Technically relevant properties of auxetic materials are high indentation resistance. Commercially available materials like pyrolytic graphite is used as thermal protection in aerospace applications or large single crystals of Ni_3Al for vanes of aircraft gas turbine engines. Some suggested applications are sponges, robust shock-absorbing materials, filters and fasteners [13, 14, 29].

This thesis studies the deformation of two-dimensional objects which will not be considered as continuum matter but have an underlying interior structure. The interior structure is a common characteristic of auxetic materials. The simple common 2d explanation of materials with negative Poisson's ratio is the re-entrant honeycomb model, as illustrated in Fig. 1.2. This model consists of two components, rigid bars and joints, denoted in this thesis as *skeletal structure* [4]. The bars are the edges of the polygons and the joints are the corners. If the bars can rotate at the joints the normal hexagon pattern will contract by pulling in the vertical direction. In contrast in the re-entrant case the opposite happens: A vertical pulling leads to expansion of the structure in the perpendicular direction.

The polymer foam of Lakes is a porous medium consisting of open cells which can be convex or have re-entrant elements. This can be interpreted in first order as skeletal structure (Fig. 1.3).

In the literature some other skeletal structures have been proposed, but a systematic search in such structures does not exist. Plane tessellations by polygons [24] are numerous and can be interpreted as such ones. The main motivation for this thesis is the question: Are there other skeletal structures with auxetic mechanisms?

A crucial and also apparent problem is the large number of degrees of freedom of such skeletal structures. Which is the physical reasonable deformation mechanism? We have extended the constraints of the bar rigidity, through symmetry constraints which the original tessellation possesses and asks for their conservation under deformation.

Another motivation for this thesis is the apparent relationship between the cell geometry and the deformation behaviour, characterised by the moduli, like the Poisson's ratio. Lakes has produced a polymer foam by increasing the number of re-entrant cells. The result is

[4] The term skeletal structure is borrowed from [30]

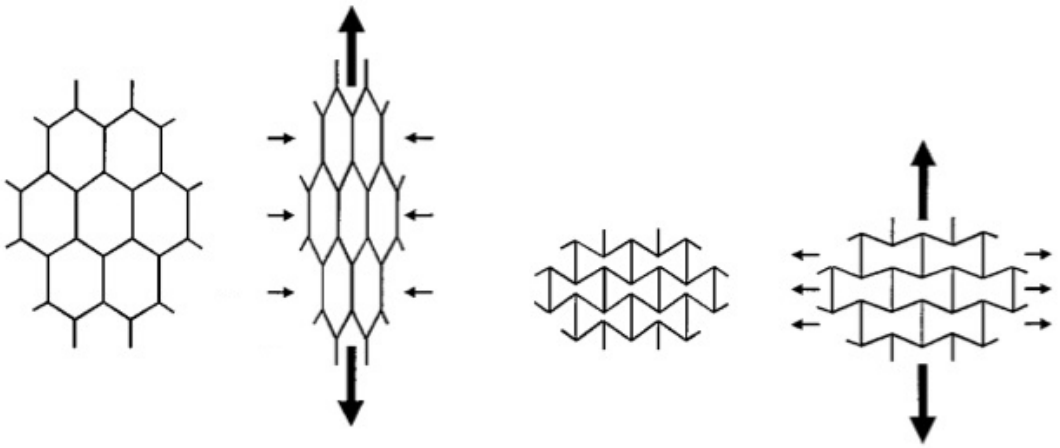

(a) *Hexagon Pattern with no re-entrant angles*

(b) *Honeycomb structure with re-entrant angles*

Figure 1.2: *Standard explanation for negative Poisson's ratio behaviour (images from [13]); The imposed pulling is indicated by the stronger vertical arrows and the material response by the three smaller arrows on each side.*

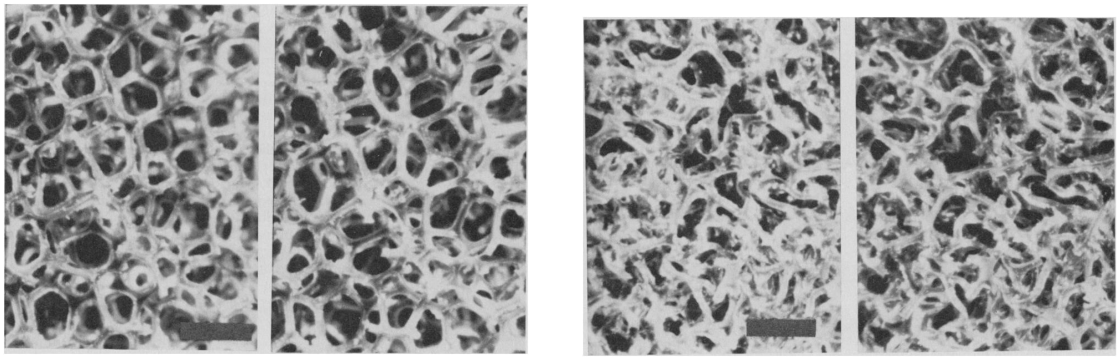

(a) *Conventional open-cell polymer foam*

(b) *Re-entrant foam. Permanent volumetric compression factor is 2.7. Poisson's ratio is* −0.6.

Figure 1.3: *Stereo photographs of polymer foams. Scale marks 2mm. Extracted from [29]*

the foam with a negative Poisson's ratio. Can we formulate a morphological/geometric condition for the microstructure of a material such that its Poisson's ratio is negative?

The determined Poisson's ratio shows that almost all uniform tessellations have under certain constraints auxetic mechanisms. The numerical solution that is derived in this thesis allows to determine finite deformations. These can lead to strongly changed geometries which can also show auxetic behaviour.

This thesis is organised as follows: Chapter 2 introduces skeletal structures and explains what the deformations of those structures are. The problem of an commonly encountered underdetermined situation is discussed. Chapter 3 explains the considered uniform tessellations and the plane groups which describes all possible geometric symmetries of periodic objects of the plane. The computer based generation of the data (coordinates of the joints, set of bars, symmetry relations) for the deformation program is presented. The multivariate system of quadratic equations is solved by the multi-dimensional Newton-Raphson-method. The solution of the linear steps are done with the singular value decomposition.

This is necessary because there often occur underdetermined situations. This and the concept of the deformation program will be presented in chapter 4. Chapter 5 discusses the highlights of the presented catalogue-like numerous results of the sixth chapter. The conclusion and an outlook will be given in chapter 7.

2 Skeletal structures

This chapter gives a precise definition of the considered model, denoted *plane skeletal structure,* and its deformation as a continuous one-parameter family of permissible configurations. General issues such as the existence and uniqueness of deformations are discussed that means the rigidity and the dimension of the solution space. Basic aspects of the rigidity theory for infinitesimal deformations are presented.

The *plane skeletal structure* model consists of rigid bars linked freely at joints. In Fig. 2.1 a model made up of aluminium slats with drilled holes where different slats are fixed to other ones is shown. The two shown states can be transformed into each other by the continuous movement of splints. During this movement the slats rotates at the splints.

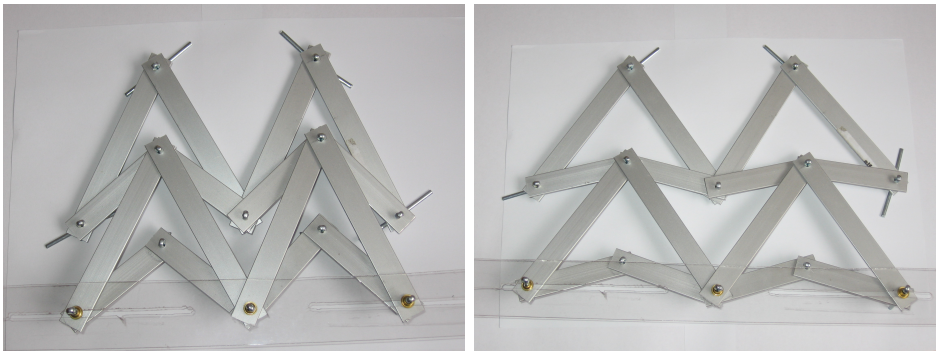

(a) **(b)**

Figure 2.1: *A non-rigid skeletal structure made from aluminium slats*

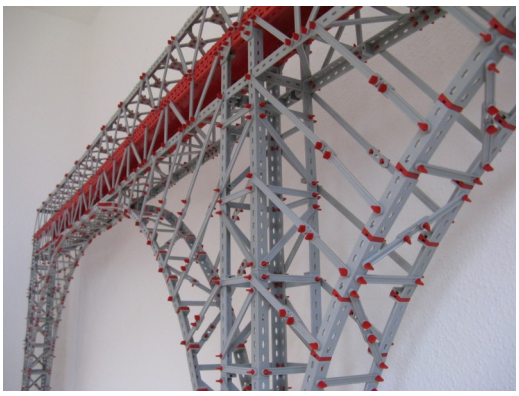

Figure 2.2: *Real, hopefully rigid, skeletal structure: "*Fischer Technik*" model of a truss bridge (from[37])*

2.1 Skeletal structures as first-order models of deformation

A deformation of a body is the result of acting forces and the material's response, e.g. quantified by elastic moduli. The corresponding physical theories are elasticity and plasticity theory. Instead of considering bendable cell walls (Figs. 2.3 and 2.5) or an atomic description of the movement in interaction potentials (Fig. 2.4) which leads to specific matter distributions, we consider model structures with degrees of freedom in their geometry or shape as simple models of the physical systems. These simplified models nevertheless reproduce the principal characteristics of the deformation behaviour.

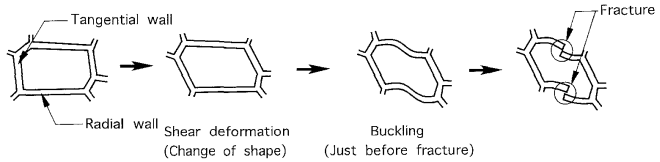

Figure 2.3: *Deformation of a wood cell [2]*

In this thesis models are considered which are networks of rigid bars linked at joints, where the bars can rotate without friction. Figs. 2.4 and 2.5 show two physical systems and their corresponding skeletal structure.

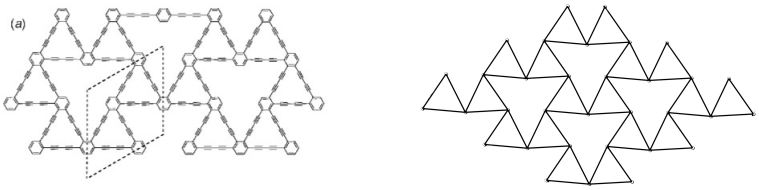

(a) *Molecule structure* **(b)** *Skeletal structure*

Figure 2.4: *Polyphenylacetylen network [21]*

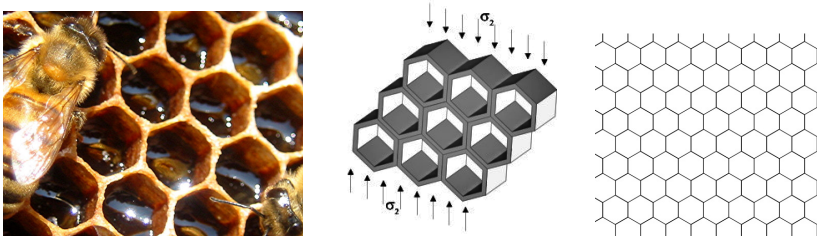

(a) *Reality* **(b)** *3d model with cell walls with elastic moduli* **(c)** *Periodic, plane, skeletal structure*

Figure 2.5: *Honeycombs*

2.2 Mathematical definition

Mathematically speaking, a skeletal structure is a graph with an assignment of the nodes of the graph to a set of coordinates.

A *graph* Γ consists of a finite set K of nodes and a set E of edges that is a subset of all pairs $\mathcal{P}(K)$ of the nodes K. A graph is denoted $\Gamma(K, E)$.

$\mathcal{P}(K) = \{\{x, y\} \mid x \neq y \; \forall x, y \in K\}$; hence $\mathcal{P}(K)$ is the set of all subsets of K which contain exactly two different elements of K ($|\mathcal{P}(K)| = \frac{1}{2}|K|(|K|-1)$).

$N := |K|$ is the number of nodes and $B := |E|$ is the number of bars.

The *coordination number* of a node $a \in K$ is the number of edges emanating from that node, i.e. the number of those $b \in K$ for which $\{a, b\} \in E$ (the neighbours of a). In Fig. 2.6 the coordination number of all nodes is 3.

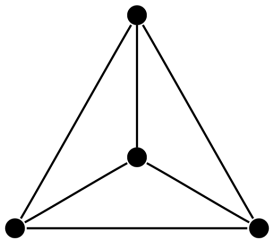

Figure 2.6: *A graph with N=4 nodes and B=6 edges*

The *Configurationspace* $\mathbb{P}$ is a $D \times N$ dimensional vector-space of real numbers $\mathbb{R}$. Every element of the configuration space describes a configuration, i.e. the N joint positions with D coordinates each. In general only a subspace of $\mathbb{P}$ represents permissible configurations that preserve the correct edge lengths.

Consider a configuration $\mathbf{P}$ of $\mathbb{P}$: it has as components labelled points $\mathbf{p}_1, \ldots, \mathbf{p}_N$, where each $\mathbf{p}_i$ is given in the Euclidean space $\mathbb{R}^D$. Let Γ be a graph, whose nodes corresponds to the labels $\{1, \ldots, N\}$. The in this way combined objects represents a skeletal structure.

For example consider the configuration

$$\mathbf{P} = ((0,0), (1,0), (1,1), (0,1))$$

and the graph

$$\Gamma(\{1,2,3,4\}, \{\{1,2\}, \{2,3\}, \{3,4\}, \{1,4\}\}).$$

This skeletal structure is represented in Fig. 2.7.

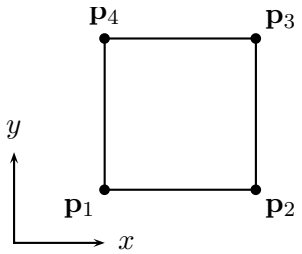

Figure 2.7: *A skeletal structure in* $\mathbb{R}^2$

This is summarised in the following definition:

A *plane skeletal structure* is a configuration $\mathbf{P} \in \mathbb{P}(\mathbb{R}^2)$ together with a graph $\Gamma(K, E)$, where the labelled points of the configuration are assigned to the elements of set of nodes K, and is denoted by $(\Gamma, \mathbf{P})$ [1][2].

In the context of skeletal structures we denote the nodes of a the graph Γ as *joints* and the edges of Γ as *bars*.

[1] Skeletal structures have also been termed pin-jointed framework [25, 12], pin-jointed truss [27], articulated structure [30], bar-and-joint framework [7] or often briefly only framework.

[2] This thesis deals only with plane skeletal structures so the adjective *plane* will be suppressed.

2.3 Deformation of skeletal structures

The rigidity of the bars defines distance equations which must hold for any permissible deformation:

$$|\mathbf{p}_i - \mathbf{p}_j| = l_{\{ij\}} \quad \text{if } \{i,j\} \in E.$$

If $\{ij\}$ is a bar, then during any deformation, the distance from $\mathbf{p}_i$ to $\mathbf{p}_j$ must remain unchanged. The distance between nodes not connected by a bar is not constrained.

A *deformation of a skeletal structure* is a continuous one-parameter family $\mathbf{P}(\delta) = (\mathbf{p}_1(\delta) \dots \mathbf{p}_N(\delta))$ with $\mathbf{P}(0) = \mathbf{P}$ and

$$\big(\mathbf{p}_i(\delta) - \mathbf{p}_j(\delta)\big) \cdot \big(\mathbf{p}_i(\delta) - \mathbf{p}_j(\delta)\big) - l^2_{\{ij\}} = 0 \qquad \forall \{i,j\} \in E. \tag{2.1}$$

Trivial deformations of skeletal structures are pure rotations or translations, i.e. deformations as defined above but with the distances between *all* pairs of joints unchanged. Equation (2.1) holds for all $\{i,j\} \in \mathcal{P}(K)$ and not just for those linked by bars.

The set of equations (2.1) represents a multivariate system of quadratic equations. The solutions are permissible configurations of the joints compatible with the linking edges.

The branch of mathematics that considers such systems of algebraic equations, is the Algebraic Geometry [8]. The geometric object corresponding to the polynomials embedded in the configuration space is called an *affine variety*.

Such a deformation is an affine variety which is a one dimensional hyperpath through the configuration space. The affine variety of the equations is not necessarily one-dimensional, but it can be the empty set, discrete points (one or more rigid configurations) or higher dimensional objects like surfaces, bodies or hyperbodies.

Note that in the higher dimensional case a given structure has multiple different deformations which we laxly call deformation modes or deformation mechanism. The question whether a given structure has any deformations, a unique single deformation or a continuum of finite deformations is one of the key question of this thesis.

Existence - Fundamental question about non-rigidity

With respect to deformations the essential information about a skeletal structure is if it is either flexible or rigid. In 1864, J.C. Maxwell published a relationship between the number of bars and the number of joints to give a necessary but not sufficient criterion to decide whether a structure can be rigid [33]. It is a purely topological criterion; the real distribution of the bars to joints and the length of the bars is not included.

Maxwells rule Every point-like object, as our joints, not fixed by bars, can move in every space direction and has D degrees of freedom. If you can fix one component, you can reduce one degree of freedom. That is e.g. possible by linking this object with a bar to another one. In spherical coordinates it is easy to see that the joint fixed with one bar can move on a circle (2D) or on a sphere (3D).

So it is apparent that the possible number of degrees of freedom is related to the number of joints N and bars B,

$$D \cdot N - B = F'. \tag{2.2}$$

The trivial deformations are not counted because rigid structures have also these freedoms and hence not relevant for the criterion; the translational and rotational degrees of freedom are subtracted, yielding:

$$2 \cdot N - B - 3 = F \qquad \text{Maxwell's rule in 2D} \tag{2.3}$$

Rigid structures must satisfy this equation with $F \leq 0$. But it is only a necessary but not a sufficient condition. There can be redundant bars, so that the number F cannot give you in general the actual number of degrees of freedom. However if $F > 0$ there must be at least F degrees of freedom. This means the structure has flexes and has finite mechanism(s). Hence it is a sufficient condition to decide, whether a structure must be flexible. Of course it cannot be a necessary condition due to the possibility of partially redundant bars. In other words F is a lower bound for the degrees of freedom.

Example for a unique deformation: To gain an impression of the one-parameter family, we consider the easiest deformable skeletal structure: the square. The corners are the joints and the edges are the bars (Fig. 2.8a). In order to avoid trivial deformations, i.e. translations and rotations, the positions of joints of $\mathbf{p}_1$ and $\mathbf{p}_2$ are fixed. Maxwell's rule states that there must be at least one finite mechanism ($2 \cdot 4 - 4 - 3 = 1$).

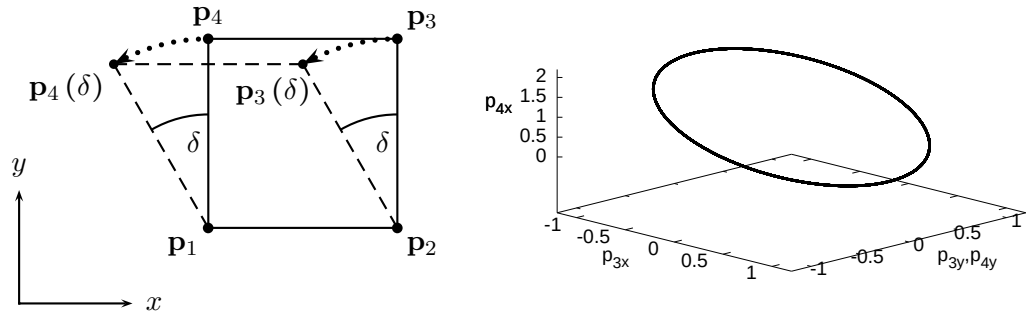

(a) **(b)**

One possible parametrisation of the deformation and in this case of the complete variety of the system of equations (2.1) with bar lengths set to one is

$$\mathbf{p}_1(\delta) = \begin{pmatrix} 0 \\ 0 \end{pmatrix}, \quad \mathbf{p}_2(\delta) = \begin{pmatrix} 1 \\ 0 \end{pmatrix}, \quad \mathbf{p}_3(\delta) = \begin{pmatrix} 1 - \sin(\delta) \\ \cos(\delta) \end{pmatrix}, \quad \mathbf{p}_4(\delta) = \begin{pmatrix} -\sin(\delta) \\ \cos(\delta) \end{pmatrix}. \tag{2.4}$$

There is only one scalar parameter δ so the deformation mode is unique. To illustrate this a subspace of the configuration space is plotted in Fig. 2.8b. The result is a 1d path in the 4-dimensional configuration space.

Uniqueness of the deformation

Example for a strut framework with two degrees of freedom We extend the square by a further point and introduce two parameters δ_1 and δ_2 (see Fig. 2.8). The joints $\mathbf{p}_1$ and $\mathbf{p}_2$ are still fixed because of trivial deformations:

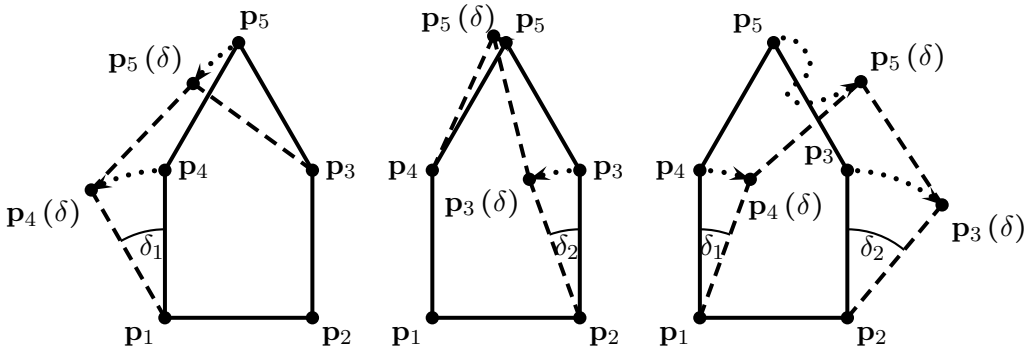

(a) $\mathbf{p}_3$ *fixed,* δ_1 *single parameter* **(b)** $\mathbf{p}_4$ *fixed,* δ_2 *single parameter* **(c)** δ_1 *and* δ_2 *independent except for equation* (2.6)

Figure 2.8: *5-gon: non-unique deformation, 2 degrees of freedom*

The explicit expressions for $P(\delta) = (\mathbf{p}_1(\delta), \mathbf{p}_2(\delta), \mathbf{p}_3(\delta), \mathbf{p}_4(\delta))$ in this parametrisation

$$\mathbf{p}_3(\delta) = \begin{pmatrix} 1 - \sin(\delta_1) \\ \cos(\delta_1) \end{pmatrix}, \qquad \mathbf{p}_4(\delta) = \begin{pmatrix} -\sin(\delta_2) \\ \cos(\delta_2) \end{pmatrix}, \qquad \mathbf{p}_5(\delta) = \begin{pmatrix} f(\delta_1, \delta_2) \\ f(\delta_1, \delta_2) \end{pmatrix}. \tag{2.5}$$

$$|\mathbf{p}_4(\delta) - \mathbf{p}_3(\delta)| \leq 2 \qquad \leftrightarrow \qquad \sin(\delta_1) - \sin(\delta_2) + \cos(\delta_1 - \delta_2) \leq \frac{1}{2} \tag{2.6}$$

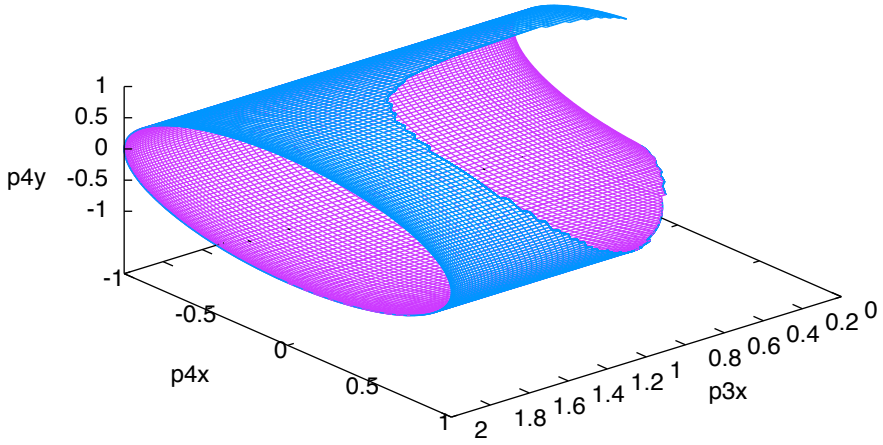

Figure 2.9: *The 2-dimensional solution space in a subspace of the full configuration space*

The two parameters generate a variety which represents a surface in the 10 dimensional configuration space. We can again plot the variety in a subspace of $\mathbb{P}$ (Fig. 2.9). Every arbitrary path on the surface represents a possible deformation mode.

To select one of the continuum of possible ones or analyse the complete ensemble, we must either extend the model or use statistical methods. This important aspect will be discussed in the section 2.6.

Dependency on the dimension of the embedding space

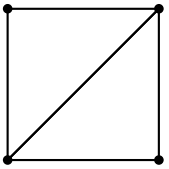

Rigid in 2d,
flexible in 3d

The dimension of the embedding space influences the degrees of freedom. For example a triangulated square embedded in the plane is rigid, but is unique flexible in 3d. In three dimensions there are 6 degrees of freedom of trivial deformations (instead of 3). The fixation of 2 linked joints reduces 5 degrees of freedom. One component of another adjacent joint must be fixed. Together with the bar this joint has only one degree freedom anymore. If you consider the square of Fig. 2.8a in three dimensions, the removal of translations and rotations leads to a situation in which all 4 joints are fixed in a plane which corresponds to the discussed 2d case. Hence the square has no dependency of the embedding space dimension.

2.4 Periodic skeletal structures

This thesis deals with deformations of periodic tessellations which cover the full plane (see chapter 3). Therefore the number of joints and bars is infinite ($N = \infty$, $B = \infty$) and the tessellations must be limited to a finite part of the plane.

A periodic tessellation is one which has elements which occurs in equidistant places again and again. 2d periodic tessellations have elements that occurs in two non collinear directions. The two minimal location differences represent the translation vectors of the tiling. These vectors represents the reduced basis system, e.g. systematically determinable by the Delaunay-Reduction [5]. They are denoted in this thesis as **a** and **b**.

A grid underlies every periodic tessellation, i.e. it is possible to mark one arbitrary point in the plane and by adding the vectors of translation a net of points will be generated. This grid is not unique and can arbitrarily shifted and rotated as a whole and is furthermore a grid of the tiling. The neighbourhood of every point is identically to all other points of the net. For instance a possible grid of the honeycomb pattern is plotted in Figure 2.10, denoted by x.

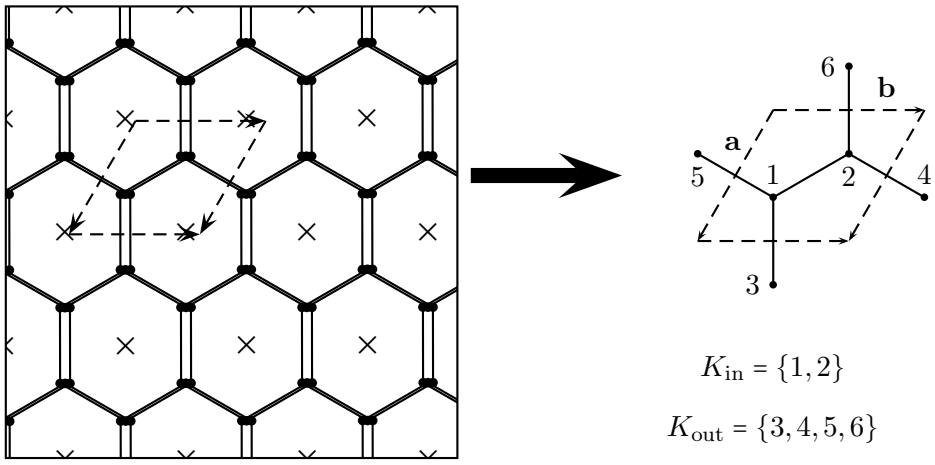

Figure 2.10: *Honeycomb pattern: Translational unit cell with neighbouring joints K_{out} and the linking bars $\{5,1\}, \{2,4\}, \{3,1\}, \{2,6\}$. $Z_{Maxwell} = 2 \cdot N_{in} + 1 - B = 2 \cdot 2 + 1 - (1 + \frac{4}{2}) = 2$*

A *primitive cell* is the minimal area of the tiling which does not contain any elements which corresponds to each other due to the periodicity. In other words it contains only one lattice point (Fig. 2.10). Again this is not unique.

One assumption which is used in this thesis, is that the deformation results should again be a periodic tessellations. The primitive cell is the smallest part of the periodic plane which under periodic boundaries can be deformed to give a element which can be used as a tile to tessellate the plane without overlaps and gaps.

Therefore is the considered finite part of the tessellation a primitive cell. However some reasons in the context of symmetric tessellations leads to an other choice of the unit cell.

The choice is done as the standard tables [24] suggests and will be discussed in chapter 3.

To illustrate this step of reduction consider the honeycomb pattern in Fig. 2.10. One question occurs about the crossing bars which link joints of the unit cell and ones of neighbouring cells which actually are related due to the translation. How should they be handled during the deformation?

These bars will be considered as one of the unit cell. But their linked joints outside of the unit cell are identified with the one in the unit cell with an addition of the lattice vectors.

The introduced symbols for the set of joints and bars are used for the translational unit cell part of the infinite periodic tiling. But additional symbols for the sets of joints which are identified, will be introduced K_{out} and K_{in} which represents the joints outside of the unit cell and in the inside.

$$f_{\{ij\}} = (\mathbf{p}_i - \mathbf{p}_j) \cdot (\mathbf{p}_i - \mathbf{p}_j) - l^2_{\{ij\}} = 0 \qquad \forall \{i, j\} \in E \tag{2.1}$$

$$\mathbf{p}_i(\delta) = \mathbf{p}_j(\delta) + n\mathbf{a}(\delta) + m\mathbf{b}(\delta) \quad \forall i \in K_{\text{out}} \quad \text{with} \quad j \in K_{\text{in}} \tag{2.7}$$

The number of bars of the unit cell will be given as follows: The bars which only link joints inside the cell are of course counted as usually. But the number of bars crossing the border will be counted one half $B = \left(B_{\text{in}} + \frac{B_{\text{cross}}}{2}\right)$. This number must be even due to the translational periodicity.

Maxwell's number for periodic skeletal structures For all results a number Z_{Maxwell} according to the Maxwell's rule is given as an indicator, whether the structure can be rigid or must be flexible. Due to the periodicity only the coordinates of the joints of one unit cell are independent. However the translational related joints can change their position relatively because of changing lattice vectors. So the degrees of the lattice vectors are added ($D \cdot D$). For the general D-dimensional case this number, denoted Z_{Maxwell} is defined as

$$Z_{\text{Maxwell}} = \underbrace{D \cdot N_{\text{in}} + D \cdot D}_{\text{freedoms}} - \underbrace{B}_{\text{constraints}} - \underbrace{\frac{D(D+1)}{2}}_{\text{trivial freedoms}} \qquad \text{with} \quad N_{\text{in}} = |K_{\text{in}}|.$$

For $D = 2$ this equation simplifies to

$$Z_{\text{Maxwell}} = 2 \cdot N_{\text{in}} + 1 - B. \tag{2.8}$$

Following two statements are the possible informations that the number can give or must fulfil. If $Z_{\text{Maxwell}} > 0$, there are freedoms and hence the structure must be flexible. Otherwise if the skeletal structure is rigid, the number must be zero or negative (cf. sect. 6.6). However the converse statements do not hold. If $Z_{\text{Maxwell}} \leq 0$, the skeletal structure can be flexible or rigid.

A modified Maxwell number is necessary for additional symmetry constraints. Especially in the case of centerings and their subgroup $c1$.

2.5 Uniaxial deformations of unit cells

Deformations of continua and the strain field

In order to characterise whether a periodic tessellation is auxetic Poisson's ratio ν must be determined. Obviously the infinite plane will stay infinite under any finite deformations so the limitation of the previous section is anyway necessary to be able to measure finite lengths as needed for the Poisson's ratio. Hence the object which is considered for deformation is the skeletal structure restricted to the conventional unit cell with periodic boundary conditions.

In continuum theories Poisson's ratio is well defined by other quantities like the strain tensor. As noted in the introduction the Poisson's ratio is one of the elastic moduli which can be expressed by other in the linear elastic homogeneous isotropic case. In this case it can be shown that ν is bounded: $-1 \leq \nu \leq 1$ 2D and $-1 \leq \nu \leq \frac{1}{2}$ 3D. And if ν equals one (one half (3d)) there is no change in volume. However the finite, inhomogeneous and also anisotropic case will be considered so this restrictions are not valid.

A short review of the deformation in continuum is given to motivate an appropriate deformation of the lattice to measure the Poisson's ratio as function of the imposed change of the lattice vectors and their resulting perpendicular change due to the skeletal structure.

An arbitrary deformation of a macroscopic body causes a relative displacement of different material points. Deformations, where the relative positions of all material points are unchanged, so the object as a whole is shifted, are excluded by fixing one point, namely the origin. As below explained rotations that also is a isometry are accepted, to allow shears which are the product of a pure deformation and a pure rotation.

The basic object of deformation in general is the strain field $\mathbf{u}_\tau(\mathbf{r})$, whose action is described in Fig. 2.11. This quantity describes the local change of material points during the deformation. It is a continuous one-parameter (τ) non-uniform vector field, which determines the new coordinates of the material points as follows

$$\mathbf{r}_\tau = \mathbf{r} + \mathbf{u}_\tau(\mathbf{r}) . \tag{2.9}$$

During the continuous deformation time τ the coordinates are changed from their initial position to the end position of the imposed deformation. For $\tau = 0$ is $\mathbf{u}_\tau(\mathbf{r}) = 0 \ \forall \mathbf{r} \in \mathbb{R}^D$.

By comparing start and end point the parameter τ can be suppressed to simplify notation.

It is more interesting in the continuum view to analyse the local or relative displacement than the absolute displacement.

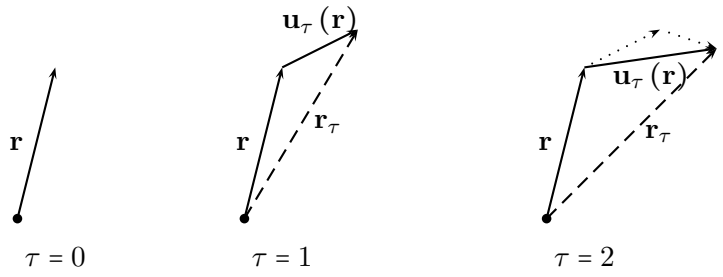

Figure 2.11: *A deformation is a continuous movement of individual material points, described by the strain field. τ parametrises this continuous process.*

We consider two neighbouring points P and Q and their respective displacement (Fig. 2.12).

$$\mathrm{d}\mathbf{r}' = \mathrm{d}\mathbf{r} + \mathbf{u}(\mathbf{r}+\mathrm{d}\mathbf{r}) - \mathbf{u}(\mathbf{r}) \tag{2.10}$$

$$\mathrm{d}\mathbf{u} = \mathbf{u}(\mathbf{r}+\mathrm{d}\mathbf{r}) - \mathbf{u}(\mathbf{r}) = \mathrm{d}\mathbf{r}' - \mathrm{d}\mathbf{r} \tag{2.11}$$

Because they are infinitesimal near points, we can replace $\mathbf{u}(\mathbf{r}+\mathrm{d}\mathbf{r})$ by its Taylor expansion up to the first term:

$$\mathrm{d}\mathbf{u} = (\mathrm{d}\mathbf{r}\cdot\nabla)\,\mathbf{u}(\mathbf{r}) \tag{2.12}$$

$$\mathrm{d}\mathbf{r}' = \mathrm{d}\mathbf{r} + (\mathrm{d}\mathbf{r}\cdot\nabla)\,\mathbf{u}(\mathbf{r}) \tag{2.13}$$

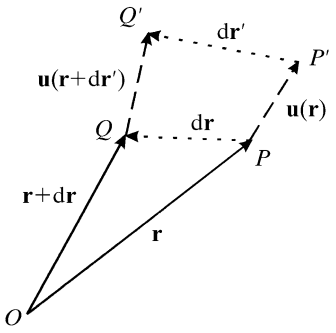

Figure 2.12: *Neighbouring points and their displacement after some deformation, extracted from [26] Vol D 1.3*

By using Einsteins summation convention we can reformulate the above equation and introduce a two-index object (non-curvilinear basis) $M_{ij} = \frac{\partial u_i}{\partial x_j}$:

$$\mathrm{d}u_i = \frac{\partial u_i}{\partial x_j}\mathrm{d}x_j \qquad = M_{ij}\mathrm{d}x_j \tag{2.14}$$

$$\mathrm{d}x_i' = \mathrm{d}x_i + \frac{\partial u_i}{\partial x_j}\mathrm{d}x_j = (M_{ij} + \delta_{ij})\,\mathrm{d}x_j \tag{2.15}$$

Homogeneous deformation and the polar decomposition If the components of M_{ij} are constant, equations (2.14) and (2.15) can be integrated,

$$\mathbf{u} = M\mathbf{r} \tag{2.16}$$

$$\mathbf{r}' = (M + \mathbb{1})\mathbf{r}. \tag{2.17}$$

They are linear equations. The deformation of the points is described by the constant object $B := M + \mathbb{1}$, denoted as *deformation matrix*.

B is only a scalar in the one-dimensional case and the deformation is equal to a multiplication of a number, as shown in Fig. 2.13:

In higher dimensions is the effect of a homogeneous deformation also simple. Every line (plane 3d) remains a line after the deformation. It can only be rotated and shifted. To

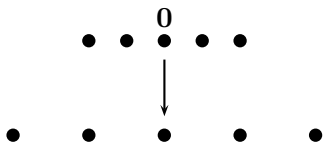

Figure 2.13: *Homogeneous deformation in 1d with $B > 0$*

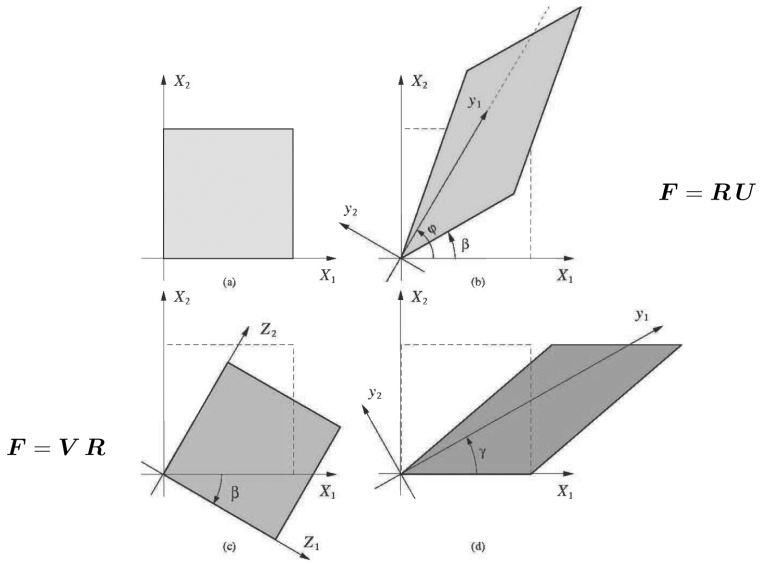

Figure 2.14: *Polar decomposition*

make this more explicit: Every real matrix F can be written as a product of an orthogonal R and a symmetric matrix U that is called the *polar decomposition*

$$F = RU. \tag{2.18}$$

1. *Pure rotation:* orthogonal matrix R. A orthogonal matrix is a isometry, i.e. it remains any distance. A orthogonal matrix is a rotation with a possibly negative determinant and hence an additional change of orientation.
2. *Pure Deformation:* symmetric matrix U. Vectors in direction of the eigenvectors remain unchanged. Every symmetric matrix can be diagonalised by an orthogonal matrix $T^{-1} = T^t$, so that $T^{-1}VT = S$ with S as diagonal matrix (*Principal Axis Transformation*).

A general homogeneous deformation divided into these two operations is shown in Fig. 2.14.

The deformation matrix B can be expressed by 4 matrices: $B = RTST^{-1}$, three orthogonal and one diagonal matrices. Hence it is obvious that a homogeneous deformation retains lines and in 3D planes, they can only be rotated and shifted. However distances of different points on the same line can have changed due to the diagonal matrix S.

Therefore the main characteristic of a homogeneous deformation is that lattices remain lattices. For instance a thermal expansion is such a homogeneous deformation.

This is a necessary condition for deformation to retain periodicity. That is not as so important for the considered deformation approach as one could assume. Because of the

restriction to the unit cell, the unit cell will be modified for itself. So the two lattice vectors will be changed to two new ones which obviously span in the case of non-co-linearity a lattice again.

The examined model of skeletal structure is a porous material and not a continuum. The strain field are complicated to formulate for the joints. The movement of the joints is quite different and far away from homogeneous. Joints can move in opposite directions, so the explicit movement is not characterisable by a homogeneous strain field or deformation matrix B.

The chosen deformation approach tries to deform the lattice, unit cell respectively and the numerical method checks if there is a compatible solution of the edge equations.

Deformation of the unit cell

The requirement that during the deformation of a skeletal structure at least the periodicity will be retained albeit with changed lattice vectors leads to a new lattice with new lattice vectors. Due to the continuity of the deformation the deformed lattice vectors are just the initial lattice vectors

$$\mathbf{a}(\tau) \to \mathbf{a} \quad \text{and} \quad \mathbf{b}(\tau) \to \mathbf{b} \quad \text{for } \tau \to 0.$$

The question dealt with by this section is what the best way is to impose a deformation, in order to obtain a sensibly defined Poisson's ratio.

As mentioned in the introduction, by deforming a body in one direction (uniaxial), the Poisson's ratio tells how the material will expand or shrink in the perpendicular direction.

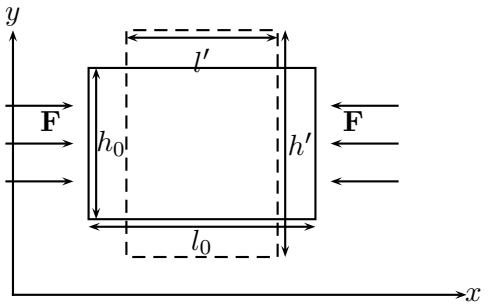

Figure 2.15: *Deformation of a non-auxetic material block: imposed contraction leads to a transversal expansion*

The material property *Poisson's ratio* contains the pure information of the orthogonal reaction. We stress that the deformation must be uniaxial to avoid imposed perpendicular strains. Alternatively, by imposing a general biaxial deformation, there is an imposed deformation in two directions. Hence the measured strain is not necessarily the pure material response. It is a superposition of imposed and answering strain.

For the sake of simplicity a uniaxial strain is imposed and the orthogonal strain is determined. In two dimensions is the orthogonal direction unambiguous. The imposed uniaxial strain is named δ and the unknown orthogonal strain X. The Poisson's ratio can be calculated by these two strains as

$$\nu = -\frac{X}{\delta}. \tag{2.19}$$

We have not yet declared which quantities are used to calculate the strain. A common used strain is the *Cauchy* or also called *engineering strain* which is the relative length change to its undeformed initial value,

$$e = \frac{l' - l_0}{l_0}. \tag{2.20}$$

For finite deformations this is not the best definition, see below. Importantly it is the relative difference between new length to prior length.

Consider the rectangular in Fig. 2.15. The length of the medium in deformation direction is denoted with l and in orthogonal direction with h (height), the initial values l_0, h_0 respectively and the deformed values with l', h' respectively. Hence the strains as determined in equations (2.20) substituted in (2.19) lead to following expression for the Poisson's ratio ν:

$$\nu = -\frac{\frac{h'-h_0}{h_0}}{\frac{l'-l_0}{l_0}}. \tag{2.21}$$

This can be assigned to the rectangular unit cells. But that is not possible in the case of non-rectangular unit cells. In this thesis length and height of the general unit cell are defined as the sum of the moduli of the projected lattice vectors $\mathbf{a}$ and $\mathbf{b}$ onto the deformation direction $\mathbf{e}_{\parallel}$ and its orthogonal direction $\mathbf{e}_{\perp}$ (see Fig. 2.16).

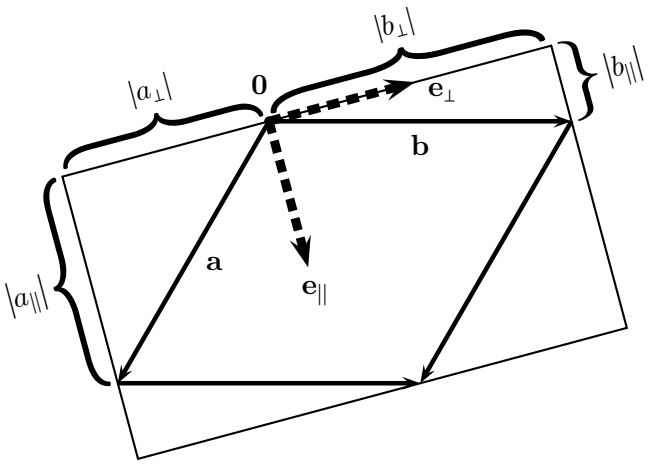

Figure 2.16: *Projected lattice vectors to determine Poisson's Ratio*
The unit cell is described by the lattice vectors $\mathbf{a}$, $\mathbf{b}$ *and the deformation direction is indicated by* $\mathbf{e}_{\parallel}$.

Under deformations the vectors $\mathbf{e}_{\parallel}$ and $\mathbf{e}_{\perp}$ does not change, and we can declare them as an alternative orthonormal basis. Instead of talking of projections the lattice vectors are formulated in the orthonormal basis $\left\{\mathbf{e}_{\parallel}, \mathbf{e}_{\perp}\right\}$.

$$\mathbf{a} = a_{\parallel}\,\mathbf{e}_{\parallel} + a_{\perp}\,\mathbf{e}_{\perp} \tag{2.22}$$

$$\mathbf{b} = b_{\parallel}\,\mathbf{e}_{\parallel} + b_{\perp}\,\mathbf{e}_{\perp} \tag{2.23}$$

$$\mathbf{a}\,(\delta) = a_{\parallel}\,(\delta)\,\mathbf{e}_{\parallel} + a_{\perp}\,(\delta)\,\mathbf{e}_{\perp} \tag{2.24}$$

$$\mathbf{b}\,(\delta) = b_{\parallel}\,(\delta)\,\mathbf{e}_{\parallel} + b_{\perp}\,(\delta)\,\mathbf{e}_{\perp} \tag{2.25}$$

The Poisson's ratio can be expressed by these quantities as

$$\nu = -\frac{\left(\left|a_{\perp}(\delta)\right| + \left|b_{\perp}(\delta)\right| - \left(\left|a_{\perp}\right| + \left|b_{\perp}\right|\right)\right) / \left(\left|a_{\perp}\right| + \left|b_{\perp}\right|\right)}{\left(\left|a_{\parallel}(\delta)\right| + \left|b_{\parallel}(\delta)\right| - \left(\left|a_{\parallel}\right| + \left|b_{\parallel}\right|\right)\right) / \left(\left|a_{\parallel}\right| + \left|b_{\parallel}\right|\right)}. \tag{2.26}$$

By comparing equation (2.19) with (2.26)

$$(1+\delta)\left(\left|a_{\parallel}\right| + \left|b_{\parallel}\right|\right) = \left|a_{\parallel}(\delta)\right| + \left|b_{\parallel}(\delta)\right|. \tag{2.27}$$

A symmetric fragmentation of the imposed strain δ on both lattice vectors leads to following two equations which describes the imposed change of the projection of the lattice vectors in deformation direction:

$$\left|a_{\parallel}(\delta)\right| = (1+\delta)\left|a_{\parallel}\right| \tag{2.28}$$

$$\left|b_{\parallel}(\delta)\right| = (1+\delta)\left|b_{\parallel}\right| \tag{2.29}$$

The orthogonal projections $a_{\perp}(\delta), b_{\perp}(\delta)$ are variables.

However these are assumptions and other choices are possible. In the following this and another deformation approach are discussed. They should provide following features and fulfil following conditions:

- The deformation process must be parameterisable which represents the amplitude of axial strain δ.
- In order to avoid translations one point, namely the origin, must be kept fixed.
- Simple elongations to verify uniqueness ($\nu = 0$) should be possible
- Pure rotations must be excluded.

This wishes exclude the approach of directly modifying the metric parameters $(|\mathbf{a}|, |\mathbf{b}|, \gamma)$, because pregiven value of δ has influence on all three, but in unknown manner (compare e.g. Fig. 2.17). Explicitly the square is uniaxial, homogeneous deformable in 45° direction, where δ is dependent on all three values of the metric parameter.

2.5.0.1 Uniaxial homogenous deformation

If consider the surrounding rectangular is handled as continuum of matter, a deformation can be expressed by the introduced deformation matrix B:

$$B = \begin{pmatrix} 1+\delta & 0 \\ 0 & 1+X \end{pmatrix}$$

$$\mathbf{a} \to \mathbf{a}' = (1+\delta)a_{\parallel}\mathbf{e}_{\parallel} + (1+X)a_{\perp}\mathbf{e}_{\perp} \tag{2.30}$$

$$\mathbf{b} \to \mathbf{b}' = (1+\delta)b_{\parallel}\mathbf{e}_{\parallel} + (1+X)b_{\perp}\mathbf{e}_{\perp} \tag{2.31}$$

This approach allows no rotation of the grid, so structures like the square cannot be deformed with this one.

2.5.0.2 Uniaxial homogeneous deformation with extension rotations

Of course by applying the deformation only onto the both lattice vectors a lattice will also be spanned by the new vectors. A modification of the above approach makes rotations possible by accepting two different orthogonal changes X_a and X_b. However there is not anymore a pure symmetric deformation matrix B which acts on all lattice points identically.

$$\mathbf{a} \to \mathbf{a}' = (1+\delta)a_{\parallel}\mathbf{e}_{\parallel} + (1+X_a)a_{\perp}\mathbf{e}_{\perp} \tag{2.32}$$

$$\mathbf{b} \to \mathbf{b}' = (1+\delta)b_{\parallel}\mathbf{e}_{\parallel} + (1+X_b)b_{\perp}\mathbf{e}_{\perp} \tag{2.33}$$

Lattice vectors which are directed in deformation direction have $a_{\perp} = 0$ and so will never show after deformation direction. So shears as presented in Fig. 2.17 are not possible by deformation in lattice direction. A small modification would allow such rotation.

$$\mathbf{a} \to \mathbf{a}' = (1+\delta)a_{\parallel}\mathbf{e}_{\parallel} + a_{\perp}(\delta)\mathbf{e}_{\perp} \tag{2.34}$$

$$\mathbf{b} \to \mathbf{b}' = (1+\delta)b_{\parallel}\mathbf{e}_{\parallel} + b_{\perp}(\delta)\mathbf{e}_{\perp} \tag{2.35}$$

This is the above mentioned deformation approach. However vectors which are perpendicular to the deformation direction are so after the deformation. If $\mathbf{b}$ is orthogonal in respect to the deformation direction, it will be so forever.

Following physical imagination of the deformation can explain this approach: Consider two parallel plates symbolised in Fig. 2.18 by the horizontal dashed lines. The uniaxial deformation process shifts them. To avoid the pure translation the line through the origin is kept fixed.

Due to the occurring rotation the projection of the lattice vectors changes and not only of the deformation. This influences the Poisson's ratio.

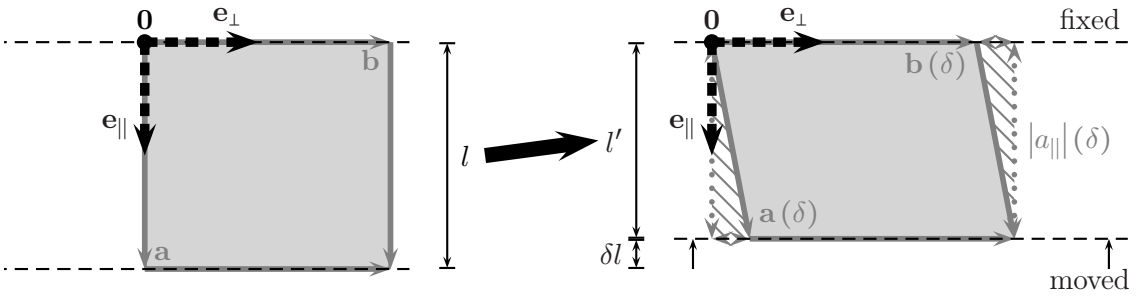

Figure 2.17: *Deformation approach rectangular case according to equations* (2.34) *and* (2.35)

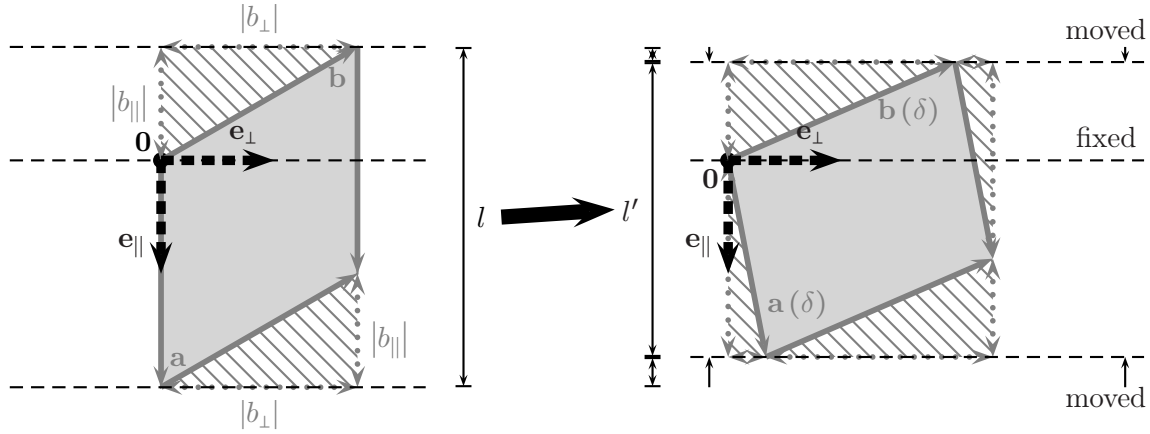

Figure 2.18: *Deformation approach non rectangular case according to equations* (2.34) *and* (2.35)

Poisson's ratio and finite strains As mentioned earlier the Cauchy strain is not the best choice as the strain for the Poisson's ratio for finite deformations. The reason is the permanent comparison to the initial structure. During such large deformations there are changing points, where the perpendicular elongation changes to contraction. So the instantaneous material behaviour becomes auxetic. However the Poisson's ratio based on the Cauchy strain becomes only negative if the current height is smaller than the initial height and that can appear later or never. To identify such reversal points an instantaneous strain will be defined.

$$e_{\text{inst}}(\delta) = \lim_{\zeta \to 0} \frac{l(\delta) - l(\delta - \zeta)}{l(\delta - \zeta)} \tag{2.36}$$

This represents the comparison between two configurations which appears in the continuous deformation process as immediate neighbours.

2.6 Multidimensional deformation spaces

As explained in chapter 2.3 the problem that must be solved is a system of quadratic multivariate equations, with different possible dimensions of the solution spaces:

$$f_{\{ij\}}(\delta) = (\mathbf{p}_i(\delta) - \mathbf{p}_j(\delta)) \cdot (\mathbf{p}_i(\delta) - \mathbf{p}_j(\delta)) - l_{\{ij\}}^2 = 0 \qquad \forall \{i,j\} \in B \tag{2.1}$$

We are interested in one 1-dimensional path $\mathbf{P}(\delta)$ that does not represent a trivial deformation.

What is the physically reasonable path if the solution space is higher dimensional and every path on the surface or through the hyperbody represents a possible deformation? Note that a multi-dimensional solution space is common for the analysed 2d tessellations (e.g. see Fig. 2.19).

An illustration of this problem by the numerical method is given in sect. 4.4.

In order to deal with those situations, where the solution spaces are multidimensional, different approaches will be discussed in the following two subsections:

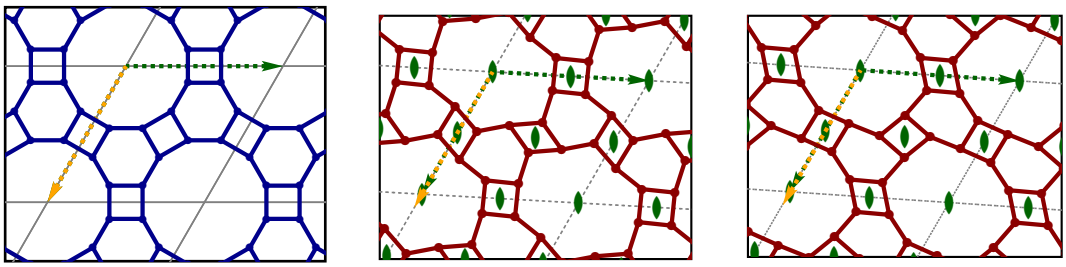

(a) $\delta = 0$ **(b)** $\delta = -0.1$ **(c)** $\delta = -0.1$

Figure 2.19: *Comparison of two deformation runs: the image (c) shows a run, where random numbers are added to the start value of the initial Newton step*

Harmonic joint-angle energy

The considered model and their deformations represents structures which can be deformed without cost of energy. In other words when loaded the bars rotate at the joints without friction and the structure collapses immediately. In the opposite a rigid skeletal structure cannot be deformed and the bars support axial loads, tensile in some, compressive in some others [12]. So in this view a rigid skeletal structure is stable in reality and can be deformed with bars of specific elastic moduli which for instance means they can be elongated dependent on Young's modulus.

So to link this model and the above defined deformations in general with real structures as e.g. compared in sect. 2.1 the model must be extended to include the cost of bending of cell walls or movement of particles in repulsing coulomb potentials or similar processes. The strongest simplification is the free rotation of the bars about the joints. This can be fixed by the introduction of an energy-functional which assigns to every configuration a specific value. This enables the distinction between deformation modes. Its dependency could be e.g. the magnitude of change of the angles at the joints between the bars:

$$H\left[\mathbf{P}\left(\delta\right)\right] = \sum_{\{ijk\}} \left(\alpha_{\{ijk\}}\left(\mathbf{P}\left(\delta\right)\right) - \alpha_{\{ijk\}}\left(\mathbf{P}\left(0\right)\right)\right)^2,$$

with α as the angle between two bars$\{ij\}, \{jk\}$ connected at one joint j. We say that the change of the angle costs energy, so the minimum of H is the path we select. To illustrate this extension in relationship to a real physical system consider the honeycomb pattern in reality with actual cell walls. As real physical explanation you can think of a cell with walls of a specific thickness and the joints are the locations, where the walls are fixed with each other (no free pivoting there like in our model [19]. If the cell is deformed the walls will bend (energy). The same configuration of the joints can be achieved by only changing the angle (only first order: stronger bending will change the distance of a bar significantly, is not covered by the considered model).

Another Hamiltonian could be in analogue to a Coulomb-potential which can maximises the distances of joints which are not fixed directly by a bar.

$$H\left[\mathbf{P}\left(\delta\right)\right] = \sum_{\{i,j\}\in\mathbb{P}(K)/B} Q_i Q_j \left|\mathbf{p}_i\left(\mathbf{P}\left(\delta\right)\right) - \mathbf{p}_j\left(\mathbf{P}\left(\delta\right)\right)\right|^n$$

The Q_i are determined by thermal equilibrium configuration, e.g. initial configuration (possible in the case of no redundant bars (no self-stresses).

With a defined Energy functional E, the task becomes to find either the groundstate deformation that minimises $E[P(\delta)]$ for each value of δ or to obtain averages of e.g. Poisson's ratio over all possible configurations each with a Boltzmann like weight.

Conservation of geometric symmetries

Physical systems which possess a high degree of symmetry (translational and further symmetries like rotations, mirror planes,...), adopt this state, because it is the most energetic favourable one (atoms in a crystal). The deformation may not destroy or outperform the physical reason behind the symmetry. So we can ask to keep all or parts of the symmetry to limit the solution space. That means this approach can reduce the dimension, because the number of independent variables decreases. For instance the 5-gon of section 2.3 has a mirror line in the initial configuration. The requirement of conservation of this symmetry leads to a unique deformation (cf. Fig. 2.20).

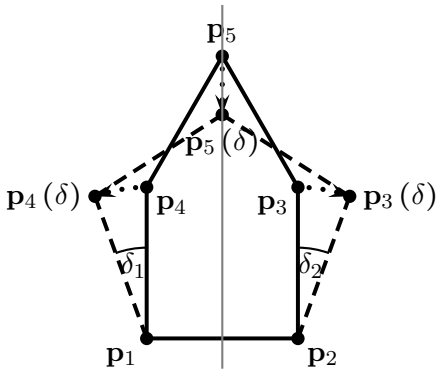

Figure 2.20: *Deformation of the 5-gon, with a geometric constraint: retaining the mirror line through point 5*

The easier and chosen approach is to retain the geometric symmetries. Most of the tilings presented in Grünbaum and Shephard [24] exhibit several symmetry elements. In many cases we can obtain a 1-dimensional solution space.

2.7 Infinitesimal and finite deformations

Rigidity theory - Infinitesimal flexes The rigidity theory [45] deals with such questions but considers the Taylor expansion in δ of the system of equations (2.1) [7]. Therefore it considers only smooth paths. However the given definition of the deformation in subsection 2.3 allows also non-smooth paths and hence this represents already a limitation of possible deformations.

First-order-rigidity means the reduction to the following system of equations by the expansion of $f_{\{ij\}}$ in $\delta = 0$ ($p' := \frac{dp}{d\delta}$)

$$(\mathbf{p}_i(\delta) - \mathbf{p}_j(\delta)) \cdot (\mathbf{p}_i'(0) - \mathbf{p}_j'(0)) = 0 \quad \forall \{i,j\} \in E. \tag{2.37}$$

$(p_i(\delta) - p_j(\delta))$ can be formulated as a matrix, the rigidity matrix. The nullspace of the rigidity matrix represents the infinitesimal deformations and trivial deformations. Therefore the dimension is at least *three* that corresponds to infinitesimal rigid skeletal structure.

The first observation one can make, is that Eq. (2.37) asks for the orthogonality of the bar vector and the difference vector of the velocity vectors which belongs to both joints of the bar. In the following are two examples presented which make clear that rigid structures can have infinitesimally flexes and this can be seen just of this orthogonality.

Infinitesimal rigidity implies rigidity [42]. But the converse is not true. The nullspace of the rigidity matrix can contain also deformations beside the trivial deformations which however lead to a small change in length of bars. They will be termed as infinitesimal flexes. Fig. 2.21 shows a skeletal structure embedded in the plane which has an infinitesimal flex but is rigid [42]. Holding the lower triangle fixed, the outer equal-length vertical bars force every point of the upper triangle to move in a circular path whose radius is equal to the length of those bars. The middle vertical bar however forces the lower point to move in a circle of strictly smaller radius and so the framework is rigid in the plane.

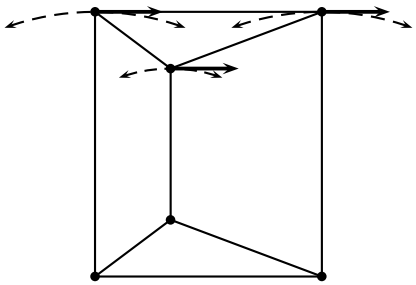

Figure 2.21: *A rigid, but infinitesimally flexible skeletal structure. The lower triangular is fixed. In order to move the upper triangular the three joints move on circles due to the rigid bars. However the radius of the two joints on the top is larger than that of the third joint and therefore this skeletal structure is rigid.*

A further example is shown in Fig. 2.22.

The rigidity theory can give a sufficient but not necessary condition for rigidity. The rank of the rigidity matrix can exclude rigid structures but cannot determine flexible structures in the sense of this thesis.

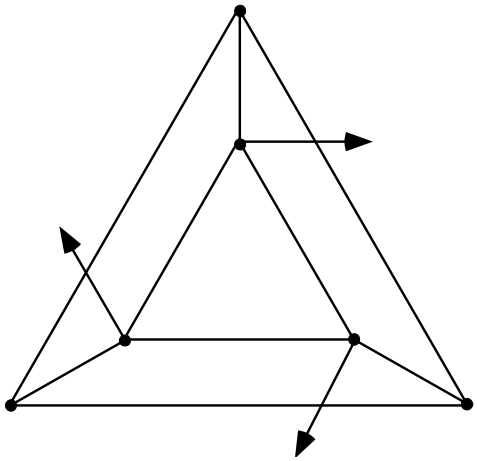

Figure 2.22: *Another example of a rigid skeletal structure which has an infinitesimal flex. The velocity vectors are perpendicular to the bars linking the inner with the outer circle. The pairwise addition of the velocity vectors leads to orthogonal vectors in respect to the edges vectors. Therefore the shown set of vectors belong to a deformation which is non trivial because not all points are transformed in the way.*

In this thesis small deformations are considered. But these deformations retain the length of the bars absolutely (maximal numerically).

3 Periodic and symmetric tessellations by polygons

The aim of this thesis is to gain an understanding of deformation mechanisms of symmetric, periodic skeletal structures, and in particular to identify novel auxetic examples. This chapter introduces symmetric periodic tessellations of the plane by polygonal tiles. These provide a "catalogue" of skeletal structures, whose deformation behaviour is analysed in this thesis. This chapter also discusses the embedding of tessellations in different plane groups, either the highest possible symmetry group or one of its subgroups with fewer symmetries. The different symmetry requirements are later used to restrict the solution space of deformations.

3.1 Tessellations by polygons

The reference book which treats the topic of tessellations comprehensively is: *Tilings and Patterns* by Grünbaum and Shephard [24]. A *tiling* is defined as the countable family of closed sets $\mathcal{T} = \{T_1, T_2, \dots\}$, which cover with *tiles* T_i the plane without gaps and overlaps, see Fig. 3.1. The term *tessellation* is used as a synonym for tiling.

The intersection of any finite set of tiles has necessarily zero area, but need not to be empty and can consist of points or arc segments. The points and arc segments, respectively are called the *vertices* and the *edges*, respectively, of the tiling.

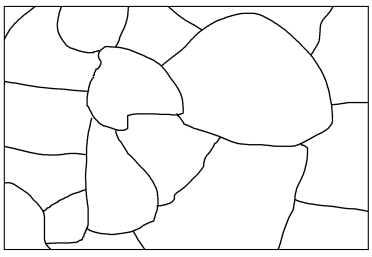

Figure 3.1: *Clipping of a tiling. The tiles match to each other perfectly, i.e. there are no gaps between the tiles or different tiles cover a common part of the plane.*

This definition is too general for our purposes. Tilings with exclusively polygons as tiles and all intersection of adjacent tiles are either corners or whole sides of the polygons will be considered ("edge-to-edge" tiling[1]). Every vertex has at least three adjacent edges. Corners that are not vertices of the tiling have only two adjacent edges.

[1] [24] defines on p.18 the term "edge-to-edge" tiling as a tiling by polygons where all corners and sides of the polygons coincide with the vertices and edges of the tiling. However on p.83 tilings with star polygons that have corners that are not vertices is denoted as "edge-to-edge". The inverse of the first statement would make this consistent i.e. every vertex coincide with a corner of a polygon.

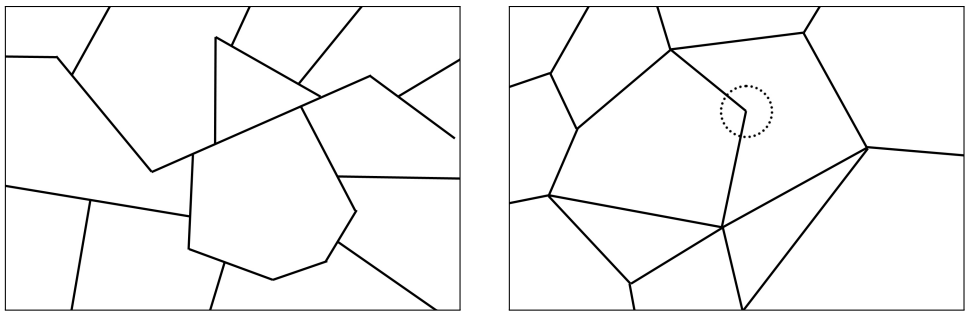

(a) **(b)**

Figure 3.2: *Comparison of a non-edge-to-edge tiling to an edge-to-edge tiling.* ***(a)*** *Tessellation with tiles which are polygons, but it is not edge-to-edge because there are intersections of different tiles which do not represent a corner or an edge of the polygons.* ***(b)*** *Edge-to-edge tessellation with a shared corner of two polygons which is not a vertex of the tiling (highlighted by the dotted circle).*

The tiles are geometric shapes with straight edges and all vertices are corners of the polygons (but not all corners are necessarily vertices of the tiling, see Fig. 3.2b). This represents a skeletal structure as defined in chapter 2 which covers the plane. The polygons are not required to be regular but can be non-regular or non-convex, e.g. star-polygons.

The re-entrant honeycomb structure (Fig. 1.2b) is the strongly deformed skeletal structure consisting of repetitive edge-to-edge regular hexagons. This object belongs to the so-called 11 Archimedean Tilings [2] (Fig. 3.3). They are a complete group of tilings, with one common property. The tilings consist only of regular polygons and have only one vertex type, respectively. There are no more tilings with this property. A type denotes the number of the different regular polygons which meet at the vertex and their order. On the other hand the species of a vertex is the pure number of different polygons. For example the vertices $3^3.4^2$ and $3^2.4.3.4$ are of different type, but belong to the same species. There are infinitely number of tilings with vertices of the same species (e.g. [24]). The distinction based on the order, a stronger requirement, will limit the tilings with one vertex type. That are the Archimedean tilings. They are also isogonal that means every pair of vertex are equivalent under some symmetry operations of the tiling. Hence the Archimedean tilings are also called 1-uniform. The 2-uniform tilings have 2 types of vertices which among each other can be mapped by symmetry operations. There are precisely 20 of them.

As another appropriate complete class of tilings presented in [24] the 4 uniform tilings by regular polygons and star polygons, in which every corner of the star is vertex of the tiling (Fig. 3.4).

Some other classes of tilings are not completely presented in [24] because not all are known or it is not yet proved that there are not more. The 17 tilings consisting of regular and star shaped polygons but with corners of the stars which are not vertices of the tiling. Nevertheless they are edge-to-edge tilings. And of course there is not enough space for all known k-uniform tilings by regular polygons, e.g. there are 61 3-uniform and 151 4-uniform tessellations [18].

In this thesis we restrict our analysis to the following types of uniform tessellations:

[2] The Archimedean Tilings are systematically investigated for the first time by Kepler in *Harmonics Mundi*, 1619 [24].

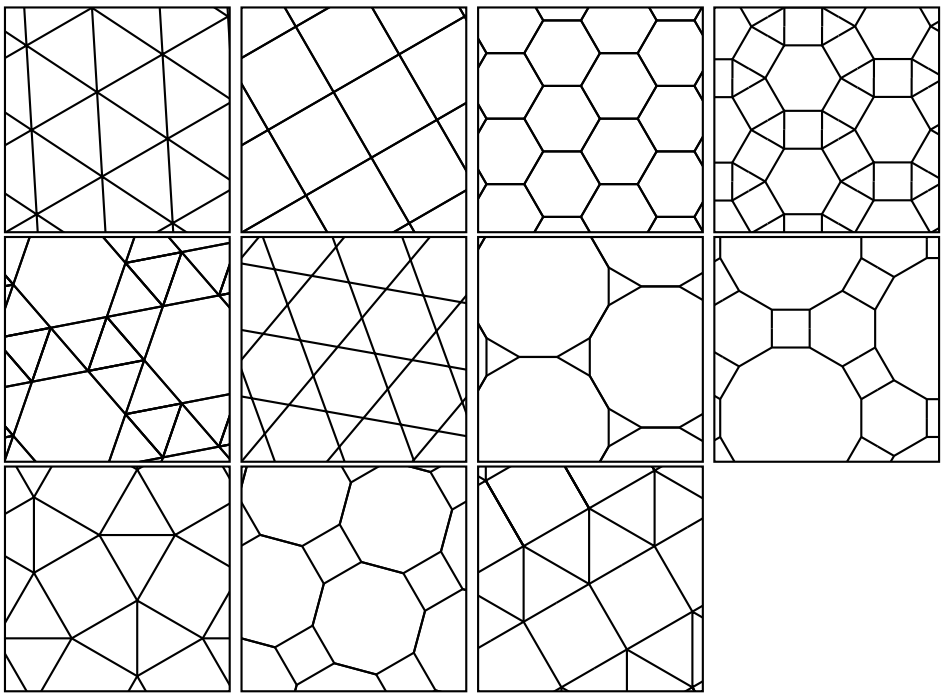

Figure 3.3: *The 11 Archimedean tilings. These 11 are the only ones which consists of regular polygons and have one vertex of the same type (see text for explanation of a type of a vertex).*

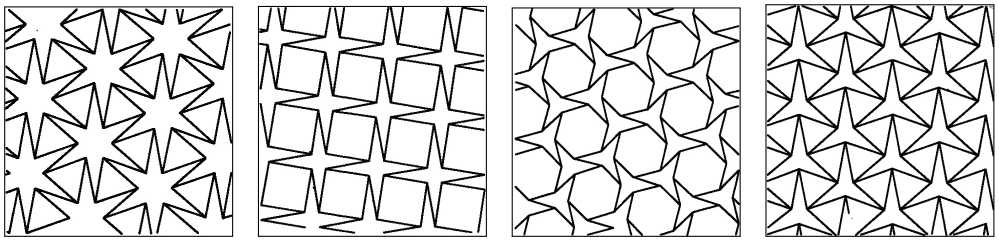

(a) $(3.6^{*}_{\alpha}.6^{**}_{\alpha})$ **(b)** $(4.4^{*}_{\alpha}.4^{**}_{\alpha})$ **(c)** $(6.3^{*}_{\alpha}.3^{**}_{\alpha})$ **(d)** $(3.3^{*}_{\alpha}.3.3^{**}_{\alpha})$

Figure 3.4: *Uniform tilings by regular and star polygons (extracted from [24])*

1. the 11 Archimedean tilings,

2. the 20 2-uniform tilings,

3. the 4 uniform tilings by regular polygons and regular star polygons, where all corners are vertices,

4. and 17 uniform tilings by regular polygons and regular star polygons, where not all corners are vertices

Additional ones which are periodic tilings but do not belong to the uniform tilings, but are interesting auxetic cases, will be called simple *periodic tilings*. That are the inverted honeycomb, inverted rhombus and a pattern of swastika.

Thus the total number of considered tilings is 55.

3.2 Periodicity and the 17 crystallographic plane groups

As already motivated we are interested in the geometric symmetries of the examined skeletal structures. The group theory is the proper tool to study their symmetries. Every planar, in linear independent directions repetitive pattern belongs to exactly one of the known 17 plane crystallographic groups [26, 5] [3].

A such symmetry group has as its members the symmetry operations of the tessellation. Symmetry operations are mappings of the plane which keep all distances invariant (*isometries*) and map the object onto itself. But not every point is necessarily mapped onto itself.

Every isometry in 2D is one of the following four types (provable, e.g. [9]):

1. **Translation** in a given direction through a given distance
2. **Rotation** about a given point O through a given angle θ
3. **Reflection** in a given Line (the mirror or line of reflection)
4. **Glide Reflection** reflection in a line L with an additional translation through a given distance parallel to L.

You cannot combine arbitrary symmetry operations to build a group. Symmetry operations can require or generate another operation and so are dependent. The completeness of a group induce the 17 groups, as shown in Fig. 3.5. These figures show the crystallographic unit cell and the occurring symmetry elements. These symbols are representatives of the symmetry operations.

The groups are denoted by the short or the full Herman-Mauguin symbol which consists of two parts: a letter which describes the kind of the conventional unit cell, either primitive (p) or centered (c), and a second part a set of characters which denotes the symmetry elements of the plane group. This is a modified point-group symbol.

The reason for the two types of unit cells, lies in the motivation to describe symmetry operations by same matrices possible by the introduction of specific basis for the individual groups.

Some notes about identification of symmetry groups The knowledge about the 17 groups allows to determine the symmetry group of a tessellation by checking few and simple symmetries. E.g. following conditions in this order are sufficient:

1. 6-fold rotation: no mirror lines p6, mirror lines $p6mm$.
2. 3-fold rotation: no mirror lines p3, mirror lines $p3m1$ (long diagonal mirror line in primitive unit cell) $p31m$ (short diagonal mirror line in primitive unit cell).
3. 4-fold rotation, no mirror lines p4, mirror line through 4-fold: $p4mm$, no mirror lines through: 4-fold $p4gm$.
4. 2-fold rotation: primitive cell diagonal mirror lines: $c2mm$, no diagonal: orthogonal mirror lines $p2mm$, no mirror lines $p2gg$, mirror lines only in one direction $p2mg$, no glide-mirror lines $p2$

[3] also called wall-paper groups, 7 stripe patterns, 3D: 230 space groups

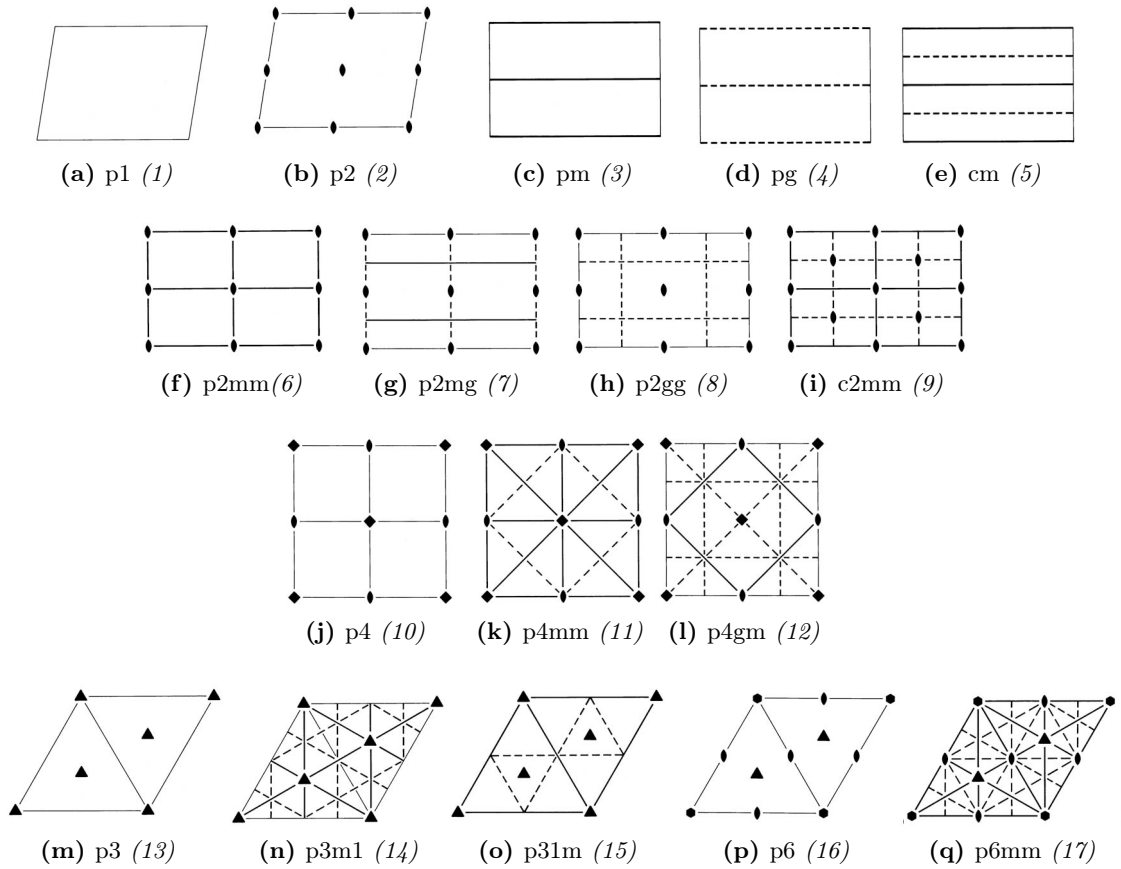

Figure 3.5: *The 17 crystallographic plane groups, represented by diagrams of the symmetry elements in the unit cell (extracted from [26], Vol. A)*

5. no rotation: mirror lines pm, no mirror lines but glide mirror lines pg, mirror lines and glide
6. if all above symmetry checks fail: $p1$

3.3 The crystallographic basis and symmetries

The *Voronoi polygon*[4] describes that area which contains all points which have one common nearest lattice point. In the plane there are two general types of Voronoi polygons: 6-gon, with parallel opposite edges (s), or a rectangular (v). The analysis of the point symmetries of all possible occurring Voronoi polygons leads to the point groups of the plane [5]. In the plane there are exactly four such groups, called *holoedries*, denoted by the point group symbols: 2, $2mm$, $4mm$, $6mm$. These symbols denotes the highest rotational symmetry of the lattice and if there are additional mirror lines along the crystallographic directions. These mirror lines are not necessarily in the direction of the reduced lattice vectors but the next discussed choice of the crystallographic coordinate system lead to the situations where the lines are directed along the crystallographic lattice vectors.

[4]also called *Dirichlet region*, *Wigner-Seitz cell* or *Brillouin-zone* of the reciprocal lattice

The representation of the symmetry operations of the point groups as matrices depend on the chosen basis. There exist a conventional basis suggested by crystallographer. The motivation is to represent all occurring matrices of the same symmetry element of the same point group identically.

The matrices are different between the two Voronoi polygon types for the point group 2mm. If you choose directions for the basis vectors parallel to symmetry lines, you can get such a unique representation. However the basis for s(2mm) is not necessary a basis of the point net anymore. There can occur the situation of an additional lattice point in the middle of the crystallographic cell, called *centered cell*. To ensure the same translational periodicity, the centerings have to be included by further symmetry relations.

In Fig. 3.6 are shown the four crystallographic coordinate systems corresponding to the four holoedries.

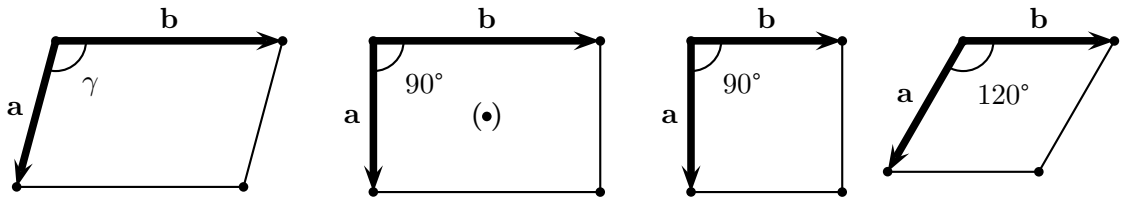

Figure 3.6: Crystallographic *coordinate systems of the point nets of the plane:* oblique, rectangular, square *and* hexagonal. *In the middle of the rectangular system is indicated by an additional lattice point in brackets that there can be a further lattice point (centered cell).*

Fixation of skeletal structure in the symmetry scaffold The decision of the unit cell is not always unique. Group $p1$ is completely arbitrary, pm, pg, cm can shifted along the mirror lines. All other groups without the p31m, p6, p6mm have different discrete alternative positions (not addition of a linear combination of translations vectors with integer coefficients). Beside the continuous arbitrary cases after the first unit cell decision the skeletal structure is fixed during the deformation.

The continuous cases of $p1, pm, pg, cm$ can lead to trivial translations which can be removed by fixing components. Especially to compare different results of multiple program runs to verify that the result are identically or not.

Basis transformation: ONB to crystallographic Basis As in section 2.5 explained the deformation will be imposed by changing lattice vectors. If the joints are given instead of in the orthonormal basis ($e_1 = (1,0)$ and $e_2 = (0,1)$) in the lattice basis $\mathbf{a}$ and $\mathbf{b}$, the symmetry relations are invariant due to the change of basis vectors.

Scalar product in non orthonormal basis As above denoted the crystallographic vectors are not necessary orthogonal or have length one. Hence the crystallographic basis is not necessary an ONB, so some accustomed expressions like that for the scalar product must regard to this.

$$\mathbf{p}_1 \cdot \mathbf{p}_2 = \left(p_{1_x}\mathbf{a} + p_{1_y}\mathbf{b}\right) \cdot \left(p_{1_x}\mathbf{a} + p_{1_y}\mathbf{b}\right) = g_{\alpha\beta} p_{1_\alpha} p_{2_\beta} \tag{3.1}$$

$$\text{with } (g_{\alpha\beta}) = \begin{pmatrix} \mathbf{a}\cdot\mathbf{a} & \mathbf{a}\cdot\mathbf{b} \\ \mathbf{a}\cdot\mathbf{b} & \mathbf{b}\cdot\mathbf{b} \end{pmatrix}$$

System of bar equations must only be rewritten by the given expression. From this equation it is already obvious if **a** and **b** are modified by the deformation approach of sect. 2.5, the joint configuration will not represent a root of this perturbed system anymore.

3.4 Subgroups and basis transformations

We analysed the symmetries to retain unique deformations. But this artificial extension is not unique. We could ask only for subgroups of the original symmetries. So one interesting question is: How do the degrees of freedom depend on the different retained symmetries? Are all symmetries are necessary or does a subgroup suffice?

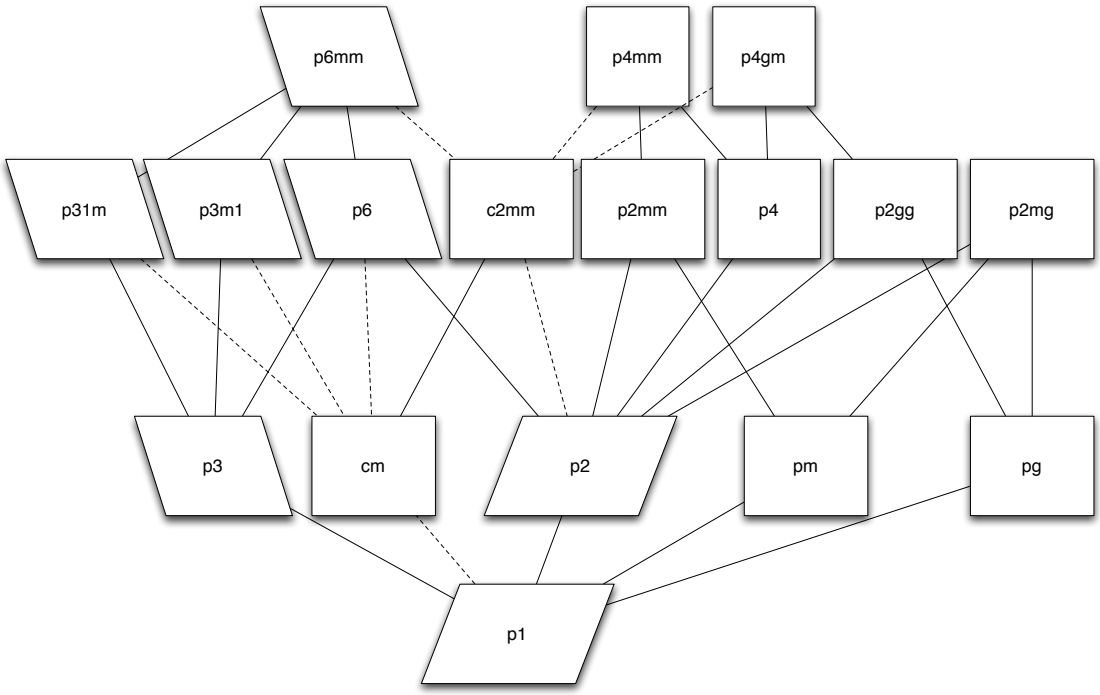

Figure 3.7: *All t-subgroup relations; A change of the cell type is indicated by the dotted line. Nevertheless there can also be necessary basis transformations between groups with the same cell type. These transformations are rotations and translations. They allow in some situations embeddings of the same subgroup in non-symmetric equivalent directions, e.g. compare* pm *as subgroup of* p2mm*. The relations are extracted from [26] Volume A1.*

Considered Subset of all possible subgroups We can classify subgroups into three groups, namely *translationengleiche* (short t-subgroups), *klassengleiche* (short k-subgroups) and general subgroups.

To reduce the large number of (isomorphic) subgroups, we will consider in this thesis only t-subgroups that are those who have the same translational symmetry. Fig. 3.7 shows the relations between the different groups and their t-subgroups.

Subgroups in the basis of the main groups The initial group and its subgroups are considered in the same basis to avoid basis transformations which transform the lattice vectors $\mathbf{a}$ and $\mathbf{b}$. This is done because the chosen deformation approach modifies the vectors directly and hence a change of the vectors would influence the effect of the deformation approach what is not intended by the consideration of different symmetries of one tiling. But it is not possible to give one single basis for all groups and all their subgroups. For instance the isomorphic case of the different embeddings of *pm* in *p2mm* makes already clear that there are two representations of one group necessary (see Fig. 3.9).

Further the suggested representation in [26] for two groups is one with a centered unit cell (*c2mm cm*). But they are subgroups of groups with a suggested primitive cell. This also needs to express these two in a representation with a primitive cell.

Hence there are multiple representations of the same groups necessary in the case of the different occurring situations as subgroups. There are much more which are not all in detail here discussed.

In particular the decentering of the centered groups lead to a further unit cell type, namely *rhombus*, with the constraint $|\mathbf{a}| = |\mathbf{b}|$ (cf. Fig. 3.8).

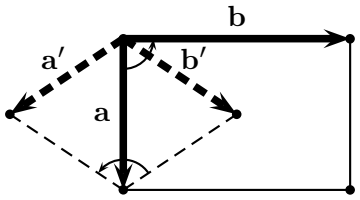

Figure 3.8: *Centered cell (solid lines) and primitive cell (dashed lines): the lattice vector constraint is in the case of the centered cell the orthogonality of both vectors* $(\mathbf{a}, \mathbf{b})$ *and in the case of primitive cell the equality of the lengths of the vectors* $(\mathbf{a}', \mathbf{b}')$.

Explicitly the transition from the centered cell lattice vectors $(\mathbf{a}, \mathbf{b})$ to the one of the primitive cell $(\mathbf{a}', \mathbf{b}')$ and vice versa is

$$\mathbf{a}' = \frac{1}{2}(\mathbf{a} - \mathbf{b}) \qquad \mathbf{a} = \mathbf{a}' - \mathbf{b}'$$
$$\mathbf{b}' = \frac{1}{2}(\mathbf{a} + \mathbf{b}) \qquad \mathbf{b} = \mathbf{a}' + \mathbf{b}'$$

and the lattice constraint leads to the equality of the lengths of the new lattice vectors however with an arbitrary angle between them,

$$\mathbf{a} \cdot \mathbf{b} \Leftrightarrow (\mathbf{a}' - \mathbf{b}') \cdot (\mathbf{a}' + \mathbf{b}') = 0 \Leftrightarrow \mathbf{a}'^2 = \mathbf{b}'^2.$$

Fig. 3.10 shows all subgroups of the group *p4mm* in one basis.

Different embeddings of one subgroup The group *p2mm* has *pm* as one subgroup. There are two possibilities to embed this (Fig. 3.9).

However if *p2mm* is on its part a subgroup of *p4mm* then the two directions are symmetric equivalent and hence no difference in the embedding of *pm*.

The mathematical derivation of the subgroups provides the possibility to deduce this difference.

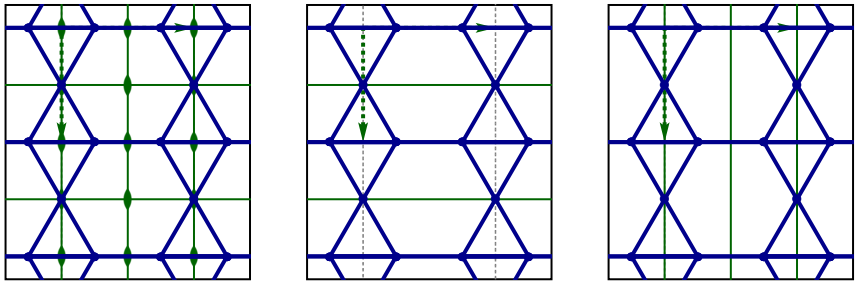

(a) **(b)** **(c)**

Figure 3.9: ***(a)*** *Group p2mm embedded in the 2-uniform tiling 15.* ***(b)***, ***(c)****: The subgroup pm can be embedded differently.*

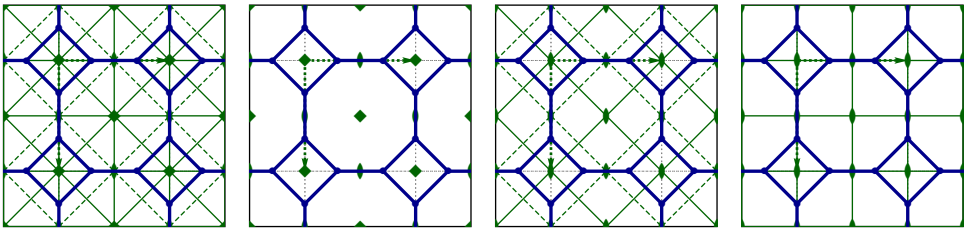

(a) *group: p4mm (11)* **(b)** *subgroup: p4 (10)* **(c)** *subgroup: p21m$_r$ (30)* **(d)** *subgroup: p2mm (6)*

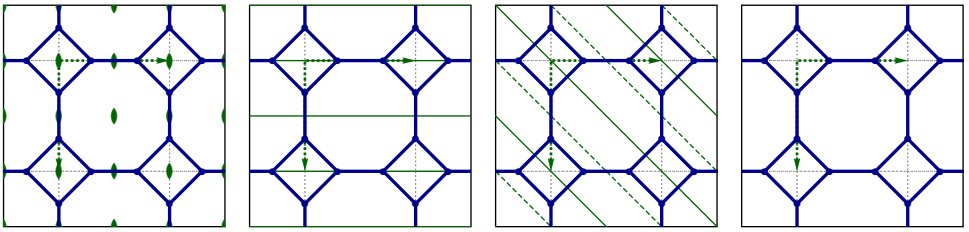

(e) *subgroup: p2 (2)* **(f)** *subgroup: pm (3)* **(g)** *subgroup: pm$_r$ (26)* **(h)** *subgroup: p1 (1)*

Figure 3.10: *All t-subgroups of p4mm*(11)*; The shown structure is the Archimedean tiling* (4.6.4.6)*, also called Truncated Square tiling. However due to the representation in the basis of p4mm the representation of c2mm and cm differs from those given in [26], indicated with an own used group name and group number (p21m$_r$*(30)*, pm$_r$*(26)*). In this cases the differences regard to the different type of unit cells. Note due to the original 4-fold symmetry the two different embeddings of pm and pm$_r$ are not considered.*

3.5 Computer-based generation of periodic and symmetric tessellations

A systematic generation of the required data for the deformation has been developed. The computer implementation of the complete problem is separated into three programs:

- `subgroup`
- `tesselate`
- `deform` (see Chapt. 4)

Unit cell and its asymmetric part As in section 2.4 has been explained only the unit cell plus neighbouring joints will be considered. The coordinates of the joints, the set of the bars and the symmetry group are needed. In the unit cell positions exist which equal each other because of symmetries. Such positions are assigned one common letter, the *Wyckoff letter*. Thus the complete unit cell contains redundant data dependent on the symmetry group. The minimal necessary part of the unit cell is called asymmetric unit. To avoid inconsistent input data the user must only provide the joints and bars of the asymmetric unit with noting the right symmetry group. An example user input file is printed below Fig. 3.11. The program `tesselate` generates from this input file a new data file with all joints and bars of the unit cell with all symmetry relations between joints which are symmetric equivalent.

Generation of subgroup data The program `subgroup` serves for the purpose to extend the asymmetric unit to the new asymmetric unit with additional joints and bars. This is illustrated in the following two columns by the *Truncated Square tiling* which belongs to the group *p4mm*.

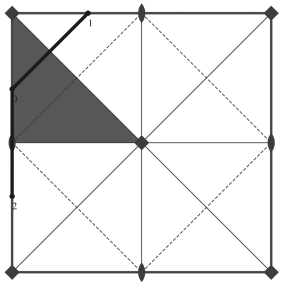

Figure 3.11: *The minimal not redundant structure information of the unit cell, the asymmetric unit (group* p4mm*)*

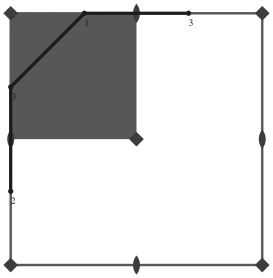

Figure 3.12: *The result of the subgroup program: the extended asymmetric unit of the group* p4

```
# Basic Informations:
name : Truncated Square Tiling
# Group:
group : p4mm


# Basis:
a : 1
b : 1
angle : 90

# Asymmetric unit
# Nodes:
# node : x,y # i
node : 0.292893218813452,0 # 1
node : 0,0.292893218813452 # 2
node : 0.707106781186548,0 # 3

# Edges:
# edge  : i;j
edge  : 1;2
edge  : 1;3
```

```
# Basic Informations:
name : Truncated Square Tiling
# Group:
group : p4
original_group : p4mm

# Basis:
a : 1
b : 1
angle : 90

# Asymmetric unit:
# Nodes:
node : 0.292893218813452,0 # 1
node : 0,0.292893218813452 # 2
node : 0.707106781186548,0 # 3
node : 0,0.707106781186548 # 4

# Edges:
edge : 1;2
edge : 1;3
edge : 2;4
```

3.6 Constraints to the unit cell deformation in different groups

The given deformation approach of the lattice vectors in subsection 2.5 by the equations (2.34) and (2.35) allow rotations and as well length changes of the vectors. Maintaining the symmetries of given symmetry groups during the deformation leads to further constraints on the lattice vectors. The complete unconstrained deformation of the unit cell is given only at the lattice type *oblique* of the groups *p1* and *p2*. All other groups do not allow an independent change of $\mathbf{a}$ and $\mathbf{b}$. Either the angle between $\mathbf{a}$ and $\mathbf{b}$ remains constant or keep their lengths.

These constraints will affect or even determine the Poisson ratio.

Specific relationships between both lattice vectors must always be satisfied. The deformation is imposed on the lattice by the referenced equations:

$$\mathbf{a}(\delta) = (1+\delta)a^{\parallel}\mathbf{e}^{\parallel} + a^{\perp}(\delta)\,\mathbf{e}^{\perp} \tag{2.34}$$

$$\mathbf{b}(\delta) = (1+\delta)b^{\parallel}\mathbf{e}^{\parallel} + b^{\perp}(\delta)\,\mathbf{e}^{\perp} \tag{2.35}$$

with δ as the deformation parameter (longitudinal imposed strain), $a^{\parallel}, b^{\parallel}, \mathbf{e}^{\parallel}, \mathbf{e}^{\perp}$ constants and $a^{\perp}(\delta), b^{\perp}(\delta)$ possible variables.

The four conventional lattice types *oblique, rectangular, square*, *hexagonal* and the decentered type *rhombus* are constrained as follows

oblique No relationship between $\mathbf{a}(\delta)$ and $\mathbf{b}(\delta)$. Both $a^{\perp}(\delta), b^{\perp}(\delta)$ are independent variables.

rectangular $\mathbf{a}(\delta)$ and $\mathbf{b}(\delta)$ must be orthogonal for all δ.

$$\mathbf{a}(\delta)\cdot\mathbf{b}(\delta) = 0 \Leftrightarrow (1+\delta)a^{\parallel}(1+\delta)b^{\parallel} + a^{\perp}(\delta)\,b^{\perp}(\delta) = 0 \tag{3.2}$$

Only one of $a^{\perp}(\delta), b^{\perp}(\delta)$ is an independent variable.

square $\mathbf{a}(\delta)$ and $\mathbf{b}(\delta)$ must be orthogonal and have the same modulus for all δ.

$$\mathbf{b}(\delta) = R\left(\frac{\pi}{2}\right)\mathbf{a}(\delta) = \underbrace{(1+\delta)\,a^{\parallel}}_{b^{\perp}(\delta)}\mathbf{e}^{\perp}\ \underbrace{-a^{\perp}(\delta)}_{(1+\delta)b^{\parallel}}\mathbf{e}^{\parallel}$$

$$\mathbf{a}^{\perp}(\delta) = -(1+\delta)\,b^{\parallel} \tag{3.3a}$$

$$\mathbf{b}^{\perp}(\delta) = (1+\delta)\,a^{\parallel} \tag{3.3b}$$

The lattice vectors are fully defined by modification of δ.

hexagonal $\mathbf{a}(\delta)$ and $\mathbf{b}(\delta)$ angle of +120° and same modulus for all δ.

$$\begin{aligned}\mathbf{b}(\delta) &= R\left(\frac{2\pi}{3}\right)\mathbf{a}(\delta) = -\frac{1}{2}\begin{pmatrix}1 & \sqrt{3}\\ -\sqrt{3} & 1\end{pmatrix}\mathbf{a}(\delta)\\ &= \underbrace{-\frac{1}{2}\left((1+\delta)\,a^{\parallel}+\sqrt{3}a^{\perp}(\delta)\right)}_{(1+\delta)b^{\parallel}}\mathbf{e}^{\parallel}\underbrace{-\frac{1}{2}\left(a^{\perp}(\delta)-\sqrt{3}\,(1+\delta)\,a^{\parallel}\right)}_{b^{\perp}(\delta)}\mathbf{e}^{\perp}\end{aligned}$$

$$a^{\perp}(\delta) = -\frac{1}{\sqrt{3}}(1+\delta)\left(a^{\parallel}+2b^{\parallel}\right) \quad (3.4a) \qquad b^{\perp}(\delta) = \frac{1}{\sqrt{3}}(1+\delta)\left(2a^{\parallel}+b^{\parallel}\right) \quad (3.4b)$$

The lattice vectors are fully defined by modification of δ.

rhombus The transition from the centered cell to the primitive cell alter the constraint for the lattice vectors. Instead of the orthogonality they must be of equal length.In the decentered case $\mathbf{a}(\delta)$ and $\mathbf{b}(\delta)$ must have the same modulus $|\mathbf{a}(\delta)| = |\mathbf{b}(\delta)|$.

We introduce as the variable the angle α between both lattice vectors:

$$\begin{aligned}\mathbf{b}(\delta) &= R(\alpha)\,\mathbf{a}(\delta) = \begin{pmatrix}\cos(\alpha) & -\sin(\alpha)\\ \sin(\alpha) & \cos(\alpha)\end{pmatrix}\mathbf{a}(\delta)\\ &= \underbrace{\left(\cos(\alpha)\,(1+\delta)\,a^{\parallel}-\sin(\alpha)\,a^{\perp}(\delta)\right)}_{(1+\delta)b^{\parallel}}\mathbf{e}^{\parallel}+\underbrace{\left(\sin(\alpha)\,(1+\delta)\,a^{\parallel}+\cos(\alpha)\,a^{\perp}(\delta)\right)}_{b^{\perp}(\delta)}\mathbf{e}^{\perp}\end{aligned}$$

$$a^{\perp}(\delta) = \frac{(1+\delta)\left(a^{\parallel}\cos(\alpha)-b^{\parallel}\right)}{\sin(\alpha)} \quad (3.5a) \qquad b^{\perp}(\delta) = \frac{(1+\delta)\left(a^{\parallel}-b^{\parallel}\cos(\alpha)\right)}{\sin(\alpha)} \quad (3.5b)$$

Consequences of the constraints for the Poisson's ratio

Square and hexagonal groups: Insert the calculated expressions of $a^{\perp}(\delta)$ and $b^{\perp}(\delta)$ into the equation for the Poisson ratio 2.26:

$$\nu = -\frac{\left(|a_{\perp}(\delta)|+|b_{\perp}(\delta)|-\left(|a_{\perp}|+|b_{\perp}|\right)\right)/\left(|a_{\perp}|+|b_{\perp}|\right)}{\left(\left|a_{\parallel}(\delta)\right|+\left|b_{\parallel}(\delta)\right|-\left(\left|a_{\parallel}\right|+\left|b_{\parallel}\right|\right)\right)/\left(\left|a_{\parallel}\right|+\left|b_{\parallel}\right|\right)} \quad (2.26)$$

This expressions cancels to a constant of −1. Therefore the Poisson ratio is always −1 for hexagonal and square groups. Of course the skeletal structure must be flexible, but nevertheless the deformations have not to be unique.

Rhombus with rectangular starting unit cell

$\alpha = 0°$

Analytical expression:

$$\nu(\delta) = -\frac{\sqrt{2\delta-\delta^2}}{\delta} \quad (3.6)$$

The Poisson's ratio diverges for $\delta \to 0$ for deformation directions in $\mathbf{a}$ and $\mathbf{b}$ directions (Fig. 3.13). Beside the constraints of the group, this result appears also in the square tiling and other only shearing tilings like the elongated triangular tiling in group *p1*.

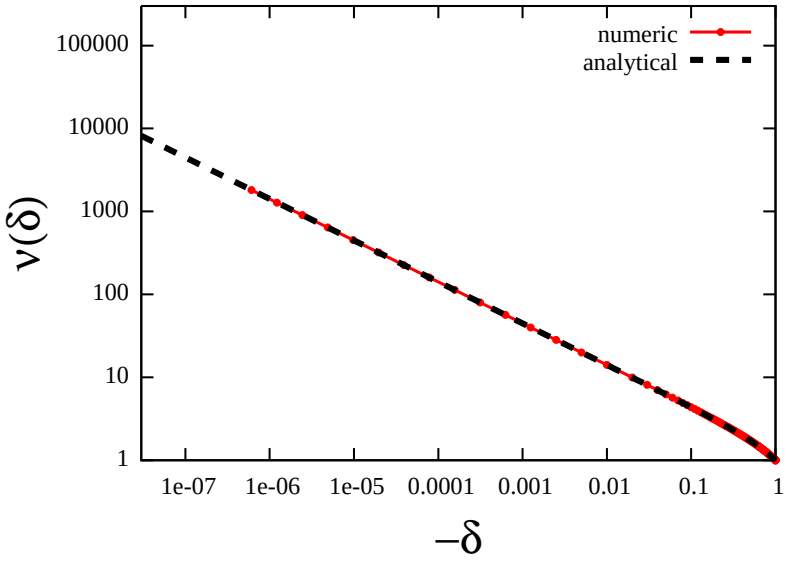

Figure 3.13: *Comparison of analytical determined Poisson's ratio as function of δ and the numerical determined Poisson's ratio calculated by the deformation results of the* square tiling *6.2.1. The analytical function is* $\nu(\delta) = -\frac{\sqrt{2\delta-\delta^2}}{\delta}$

4 Numerical solution of the edge equations

The multivariate system of quadratic equations of the bars cannot be solved in general analytically. The initial joint configuration represents a valid configuration, which satisfies the edge equations. As detailed discussed this thesis considers unique mechanisms. If the lattice is hold fixed, then only indifferent and so non-unique skeletal structures can undergo a deformation. These cases are excluded and so the fixation of the lattice leads to a rigid situation. Through the imposed change of the lattice vectors the system of edge equations is perturbed and the skeletal structure must deform if possible. The solution of this modified system are tried to calculate. In this thesis this problem will be handled numerically by the multidimensional Newton-Raphson method. The occurring linear equations during the single steps of the numerical method will be solved with singular value decomposition of the Jacobian. This chapter presents the numerical method and its implementation in the context of the periodic tessellations.

4.1 Mathematical formulation of the deformation problem

Beside the system of equations which describes the bar extensions, furthermore equations are introduced through the asking of retaining periodic and symmetric properties of the tessellations. That are the identification of neighbouring joints and symmetry relations between joints which are symmetrically equivalent. Moreover because of the convenient formulation of the symmetry relations in the crystallographic basis the chosen basis is not anymore an orthonormal one. Hence the scalar product must be formulated in a more general way as done in equation (4.1),

$$f_{\{ij\}} = g_{\alpha\beta}(\mathbf{p}_i - \mathbf{p}_j)_\alpha(\mathbf{p}_i - \mathbf{p}_j)_\beta - l^2_{\{ij\}} \stackrel{!}{=} 0 \tag{4.1}$$

$$\text{with } \left(g_{\alpha\beta}\right) = \begin{pmatrix} \mathbf{a}\cdot\mathbf{a} & \mathbf{a}\cdot\mathbf{b} \\ \mathbf{a}\cdot\mathbf{b} & \mathbf{b}\cdot\mathbf{b} \end{pmatrix}.$$

The Greek indices's denote the components of the vectors. The Latin indices's are the labels of the joints.

The additional symmetry relations will be substituted in 4.1:

$$(\mathbf{p}_i, 1) = S_{\{ij\}}\,(\mathbf{p}_j, 1) \quad S_{\{ij\}} = \begin{pmatrix} R_{\{ij\}} & \mathbf{t}_{\{ij\}} \\ \mathbf{0} & 1 \end{pmatrix} \qquad \Leftrightarrow \mathbf{p}_i = R_{\{ij\}}\mathbf{p}_j + \mathbf{t}_{\mathbf{\{ij\}}} \tag{4.2}$$

$S_{\{ij\}}$ is an augmented matrix $(D+1)\times(D+1)$ which has in general a rotational and translational part. These equations do not depend on the changing lattice, e.g. if a joint is related due to translational symmetry the corresponding equations is $\mathbf{p}_i = \mathbf{p}_j + (1,0)$.

The desired deformation magnitude δ, the strain in deformation direction which the user sets, has the following range:

- $-1 \leq \delta < 0 \Leftrightarrow$ contraction

  At $\delta = -1$ the unit cell is completely collapsed to a line, its length in the parallel direction is zero. A smaller value than -1 leads to expansion in the other direction.

- $\delta > 0 \Leftrightarrow$ expansion

This parameter will modify the lattice vectors in the following way (cf. sec. 2.5):

$$\mathbf{a} = (1+\delta) a_{\|} \mathbf{e}_{\|} + a_{\perp}(\delta)\, \mathbf{e}_{\perp} \tag{2.34}$$

$$\mathbf{b} = (1+\delta) b_{\|} \mathbf{e}_{\|} + b_{\perp}(\delta)\, \mathbf{e}_{\perp}. \tag{2.35}$$

$\mathbf{e}_{\|}$ which the user can choose, determines the deformation direction that means the given length of the rectangular which encloses the unit cell and is parallel to $\mathbf{e}_{\|}$.

The unknowns, are such components of the joints and lattice parameters which are not dependent or predefined due to symmetry:

$$p_{i_\alpha}(\delta) \quad \text{and} \quad a_{\perp}(\delta), b_{\perp}(\delta)$$

In the case of *p1*, the only dependent components of the joints are the one who belongs to the neighbouring cells and are related by translation.

4.2 Local Newton-Raphson-method

The general problem can be expressed as follows:

Find for a given function $\mathbf{f} = (f_1, \ldots, f_n) : \mathbb{R}^m \to \mathbb{R}^n$ a $\mathbf{x}^* = (x_1^*, ..., x_m^*) \in \mathbb{R}^m$, so that $f_1(x^*) = 0, \ldots, f_n(x^*) = 0$. $\mathbf{x}^*$ is a common root of all n equations. This multidimensional problem of finding zeros cannot be solved in general.

In our case the equations are the edge equations $f_{\{ij\}}$ (4.1) with an order of 2.

The Newton-Raphson-method [38, 44] is an iterative method which can find approximation of zeros of such systems if a sufficient good first guess of the desired root is known. The form of iterative methods is: beginning with the given start value x_0, successive approximates $x_i, i = 1, 2 \ldots$ to $\mathbf{x}^*$ are calculated with the aid of an iteration function Φ evaluating the prior value to gain a closer approximate: $x_{i+1} := \Phi(x_i)$ with $i = 0, 1, 2, \ldots$.

The idea beyond this method is the Taylor expansion. A differentiable function can be expressed by the Taylor series. In one dimension this is

$$f(x) = \sum_n \frac{f^{(n)}(x_0)}{n!} (x - x_0)^n. \tag{4.3}$$

If only x in the neighbourhood of x_0 are considered that means only small deviation ϵ of x_0, the higher orders will become smaller due to the higher power and can be neglected to get nonetheless a good approximation of the actual values of x:

$$f(x_0 + \epsilon) \approx f(x_0) + f'(x_0)\epsilon \qquad \left(+ \frac{f''(x_0)}{2} \epsilon^2 + \ldots \right). \tag{4.4}$$

So the root of the linearised (classical Newton) represents the next better approximate of x^*,

$$f(x_0 + \epsilon) = 0 \quad \Rightarrow x_1 = x_0 - \frac{f(x_0)}{f'(x_0)} \qquad \text{with } f'(x_0) \neq 0. \tag{4.5}$$

The iterative function of the one-dimensional Newton-Raphson is $\Phi(x) := x - \frac{f(x)}{f'(x)}$.

In the 1d case this procedure can be visualised as done in Fig. 4.1. Through the neglecting of higher orders the function is approximated by its tangent in the starting point. The root of the tangent is nearest to the actual root. Nevertheless it is not possible to determine

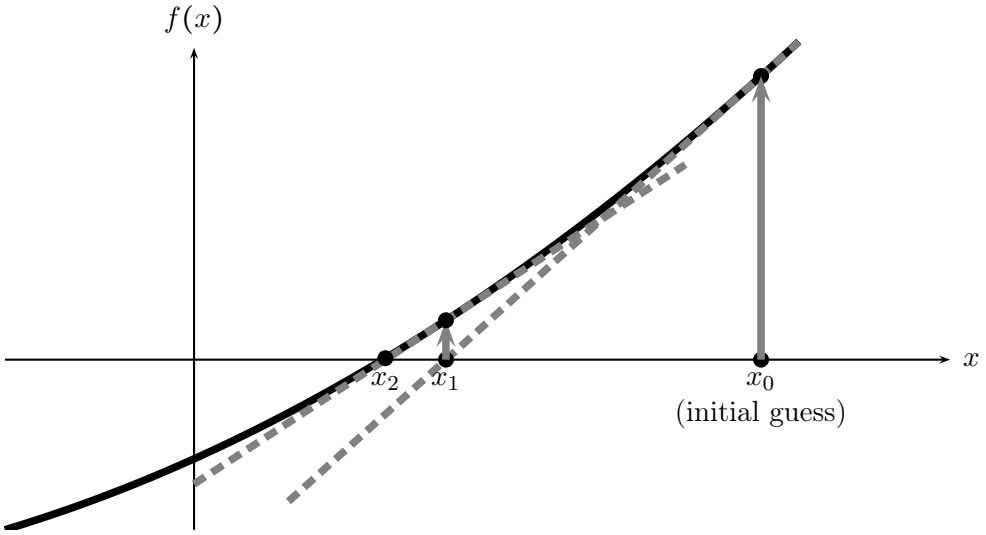

Figure 4.1: *1-d Newton-Raphson Method: root of the tangent is the next better approximate value*

the exact root in a finite number of steps. However the results are correct in sufficient decimals.

If the deformation is not too large, the deviation of the initial configuration is close to the new solution and can therefore be a good start value. However if the desired maximal deformation δ represents a large deformation the new configuration can considerably change. The initial configuration will not be longer a good guess for the root. Therefore the deformation will be divided in smaller but nevertheless finite steps (parameter: `max-step`), so that the Newton-Method can succeed.

Beside the advantage of the Newton-method, its rate of convergence, the method is not water-proof. It is not a global convergent method, hence it can fail if the initial point is not good enough. For example if the derivative is zero of the initial or a subsequent values the Newton method cannot improve the approximation (anymore).

In our case there are situations (kagome), where the initial configuration is indefinite. The method fails while the initial configuration is not modified by an addition of random numbers (starting value must be a saddle point or extrema, two equivalent paths are possible, symmetry around this point ⇒ must be local extrema).

Also if there are local extrema between the initial value and the searched root, newton method will converge again this local extrema.

A further problem appears at functions which have not the complete $\mathbb{R}$ as their domain of definition (e.g. *ln* with initial guess greater than 1). The zero of tangent can lie in the region, where the function is not defined. But that does not regard to our equations, because they are defined for all $\mathbf{p} \in \mathbb{P}$.

So far the presentation of the one dimensional case explains already some important aspects of the newton method: need of a good start value due to the lack of the global convergence, there some situations where the method fails, which can occur accordingly in the multidimensional case too.

The multidimensional Taylor expansion up to the first order can be written conveniently with the Jacobi-Matrix J,

$$\mathbf{f}(\mathbf{x} + \delta\mathbf{x}) \approx \mathbf{f}(\mathbf{x}) + J \cdot \delta\mathbf{x}. \tag{4.6}$$

As done in 1d case the system is considered in this approximation and its root determined,

$$\mathbf{f}(\mathbf{x} + \delta\mathbf{x}) = 0 \Leftrightarrow \mathbf{f}(\mathbf{x}) = -J \cdot \delta\mathbf{x}. \tag{4.7}$$

The equation (4.7) is a system of linear equations, whose solution space is defined by the rank of the matrix.

As discussed the skeletal structures can have a continuum of possible paths that means the system of edge equations must be under-determined in the context of limiting the joints. Different possible configurations are compatible with one deformation of the unit cell. That means the disturbed system of equations will have a continuum as solution space. Different Newton paths on the function manifold from the same starting point can lead to different admissible roots. This is not unique as in one 1d where concept of walking downhill is unique.

Hence the approximated linear system of equations will have degrees of freedom and so the matrix will be under-determined and have a continuum of solutions. All these different $\delta\mathbf{x}$ are reasonable steps to approximate different or maybe even the same roots.

Therefore the inverse of the Jacobi will surely not always exist.

In order to choose always a solution the pseudo inverse of the Jacobi through the singular value decomposition is calculated. That means the single steps of the Newton method are those with the smallest coordinate deviation.

We stress, other steps are also admissible ones and would also lead to approximation of perhaps an other point of the continuum of possible solution. The singular value decomposition excludes such paths.

4.3 Singular value decomposition

The cases of Jacobi matrices with a rank deficiency do not have a unique solution. the singular value decomposition can be used to select the one with the smallest modulus of $\delta\mathbf{x}$:

$$\delta\mathbf{x}_{\min} = \min\{|\delta\mathbf{x}| \mid J\delta\mathbf{x} = -\mathbf{f}(\mathbf{x})\}$$

.

Following mathematical formulation describes the decomposition and a prove can be found e.g. in [20]:

Singular Value Decomposition If A is a real $m \times n$ matrix, then there exist orthogonal matrices

$$U = [u_1, \ldots, u_m] \in \mathbb{R}^{m\times m} \quad und \quad V = [v_1, \ldots, v_m] \in \mathbb{R}^{n\times n}$$

such that

$$U^T AV = \operatorname{diag}(\sigma_1, \ldots, \sigma_p) \in \mathbb{R}^{m\times n} \qquad p = \min\{m, n\}$$

with $\sigma_1 \geq \sigma_2 \geq \cdots \geq \sigma_p \geq 0$ (singular values)

Hence every real matrix can be expressed through a product of three matrices, two orthogonal and one diagonal. The inverse of a matrix (pseudo inverse in the case of singular situations) is

$$A^{-1} = U \operatorname{diag}(\sigma_1, \ldots, \sigma_p)V^T,$$

which is also called the Moore-Penrose inverse.

The only thing that can go wrong with this construction is for one of the σ_i's to be zero, or (numerically) for it to be so small that its value is dominated by round-off error and therefore unknowable. If more than one of the σ_i's has this problem, then the matrix is even more singular. So, first of all, SVD gives you a clear diagnosis of the situation.

In the under-determined situation there will be some zeros and hence there exist a null-space of dimension greater than 0. However the SVD selects that solution with the smallest modulus and hence that with the smallest change in coordinates [38].

4.4 Numerical results in the case of the multidimensional solution space

The numerical method selects for each small deformation step the one with the smallest coordinate deviation due to solving with the singular value decomposition (see sect. 4.3). However this is not unique. Fig. 4.2 displays two different deformations of the same structure. The executed deformations differ in the reached configuration of the joints. This can be reached by modifying the start values of the Newton method by adding random numbers.

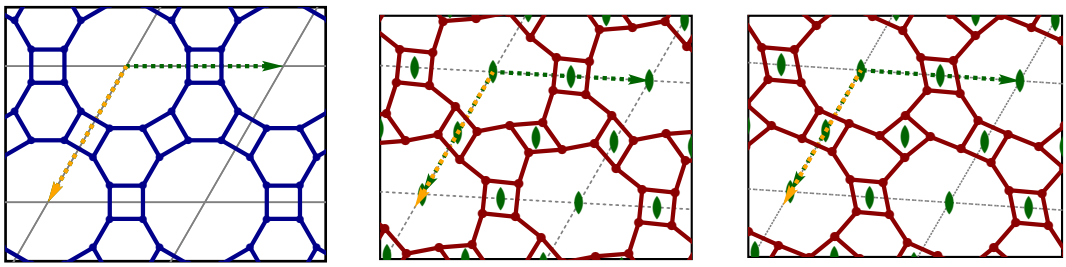

(a) $\delta = 0$ **(b)** $\delta = -0.1$ **(c)** $\delta = -0.1$

Figure 4.2: *Comparison of two deformation runs: the image (c) shows a run, where random numbers are added to the start value of the initial Newton step*

To measure Poisson's ratio an elongation of the lattice vectors is imposed in a given direction and let the orthogonal parts of the lattice vectors as variables which will be determined by the numerical method. If the joint configurations are different, we can check if the change of the orthogonal part is predetermined by the skeletal structure or is arbitrary. The orthogonal parts will be fixed and again the deforamtion on the parallel parts are imposed. So one Poisson's ratio for the structure cannot be given. See Fig. 4.3 where the orthogonal expansion differs at the same axial strain δ.

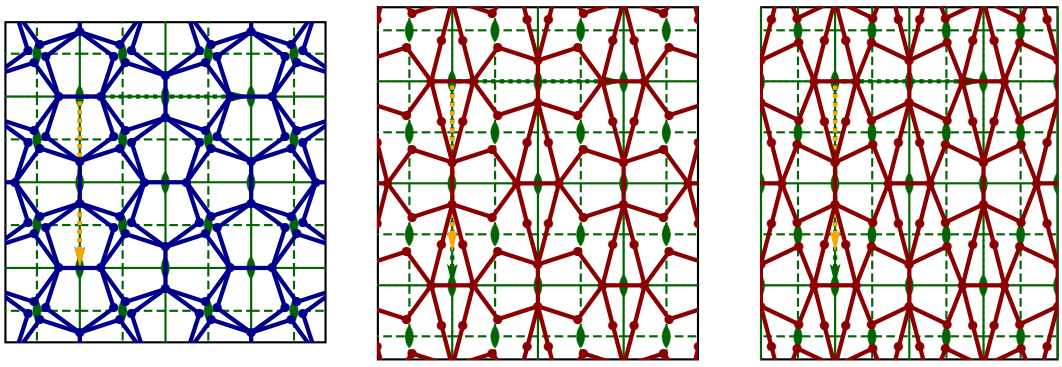

(a) *Original structure* **(b)** $b_\perp$ *is fixed.* **(c)** $b_\perp$ *is variable.*

Figure 4.3: *Comparison of two deformation runs: with and without fixation of* $b_\perp$*, the horizontal width differs between image (b) and (c).*

5 Common features of deformations with negative Poisson's ratio

The program to calculate deformations of skeletal structures developed in this thesis has been applied systematically to large classes of known tessellations, extracting in particular instantaneous and finite Poisson's ratios. The data obtained is compiled in chapter 6. By this systematic analysis we have identified a few common features of deformations of tessellations that are summarised in this chapter: Among the tessellations with auxetic behaviour there are two common mechanisms, *re-entrant* and *rotating substructures*. Numerous tessellations with hexagonal or square symmetry can be deformed in hexagonal or square symmetry embedding and then have Poisson's ratio -1, both for finite and infinitesimal deformation (Sect. 5.1). For two of these tessellations these mechanisms remain unique without symmetry constraints leading to as yet unknown auxetic skeletal structures (Sect. 5.3). Most tessellations become auxetic if a sufficiently large strain is applied (Sect. 5.2). For a number of tessellations the infinitesimal Poisson's ratio is infinity, however a finite deformation is well-defined.

Common auxetic behaviour The found auxetic deformation mechanisms can be categorised in two types:

1. skeletal structures with one or more elements in the unit cell that rotate, e.g. *star tiling IB* in $p4$ see Fig. 5.1.
2. re-entrant structures like the inverted honeycomb pattern, see Fig. 5.3

Non-affine deformations lead to auxetic behaviour. The re-entrant case occurs in the uniform tessellations only at finite deformations, because they consist only of convex polygons. Of course this regards not to the star tilings.

5.1 Deformations in square and hexagonal groups

Most considered tessellations that belong to hexagonal or square symmetry groups have unique deformations in the maximal hexagonal or square symmetry group, in which the tiling is not rigid. By constraining the deformation to maintaining hexagonal or square symmetry the Poisson ratio is fixed to -1 (cf. Sect. 3.6) and these structures are hence auxetic. While auxeticity is an imposed feature for these tessellations it is interesting to note that typically the deformation behaviour involves the rotation of some elements of the elements structure. It is also noteworthy that, upon sufficiently large deformations, these tilings often convert to other well-known tessellations.

An example for the rotating element is given by the "star tiling b" $(4.4^{*}_{\alpha}.4^{**}_{\alpha})$, see Fig. 5.1. Its highest possible symmetry group $p4$ is retained during the deformation, hence. By stretching it to its maximum, the star tiling becomes the Archimedean Truncated Square

tiling (cf. Fig. 5.3). During the deformation, the square elements of the tessellation rotate around the four-fold rotation sites, retaining their square shape because of the imposed symmetry *p4*. Deformations of this tessellation in lower symmetry groups are not unique.

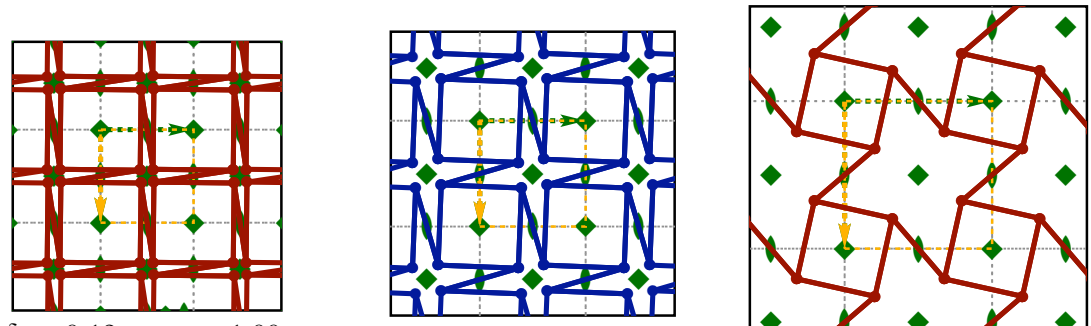

Figure 5.1: *Deformation of the "star tiling b" under the constraint that its symmetry group* p4 *is fully retained. The central image shows the initial tiling with its joints and bars in blue, symmetry elements in green and the deformation direction in orange, the underlying grid as dotted gray points. The left image is the contracted and the right the elongated one. Deformed skeletal structures are printed in red. When stretched to its maximal value* $\delta = 0.831$ *it becomes the* truncated square tiling *(cf. Fig. 5.3). The maximal contraction before bars collapse onto each other is* $\delta = -0.25$.

Similarly rotating elements are observed in the "2-uniform tiling 11" $(3^3.4^2;3.4.6.4)$, with two elements that rotate in opposite directions. The deformation in spacegroup *p6* is shown in Fig. 5.2. The rotating elements are on the one hand the hexagons centered around the 6-fold site symmetry at the corners of the unit cell and on the other hand triangle's consisting of 4 smaller triangles located at 3-fold site symmetry. Deformations of this tessellation in a lower symmetry group is shown in sect. 6.3.14 which show a re-entrant behaviour from $\delta = -0.1$.

At $\delta = -0.3$ the squares are fully collapsed. Due to the collapsed and so disappeared squares the picture is identically to the rigid Archimedean snub hexagonal tiling (6.6.2). In this symmetry group (*p6*) "2-uniform tiling 11" cannot be expanded.

There are four uniform tessellations that are rigid in hexagonal or square symmetry group embedding but are flexible in lower rectangular or oblique groups. These are the Archimedean tilings, square, hexagonal and snub square (cf. Tables 6.3, 6.4) and the 2-uniform tiling 9 (cf. Table 6.6).

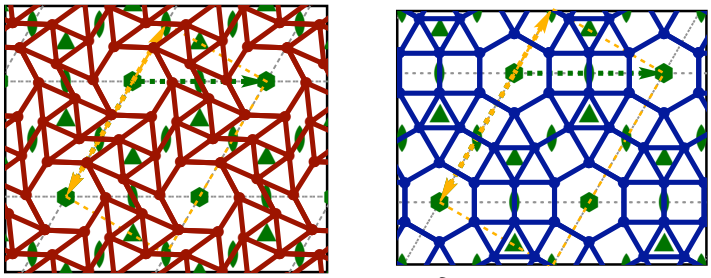

Figure 5.2: *Deformation of 2-uniform tiling* $(3^3.4^2;3.4.6.4)$ *in* p6. *Under this constraint the tiling is only deformable. The hexagonal elements at the* 6*–fold sites rotate in alternating direction as the compound triangular of 4 smaller triangles at the* 3*–fold sites.*

5.2 Auxetic behaviour in finite deformations

All uniform tessellations are composed of regular polygons. They are convex, hence there are not any re-entrant elements. Nevertheless many of them become auxetic when the applied strain δ is sufficiently large. Re-entrant elements then emerge. To ensure unique mechanisms at large strain, symmetry constraints are usually necessary. This relatively common auxetic behaviour at large strains provides is not often discussed, as analyses are often restricted to infinitesimal or small strains.

The "Archimedean Truncated Square tiling" belongs to this case. The deformation in symmetry group $p21m_r$ is shown in Fig. 5.3. The left image of Fig. 5.3 shows the deformed tiling for a sufficiently large value of δ such that re-entrant cells have formed. The Poisson ratio as function of δ is shown in Fig. 5.4. The value of $\delta = -0.4$ for which $\nu(\delta) = 0$ corresponds exactly to the transition from a structure with to a structure without re-entrant cells. The symmetry group $p21m_r$ does not permit rotation of any of the elements.

The deformation behaviour of the "Archimedean Truncated Square tiling" depends on the retained symmetries. It has three different unique deformation modes dependent in which symmetry group it is embedded. In the *p4* it is infinitesimally auxetic and corresponds to the shown star tiling b of the previous section (5.1). The unique deformation in *p2mm* is not auxetic for any degree of deformation.

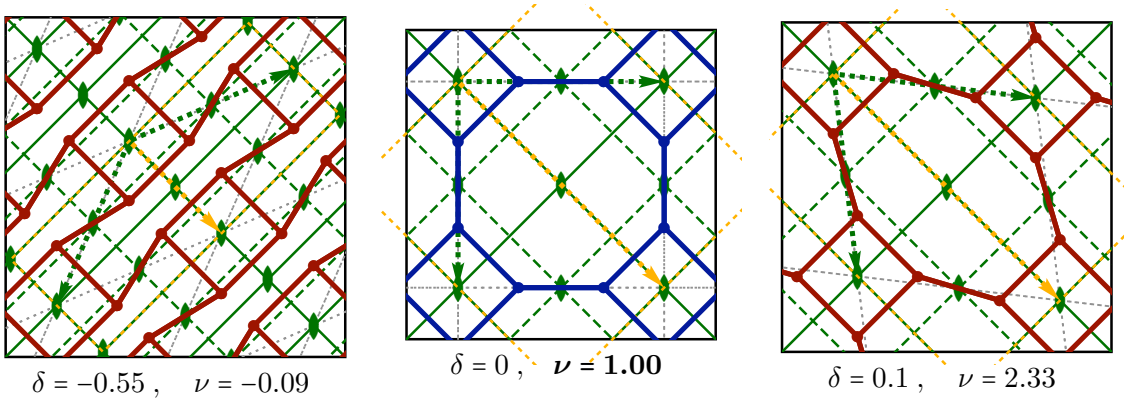

Figure 5.3: *Deformation of the Truncated Square Tiling.*

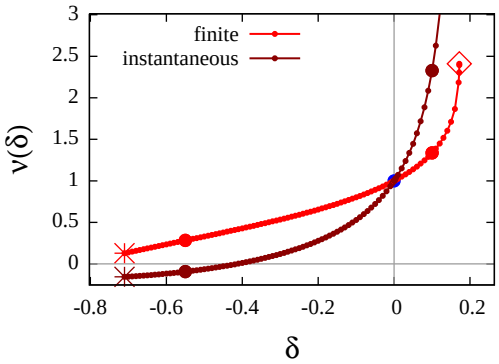

Figure 5.4: *Poisson's ratio of the Truncated Square Tiling*

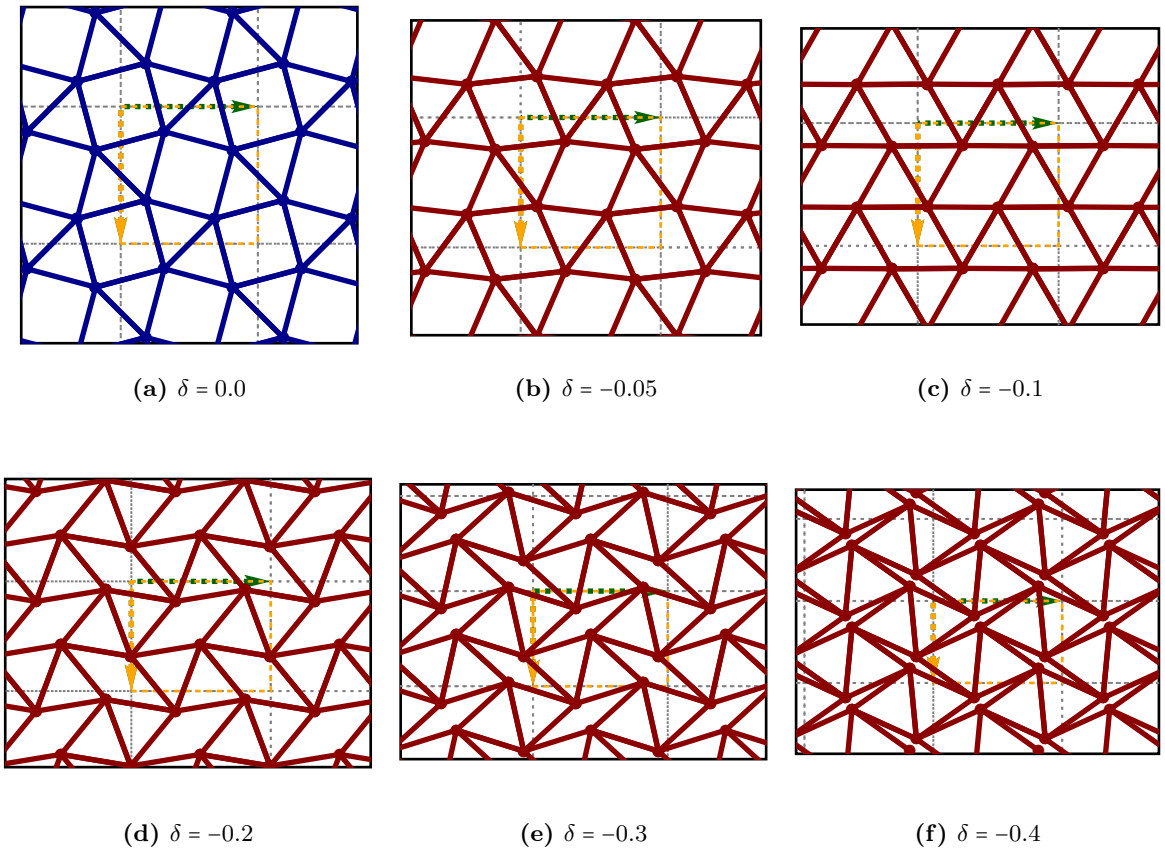

(a) $\delta = 0.0$ **(b)** $\delta = -0.05$ **(c)** $\delta = -0.1$

(d) $\delta = -0.2$ **(e)** $\delta = -0.3$ **(f)** $\delta = -0.4$

Figure 5.5: *Deformation of the snub square tiling in group p*1

The snub square tiling, $(3^2.4.3.4)$, is not infinitesimally auxetic. It does not have any re-entrant elements as it consists only of squares and triangles. However the skeletal structure becomes auxetic if the imposed contraction is smaller than −0.1. This auxetic behaviour is due to rotating elements. These are the triangulated rhombi, as shown in Fig. 5.5.

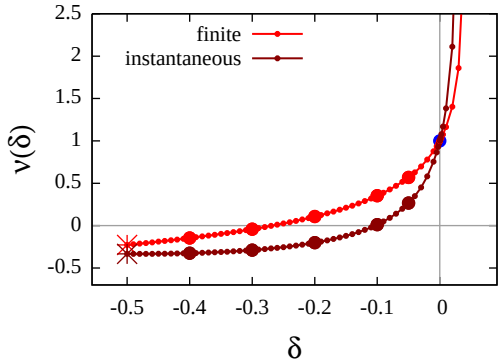

Figure 5.6: *Poisson's ratio of the snub square tiling in* p1. *The maximal contraction is given by* $\delta = -0.5$ *the edges of the squares collapse. A greater contraction would only be possible when allowing overlap of the joints. The maximal stretching is given by* $\delta = -0.5$ *when the squares collapses. The value of* $\delta \approx -0.1$ *when* $\nu(\delta)$ *becomes negative corresponds to Fig. 5.5c.*

5.3 Auxetic skeletal structures with unique mechanisms without symmetry constraints

Among the considered uniform tessellations there are four tessellations that have a unique deformation in *p1*, i.e. no symmetry constraints except for periodicity, and that are auxetic. This number reduces to three as the star tiling d and the Archimedean kagome tiling represent the same structure at different states of the deformation. The kagome tiling has already been suggested as an example of an auxetic structure [21, 22], see 6.2.17 and 6.4.4. The remaining "2-uniform tessellation" 7, denoted in the vertex notation as $(3^6;3^2.6^2)$ and "2-uniform tessellation" 5 $(3^6;3^2.4.3.4)$ have been identified as infinitesimally auxetic in this thesis.

The 2-uniform tiling 7 is the unique version of the star tiling c. That means they both have the same deformation behaviour, however additional symmetry constraints are necessary for the star tiling c to reach this unique behaviour (cf. 6.4.3). Also the 2-uniform tilign 5 is a unique version of a different tiling, the small rhombitrihexagonal tiling (6.2.18). The deformation consists of the same rotating elements, hexagons centered in the corners of the unit cell which is retained due to triangulation in the 2-uniform tiling and in the star tiling c by the 6-fold symmetry at the lattice points.

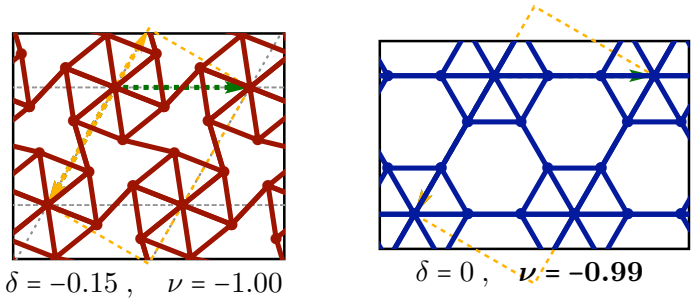

Figure 5.7: *Deformation of the 2-uniform 7 tiling: it can only be compressed, but is unique in* p1 *and has a constant negative Poisson's ratio of* -1. *The skeletal structure itself retains the symmetries of group* p6 *which is line with the constant Poisson's ratio.*

The "2-uniform tessellation 5", $(3^6;3^2.4.3.4)$ has a unique auxetic deformation mechanism that has not been published and that is not an analogue of a previously published case. Figure 5.8 shows its deformation. During the deformation some elements rotate. In the corners of the unit cell there are triangulated hexagons which rotate. The Poisson's ratio in $p1$ is found to be -1 for all values of δ (note that it is not a priori constraint to this value). The tessellation is also not rigid in hexagonal or square embeddings and has the same deformation mechanism in this groups as in $p1$, cf. Table 6.3.

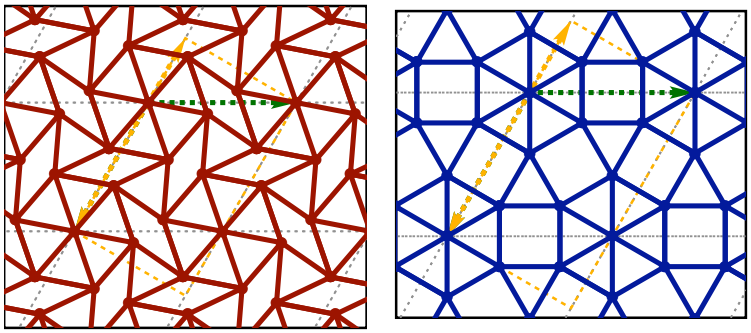

Figure 5.8: *2-uniform 5* $(3^6;3^2.4.3.4)$*: unique auxetic deformation in* p1 *with a constant Poisson's ratio of* -1

6 Systematic deformation analysis of tessellations

The deformation behaviour is systematically analysed for a large number of known tessellations, motivated by the search for yet unknown auxetic mechanisms. For each tessellation, and for each of the possible symmetry groups in which it can be embedded, the finite and instantaneous Poisson's ratio are shown as function of the strain δ. The infinitesimal Poisson's ratios are tabulated for all tessellations and all symmetry groups in Tables 6.2 to 6.9. Specifically, our analysis includes all 11 Archimedean tilings (sect. 6.2), all 20 2-uniform tilings (sect. 6.3), 21 uniform tilings of the plane by star polygons (sections 6.4 and 6.5), and 3 other tilings of general interest (sect. 6.1). Except for a few notable exceptions, the analysis is restricted to strain directions corresponding to translation vectors.

As detailed in the previous chapters, the deformation behaviour of the tessellations depends on the strain direction and on the symmetries that are retained during the deformation. Depending especially on the embedding symmetry group, a given tessellation may be rigid or have a unique deformation or ambiguous deformation modes, see the Tables 6.2 to 6.9. For the purpose of this thesis the Poisson's ratio is only well-defined for unique deformations.

The Poisson's ratio of a skeletal structure depends in general on the embedding symmetry group. In particular all tessellations with square or hexagonal symmetry are either rigid or have a Poisson's ratio of -1 (for hexagonal or square structures with ambiguous deformations all deformations yield the same value -1), see also section 3.6. Among the 52 uniform tessellations analysed in this chapter, 34 are not rigid when embedded in a hexagonal or square symmetry group and hence have a negative Poisson's ratio -1, independent of the degree of strain applied (this includes 5 of the 11 Archimedean tilings. While the constraint imposed by the high symmetry groups is substantial, it demonstrates the strong influence that symmetry has on deformation behaviour.

The finite deformation modes lead to a Poisson's ratio which depends on the magnitude of deformation. Therefore the data presented in this chapter includes both an instantaneous Poisson's ratio (i.e. the Poisson's ratio observed for a structure that has already been deformed by a strain δ if a further infinitesimal strain is applied) and the finite Poisson's ratio (i.e. the difference between undeformed tessellation and the tessellation at strain δ). Again, also this finite deformation behaviour is dependent on the symmetries retained during the deformation, see e.g. truncated square tiling 6.2.10 ($p4mm$), 6.2.11 (pm_r), 6.2.12 ($p2mm$).

For many of the analysed tessellations and in many of the possible symmetry embeddings there is a threshold for the strain δ above which the deformation becomes auxetic, see for example the truncated square tiling in the symmetry group pm_r 6.2.11. Out of the *five* tessellations that have unique deformations in rectangular or oblique space groups (i.e. those without an a priori constraint on ν) there are *two* tessellations that become auxetic at finite strain. For *two* out of these, this behaviour persists in the case of pure

translational periodicity without further symmetries. This further supports the claim that auxetic mechanisms are a common feature of symmetric and periodic tessellations, especially when applying finite strains.

The deformations analysed contain 2 tessellations that are auxetic at infinitesimal deformation without any symmetry constraints and that had not been identified as such, see 2-uniform 5 and 7 (6.3.6, 6.2.17). These are presented alongside one other known infinitesimally auxetic uniform tessellations (6.4.4).

Finally we describe 8 tessellations for which the infinitesimal Poisson's ratio is infinite, as $\nu(\delta)$ diverges for small strains δ, see Archimedean tilings: square and elongated triangular. However for finite δ the deformation behaviour is finite, demonstrating that the numerical approach of analysing finite deformations reveals some insight that the infinitesimal treatment by rigidity theory lacks.

Presentation of data

Tabulated characteristics of infinitesimal deformations

Tables 6.2 to 6.9 show the numerical results for the infinitesimal deformations of symmetric tessellations, sorted by tessellation type. The purpose of the tables is to list the infinitesimal Poisson's ratio of the considered structures in their different t-subgroups.

The first column specifies the name of the skeletal structure and its (highest possible) symmetry group embedding. Additional the main deformation characteristic is given. Either a tiling is rigid or not, the provided deformation mechanism is unique without symmetry constraints or becomes unique under symmetries or is in all settings not unique. The following 17 columns correspond to the 17 plane groups; if the skeletal structure can be embedded in a symmetry group, the deformation results in that symmetry group are given. The nomenclature of these tables is summarised in Tab. 6.1. The symmetry group names refer to those in [26].

A detail regarding 10 of 17 groups requires special attention: [26] suggests for each group a specific unit cell and its orientation in respect to the symmetry elements, i.e. both lattice vectors are given and the symmetry relations in the basis of these. Through the reduction of symmetries subgroups are generated from the initial group. The lattice vectors and hence the basis are not changed. But the new subgroups with the original basis are not necessary in the suggested setting. Hence the data of the tables are not usable as given. For instance the original group has a primitive cell but has a subgroup which has a suggested setting with a centered cell. If such a difference occur this is denoted with an index of an integer number referring to the appendix where all such cases are listed for the t-subgroups. Especially this info is helpful to know which deformation direction is used without giving the initial group.

There are groups which have t-subgroups which can be differently embedded into the structure. That means there are equal symmetry elements but oriented in different directions. If this aren't symmetric equivalent orientations due to symmetry, these isomorphic cases will also be considered. Hence there are tabulated beside the two values for **a**, **b** direction, values for the different embeddings of the symmetry group (c.f. *p2mm* as discussed in 3.4)

An in-depth analysis of the direction dependence of deformation behaviour is important but beyond the scope of this thesis (although numerically easily feasible with the implemented program). Except for a few exceptions, values for the deformations are only given for the two lattice vector directions **a** and **b**. Exceptions are made for some auxetic structures or for skeletal structure that are rigid w.r.t. deformations in **a** or **b** but not rigid in other directions. A list of totally rigid tilings is given in section 6.6.

Table 6.1: *List of used symbols in the tables of the infinitesimal Poisson's ratios. X is a placeholder for a number or a letter.*

-	:	The tiling does not have these symmetries or cannot be embedded in this group without change of the translational periodicity.
<number>	:	The infinitesimal Poisson's ratio $\nu(\delta \to 0)$ is given explicitly if the tiling has a unique deformation mode.
R	:	The tessellation cannot be deformed in this group. It is rigid.
U	:	The deformation of the tiling is not unique, i.e. the skeletal structure and symmetry group does not determine the deformation mode. Therefore no Poisson's ratio can be given.
N	:	The infinitesimal Poisson's ratio is discontinuous at $\delta = 0$. The left infinitesimal Poisson's ratio differs from the right.
∞	:	The Poisson's ratio diverges for $\delta \to 0$.
$X^{\ddagger}$	:	This regards to two situations. First tessellations with rotating elements which can rotate in two directions but else the deformation is unique (e.g. *trihexagonal tiling* 6.2.17). Second structures which shear have often two directions for the shear (e.g. *square tiling* 6.2.1 or *2-uniform 8* 6.3.11).
$X^{\downarrow}$	:	The skeletal structure can only be compressed, not elongated.
$X^{x^{\circ}}$	:	The deformation direction in respect to $\mathbf{a}\,(\delta = 0)$
$X_{\text{<integer>}}$	:	The chosen basis of the subgroup differs to the conventional one (unchanged basis of the original group). In the appendix are listed such representations of groups.
$\underline{X}$	:	The results of the finite deformation in this setting are shown in one of the sections listed in the first chapter.

Presentation of finite deformations

In contrast to rigidity theory the numerical approach demonstrated in this thesis allows the analysis of deformations with finite strain. Our analysis of such finite deformations of symmetric tessellations demonstrates that auxetic behaviour is relatively common. It also shows some less obvious deformation pathways between several structures.

All tilings are characterised by their symmetry group, which contains all symmetries which a tiling possesses. This is at least the periodicity which asks for periodic boundary conditions. This is retained in all cases. In addition a tiling can have symmetries like (glide) mirror lines and point symmetries. The deformation of a tiling is dependent on the direction and the retained symmetry group. This is called a deformation setting. But there are cases where the retaining of different groups lead to the same mechanism. Then only one of them is displayed (e.g. inverted honeycomb pattern in the groups $c2mm, c11m, cm$).

For each deformation setting of a structure the results are printed in one block on a half-page. This block consists of a title line with the name of the tiling and the deformation direction. The second line gives alternative names or a mathematical expression like the vertex notation which describes the tiling uniquely. Furthermore the symmetry group as well as the group which is retained under the deformation. Under them there are shown three images. The middle of them is the initial structure. The left is a deformed one with $\delta < 0$ and the right one consequently with $\delta > 0$. Instantaneous and the Poisson's ratio in relation to the initial configuration are plotted. Furthermore some information about the structure which determines the degrees of freedom are given. As an example the results of the re-entrant honeycomb pattern is shown below. The listing 1 describes the details of all given informations.

Re-entrant Honeycomb

→ 90°

Inverted Honeycomb | $c2mm$ (rectangular)

$c11m$ (rectangular)

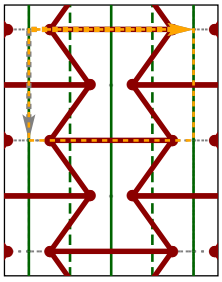

$\delta = -0.10$, $\nu = -1.06$

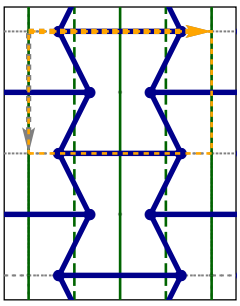

$\delta = 0$, $\boldsymbol{\nu = -0.75}$

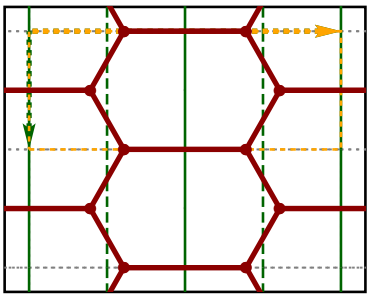

$\delta = 0.7$, $\nu = 1.48$

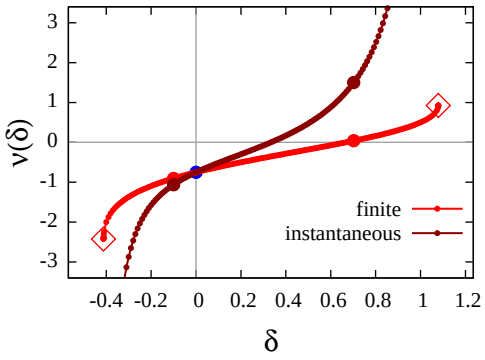

B: tuc | cross	:	6 | 2
N: tuc | neigb. | tot	:	$1 \times 4\, b(1)$ | 4 $\sum = 8$
Free|Dep.|Fix $p^i_{x,y}$	:	1 | 14 | 1 $\sum = 16$
Set|Free|Dep.|Fix	:	$a^{\parallel}, b^{\parallel}$ | $a^{\perp}$ | $b^{\perp} = -\frac{a^{\parallel} b^{\parallel}}{a^{\perp}}$ | none
$\langle \frac{B}{N} \rangle$	:	3.00
$Z_{Maxwell}$	:	3
Reference(s)	:	[1], [19] p.63

Infinitesimally **auxetic**

Listing 1 Explanation for the presented information of the results of the finite deformations

Name of tiling

Alternative term | **group** of tiling (lattice type)

Deformation direction related to a_0
retained (sub)group

snapshot of deformed tiling with $\boldsymbol{\delta < 0}$	clipping of initial tiling ($\boldsymbol{\delta = 0}$)	snapshot of deformed tiling with $\boldsymbol{\delta > 0}$

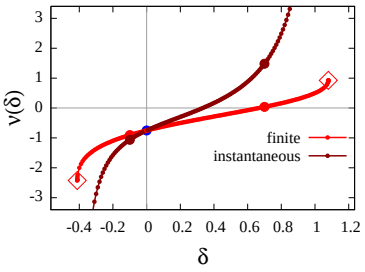

The plot on the left shows the finite as well as the instantaneous Poisson's ratio as a function of the deformation magnitude $\boldsymbol{\delta}$. The explicit definitions of the two Poisson's ratio are given in section 2.5. Negative values of the instantaneous Poisson's ratio represent regions, where the mechanism is auxetic.
The plot stops at the maximal deformation marked by a diamond symbol ◇. There are situations which lead to an overlap of joints and bars. In this cases the deformation is stopped indicated by a star ✳.

The list on the right of the plot gives details regarding to the degrees of freedom which the tiling possesses due to the skeletal structure and the retained symmetries.

$\boldsymbol{B}$**: tuc**	:	Number of bars in the unit cell. Bars that connect points within the unit cell to points in adjacent unit cell count as $\frac{1}{2}$.
$\boldsymbol{B}$**: cross**	:	Half the number of bars which crosses the border of the unit cell. They ensure the periodic boundary conditions.
$\boldsymbol{N}$**: tuc**	:	Number of joints in the unit cell: number of occupied Wyckoff positions with their corresponding multiplicity and type of site symmetry. These numbers determine the degree of freedoms beside the rigid bars.
$\boldsymbol{N}$**: neighbour**	:	Number of joints in the neighbouring unit cells, which are linked with a bar to the unit cell
$\boldsymbol{N}$**: total**	:	The total number of considered joints. This is just the sum of the two prior values.
Free $\mathrm{p}^{i}_{x,y}$	:	The actual number of free components of the joints. It may be an odd number because of fixation on mirror lines.
Depend. $\mathrm{p}^{i}_{x,y}$	:	Number of joints whose location is fully determined by symmetry or periodicity.
Fixed $\mathrm{p}^{i}_{x,y}$	:	The skeletal structure is kept fixed relative to the symmetry scaffold. The groups ***pm***, ***pg***, ***cm*** and ***p1*** allow a trivial translation which can be avoided by fixing additional components.
Lattice vector components:		
Set	:	As explained in sect. 2.5 the parallel parts of the lattice vectors are imposed deformed $\boldsymbol{a_{\parallel} \to (1+\delta) a_{\parallel}}$. This entry is always equal.
Free	:	This entry indicates whether both, one or none of the orthogonal parts of the lattice vectors are free.
Depend.	:	Due to symmetry orthogonal parts can depedent on the parallel parts. This entry shows this dependency.
Fixed	:	The user has the possibility to fix if possible one orthogonal component of the lattice vectors.
$\langle \frac{B}{N} \rangle$	:	Average coordinate number of the joints. Coordinate number is the number of bars emanating form the joint (sect. 2.2)
$\mathbf{Z_{Maxwell}}$	:	Maxwell number $\boldsymbol{Z = 2 \cdot N_{\mathrm{in}} + 1 - B}$ (sect. 2.4)
Reference(s)	:	Publications which present this structure and in some cases have already suggested it as a model for auxetic behaviour.

Table 6.2: *Infinitesimal deformation behaviour of periodic tessellations, see Table 6.1 for explanation of symbols*

Group	**p6mm**	**p6**	**p31m**	**p3m1**	**p3**	**p4gm**	**p4mm**	**p4**
Lattice type	hexagonal					square		
Re-entrant Honeycomb (c2mm) **1 sym. mode:** 6.1.2, 6.1.1	-	-	-	-	-	-	-	-
Re-entrant Rhombs (pm) **unqiue:** 6.1.4, 6.1.3	-	-	-	-	-	-	-	-
Swastika (p4) **1 sym. mode:** 6.1.5	-	-	-	-	-	-	-	**–1**

6.1 Periodic tilings

The set of tilings, denoted *periodic tilings*, contains three tilings, which have known auxetic mechanisms. The results for infinitesimal small deformations are listed in Table 6.2.

In the introduction the honeycomb pattern as a possible auxetic mechanism has been presented. The regular case belongs to the Archimedean tilings where the reentrant case can be achieved by a finite symmetric deformation. But here will be considered a pattern 6-gons, with two different length of the edges. Top and bottom edge length is double as along as the four side edges, see 6.1.1. As initial configuration the reentrant case is chosen. It provides one unique deformation mechanism in the groups $c2mm, cm$ and $c11m$. In order to compare this with the complete regular one (*hexagonal tiling* in 6.2.3) a finite deformation is imposed to that state where all angles are equal 120°. The instantaneous Poisson's ratio of the non-regular differs to the regular infinitesimal Poisson's ratio. This supports the assumption that deformation properties are dependent on the geometry.

The second considered tiling is a pattern build up by folded rhombi, also denoted as inverted rhombi like in the honeycomb case. This skeletal structure have exactly one degree of freedom which retains the mirror lines and hence is deformable also in *pm* 6.1.4. This periodic tiling represents the auxetic skeletal structure with the smallest number of bars in the unit cell which provide a unique deformation mechanism without symmetry constraints.

The last one in this set is a suggested model for the explanation of an auxetic foam. A foam of a conventional diamond-shaped honeycomb model is during a compression and heating process modified so that ribs are broken. This auxetic foam is idealised described as a pattern of swastika [23]. The mechanism of the pattern of swastika represents a typical detected auxetic mechanism in the uniform tilings, where rigid elements rotate (cf. e.g. *truncated square tiling* in group *p*4 (6.2.10), 2-Uniform 16 $(3.4.3.12; 3.12^2)$ in group *p*4 (6.3.21)). Similar behaviour can be found in many hexagonal cases (e.g. *truncated hexagonal tiling* 6.2.13).

Table 6.2: *Infinitesimal deformation behaviour of periodic tessellations, see Table 6.1 for explanation of symbols*

c2mm	p2gg	p2mg	p2mm	cm	pg	pm	p2	p1
rectangular (or rhombus in specific subgroups)							oblique	
−1.33$^{0°}$ **−0.75**$^{90°}$	-	-	-	**−1.33**$^{0°}$, **−1.33**$^{0°}_{25}$ **−0.75**$^{90°}$, **−0.75**$^{90°}_{25}$	-	-	U_{19}	U_{18}
-	-	-	-	-	-	**−3.2** $^{0°}$ **−0.31** $^{90°}$	-	**−3.2** $^{0°}$ **−0.31** $^{90°}$
-	-	-	-	-	-	-	U	U

6.1.1 Re-entrant Honeycomb

→ 90°

Inverted Honeycomb | *c2mm* (rectangular)

c11m (rectangular)

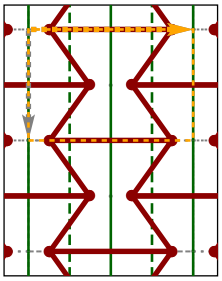

$\delta = -0.10$, $\nu = -1.06$

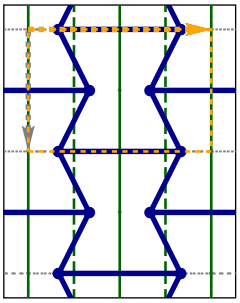

$\delta = 0$, $\boldsymbol{\nu = -0.75}$

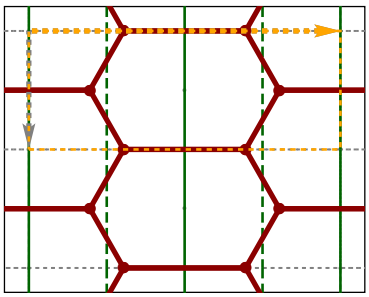

$\delta = 0.7$, $\nu = 1.50$

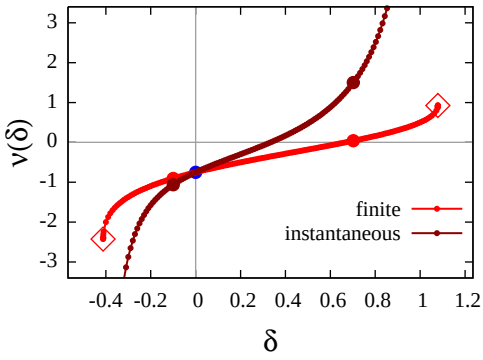

***B*: tuc | cross**	:	6 | 2
***N*: tuc | neigb. | tot**	:	$1 \times 4\, b(1)$ | 4 $\sum = 8$
Free|Dep.|Fix $p^i_{x,y}$	:	1 | 14 | 1 $\sum = 16$
Set|Free|Dep.|Fix	:	$a^{\parallel}, b^{\parallel}$ | $a^{\perp}$ | $b^{\perp} = -\frac{a^{\parallel} b^{\parallel}}{a^{\perp}}$ | none
$\langle \frac{B}{N} \rangle$	:	3.00
$\mathbf{Z}_{\mathbf{Maxwell}}$	:	3
Reference(s)	:	[1], [19] p.63

Infinitesimally **auxetic**

6.1.2 Re-entrant Honeycomb

↓ 0°

Inverted Honeycomb | *c2mm* (rectangular)

***c*11*m* (rectangular)**

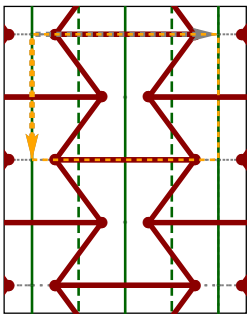

$\delta = -0.10$, $\nu = -0.91$

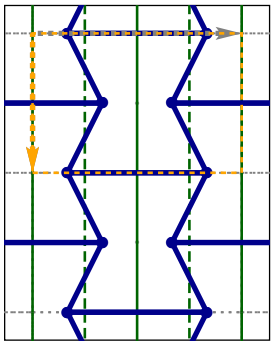

$\delta = 0$, $\boldsymbol{\nu = -1.33}$

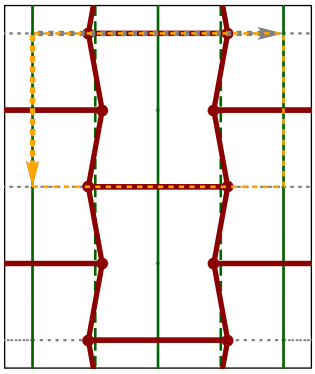

$\delta = 0.1$, $\nu = -3.36$

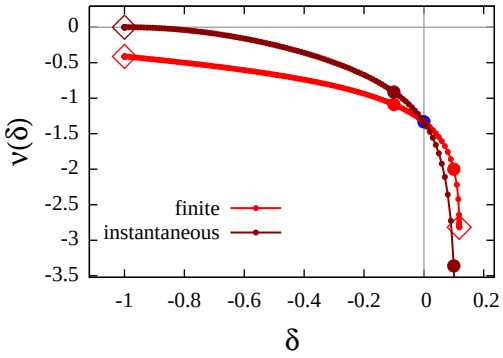

***B*: tuc | cross**	:	6 | 2
***N*: tuc | neigb. | tot**	:	$1 \times 4\, b(1)$ | 4 $\sum = 8$
Free|Dep.|Fix $\mathrm{p}^i_{x,y}$	:	1 | 14 | 1 $\sum = 16$
Set|Free|Dep.|Fix	:	$a^{\parallel}, b^{\parallel}$ | $b^{\perp}$ | $a^{\perp} = -\frac{a^{\parallel} b^{\parallel}}{b^{\perp}}$ | none
$\langle \frac{B}{N} \rangle$	:	3.00
$\mathbf{Z}_{\mathbf{Maxwell}}$	:	3
Reference(s)	:	[1], [19] p.63

Infinitesimally **auxetic**

6.1.3 Kites

↓ 0°

Re-entrant Rhombs | *pm* (rectangular)

***p*1 (oblique)**

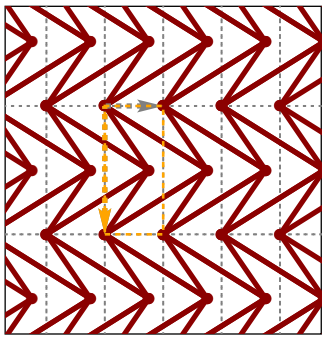

$\delta = -0.15$, $\nu = -0.91$

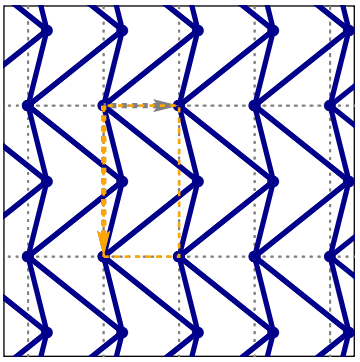

$\delta = 0$, $\boldsymbol{\nu = -3.20}$

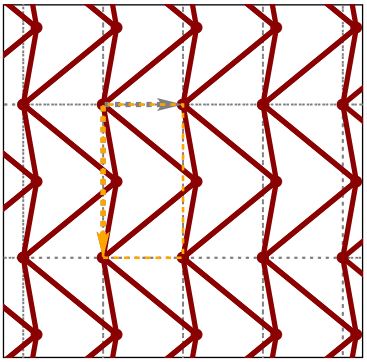

$\delta = 0.015$, $\nu = -4.63$

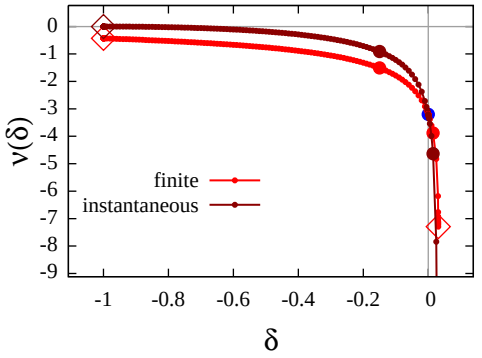

***B*: tuc | cross**	:	4 | 2
***N*: tuc | neigb. | tot**	:	$2 \times 1\, a(1)$ | 4 $\sum = 6$
Free|Dep.|Fix $\mathrm{p}^i_{x,y}$	:	2 | 8 | 2 $\sum = 12$
Set|Free|Dep.|Fix	:	$a^{\parallel}, b^{\parallel}$ | $a^{\perp}, b^{\perp}$|none|none
$\langle \frac{B}{N} \rangle$	:	4.00
$\mathbf{Z}_{\mathbf{Maxwell}}$	:	1
Reference(s)	:	[35] p.3, Fig. 1.1

Infinitesimally **auxetic**

6.1.4 Kites

→ 90°
***p*1 (oblique)**

Re-entrant Rhombs | *pm* (rectangular)

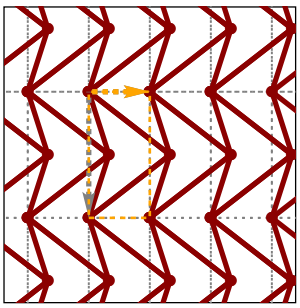

$\delta = -0.05$, $\nu = -0.41$

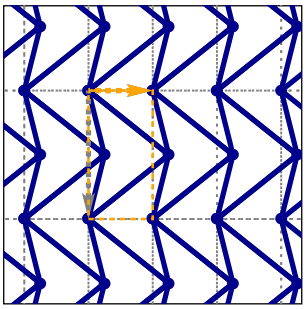

$\delta = 0$, $\boldsymbol{\nu = -0.31}$

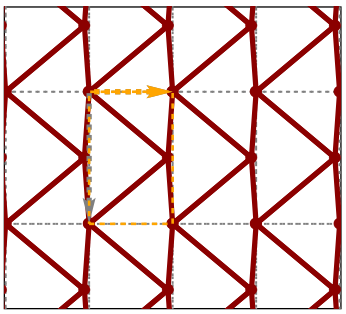

$\delta = 0.3$, $\nu = 0.08$

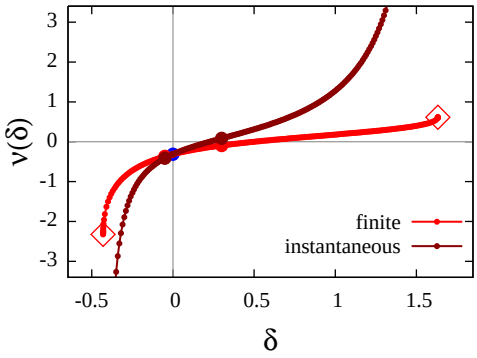

***B*: tuc | cross**	:	4 | 2
***N*: tuc | neigb. | tot**	:	$2 \times 1\, a(1)$ | 4 $\sum = 6$
Free|Dep.|Fix $\mathrm{p}^i_{x,y}$	:	2 | 8 | 2 $\sum = 12$
Set|Free|Dep.|Fix	:	$a^{\parallel}, b^{\parallel}$ | $a^{\perp}, b^{\perp}$|none|none
$\langle \frac{B}{N} \rangle$	:	4.00
$\mathbf{Z}_{\mathrm{Maxwell}}$	:	1
Reference(s)	:	[35] p.3, Fig. 1.1

Infinitesimally **auxetic**

6.1.5 Swastika

↓ 0°
***p*4 (square)**

*p*4 (square)

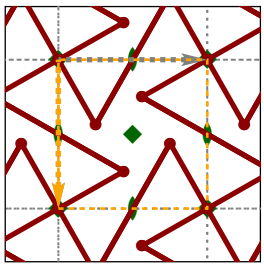

$\delta = -0.30$, $\nu = -1.00$

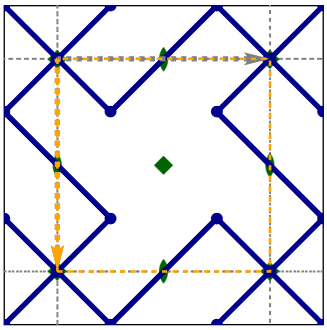

$\delta = 0$, $\boldsymbol{\nu = -1.00}$

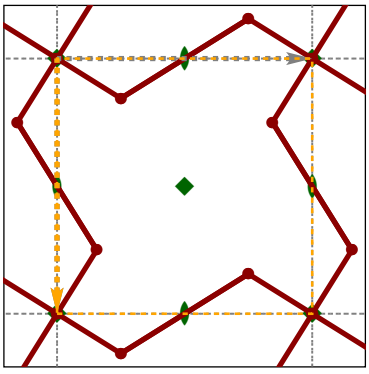

$\delta = 0.2$, $\nu = -1.00$

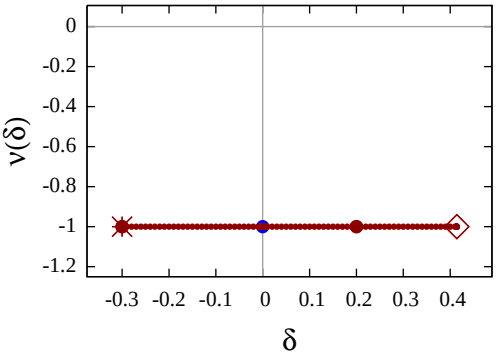

***B*: tuc | cross**	:	6 | 2
***N*: tuc | neigb. | tot**	:	$1 \times 4\, d(1), 1 \times 1\, a(4..)$ | 7 $\sum = 12$
Free|Dep.|Fix $\mathrm{p}^i_{x,y}$	:	2 | 22 | 0 $\sum = 24$
Set|Free|Dep.|Fix	:	$a^{\parallel}, b^{\parallel}$ | none | $a^{\perp} = -b^{\parallel}$, $b^{\perp} = a^{\parallel}$ | N.A.
$\langle \frac{B}{N} \rangle$	:	2.40
$\mathbf{Z}_{\mathrm{Maxwell}}$	:	5
Reference(s)	:	[23], [43]

Auxetic

6.2 Archimedean tilings

The *Archimedean tilings* are 11 plane periodic tessellations which have regular polygons as tiles and have one vertex type. They are also called *1-uniform tilings* due to the property of isogonality (cf. Sect. 3.1 and [24]).

Two of the Archimedean tilings are completely rigid because of columns and rows of triangle's which are themselves obviously rigid (*triangular* and *snub hexagonal tiling*, sect. 6.6). This is marked by the capital letter "R" in the Tables 6.3 and 6.4 of the infinitesimal results.

Albeit the table lists the infinitesimal results rigidity does not denote the term infinitesimal rigidity as defined in the *rigidity theory* (cf. Sect. 2.7 for the term infinitesimal rigidity).

The *square* and the *elongated triangular tiling* can only be sheared, i.e. the angle between the lattice vectors must change. The deformation of the square tiling in the minimal unit cell is clear by intuition (see 6.2.1 and 6.2.2). The elongated triangular tiling has a similar deformation mode in the groups $c1$ and $c2$ but in contrast the length of one lattice vector reduces (6.2.6). This explains the difference in the plots of the square tiling and of the elongated triangular tiling which reaches the negative range for the values of the Poisson's ratio. A shear deformation in direction of **a** leads also to a change of the angle. Because the lattice vector **b** reduce its length necessarily, *negative normal stress* can be observed.

Auxetic deformation occurs always in the case of non-rigidity in the hexagonal and square groups where Poisson's ratio is fully constraint to -1 due to the symmetry (cf. Sect. 3.6).

Table 6.3: *Infinitesimal deformation behaviour of Archimedean tilings, see Table 6.1 for explanation of symbols.*

Group	**p6mm**	**p6**	**p31m**	**p3m1**	**p3**	**p4gm**	**p4mm**	**p4**
Lattice Type	hexagonal					square		
Triangular Tiling ($p6mm$) **rigid:** 6.6.1	R	R	R	R	R	-	-	-
Square Tiling ($p4mm$) **unique:** 6.2.1, 6.2.2	-	-	-	-	-	-	R	R
Hexagonal Tiling ($p6mm$) **1 sym. mode:** 6.2.3, 6.2.4, 6.2.5	R	R	R	R	R	-	-	-
Elongated Triangular Tiling ($c2mm$) - **unique:** 6.2.6, 6.2.7	-	-	-	-	-	-	-	-
Snub Square Tiling ($p4gm$) **unique:** 6.2.8, 6.2.9	-	-	-	-	-	R	-	R
Truncated Square Tiling ($p4mm$) - **3 sym. modes:** 6.2.10; 6.2.11 ; 6.2.12	-	-	-	-	-	-	R	**−1**$^{\ddagger\downarrow}$

Five Archimedean tilings can uniquely be deformed in those groups (*truncated square* 6.2.10, *truncated hexagonal*, *trihexagonal* 6.2.17, *small rhombitrihexagonal* 6.2.18 and *great rhomibtrihexagonal tilings*). But even two of them show two different mechanisms dependent on different groups (*truncated hexagonal tiling* 6.2.13, 6.2.14 and the *great rhomibtrihexagonal tiling* 6.2.20, 6.2.21). One of these five is a skeletal structure which has only one degree of freedom and hence the symmetry constraints are not necessary to limit the solution space. This is the *trihexagonal tiling* also called Kagome structure which represents under the 11 Archimedean tilings the only one which is infinitesimally auxetic without additional symmetry constraints. This skeletal structure is already suggested in [21] as a model for auxetic behaviour.

However under finite deformations the *snub square tiling* which also possesses only one degree of freedom becomes auxetic (6.2.8). There are four further cases where a negative Poisson's ratio occurs under finite deformations but only under additional symmetry constraints. That are the known *hexagonal tiling* ($p2mm_r, pm_r, p11m_r$; see 6.2.3) which becomes the re-entrant honeycomb pattern, the truncated square tiling ($p2mm_r, pm_r$; see 6.2.11), the truncated hexagonal tiling ($p2mm_r, p11m_r$; see 6.2.15) and the *small rhombitrihexagonal tiling* ($p2mm_r, pm_r, p11m_r$; see 6.2.19). All have one mechanism in the different rectangular groups.

Only the *square tiling* shows in no setting auxetic behaviour. Further the *truncated square tiling* in the groups $p2mm$ and pm has a mechanism which has never a negative Poisson's ratio (6.2.12).

Table 6.3: *Infinitesimal deformation behaviour of Archimedean tilings, see Table 6.1 for explanation of symbols.*

c2mm	p2gg	p2mg	p2mm	cm	pg	pm	p2	p1
rectangular (or rhombus in specific subgroups)							oblique	
R_{30}	-	-	-	R_{26}, R_{27}	-	-	R	$\underline{R}$
$\infty_{30}^{0^\circ\ddagger\downarrow}$ $1_{30}^{45^\circ}$	-	-	R	$\infty_{26}^{0^\circ\ddagger\downarrow}$ $1_{26}^{45^\circ}$	-	R	$\infty^{0^\circ\ddagger\downarrow}$ 1^{45°	$\underline{\infty}^{0^\circ\ddagger\downarrow}$ $\underline{1}^{45^\circ}$
$N_{30}^{0^\circ}$ $1_{30}^{60^\circ}$ $1_{30}^{-30^\circ}$	-	-	-	$N_{26}^{0^\circ}$, $\underline{N}_{27}^{0^\circ}$ $1_{26}^{60^\circ}$, $\underline{1}_{27}^{60^\circ}$ $1_{26}^{-30^\circ}$, $\underline{1}_{27}^{-30^\circ}$	-	-	U	U
R	-	-	-	R, R_{25}	-	-	$\infty_{19}^{0^\circ\ddagger\downarrow}$ $1_{19}^{45^\circ\ddagger\downarrow}$ $\infty_{19}^{90^\circ}$	$\underline{\infty}_{18}^{0^\circ\ddagger\downarrow}$ $1_{18}^{45^\circ\ddagger\downarrow}$ $\underline{\infty}_{18}^{90^\circ}$
$R_{31}^{0^\circ}$ $R_{31}^{45^\circ}$	1^{0° $\mathbf{-0.76}^{45^\circ}$	-	-	$1_{28}^{0^\circ}$ $\mathbf{-0.76}_{28}^{45^\circ}$	1^{0° $\mathbf{-0.76}_{23}^{45^\circ}$	-	1^{0° $\mathbf{-0.76}^{45^\circ}$	$\underline{1}^{0^\circ}$ $\underline{\mathbf{-0.76}}^{45^\circ}$
$\infty_{30}^{0^\circ\ddagger\downarrow}$ $1_{30}^{45^\circ}$	-	-	1	$\underline{\infty}_{26}^{0^\circ\ddagger\downarrow}$ $\underline{1}_{26}^{45^\circ}$	-	$\underline{1}$	U	U

Discontinuous Poisson's ratio In the cases of the *hexagonal*, *truncated hexagonal* and *small rhombitrihexagonal tilings* the graphs of the determined Poisson's ratio as function of δ have points of discontinuity (6.2.3, 6.2.15 and 6.2.19). This occurs at $\delta = 0$. There are two different Poisson's ratios for small deformations with $\delta > 0$ and $\delta < 0$. This is denoted with the large letter "N" in the Tables 6.3, 6.4 to indicate that there is not a unique Poisson's ratio for infinitesimal compression and elongation. Additionally the *truncated hexagonal tiling* has a further point of discontinuity at $\delta \approx -0.46$ which will be discussed separately below. Particularly these jumps contain a sign change i.e. the left value and the right value have a different sign. Thus both compression and elongation lead to the same orthogonal effect, here an expansion of the surrounding rectangle. One similarity is that it occurs only in the decentered groups $pm_r, p11m_r, p2mm_r, \ldots$ with the lattice constraints $|\mathbf{a}(\delta)| = |\mathbf{b}(\delta)|$, denoted as rhombus (indicated with the small letter "r" in the subscript).

In order to understand these results which are contrary expectations the *hexagonal tiling* will be discussed here in more detail in group $p11m_r$. See 6.2.3 for the plot of Poisson's ratio which shows the jump.

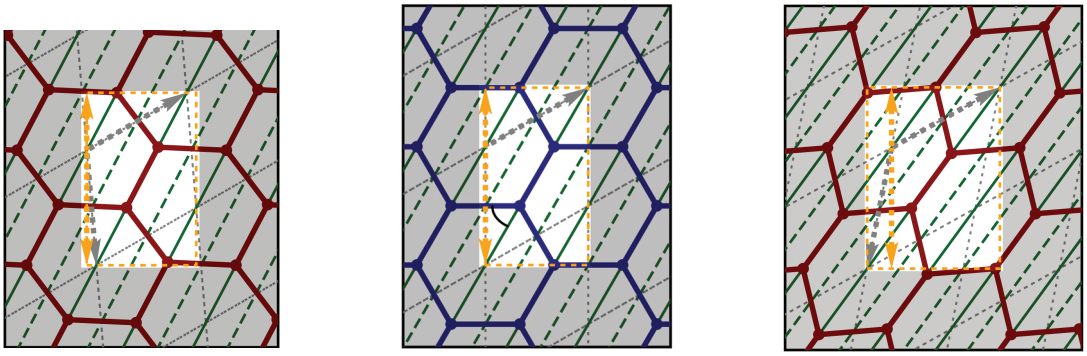

(a) $\delta < 0$ *and* $\nu > 0$ **(b)** $\delta = 0$ **(c)** $\delta > 0$ *and* $\nu < 0$

Figure 6.1: *(a) Configuration for a small vertical contraction, (b) the initial configuration and (c) the one for a small vertical expansion. Contraction as well as expansion lead to an elongation of the surrounding rectangle (orange) in perpendicular direction.*

Consider the primitive unit cell of the *hexagonal tiling* spanned by the two grey lattice vectors in Figs. 6.1a–c and is in this case a cell with equal side lengths and an angle of 120°. This cell is surrounded by the orange rectangle which represents the length and the height that determine Poisson's ratio (highlighted region). The deformation is imposed vertically indicated by the orange arrow.

There is one bar in the unit cell which lies on the diagonal mirror line (green solid line) and is hence fixed on this. The other bars which cross the border of the unit cell link further bars of the next unit cells which lie again on parallel mirror lines.

If the angle between one of the crossing bars and a mirror line is changed to contract or expand the skeletal structure, the mirrored crossing bar changes its angle correspondingly to the symmetry. Therefore a larger angle lead to a greater distance of the mirror lines and a smaller angle for more narrow mirror lines. To allow such a change induced by the skeletal structure the lattice vectors must change. There are two possibilities: Either the angle between the both lattice vectors changes or the lengths of them. But also both possibilities can occur simultaneously.

The chosen deformation approach on the unit cell impose beside the elongation of $a_{||}$ & $b_{||}$ a change of the orthogonal parts which are not independent because of the lattice constraint $|\mathbf{a}(\delta)| = |\mathbf{b}(\delta)|$ (sections 2.5 and 3.6). The angle between both must change due to the approach and is used as the independent variable. The explicit equations,

$$a^{\perp}(\delta) = \frac{(1+\delta)\left(a^{||}\cos(\alpha) - b^{||}\right)}{\sin(\alpha)} \qquad \text{and} \qquad b^{\perp}(\delta) = \frac{(1+\delta)\left(a^{||} - b^{||}\cos(\alpha)\right)}{\sin(\alpha)},$$

make clear that the original value of $a^{\perp}(\delta = 0) = 0$ becomes unequal to zero and hence the vector rotates. That also regards to the second lattice vector. Therefore the unit cell rotates and consequently the symmetry scaffold as well.

The change of the unit cell for $\delta < 0$ is that the angle and the moduli of the lattice vectors become smaller. In the opposite direction the unit cell is flattened (larger angle) with increased length of the lattice vectors.

These changes with the rotation of the unit cell in opposite directions for both deformation directions lead in both cases to a perpendicular expansion of the surrounding rectangle. This explains the result of the two different signs. But nevertheless this result is strongly influenced by the assumptions of the approach of considering the abstract unit cell together with the symmetries which restrict lattice vector changes and the surrounding rectangle which determines Poisson's ratio.

Local minimum in the finite Poisson's ratio A second jump point contains the plot of Poisson's ratio of the *truncated hexagonal tiling* with deformation direction of 0° in group $p11m_r$ but for a finite deformation ($\delta \approx -0.46$) (see Fig. 6.2). In contrast to the

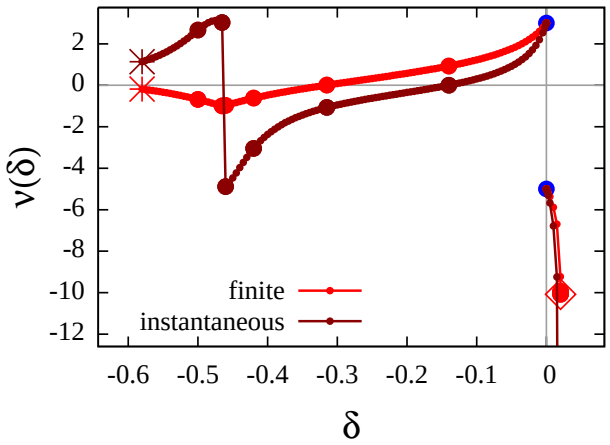

Figure 6.2: *Plot of the finite and instantaneous Poisson's ratio of the* truncated hexagonal tiling *with a deformation direction of* 0° *in the group* $p11m_r$

hexagonal tiling here is actually a change in the skeletal structure responsible. However also a rotation occurs. The skeletal structure has some similarities to the *hexagonal tiling*: a fixed part of the structure on the mirror lines and bars which link such elements between different mirror lines (Fig. 6.3a). These linking bars change their orientation and determine the distance between the different mirror lines (compare *hexagonal tiling*).

At the jump point ($\delta \approx -0.46$) the linking bars become parallel to the glide-mirror line (Fig. 6.3e). This state represents the one with the shortest length in the direction of the mirror lines (not deformation direction). Before and after this state the bars are not

anymore parallel and hence increase this length. During the deformation process this length becomes first smaller and smaller but at the jump point this length becomes again longer. This behaviour can also be seen in the graph of the finite Poisson's ratio where this turning point represents a local minimum. A deformation in mirror line direction would have this point as its maximal contraction.

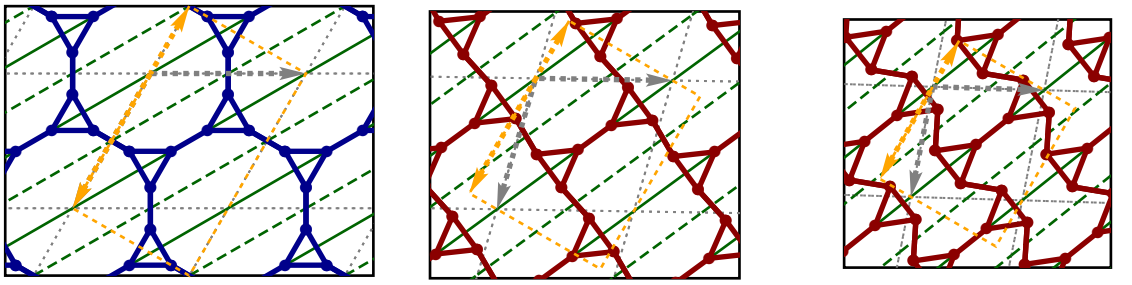

(a) $\delta = 0$ **(b)** $\delta = -0.14$ *and* $\nu_{inst.} \approx 0$ **(c)** $\delta = -0.315$ *and* $\nu_{inst.} < 0$

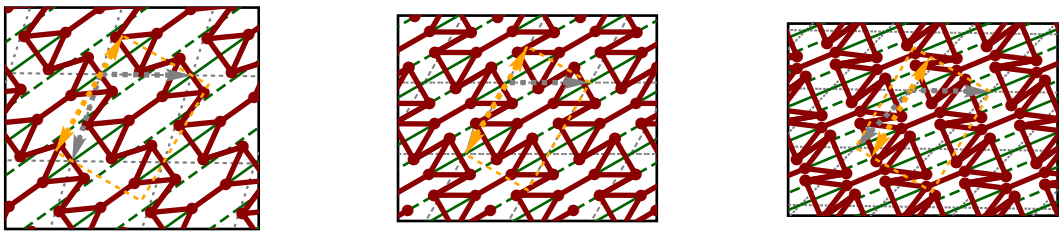

(d) $\delta = -0.42$ *and* $\nu < -5$ **(e)** $\delta = -0.46519$ **(f)** $\delta = -0.5$ *and* $\nu > 0$

Figure 6.3: *Deformation of the truncated hexagonal tiling with* $\delta < 0$

Table 6.4: *Infinitesimal deformation behaviour of Archimedean tilings.*

Group	**p6mm**	**p6**	**p31m**	**p3m1**	**p3**	**p4gm**	**p4mm**	**p4**
Lattice Type	hexagonal					square		
Snub Hexagonal Tiling ($p6$) **rigid:** 6.6.2	-	R	-	-	R	-	-	-
Truncated Hexagonal Tiling ($p6mm$) - **3 sym. modes:** 6.2.13; 6.2.14; 6.2.15, 6.2.16	R	$\underline{\mathbf{-1}}^{\ddagger\downarrow}$	$\underline{\mathbf{-1}}^{\ddagger\downarrow}$	R	U	-	-	-
Trihexagonal Tiling ($p6mm$) - **unique:** 6.2.17	R	R	$\mathbf{-1}^{\ddagger\downarrow}$	R	$\mathbf{-1}^{\ddagger\downarrow}$	-	-	-
Small Rhombitrihexagonal Tiling ($p6mm$) **2 sym. modes:** 6.2.18; 6.2.19	R	$\mathbf{-1}^{\downarrow\ddagger}$	R	R	$\underline{\mathbf{-1}}^{\ddagger\downarrow}$	-	-	-
Great Rhombitrihexagonal Tiling ($p6mm$) **2 sym. modes:** 6.2.20; 6.2.21	R	$\underline{\mathbf{-1}}^{\ddagger\downarrow}$	$\underline{\mathbf{-1}}^{\ddagger\downarrow}$	R	U	-	-	-

6.2.1 Square Tiling

$\downarrow 0^\circ$

(4^4) - Quadrille (Conway) | *p4mm* (square)

***p*1 (oblique)**

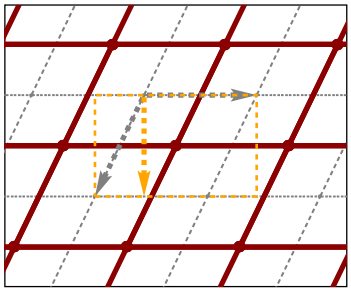

$\delta = -0.1\,, \quad \nu = 1.29$

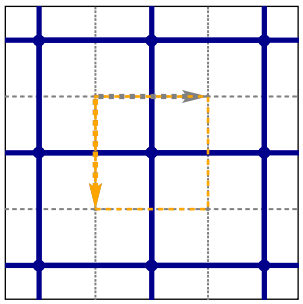

$\delta = 0\,, \quad \boldsymbol{\nu = \infty}$

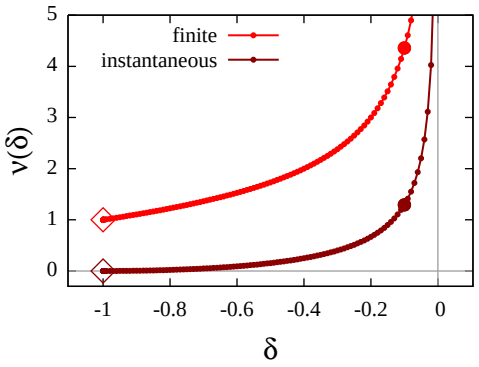

***B*: tuc | cross**	:	2 | 2
***N*: tuc | neigb. | tot**	:	$1 \times 1\, a(1)$ | 4 $\sum = 5$
Free|Dep.|Fix $\mathrm{p}^i_{x,y}$	:	0 | 8 | 2 $\sum = 10$
Set|Free|Dep.|Fix	:	$a^{\parallel}, b^{\parallel}$ | $a^{\perp}, b^{\perp}$|none|none
$\langle \frac{B}{N} \rangle$	:	4.00
$\mathbf{Z}_{\mathbf{Maxwell}}$	:	1
Reference(s)	:	[24], p.63, Fig.2

Not auxetic

Table 6.4: *Infinitesimal deformation behaviour of Archimedean tilings.*

c2mm	p2gg	p2mg	p2mm	cm	pg	pm	p2	p1
rectangular (or rhombus in specific subgroups)							oblique	
-	-	-	-	-	-	-	R	$\underline{\mathrm{R}}$
$\mathrm{N}^{0^\circ}_{30}$ $1^{60^\circ}_{30}$	-	-	-	U_{26}, $\underline{\mathrm{N}}^{0^\circ}_{27}$ $\underline{1}^{60^\circ}_{27}$	-	-	U	U
R_{30}	-	-	-	$\mathbf{-1}_{26}{}^{\ddagger\downarrow}$, R_{27}	-	-	R	$\underline{\mathbf{-1}}^{\ddagger\downarrow}$
$\mathrm{N}^{0^\circ}_{30}$ $1^{60^\circ}_{30}$	-	-	-	$\underline{\mathrm{N}}^{0^\circ}_{26}$, $\mathrm{N}^{0^\circ}_{27}$ $1^{60^\circ}_{26}$, $1^{60^\circ}_{27}$	-	-	U	U
U_{30}	-	-	-	U_{26}, U_{27}	-	-	U	U

6.2.2 Square Tiling

↘ 45°

(4^4) - Quadrille (Conway) | *p4mm* (square)

p1 (oblique)

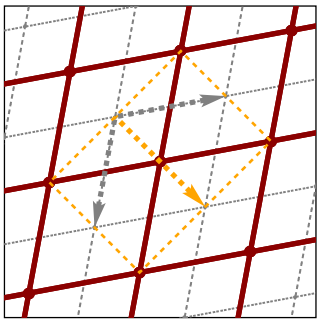

$\delta = -0.20$, $\nu = 0.47$

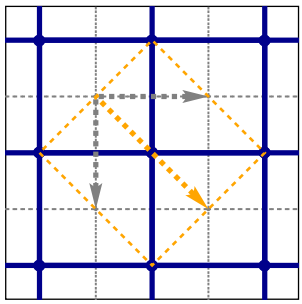

$\delta = 0$, $\boldsymbol{\nu = 1.00}$

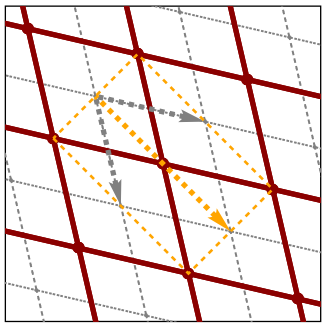

$\delta = 0.2$, $\nu = 2.57$

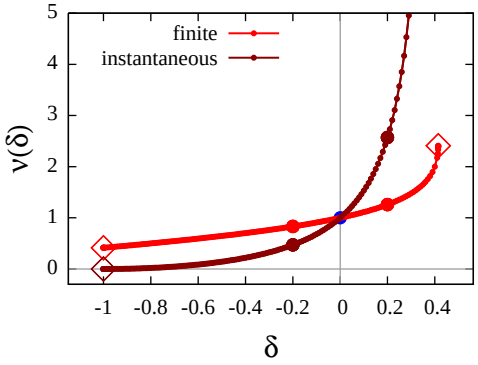

B: tuc | cross	:	2 | 2
N: tuc | neigb. | tot	:	$1 \times 1\, a(1)$ | 4 $\sum = 5$
Free|Dep.|Fix $\mathrm{p}^i_{x,y}$	:	0 | 8 | 2 $\sum = 10$
Set|Free|Dep.|Fix	:	$a^{\parallel}, b^{\parallel}$ | $a^{\perp}, b^{\perp}$|none|none
$\langle \frac{B}{N} \rangle$	:	4.00
$\mathbf{Z_{Maxwell}}$	:	1
Reference(s)	:	[24], p.63, Fig.2

Not auxetic

6.2.3 Hexagonal Tiling

↓ 0°

(6^3) - Hextille (Conway), Honeycomb | *p6mm* (hexagonal)

p11m_r (rhombus)

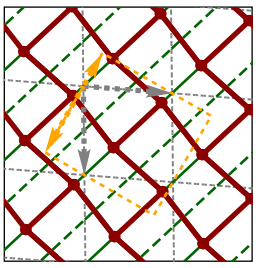

$\delta = -0.33$, $\nu = -0.01$

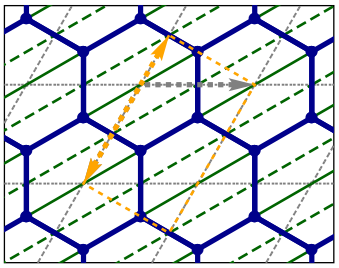

$\delta = 0$, $\boldsymbol{\nu_- = 3.00}$, $\boldsymbol{\nu_+ = -5.00}$

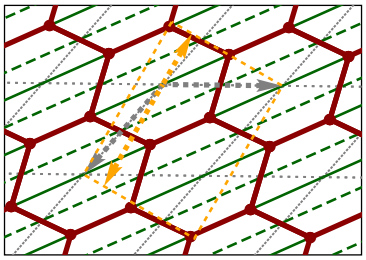

$\delta = 0.029$, $\nu = -\infty$

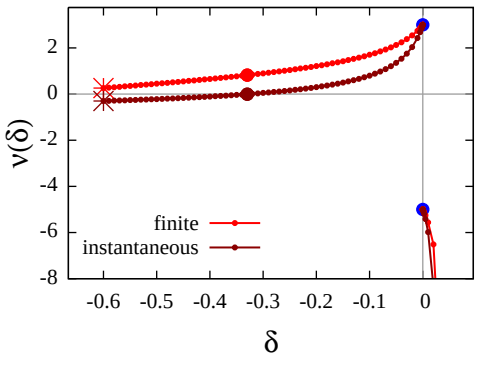

B: tuc | cross	:	3 | 2
N: tuc | neigb. | tot	:	$2 \times 1\, a(U)$ | 4 $\sum = 6$
Free|Dep.|Fix $\mathrm{p}^i_{x,y}$	:	2 | 10 | 0 $\sum = 12$
Set|Free|Dep.|Fix	:	$a^{\parallel}, b^{\parallel}$ | $b^{\perp}$ | $a^{\perp} = f(\delta, b^{\perp})$ | none
$\langle \frac{B}{N} \rangle$	:	3.00
$\mathbf{Z_{Maxwell}}$	:	2
Reference(s)	:	[24], p.63, Fig.3

Auxetic under finite deformation ↓

6.2.4 Hexagonal Tiling

↘ 60°

(6^3) - Hextille (Conway), Honeycomb | *p6mm* (hexagonal)

***p*11*m*$_r$ (rhombus)**

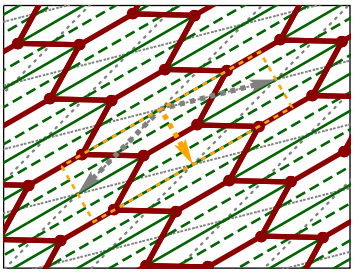

$\delta = -0.40$, $\nu = 0.17$

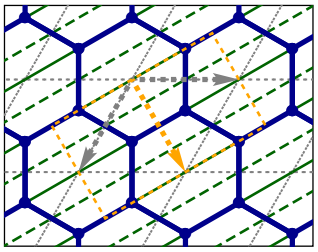

$\delta = 0$, $\boldsymbol{\nu = 1.00}$

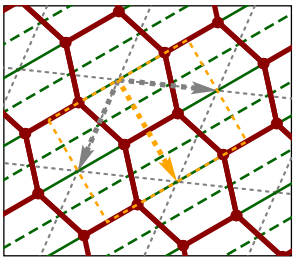

$\delta = 0.1$, $\nu = 2.29$

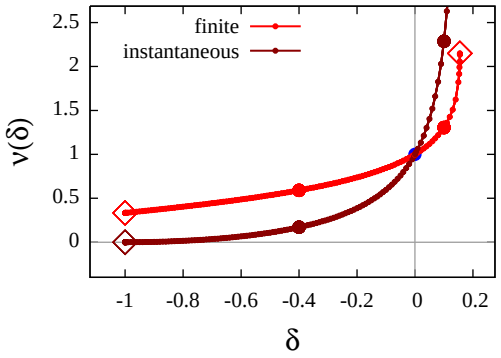

***B*: tuc | cross**	:	3 | 2
***N*: tuc | neigb. | tot**	:	$2 \times 1\, a(U)$ | 4 $\sum = 6$
Free|Dep.|Fix $\mathrm{p}^i_{x,y}$	:	2 | 10 | 0 $\sum = 12$
Set|Free|Dep.|Fix	:	$a^{\parallel}, b^{\parallel}$ | $a^{\perp}$ | $b^{\perp} = f(\delta, a^{\perp})$ | none
$\langle \frac{B}{N} \rangle$	:	3.00
$\mathbf{Z}_{\mathbf{Maxwell}}$	:	2
Reference(s)	:	[24], p.63, Fig.3

Not auxetic

6.2.5 Hexagonal Tiling

↙ 330°

(6^3) - Hextille (Conway), Honeycomb | *p6mm* (hexagonal)

***p*11*m*$_r$ (rhombus)**

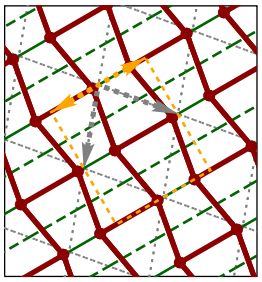

$\delta = -0.45$, $\nu = -0.15$

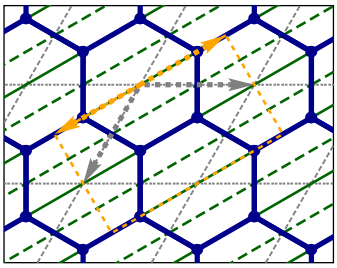

$\delta = 0$, $\boldsymbol{\nu = 1.00}$

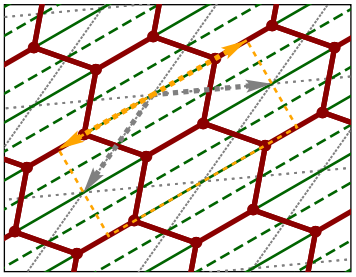

$\delta = 0.1$, $\nu = 1.86$

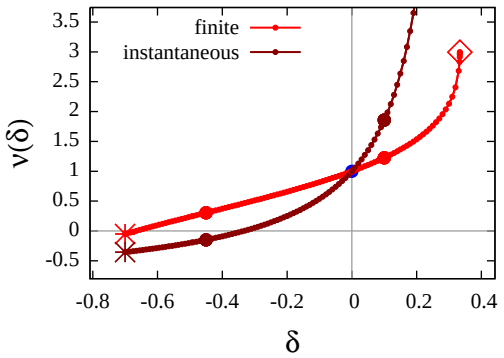

***B*: tuc | cross**	:	3 | 2
***N*: tuc | neigb. | tot**	:	$2 \times 1\, a(U)$ | 4 $\sum = 6$
Free|Dep.|Fix $\mathrm{p}^i_{x,y}$	:	2 | 10 | 0 $\sum = 12$
Set|Free|Dep.|Fix	:	$a^{\parallel}, b^{\parallel}$ | $b^{\perp}$ | $a^{\perp} = f(\delta, b^{\perp})$ | none
$\langle \frac{B}{N} \rangle$	:	3.00
$\mathbf{Z}_{\mathbf{Maxwell}}$	:	2
Reference(s)	:	[24], p.63, Fig.3

Auxetic under finite deformation

6.2.6 Elongated Triangular Tiling

$\downarrow$ **0°**

$(3^2.4^2)$ - Isosnub Quadrille (Conway) | $c2mm$ (rectangular)

***c*1 (oblique)**

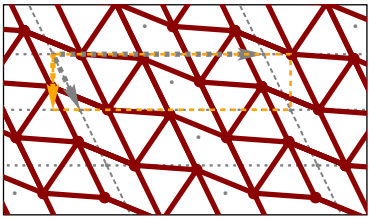

$\delta = -0.1$, $\nu = -0.26$

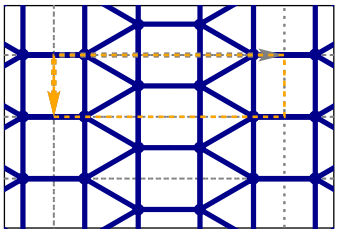

$\delta = 0$, $\boldsymbol{\nu = \infty}$

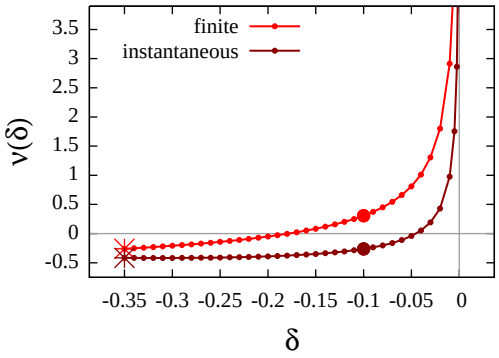

***B*: tuc | cross**	:	11 | 4
***N*: tuc | neigb. | tot**	:	$2 \times 2\,a(1)$ | 10 $\sum = 14$
Free|Dep.|Fix $\mathrm{p}^i_{x,y}$	:	2 | 24 | 2 $\sum = 28$
Set|Free|Dep.|Fix	:	$a^{\parallel}, b^{\parallel}$ | $a^{\perp}, b^{\perp}$|none|none
$\langle \frac{B}{N} \rangle$	:	5.50
$\mathbf{Z_{Maxwell}}$	:	-2
Reference(s)	:	[24], p.63, Fig.6

Auxetic under finite deformation

6.2.7 Elongated Triangular Tiling

$\rightarrow$ **90°**

$(3^2.4^2)$ - Isosnub Quadrille (Conway) | $c2mm$ (rectangular)

***c*1 (oblique)**

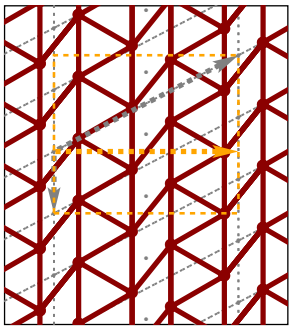

$\delta = -0.2$, $\nu = 0.94$

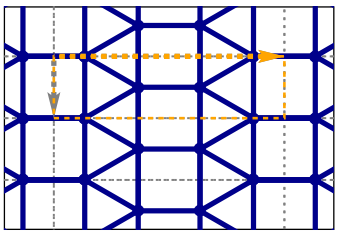

$\delta = 0$, $\boldsymbol{\nu = \infty}$

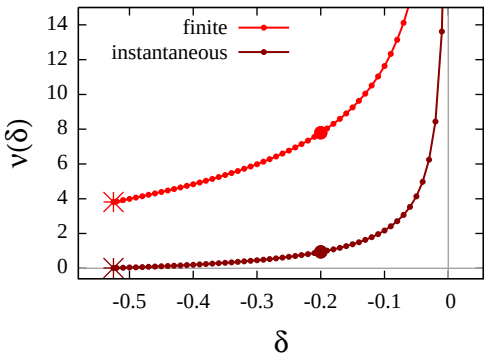

***B*: tuc | cross**	:	11 | 4
***N*: tuc | neigb. | tot**	:	$2 \times 2\,a(1)$ | 10 $\sum = 14$
Free|Dep.|Fix $\mathrm{p}^i_{x,y}$	:	2 | 24 | 2 $\sum = 28$
Set|Free|Dep.|Fix	:	$a^{\parallel}, b^{\parallel}$ | $a^{\perp}, b^{\perp}$|none|none
$\langle \frac{B}{N} \rangle$	:	5.50
$\mathbf{Z_{Maxwell}}$	:	-2
Reference(s)	:	[24], p.63, Fig.6

Not auxetic

6.2.8 Snub Square Tiling

↓ 0°

(3^2.4.3.4) - Snub Quadrille (Conway) | *p4gm* (square)

***p*1 (oblique)**

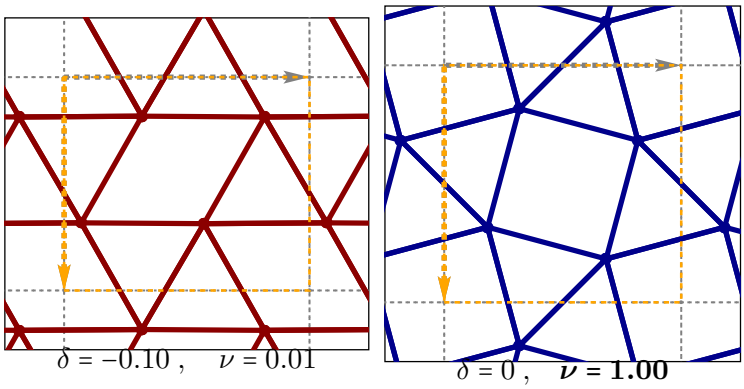

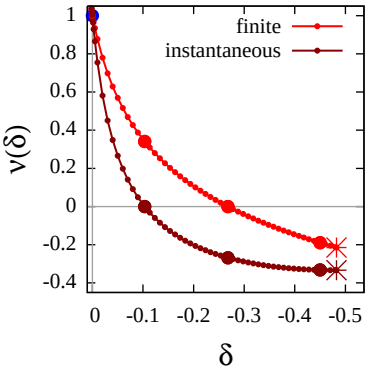

***B*: tuc | cross**	:	10 | 6
***N*: tuc | neigb. | tot**	:	$4 \times 1\, a(1)$ | 8 $\sum = 12$
Free|Dep.|Fix $p^i_{x,y}$	:	6 | 16 | 2 $\sum = 24$
Set|Free|Dep.|Fix	:	$a^{\parallel}, b^{\parallel}$ | $a^{\perp}, b^{\perp}$|none|none
$\langle \frac{B}{N} \rangle$	:	5.00
$\mathbf{Z}_{\mathbf{Maxwell}}$	:	-1
Reference(s)	:	[24], p.63, Fig.7

Auxetic under finite deformation

6.2.9 Snub Square Tiling

↘ 45°

(3^2.4.3.4) - Snub Quadrille (Conway) | *p4gm* (square)

***p*1 (oblique)**

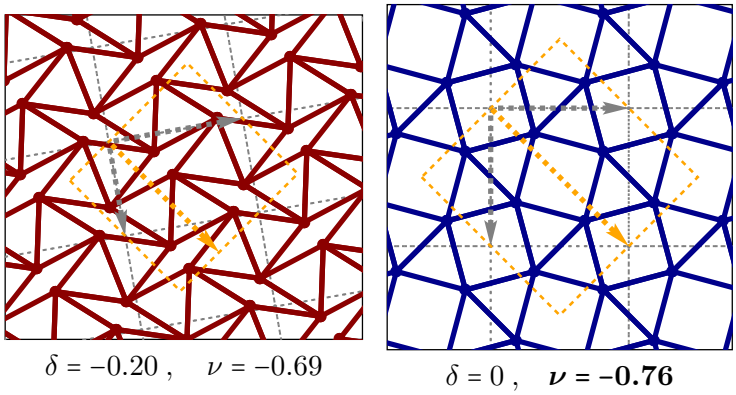

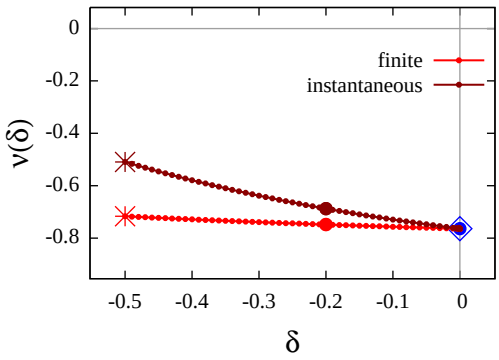

***B*: tuc | cross**	:	10 | 6
***N*: tuc | neigb. | tot**	:	$4 \times 1\, a(1)$ | 8 $\sum = 12$
Free|Dep.|Fix $p^i_{x,y}$	:	6 | 16 | 2 $\sum = 24$
Set|Free|Dep.|Fix	:	$a^{\parallel}, b^{\parallel}$ | $a^{\perp}, b^{\perp}$|none|none
$\langle \frac{B}{N} \rangle$	:	5.00
$\mathbf{Z}_{\mathbf{Maxwell}}$	:	-1
Reference(s)	:	[24], p.63, Fig.7

Auxetic

6.2.10 Truncated Square Tiling

↓ 0°

(4.8^2) - Truncated Quadrille (Conway) | *p4mm* (square)

***p4* (square)**

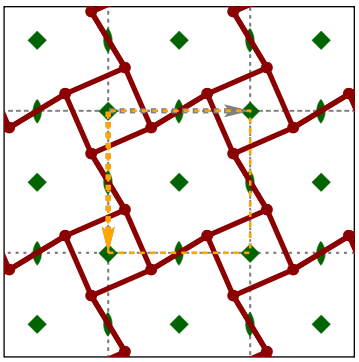

$\delta = -0.10\,, \quad \nu = -1.00$

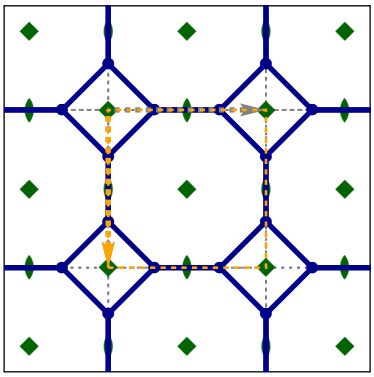

$\delta = 0\,, \quad \boldsymbol{\nu = -1.00}$

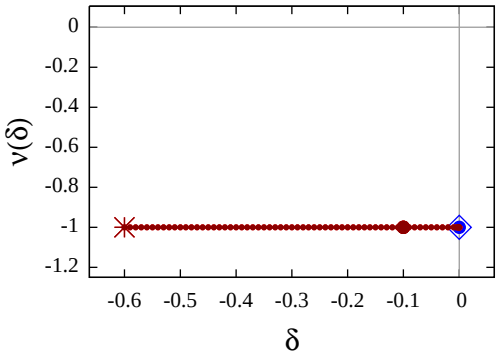

***B*: tuc | cross**	:	6 | 2
***N*: tuc | neigb. | tot**	:	$1 \times 4\,d(1)$ | 4 $\sum = 8$
Free|Dep.|Fix $\mathrm{p}^i_{x,y}$	:	2 | 14 | 0 $\sum = 16$
Set|Free|Dep.|Fix	:	$a^{\parallel}, b^{\parallel}$ | none | $a^{\perp} = -b^{\parallel}$, $b^{\perp} = a^{\parallel}$ | N.A.
$\langle \frac{B}{N} \rangle$	:	3.00
$\mathbf{Z}_{\mathbf{Maxwell}}$	:	3
Reference(s)	:	[24], p.63 , Fig.12

Auxetic

6.2.11 Truncated Square Tiling

↓ 0°

(4.8^2) - Truncated Quadrille (Conway) | *p4mm* (square)

***pm*$_r$ (rhombus)**

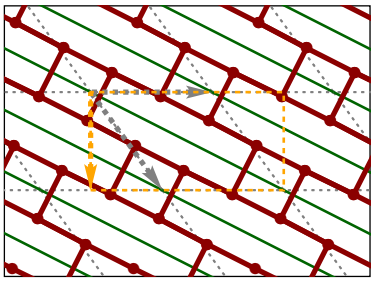

$\delta = -0.25\,, \quad \nu = 0.27$

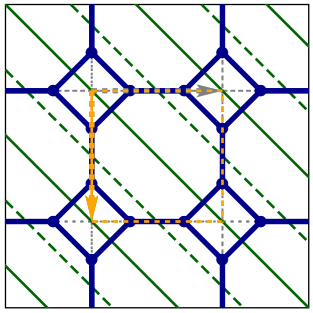

$\delta = 0\,, \quad \boldsymbol{\nu = \infty}$

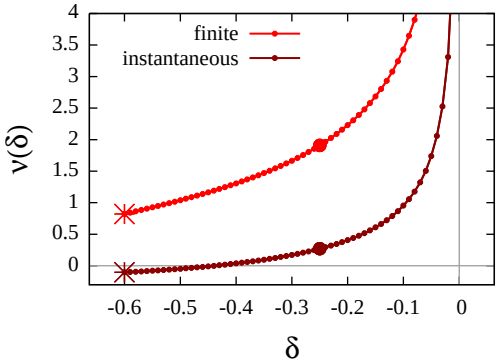

***B*: tuc | cross**	:	6 | 2
***N*: tuc | neigb. | tot**	:	$2 \times 2\,b(1)$ | 4 $\sum = 8$
Free|Dep.|Fix $\mathrm{p}^i_{x,y}$	:	3 | 12 | 1 $\sum = 16$
Set|Free|Dep.|Fix	:	$a^{\parallel}, b^{\parallel}$ | $b^{\perp}$ | $a^{\perp} = f(\delta, b^{\perp})$ | none
$\langle \frac{B}{N} \rangle$	:	3.00
$\mathbf{Z}_{\mathbf{Maxwell}}$	:	3
Reference(s)	:	[24], p.63 , Fig.12

Auxetic under finite deformation

6.2.12 Truncated Square Tiling

↓ 0°

(4.8^2) - Truncated Quadrille (Conway) | *p4mm* (square)

***p2mm* (rectangular)**

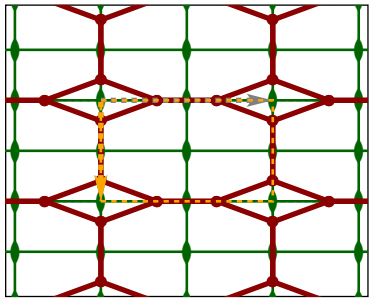

$\delta = -0.30$, $\nu = 0.22$

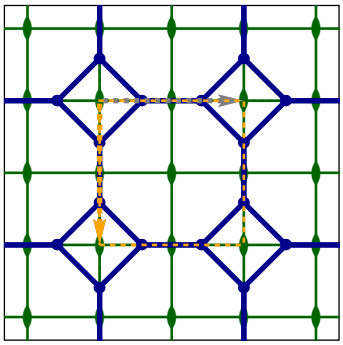

$\delta = 0$, $\boldsymbol{\nu = 1.00}$

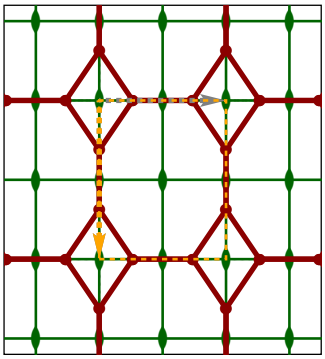

$\delta = 0.1$, $\nu = 1.85$

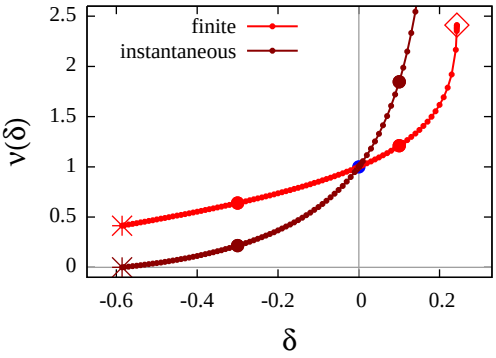

***B*: tuc | cross**	:	6 | 2
***N*: tuc | neigb. | tot**	:	$1\times 2\,g(.m.), 1\times 2\,e(..m)$ | 4 $\quad \sum = 8$
Free|Dep.|Fix $\mathrm{p}^i_{x,y}$	:	2 | 14 | 0 $\quad \sum = 16$
Set|Free|Dep.|Fix	:	$a^{\parallel}, b^{\parallel}$ | $b^{\perp}$ | $a^{\perp} = -\frac{a^{\parallel}b^{\parallel}}{b^{\perp}}$ | none
$\langle \frac{B}{N} \rangle$	:	3.00
$\mathbf{Z}_{\mathbf{Maxwell}}$	:	3
Reference(s)	:	[24], p.63 , Fig.12

Not auxetic

6.2.13 Truncated Hexagonal Tiling

↓ 0°

(3.12^2) - Truncated Hextille (Conway) | *p6mm* (hexagonal)

***p6* (hexagonal)**

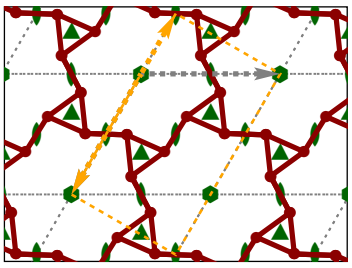

$\delta = -0.10$, $\nu = -1.00$

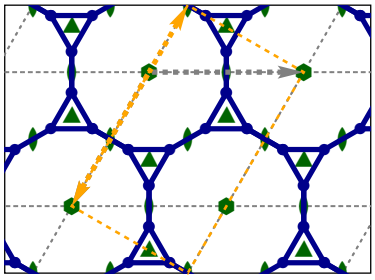

$\delta = 0$, $\boldsymbol{\nu = -1.00}$

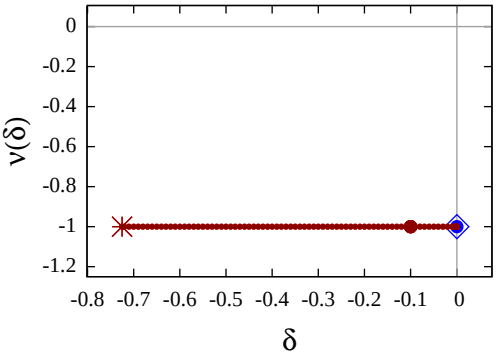

***B*: tuc | cross**	:	9 | 2
***N*: tuc | neigb. | tot**	:	$1\times 6\,d(1)$ | 4 $\quad \sum = 10$
Free|Dep.|Fix $\mathrm{p}^i_{x,y}$	:	2 | 18 | 0 $\quad \sum = 20$
Set|Free|Dep.|Fix	:	$a^{\parallel}, b^{\parallel}$ | none | $a^{\perp} = \frac{a^{\parallel}+2b^{\parallel}}{-\sqrt{3}}$, $b^{\perp} = \frac{2a^{\parallel}+b^{\parallel}}{\sqrt{3}}$ | N.A.
$\langle \frac{B}{N} \rangle$	:	3.00
$\mathbf{Z}_{\mathbf{Maxwell}}$	:	4
Reference(s)	:	[24], p.63, Fig.10

Auxetic

6.2.14 Truncated Hexagonal Tiling

↓ 0°

(3.12^2) - Truncated Hextille (Conway) | *p6mm* (hexagonal)

***p31m* (hexagonal)**

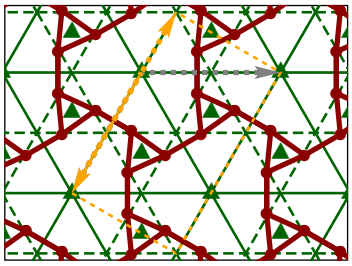

$\delta = -0.10$, $\nu = -1.00$

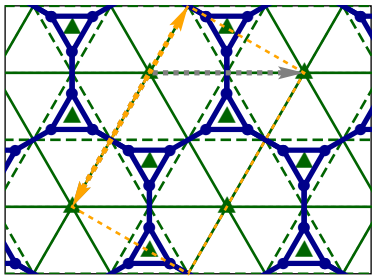

$\delta = 0$, $\boldsymbol{\nu = -1.00}$

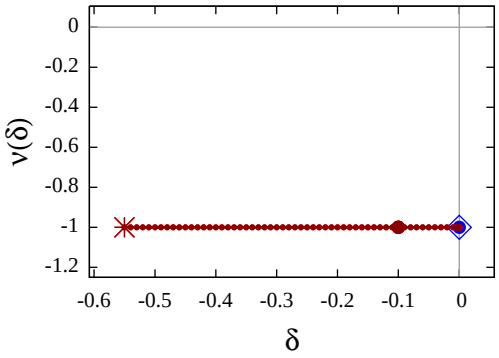

B: tuc | cross	:	9 | 2
N: tuc | neigb. | tot	:	$1 \times 6\,d(1)$ | 4 $\sum = 10$
Free|Dep.|Fix $\mathrm{p}^i_{x,y}$	:	2 | 18 | 0 $\sum = 20$
Set|Free|Dep.|Fix	:	$a^{\parallel}, b^{\parallel}$ | none | $a^{\perp} = \frac{a^{\parallel}+2b^{\parallel}}{-\sqrt{3}}$, $b^{\perp} = \frac{2a^{\parallel}+b^{\parallel}}{\sqrt{3}}$ | N.A.
$\langle \frac{B}{N} \rangle$	:	3.00
$\mathbf{Z_{Maxwell}}$	:	4
Reference(s)	:	[24], p.63, Fig.10

Auxetic

6.2.15 Truncated Hexagonal Tiling

↓ 0°

(3.12^2) - Truncated Hextille (Conway) | *p6mm* (hexagonal)

***p11m*$_r$ (rhombus)**

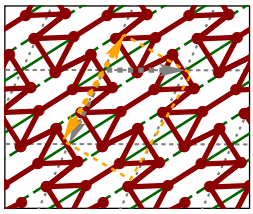

$\delta = -0.45$, $\nu = -4.47$

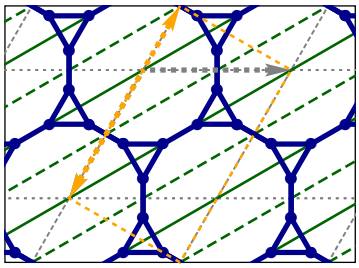

$\delta = 0$, $\boldsymbol{\nu_- = 3.00}$, $\boldsymbol{\nu_+ = -5.00}$

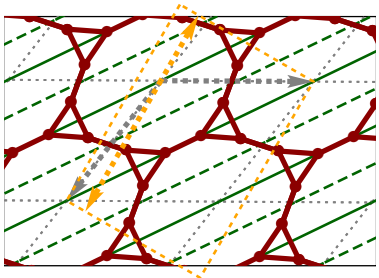

$\delta = 0.02$, $\nu = -\infty$

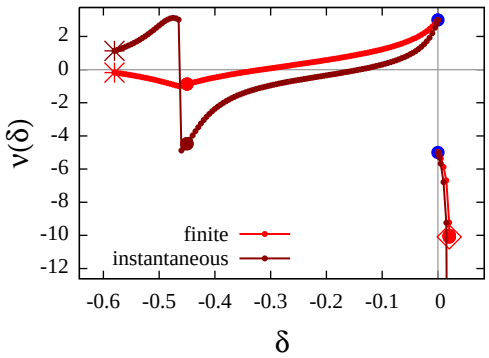

B: tuc | cross	:	9 | 2
N: tuc | neigb. | tot	:	$2 \times 2\,b(1), 2 \times 1\,a(U)$ | 4 $\sum = 10$
Free|Dep.|Fix $\mathrm{p}^i_{x,y}$	:	5 | 14 | 1 $\sum = 20$
Set|Free|Dep.|Fix	:	$a^{\parallel}, b^{\parallel}$ | $b^{\perp}$ | $a^{\perp} = f(\delta, b^{\perp})$ | none
$\langle \frac{B}{N} \rangle$	:	3.00
$\mathbf{Z_{Maxwell}}$	:	4
Reference(s)	:	[24], p.63, Fig.10

Auxetic under finite deformation ↓

6.2.16 Truncated Hexagonal Tiling

↘ 60°

(3.12^2) - Truncated Hextille (Conway) | *p6mm* (hexagonal)

$p11m_r$ (rhombus)

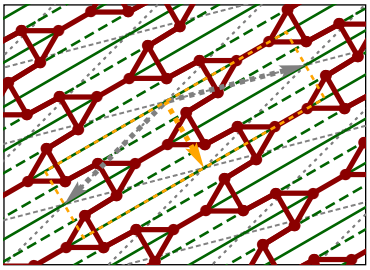

$\delta = -0.45$, $\nu = 0.01$

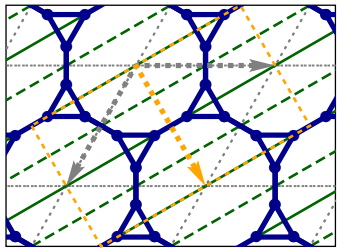

$\delta = 0$, **$\nu = 1.00$**

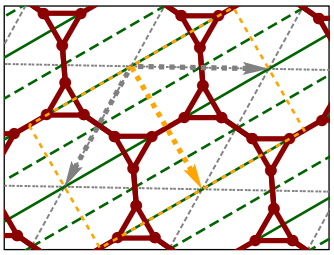

$\delta = 0.02$, $\nu = 1.27$

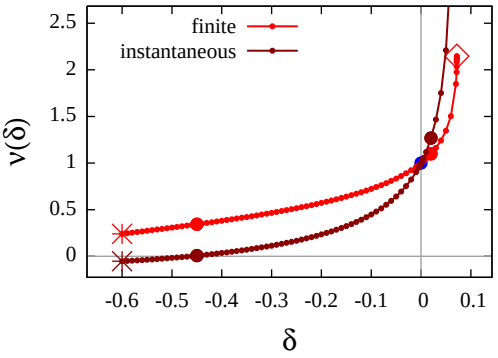

B: tuc | cross	:	9 | 2
N: tuc | neigb. | tot	:	$2\times 2\,b(1), 2\times 1\,a(U)$ | 4 $\sum = 10$
Free|Dep.|Fix $p^i_{x,y}$	:	5 | 14 | 1 $\sum = 20$
Set|Free|Dep.|Fix	:	$a^{\parallel}, b^{\parallel}$ | $a^{\perp}$ | $b^{\perp} = f(\delta, a^{\perp})$ | none
$\langle \frac{B}{N} \rangle$	:	3.00
Z_{Maxwell}	:	4
Reference(s)	:	[24], p.63, Fig.10

Auxetic under finite deformation

6.2.17 Trihexagonal Tiling

↓ 0°

$(3.6.3.6)$ - Hexadeltille (Conway), Kagome | *p6mm* (hexagonal)

$p1$ (oblique)

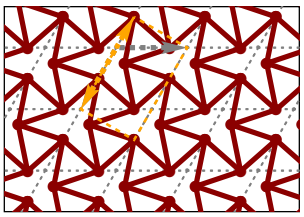

$\delta = -0.25$, $\nu = -1.00$

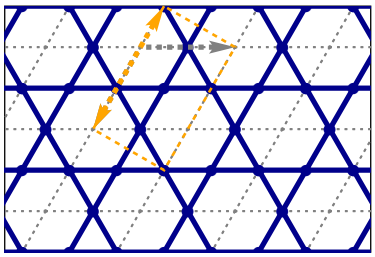

$\delta = 0$, **$\nu = -0.99$**

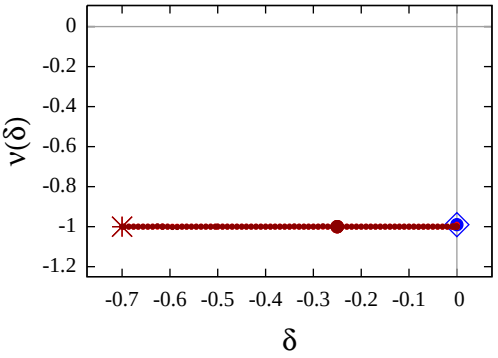

B: tuc | cross	:	6 | 0
N: tuc | neigb. | tot	:	$3\times 1\,a(1)$ | 2 $\sum = 5$
Free|Dep.|Fix $p^i_{x,y}$	:	4 | 4 | 2 $\sum = 10$
Set|Free|Dep.|Fix	:	$a^{\parallel}, b^{\parallel}$ | $a^{\perp}, b^{\perp}$|none|none
$\langle \frac{B}{N} \rangle$	:	4.00
Z_{Maxwell}	:	1
Reference(s)	:	[24], p.63, Fig.9

Auxetic

6.2.18 Small Rhombitrihexagonal Tiling

↓ 0°

(3.4.6.4) - Rhombihexadeltille (Conway) | *p6mm* (hexagonal)

***p6* (hexagonal)**

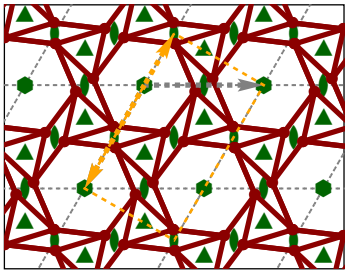

$\delta = -0.15$, $\nu = -1.00$

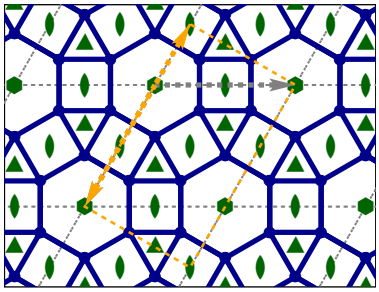

$\delta = 0$, $\boldsymbol{\nu = -1.00}$

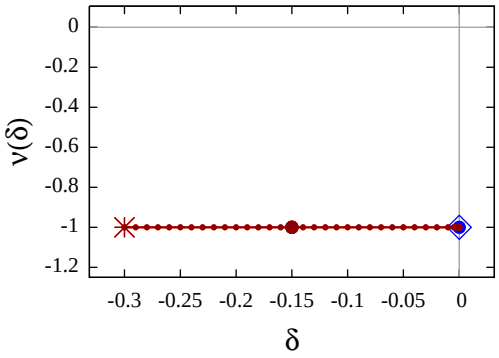

B: tuc | cross	:	12 | 4
N: tuc | neigb. | tot	:	$1 \times 6\, d(1)$ | 8 $\sum = 14$
Free|Dep.|Fix $\mathrm{p}^i_{x,y}$	:	2 | 26 | 0 $\sum = 28$
Set|Free|Dep.|Fix	:	$a^{\parallel}, b^{\parallel}$ | none | $a^{\perp} = \frac{a^{\parallel}+2b^{\parallel}}{-\sqrt{3}}$, $b^{\perp} = \frac{2a^{\parallel}+b^{\parallel}}{\sqrt{3}}$ | N.A.
$\langle \frac{B}{N} \rangle$	:	4.00
Z_{Maxwell}	:	1
Reference(s)	:	[24], p.63, Fig.8

Auxetic

6.2.19 Small Rhombitrihexagonal Tiling

↓ 0°

(3.4.6.4) - Rhombihexadeltille (Conway) | *p6mm* (hexagonal)

***pm*$_r$ (rhombus)**

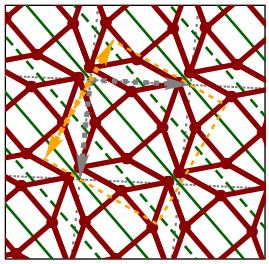

$\delta = -0.30$, $\nu = -0.34$

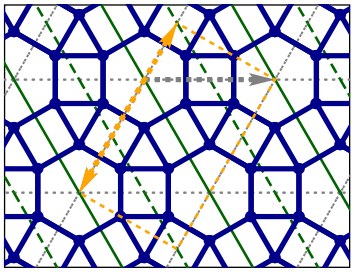

$\delta = 0$, $\boldsymbol{\nu_- = 3.00}$, $\boldsymbol{\nu_+ = -5.00}$

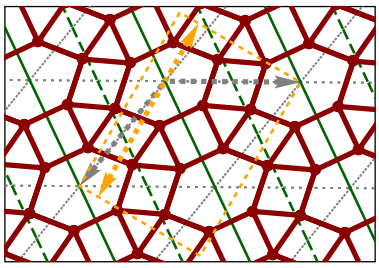

$\delta = 0.024$, $\nu = -\infty$

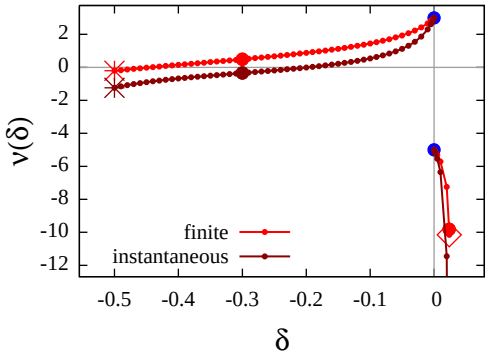

B: tuc | cross	:	12 | 4
N: tuc | neigb. | tot	:	$3 \times 2\, b(1)$ | 8 $\sum = 14$
Free|Dep.|Fix $\mathrm{p}^i_{x,y}$	:	5 | 22 | 1 $\sum = 28$
Set|Free|Dep.|Fix	:	$a^{\parallel}, b^{\parallel}$ | $b^{\perp}$ | $a^{\perp} = f(\delta, b^{\perp})$ | none
$\langle \frac{B}{N} \rangle$	:	4.00
Z_{Maxwell}	:	1
Reference(s)	:	[24], p.63, Fig.8

Auxetic under finite deformation ↓

6.2.20 Great Rhombitrihexagonal Tiling

↓ 0°

(4.6.12) - Truncated Hexadeltille (Conway) | *p6mm* (hexagonal)

***p*6 (hexagonal)**

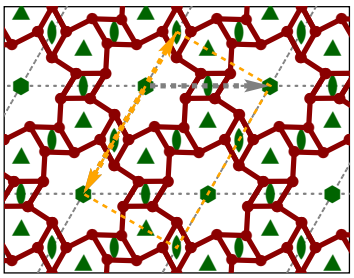

$\delta = -0.10$, $\nu = -1.00$

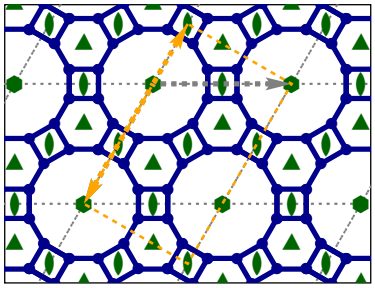

$\delta = 0$, $\boldsymbol{\nu = -1.00}$

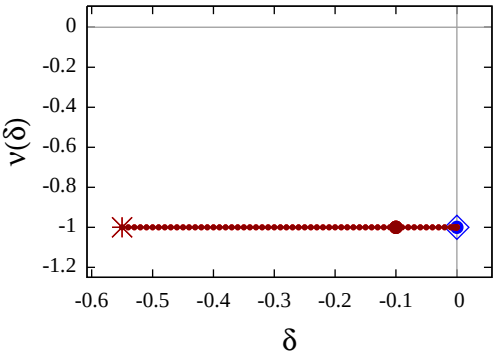

***B*: tuc | cross**	:	18 | 4
***N*: tuc | neigb. | tot**	:	$2 \times 6\, d(1)$ | 8 $\sum = 20$
Free|Dep.|Fix $\mathrm{p}^i_{x,y}$	:	4 | 36 | 0 $\sum = 40$
Set|Free|Dep.|Fix	:	$a^{\parallel}, b^{\parallel}$ | none | $a^{\perp} = \frac{a^{\parallel}+2b^{\parallel}}{-\sqrt{3}}$, $b^{\perp} = \frac{2a^{\parallel}+b^{\parallel}}{\sqrt{3}}$ | N.A.
$\langle \frac{B}{N} \rangle$	:	3.00
$\mathbf{Z}_{\mathbf{Maxwell}}$	:	7
Reference(s)	:	[24], p.63, Fig.11

Auxetic

6.2.21 Great Rhombitrihexagonal Tiling

↓ 0°

(4.6.12) - Truncated Hexadeltille (Conway) | *p6mm* (hexagonal)

***p*31*m* (hexagonal)**

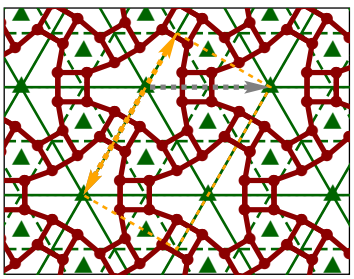

$\delta = -0.10$, $\nu = -1.00$

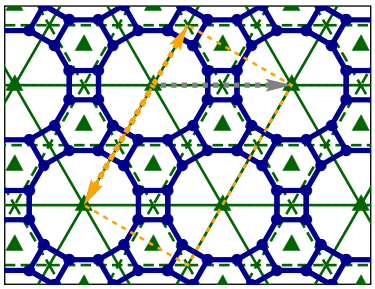

$\delta = 0$, $\boldsymbol{\nu = -1.00}$

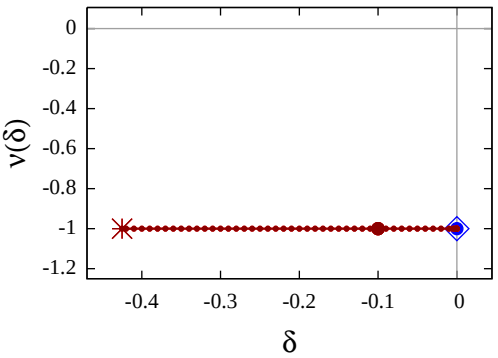

***B*: tuc | cross**	:	18 | 4
***N*: tuc | neigb. | tot**	:	$2 \times 6\, d(1)$ | 8 $\sum = 20$
Free|Dep.|Fix $\mathrm{p}^i_{x,y}$	:	4 | 36 | 0 $\sum = 40$
Set|Free|Dep.|Fix	:	$a^{\parallel}, b^{\parallel}$ | none | $a^{\perp} = \frac{a^{\parallel}+2b^{\parallel}}{-\sqrt{3}}$, $b^{\perp} = \frac{2a^{\parallel}+b^{\parallel}}{\sqrt{3}}$ | N.A.
$\langle \frac{B}{N} \rangle$	:	3.00
$\mathbf{Z}_{\mathbf{Maxwell}}$	:	7
Reference(s)	:	[24], p.63, Fig.11

Auxetic

6.3 2-Uniform Tilings

The *2-uniform tilings* are *20* tessellations with two different types of vertices. They show like the Archimedean tilings different deformation behaviour. The Tables 6.5 and 6.6 lists the infinitesimal results. There are rigid, auxetic, non-auxetic with and without symmetry constraints tilings and tilings which has in no setting a unique deformation mode.

The two rigid tilings, (*2-uniform 1* and *2*) are shown in section 6.6. Again directly neighboured triangles which share a common bar are the reason for the rigidity.

There are several tilings which can only be sheared (*2-uniform 3, 4, 8, 12, 15* and *19*) and have a diverging Poisson's ratio in the lattice directions for $\delta \to 0$. Tilings 3,4,8,15 are already in group $p1$ unique, 12 and 19 in $c2$. Tiling 19 has a different deformation behaviour in the group $c11m$, a pure auxetic (6.3.26). This behaviour shows only this tiling i.e. beside the shear having an auxetic mechanism in a different group.

Tilings 6 and 11 have two deformation mechanisms dependent on the retained symmetry group. Auxetic behaviour is imposed due to the constraining hexagonal or square groups. This regards to these (6.3.9, 6.3.14) and to the tilings 16 and 20 (6.3.21, 6.3.27). There are two tilings which are auxetic in rectangular groups (14 and 19). 2-uniform 14 have

Table 6.5: *Infinitesimal deformation behaviour of 2-uniform tessellations 1–7, see Table 6.1 for explanation of symbols*

Group	***p6mm***	***p6***	***p31m***	***p3m1***	***p3***	***p4gm***	***p4mm***	***p4***
Lattice Type	hexagonal					square		
2-Uniform 1 ($p6$) **rigid:** 6.6.3	-	R	-	-	R	-	-	-
2-Uniform 2 ($p6mm$) **rigid:** 6.6.4	R	R	R	R	R	-	-	-
2-Uniform 3 ($c2mm$) **unique:** 6.3.1, 6.3.2	-	-	-	-	-	-	-	-
2-Uniform 4 ($p2mm$) **unique:** 6.3.5, 6.3.3, 6.3.4	-	-	-	-	-	-	-	-
2-Uniform 5 ($p6mm$) **unique:** 6.3.6	R	$\mathbf{-1}^{\ddagger\downarrow}$	R	R	$\mathbf{-1}^{\ddagger\downarrow}$	-	-	-
2-Uniform 6 ($p6mm$) **2 sym. modes:** 6.3.9; 6.3.7, 6.3.8	R	$\mathbf{-1}^{\ddagger\downarrow}$	R	R	$\underline{\mathbf{-1}}^{\ddagger\downarrow}$	-	-	-
2-Uniform 7 ($p6mm$) **unique:** 6.3.10	R	$\mathbf{-1}^{\ddagger\downarrow}$	R	R	$\mathbf{-1}^{\ddagger\downarrow}$	-	-	-

two different auxetic mechanisms (6.3.18, 6.3.19) which are denoted in the Table 6.6 with numbers in bracket to indicate that different retained groups lead to the same mechanism. Both with a constant Poisson's ratio of -1. But the point of mutually overlap of joints and bars occurs at a different strain δ.

The new identified auxetic tilings are the 2-uniform 5 and 2-uniform 7 tiling which have only one degree of freedom in their skeletal structure and hence unique deformable in $p1$ (6.3.6, 6.3.10). Note the same deformation mechanism of 2-uniform 5 and the Archimedean tiling small rhombitrihexagonal (6.2.18). The only difference is that in the Archimedean case symmetries are necessary to make the hexagon rigid which is in the case of the 2-uniform 5 rigid due to triangles. The triangulation of the hexagon has lead to a structure with only one degree of freedom and so the symmetry constraints are not necessary anymore. This regards also to the truncated square tiling and some others. Hence the determination of different mechanisms of underconstrained skeletal structure with symmetries can help to find auxetic mechanisms. Some cases offers the possibility to modify in an appropriate way the skeletal structure to make symmetries redundant.

Table 6.5: *Infinitesimal deformation behaviour of 2-uniform tessellations 1–7, see Table 6.1 for explanation of symbols*

c2mm	**p2gg**	**p2mg**	**p2mm**	**cm**	**pg**	**pm**	**p2**	**p1**
rectangular (or rhombus in specific subgroups)							oblique	
-	-	-	-	-	-	-	R	$\underline{\mathrm{R}}$
R_{30}	-	-	-	R_{26}, R_{27}	-	-	R	$\underline{\mathrm{R}}$
R	-	-	-	R, R_{25}	-	-	$\infty_{19}^{0^\circ\ddagger\downarrow}$ $1_{19}^{45^\circ}$ $\infty_{19}^{90^\circ\ddagger\downarrow}$	$\underline{\infty}_{18}^{0^\circ\ddagger\downarrow}$ $1_{18}^{45^\circ}$ $\underline{\infty}_{18}^{90^\circ\ddagger\downarrow}$
-	-	-	R	-	-	R, R_{21}	R^{0° $\underline{1}^{45^\circ}$ R^{90°	$\underline{\infty}^{0^\circ\ddagger\downarrow}$ 1^{45° $\underline{\infty}^{90^\circ\ddagger\downarrow}$
R_{30}	-	-	-	R_{26}, R_{27}	-	-	$-1^{\ddagger\downarrow}$	$\underline{-1}^{\ddagger\downarrow}$
$\mathrm{N}_{30}^{0^\circ}$ $1_{30}^{60^\circ}$	-	-	-	$\underline{\mathrm{N}}_{26}^{0^\circ}$, $\mathrm{N}_{27}^{0^\circ}$ $\underline{1}_{26}^{60^\circ}$, $1_{27}^{60^\circ}$	-	-	U	U
R_{30}	-	-	-	R_{26}, R_{27}	-	-	$\mathbf{-1}^{\ddagger\downarrow}$	$\underline{\mathbf{-1}}^{\ddagger\downarrow}$

Table 6.6: *Infinitesimal deformation behaviour of 2-uniform tessellations 8–20.*

Group	**p6mm**	**p6**	**p31m**	**p3m1**	**p3**	**p4gm**	**p4mm**	**p4**
Lattice type	hexagonal					square		
2-Uniform 8 ($c2mm$) **unique:** 6.3.11	-	-	-	-	-	-	-	-
2-Uniform 9 ($p4gm$) **unique:** 6.3.12	-	-	-	-	-	R	-	R
2-Uniform 10 ($p2gg$) **unique:** 6.3.13	-	-	-	-	-	-	-	-
2-Uniform 11 ($p6mm$) **2 sym. modes:** 6.3.14; 6.3.15	R	**–1**‡	R	R	**–1**‡	-	-	-
2-Uniform 12 ($c2mm$) **1 sym. mode:** 6.3.16	-	-	-	-	-	-	-	-
2-Uniform 13 ($c2mm$) **no mode**, e.g. 6.3.17	-	-	-	-	-	-	-	-
2-Uniform 14 ($p6mm$) **2 sym. modes:** 6.3.18; 6.3.19	R	$\mathbf{-1}^{\ddagger\downarrow}_{(1)}$	$\mathbf{-1}^{\ddagger\downarrow}_{(2)}$	R	$\mathbf{-1}^{\ddagger\downarrow}_{(2)}$	-	-	-
2-Uniform 15 ($p2mm$) **unique:** 6.3.20	-	-	-	-	-	-	-	-
2-Uniform 16 ($p4mm$) **1 sym. mode:** 6.3.21	-	-	-	-	-	-	R	**–1**$^{\ddagger\downarrow}$
2-Uniform 17 ($p6mm$) **1 sym. mode:** 6.3.22	R	U	R	R	U	-	-	-
2-Uniform 18 ($p2mm$) **no mode, e.g.** 6.3.23	-	-	-	-	-	-	-	-
2-Uniform 19 ($c2mm$) **2 sym modes:** 6.3.25, 6.3.26; 6.3.24	-	-	-	-	-	-	-	-
2-Uniform 20 ($p6mm$) **1 sym. mode:** 6.3.27	R	U	**–1**$^{\ddagger\downarrow}$	R	U	-	-	-

Table 6.6: *Infinitesimal deformation behaviour of 2-uniform tessellations 8–20.*

c2mm	**p2gg**	**p2mg**	**p2mm**	**cm**	**pg**	**pm**	**p2**	**p1**
rectangular (or rhombus in specific subgroups)							oblique	
R	-	-	-	R, R_{25}	-	-	$\infty_{19}^{0^\circ\ddagger\downarrow}$ $1_{19}^{45^\circ}$ $\infty_{19}^{90^\circ\ddagger\downarrow}$	$\underline{\infty}_{18}^{0^\circ\ddagger\downarrow}$ $1_{18}^{45^\circ}$ $\infty_{18}^{90^\circ\ddagger\downarrow}$
R_{31}	1^{0°	-	-	R_{28}	R_{23}	-	1^{0°	$\underline{1}^{0^\circ}$
-	1^{0° 1^{90°	-	-	-	$1_{23}^{0^\circ}$, $1_{24}^{0^\circ}$ $1_{23}^{90^\circ}$, $1_{24}^{90^\circ}$	-	1^{0° 1^{90°	$\underline{1}^{0^\circ}$ 1^{90°
$N_{30}^{0^\circ}$ $1_{30}^{60^\circ}$	-	-	-	$\underline{N}_{26}^{0^\circ}$, $N_{27}^{0^\circ}$ $1_{26}^{60^\circ}$, $1_{27}^{60^\circ}$	-	-	U	U
R	-	-	-	R, R_{25}	-	-	$R_{19}^{0^\circ}$ $\underline{1}_{19}^{45^\circ}$ $R_{19}^{90^\circ}$	U_{18}
R	-	-	-	R, R_{25}	-	-	$\underline{U}_{19}$	U_{18}
R_{30}	-	-	-	$\underline{\mathbf{-1}}_{26,(2)}^{\ddagger\downarrow}$, R_{27}	-	-	$\underline{\mathbf{-1}}_{(1)}^{\ddagger\downarrow}$	U
-	-	-	R	-	-	R, R_{21}	R^{0° 1^{45° R^{90°	$\underline{\infty}^{0^\circ}$ 1^{45° ∞^{90°
U_{30}	-	-	R	U_{26}	-	R	U	U
$N_{30}^{0^\circ}$ $1_{30}^{60^\circ}$	-	-	-	$\underline{N}_{26}^{0^\circ}$, $N_{27}^{0^\circ}$ $1_{26}^{60^\circ}$, $1_{27}^{60^\circ}$	-	-	U	U
-	-	-	R	-	-	R, R_{21}	$\underline{U}$	U
R	-	-	-	R, $\underline{\mathbf{-0.63}}_{25}^{0^\circ\ddagger\downarrow}$ $\underline{\mathbf{-0.75}}_{25}^{45^\circ\ddagger\downarrow}$ $\underline{\mathbf{-1.58}}_{25}^{90^\circ\ddagger\downarrow}$	-	-	$R_{19}^{0^\circ}$ $\underline{1}_{19}^{45^\circ}$ $R_{19}^{90^\circ}$	U_{18}
U_{30}	-	-	-	U_{26}, U_{27}	-	-	U	U

Further tilings with one degree of freedom are the 2-uniform 9 and 10 which have the same graph of Poisson's ratio as function of the imposed strain δ (6.3.12, 6.3.13). They become auxetic at the strain magnitude of $\delta = -0.1$. There are some tilings which also have auxetic behaviour for finite deformations but with additional symmetry constraints, namely the second deformation mechanisms of the tilings 6 and 11 (6.3.7,6.3.15) and additionally the only mechanism of tiling 17 (6.3.22). These are mechanisms in the groups with a rhombus as unit cell and show also the discussed jump point at $\delta = 0$ for the deformation in lattice direction (see paragraph in section 6.2 on page 62).

The tilings 13 and 18 have in no symmetry group a unique deformation mechanism and hence no Poisson's ratio is given. For examples of non-unique deformation mechanism the results of the deformation in their highest non-rigid symmetry group are showed, 6.3.17 and 6.3.23.

6.3.1 2-Uniform 3

$\downarrow 0°$

$(3^6;3^3.4^2)_1$ | $c2mm$ (rectangular)

$c1$ (oblique)

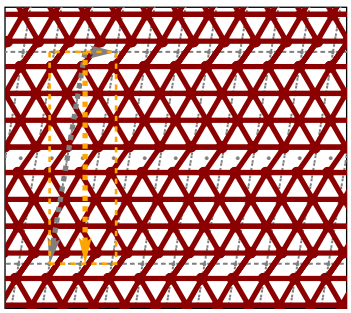

$\delta = -0.05$, $\nu = 4.57$

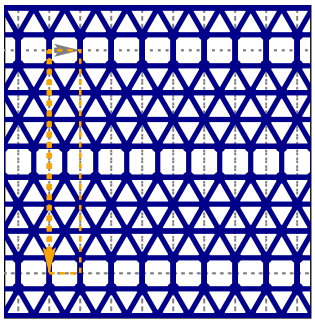

$\delta = 0$, $\boldsymbol{\nu = \infty}$

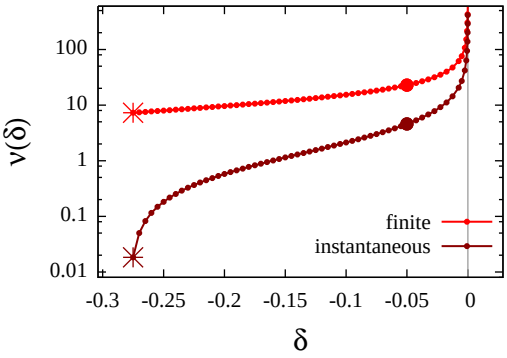

B: tuc | cross	:	23 | 6
N: tuc | neigb. | tot	:	$4 \times 2\,a(1)$ | 16 $\sum = 24$
Free|Dep.|Fix $p^i_{x,y}$	:	6 | 40 | 2 $\sum = 48$
Set|Free|Dep.|Fix	:	$a^{\parallel}, b^{\parallel}$ | $a^{\perp}, b^{\perp}$|none|none
$\langle \frac{B}{N} \rangle$	:	5.75
$Z_{Maxwell}$	:	-6
Reference(s)	:	[24], p.67 , fig.12

Not auxetic

6.3.2 2-Uniform 3

$\rightarrow 90°$

$(3^6;3^3.4^2)_1$ | $c2mm$ (rectangular)

$c1$ (oblique)

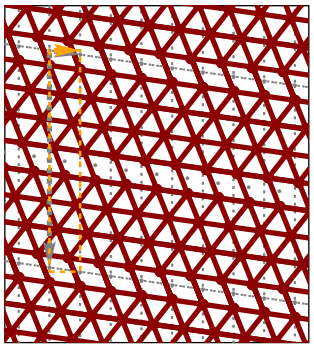

$\delta = -0.01$, $\nu = -1.74$

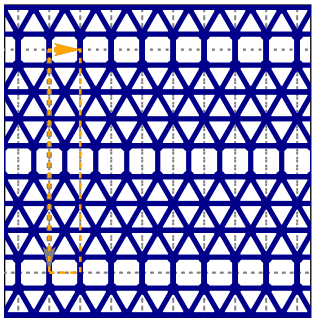

$\delta = 0$, $\boldsymbol{\nu = \infty}$

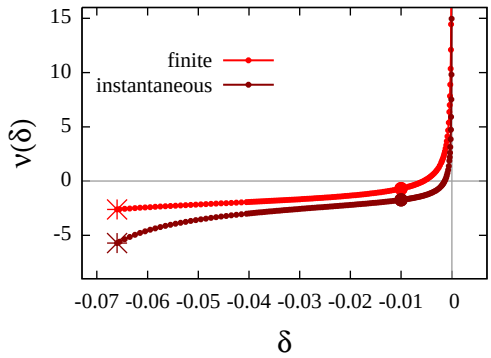

B: tuc | cross	:	23 | 6
N: tuc | neigb. | tot	:	$4 \times 2\,a(1)$ | 16 $\sum = 24$
Free|Dep.|Fix $p^i_{x,y}$	:	6 | 40 | 2 $\sum = 48$
Set|Free|Dep.|Fix	:	$a^{\parallel}, b^{\parallel}$ | $a^{\perp}, b^{\perp}$|none|none
$\langle \frac{B}{N} \rangle$	:	5.75
$Z_{Maxwell}$	:	-6
Reference(s)	:	[24], p.67 , fig.12

Auxetic under finite deformation

6.3.3 2-Uniform 4

$\downarrow 0°$

$(3^6;3^3.4^2)_2$ | $p2mm$ (rectangular) — **$p1$ (oblique)**

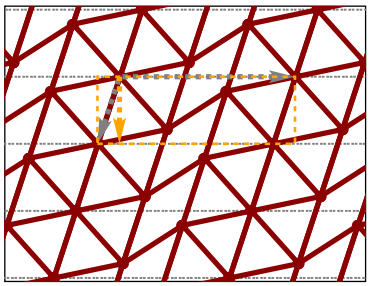

$\delta = -0.05$, $\nu = -0.71$

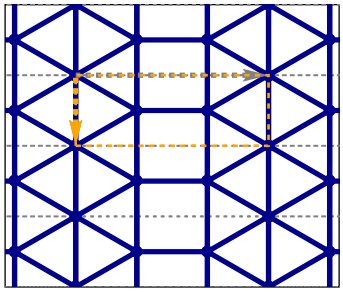

$\delta = 0$, $\boldsymbol{\nu = \infty}$

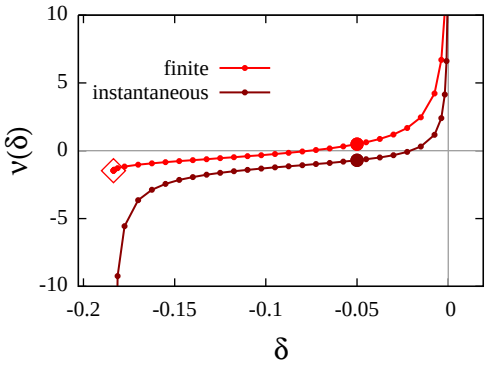

B: tuc | cross	:	8 | 3
N: tuc | neigb. | tot	:	$3 \times 1\, a(1)$ | 7 $\sum = 10$
Free|Dep.|Fix $\mathrm{p}^i_{x,y}$	:	4 | 14 | 2 $\sum = 20$
Set|Free|Dep.|Fix	:	$a^{\parallel}, b^{\parallel}$ | $a^{\perp}, b^{\perp}$|none|none
$\langle \frac{B}{N} \rangle$	:	5.33
$\mathbf{Z}_{\mathbf{Maxwell}}$	:	-1
Reference(s)	:	[24], p.67, fig.12

Auxetic under finite deformation

6.3.4 2-Uniform 4

$\rightarrow 90°$

$(3^6;3^3.4^2)_2$ | $p2mm$ (rectangular) — **$p1$ (oblique)**

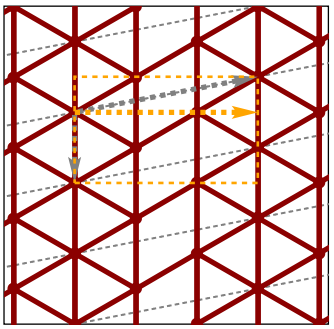

$\delta = -0.05$, $\nu = 2.95$

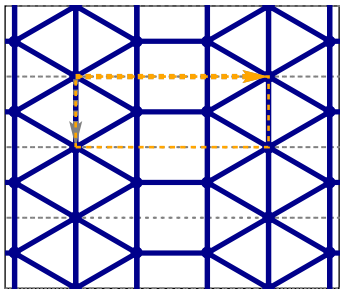

$\delta = 0$, $\boldsymbol{\nu = \infty}$

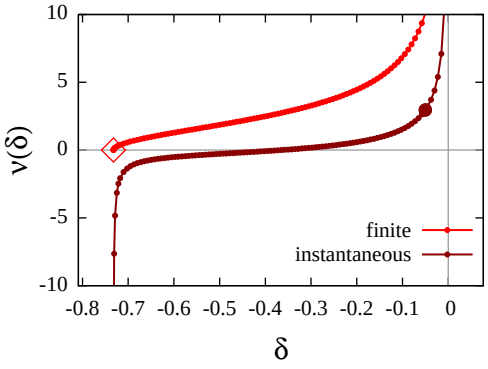

B: tuc | cross	:	8 | 3
N: tuc | neigb. | tot	:	$3 \times 1\, a(1)$ | 7 $\sum = 10$
Free|Dep.|Fix $\mathrm{p}^i_{x,y}$	:	4 | 14 | 2 $\sum = 20$
Set|Free|Dep.|Fix	:	$a^{\parallel}, b^{\parallel}$ | $a^{\perp}, b^{\perp}$|none|none
$\langle \frac{B}{N} \rangle$	:	5.33
$\mathbf{Z}_{\mathbf{Maxwell}}$	:	-1
Reference(s)	:	[24], p.67, fig.12

Auxetic under finite deformation

6.3.5 2-Uniform 4

$(3^6;3^3.4^2)_2$ | *p2mm* (rectangular)

↘ 45°
***p*2 (oblique)**

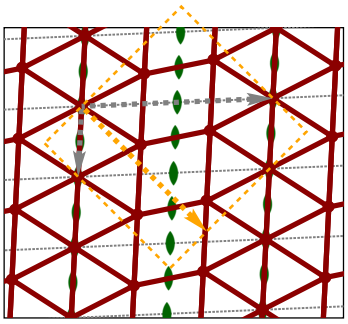

$\delta = -0.05$, $\nu = 0.50$

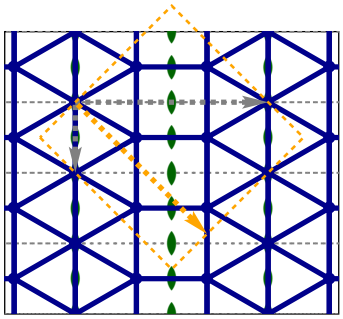

$\delta = 0$, $\boldsymbol{\nu = 1.00}$

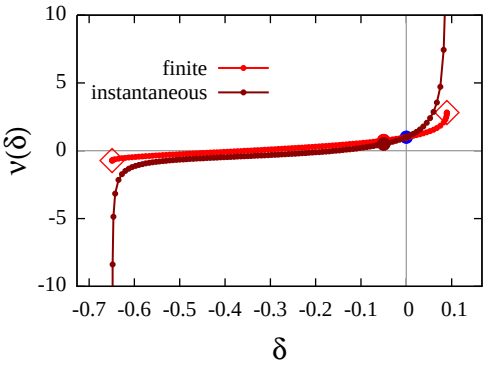

***B*: tuc | cross**	: 8 | 3	
***N*: tuc | neigb. | tot**	: $1\times 2\,e(1), 1\times 1\,a(2)$ | 7	$\sum = 10$
Free|Dep.|Fix $\mathrm{p}^i_{x,y}$	: 2 | 18 | 0	$\sum = 20$
Set|Free|Dep.|Fix	: $a^{\parallel}, b^{\parallel}$ | $a^{\perp}, b^{\perp}$|none|none	
$\langle \frac{B}{N} \rangle$	: 5.33	
$\mathbf{Z}_{\mathbf{Maxwell}}$	: -1	
Reference(s)	: [24], p.67, fig.12	

Auxetic under finite deformation

6.3.6 2-Uniform 5

$(3^6;3^2.4.3.4)$ | *p6mm* (hexagonal)

↓ 0°
***p*1 (oblique)**

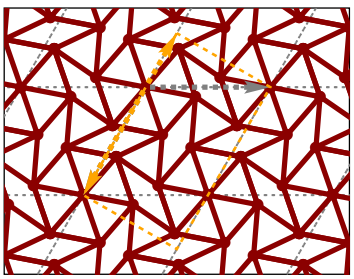

$\delta = -0.10$, $\nu = -1.00$

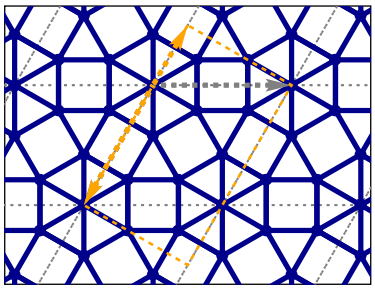

$\delta = 0$, $\boldsymbol{\nu = -1.00}$

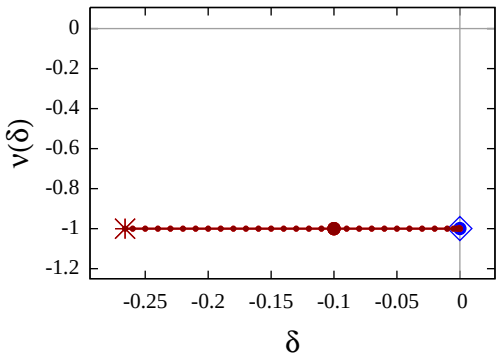

***B*: tuc | cross**	: 18 | 4	
***N*: tuc | neigb. | tot**	: $7\times 1\,a(1)$ | 11	$\sum = 18$
Free|Dep.|Fix $\mathrm{p}^i_{x,y}$	: 12 | 22 | 2	$\sum = 36$
Set|Free|Dep.|Fix	: $a^{\parallel}, b^{\parallel}$ | $a^{\perp}, b^{\perp}$|none|none	
$\langle \frac{B}{N} \rangle$	: 5.14	
$\mathbf{Z}_{\mathbf{Maxwell}}$	: -3	
Reference(s)	: [24] p. 67, Fig. 3	

Auxetic

6.3.7 2-Uniform 6

$\downarrow$ **0°**

$(3^6;3^4.4.12)$ | *p6mm* (hexagonal)

***pm*$_r$ (rhombus)**

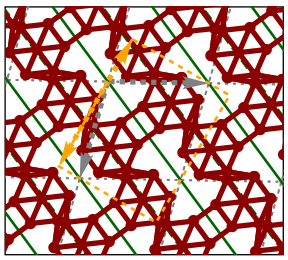

$\delta = -0.25$, $\nu = -1.25$

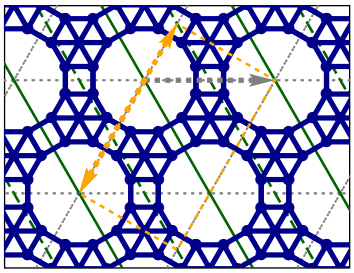

$\delta = 0$, $\boldsymbol{\nu_- = 3.00}$, $\boldsymbol{\nu_+ = -5.00}$

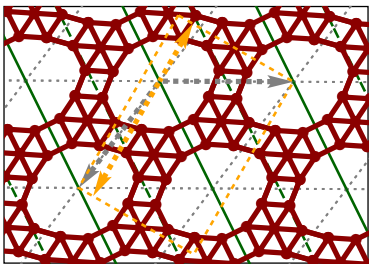

$\delta = 0.018$, $\nu = -\infty$

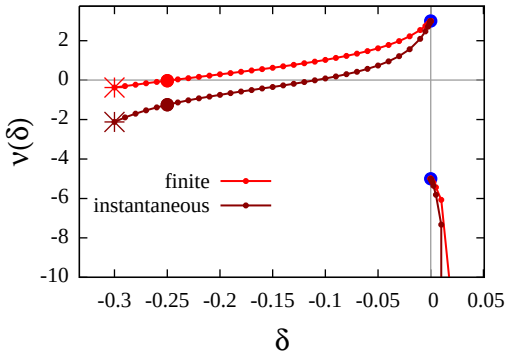

***B*: tuc | cross**	:	30 | 4
***N*: tuc | neigb. | tot**	:	$7 \times 2\,b(1)$ | 8 $\sum = 22$
Free|Dep.|Fix $\mathrm{p}^i_{x,y}$	:	13 | 30 | 1 $\sum = 44$
Set|Free|Dep.|Fix	:	$a^{\parallel}, b^{\parallel}$ | $b^{\perp}$ | $a^{\perp} = f(\delta, b^{\perp})$ | none
$\langle \frac{B}{N} \rangle$	:	4.29
$\mathbf{Z}_{\mathbf{Maxwell}}$	:	-1
Reference(s)	:	[24], p.67, Fig.12

Auxetic under finite deformation $\downarrow$

6.3.8 2-Uniform 6

$\searrow$ **60°**

$(3^6;3^4.4.12)$ | *p6mm* (hexagonal)

***pm*$_r$ (rhombus)**

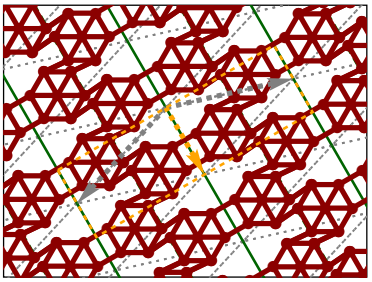

$\delta = -0.40$, $\nu = -0.02$

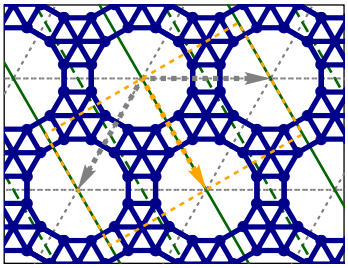

$\delta = 0$, $\boldsymbol{\nu = 1.00}$

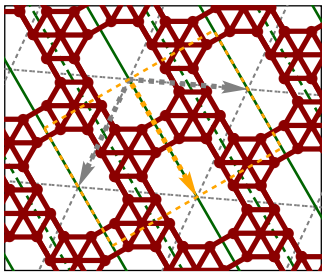

$\delta = 0.057$, $\nu = \infty$

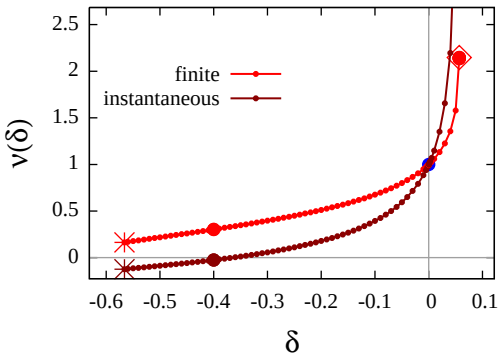

***B*: tuc | cross**	:	30 | 4
***N*: tuc | neigb. | tot**	:	$7 \times 2\,b(1)$ | 8 $\sum = 22$
Free|Dep.|Fix $\mathrm{p}^i_{x,y}$	:	13 | 30 | 1 $\sum = 44$
Set|Free|Dep.|Fix	:	$a^{\parallel}, b^{\parallel}$ | $a^{\perp}$ | $b^{\perp} = f(\delta, a^{\perp})$ | none
$\langle \frac{B}{N} \rangle$	:	4.29
$\mathbf{Z}_{\mathbf{Maxwell}}$	:	-1
Reference(s)	:	[24], p.67, Fig.12

Auxetic under finite deformation

6.3.9 2-Uniform 6

$(3^6;3^4.4.12)$ | *p6mm* (hexagonal)

↓ 0°
$p3$ (hexagonal)

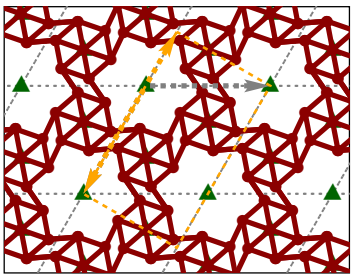

$\delta = -0.10$, $\nu = -1.00$

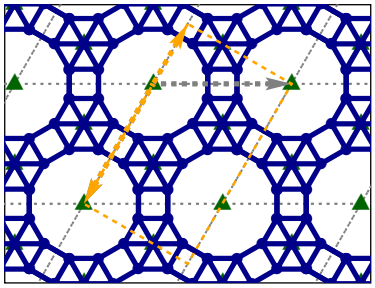

$\delta = 0$, $\boldsymbol{\nu = -1.00}$

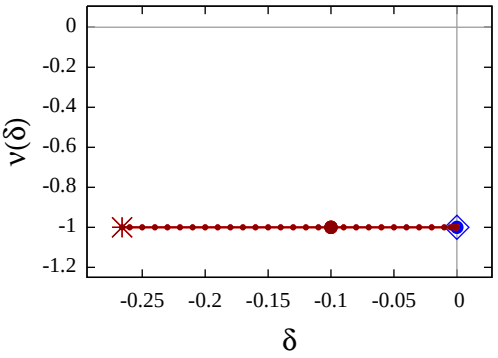

B: tuc | cross	:	30 | 4
N: tuc | neigb. | tot	:	$4\times3\,d(1), 1\times1\,c(3..), 1\times1\,b(3..)$ | 8 $\sum = 22$
Free|Dep.|Fix $\mathrm{p}^i_{x,y}$	:	8 | 36 | 0 $\sum = 44$
Set|Free|Dep.|Fix	:	$a^{\parallel}, b^{\parallel}$ | none | $a^{\perp} = \frac{a^{\parallel}+2b^{\parallel}}{-\sqrt{3}}$, $b^{\perp} = \frac{2a^{\parallel}+b^{\parallel}}{\sqrt{3}}$ | N.A.
$\langle\frac{B}{N}\rangle$	:	4.29
Z_{Maxwell}	:	-1
Reference(s)	:	[24], p.67, Fig.12

Auxetic

6.3.10 2-Uniform 7

$(3^6;3^2.6^2)$ | *p6mm* (hexagonal)

↓ 0°
$p1$ (oblique)

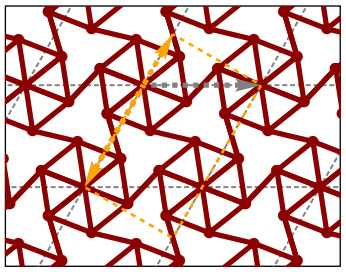

$\delta = -0.15$, $\nu = -1.00$

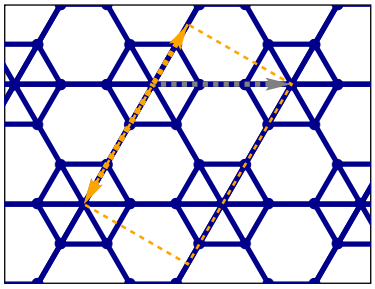

$\delta = 0$, $\boldsymbol{\nu = -0.99}$

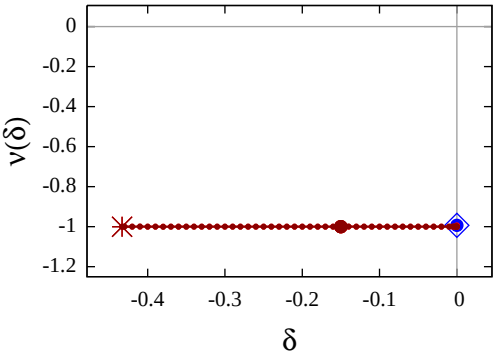

B: tuc | cross	:	15 | 6
N: tuc | neigb. | tot	:	$7\times1\,a(1)$ | 7 $\sum = 14$
Free|Dep.|Fix $\mathrm{p}^i_{x,y}$	:	12 | 14 | 2 $\sum = 28$
Set|Free|Dep.|Fix	:	$a^{\parallel}, b^{\parallel}$ | $a^{\perp}, b^{\perp}$|none|none
$\langle\frac{B}{N}\rangle$	:	4.29
Z_{Maxwell}	:	0
Reference(s)	:	[24], p.63, Fig.12

Auxetic

6.3.11 2-Uniform 8

$\downarrow 0°$

$(3^4.6;3^2.6^2)$ | $c2mm$ (rectangular)

$c1$ (oblique)

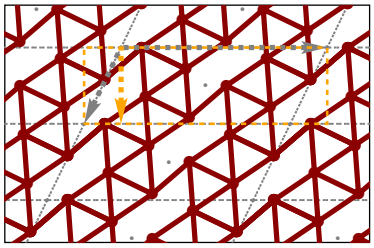

$\delta = -0.1$, $\nu = -0.87$

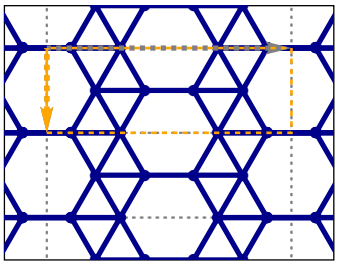

$\delta = 0$, $\boldsymbol{\nu = \infty}$

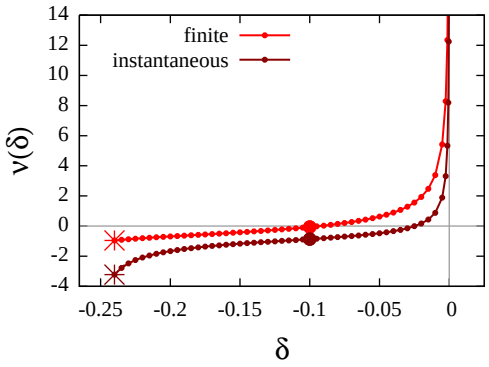

B: tuc | cross	:	19 | 4
N: tuc | neigb. | tot	:	$4 \times 2\,a(1)$ | 8 $\sum = 16$
Free|Dep.|Fix $\mathrm{p}^i_{x,y}$	:	6 | 24 | 2 $\sum = 32$
Set|Free|Dep.|Fix	:	$a^{\parallel}, b^{\parallel}$ | $a^{\perp}, b^{\perp}$|none|none
$\langle \frac{B}{N} \rangle$	:	4.75
$\mathbf{Z}_{\mathbf{Maxwell}}$	:	-2
Reference(s)	:	[24], p.67, Fig.12

Auxetic under finite deformation

6.3.12 2-Uniform 9

$\downarrow 0°$

$(3^3.4^2;3^2.4.3.4)1$ | $p4gm$ (square)

$p1$ (oblique)

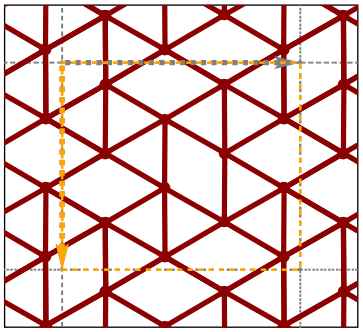

$\delta = -0.10$, $\nu = 0.01$

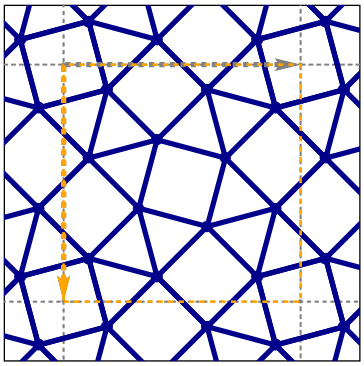

$\delta = 0$, $\boldsymbol{\nu = 1.00}$

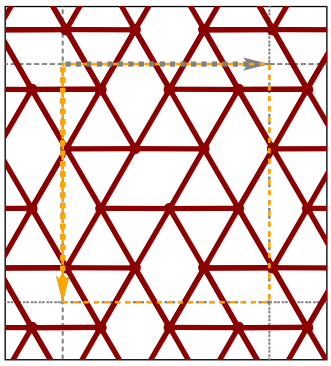

$\delta = 0.035$, $\nu = \infty$

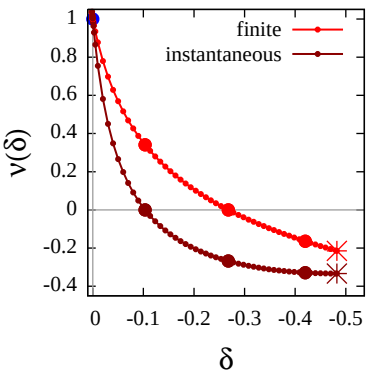

B: tuc | cross	:	30 | 10
N: tuc | neigb. | tot	:	$12 \times 1\,a(1)$ | 12 $\sum = 24$
Free|Dep.|Fix $\mathrm{p}^i_{x,y}$	:	22 | 24 | 2 $\sum = 48$
Set|Free|Dep.|Fix	:	$a^{\parallel}, b^{\parallel}$ | $a^{\perp}, b^{\perp}$|none|none
$\langle \frac{B}{N} \rangle$	:	5.00
$\mathbf{Z}_{\mathbf{Maxwell}}$	:	-5
Reference(s)	:	[24], p.67, Fig.12

Auxetic under finite deformation

6.3.13 2-Uniform 10

$\downarrow 0°$

$(3^3.4^2;3^2.4.3.4)2$ | $p2gg$ (rectangular)

***p*1 (oblique)**

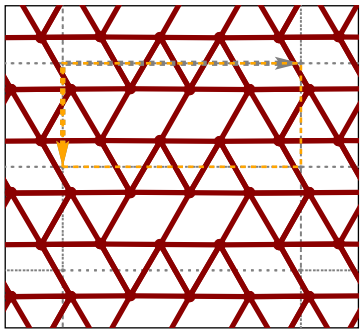

$\delta = -0.10$, $\nu = 0.01$

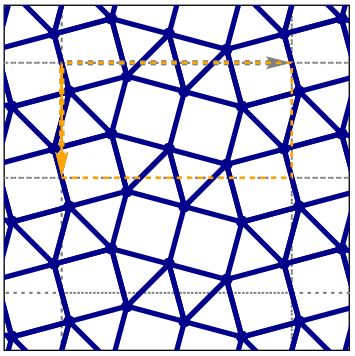

$\delta = 0$, $\boldsymbol{\nu = 1.00}$

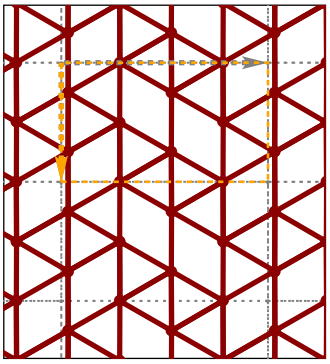

$\delta = 0.035$, $\nu = \infty$

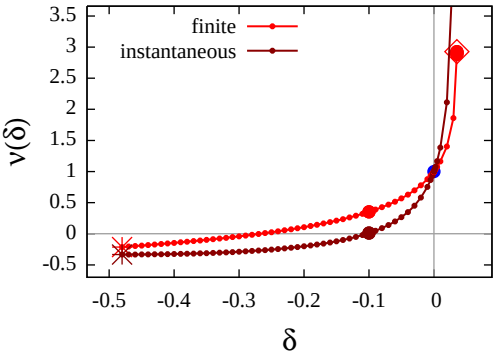

***B*: tuc | cross**	:	20 | 9
***N*: tuc | neigb. | tot**	:	$8 \times 1\, a(1)$ | 12 $\sum = 20$
Free|Dep.|Fix $\mathrm{p}^i_{x,y}$	:	14 | 24 | 2 $\sum = 40$
Set|Free|Dep.|Fix	:	$a^{\parallel}, b^{\parallel}$ | $a^{\perp}, b^{\perp}$|none|none
$\langle \frac{B}{N} \rangle$	:	5.00
$\mathbf{Z}_{\mathbf{Maxwell}}$	:	-3
Reference(s)	:	[24], p.67, Fig.12

Auxetic under finite deformation

6.3.14 2-Uniform 11

$\downarrow 0°$

$(3^3.4^2;3.4.6.4)$ | $p6mm$ (hexagonal)

***p*3 (hexagonal)**

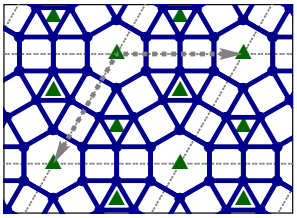

***B*: tuc | cross**	:	27 | 6
***N*: tuc | neigbour | total**	:	$4 \times 3\, d(1)$ | 12 $\sum = 24$
Free|Depend.|Fixed $\mathrm{p}^i_{x,y}$	:	8 | 40 | 0 $\sum = 48$
Set|Free|Depend.|Fixed	:	$a^{\parallel}, b^{\parallel}$ | none | $a^{\perp} = \frac{a^{\parallel}+2b^{\parallel}}{-\sqrt{3}}$, $b^{\perp} = \frac{2a^{\parallel}+b^{\parallel}}{\sqrt{3}}$ | N.A.
$\langle \frac{B}{N} \rangle$	:	4.50
$\mathbf{Z}_{\mathbf{Maxwell}}$	:	-2
Reference(s)	:	[24], p.67, Fig.12

Auxetic

6.3.15 2-Uniform 11

$(3^3.4^2;3.4.6.4)$ | $p6mm$ (hexagonal)

↓ 0°

pm_r (rhombus)

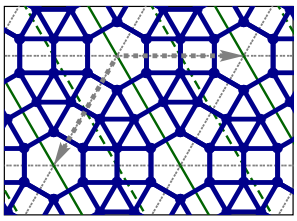

B: tuc | cross	:	27 | 6
N: tuc | neigbour | total	:	$6 \times 2\,b(1)$ | 12 $\sum = 24$
Free|Depend.|Fixed $p^i_{x,y}$	:	11 | 36 | 1 $\sum = 48$
Set|Free|Depend.|Fixed	:	$a^{\|\|}, b^{\|\|}$ | $b^{\perp}$ | $a^{\perp} = f(\delta, b^{\perp})$ | none
$\langle \frac{B}{N} \rangle$	:	4.50
$Z_{Maxwell}$	:	-2
Reference(s)	:	[24], p.67, Fig.12

Auxetic under finite deformation ↓

6.3.16 2-Uniform 12

$(3^3.4^2;4^4)1$ | $c2mm$ (rectangular)

↘ 45°

$c2$ (oblique)

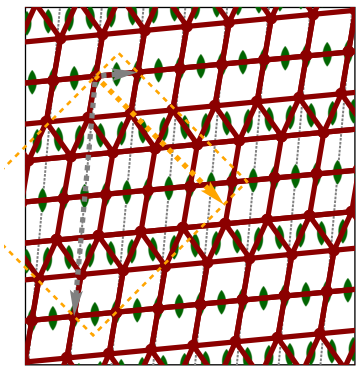

$\delta = -0.10$, $\nu = 0.52$

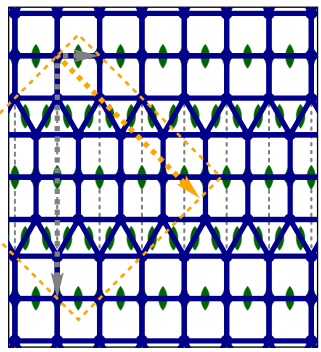

$\delta = 0$, **ν = 1.00**

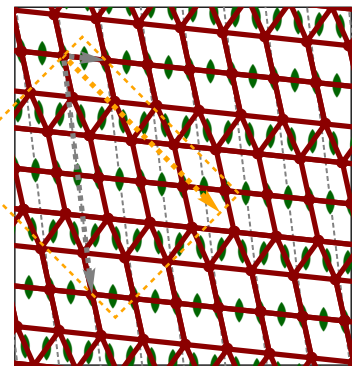

$\delta = 0.1$, $\nu = 2.23$

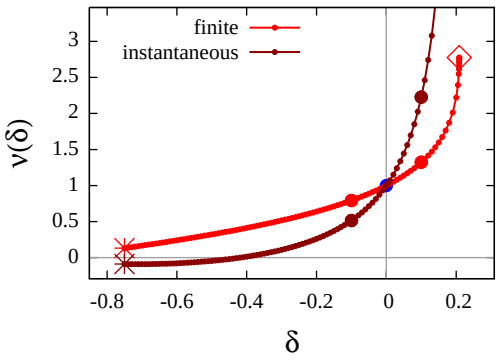

B: tuc | cross	:	14 | 6
N: tuc | neigb. | tot	:	$1 \times 4\,d(1), 1 \times 2\,a(2)$ | 11 $\sum = 17$
Free|Dep.|Fix $p^i_{x,y}$	:	2 | 32 | 0 $\sum = 34$
Set|Free|Dep.|Fix	:	$a^{\|\|}, b^{\|\|}$ | $a^{\perp}, b^{\perp}$|none|none
$\langle \frac{B}{N} \rangle$	:	4.67
$Z_{Maxwell}$	:	-1
Reference(s)	:	[24], p.67, Fig.12

Auxetic under finite deformation

6.3.17 2-Uniform 13

$\downarrow 0°$

$(3^3.4^2;4^4)2$ | $c2mm$ (rectangular)

$c2$ (oblique)

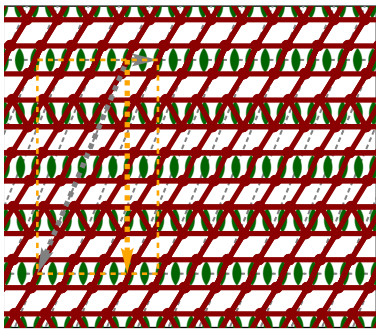

$\delta = -0.1$, $\nu = 3.08$

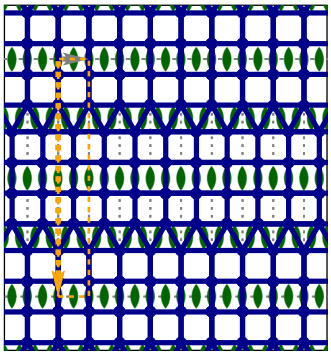

$\delta = 0$, $\boldsymbol{\nu = \infty}$

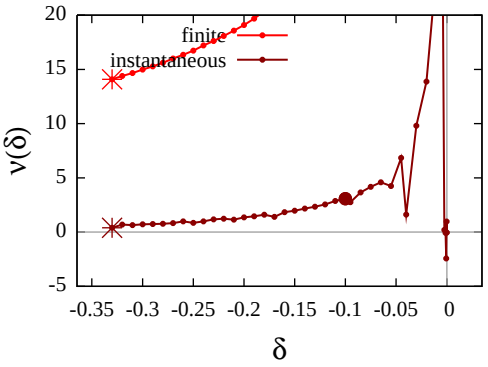

B: tuc | cross	:	19 | 8
N: tuc | neigb. | tot	:	$2\times 4\,d(1)$ | 16 $\sum = 24$
Free|Dep.|Fix $\mathrm{p}^i_{x,y}$	:	4 | 44 | 0 $\sum = 48$
Set|Free|Dep.|Fix	:	$a^{\parallel}, b^{\parallel}$ | $a^{\perp}, b^{\perp}$|none|none
$\langle \frac{B}{N} \rangle$	:	4.75
$\mathbf{Z}_{\mathbf{Maxwell}}$	:	-2
Reference(s)	:	[24], p.67, Fig.12

Auxetic under finite deformation

6.3.18 2-Uniform 14

$\downarrow 0°$

$(3^2.4.3.4;3.4.6.4)$ | $p6mm$ (hexagonal)

pm_r (rhombus)

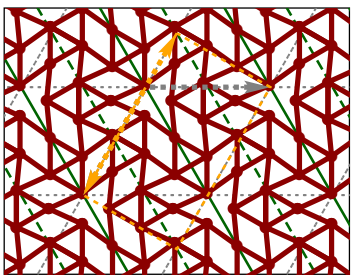

$\delta = -0.10$, $\nu = -1.00$

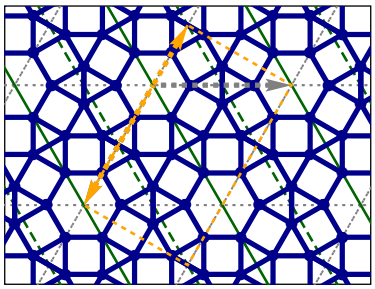

$\delta = 0$, $\boldsymbol{\nu = -1.00}$

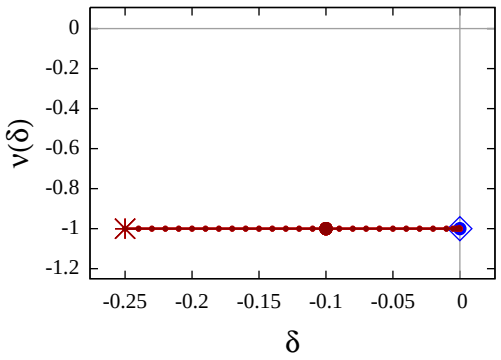

B: tuc | cross	:	27 | 2
N: tuc | neigb. | tot	:	$5\times 2\,b(1), 2\times 1\,a(U)$ | 8 $\sum = 20$
Free|Dep.|Fix $\mathrm{p}^i_{x,y}$	:	11 | 28 | 1 $\sum = 40$
Set|Free|Dep.|Fix	:	$a^{\parallel}, b^{\parallel}$ | $b^{\perp}$ | $a^{\perp} = f(\delta, b^{\perp})$ | none
$\langle \frac{B}{N} \rangle$	:	4.50
$\mathbf{Z}_{\mathbf{Maxwell}}$	:	-2
Reference(s)	:	[24], p.67, Fig.12

Auxetic

6.3.19 2-Uniform 14

↘ 60°

$(3^2.4.3.4;3.4.6.4)$ | $p6mm$ (hexagonal)

$p2$ (oblique)

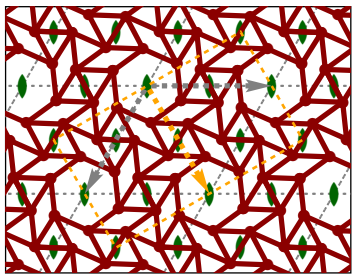

$\delta = -0.10$, $\nu = -1.00$

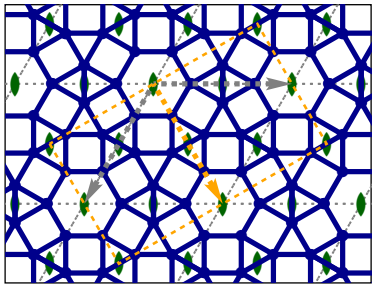

$\delta = 0$, $\boldsymbol{\nu = -1.00}$

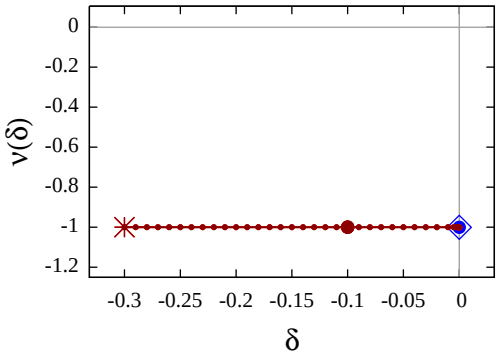

B: tuc | cross	:	27 | 2
N: tuc | neigb. | tot	:	$6 \times 2\,e(1)$ | 8 $\sum = 20$
Free|Dep.|Fix $\mathrm{p}^i_{x,y}$	:	12 | 28 | 0 $\sum = 40$
Set|Free|Dep.|Fix	:	$a^{\parallel}, b^{\parallel}$ | $a^{\perp}, b^{\perp}$|none|none
$\langle \frac{B}{N} \rangle$	:	4.50
$\mathbf{Z}_{\mathbf{Maxwell}}$	:	-2
Reference(s)	:	[24], p.67, Fig.12

Auxetic

6.3.20 2-Uniform 15

↓ 0°

$(3^2.6^2;3.6.3.6)$ | $p2mm$ (rectangular)

$p1$ (oblique)

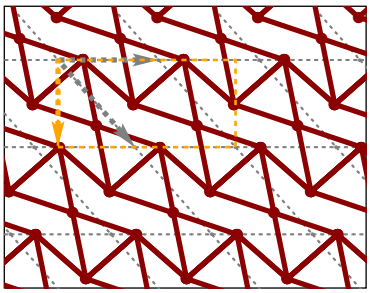

$\delta = -0.25$, $\nu = -0.01$

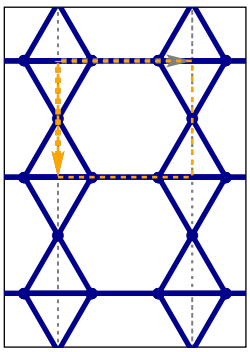

$\delta = 0$, $\boldsymbol{\nu = \infty}$

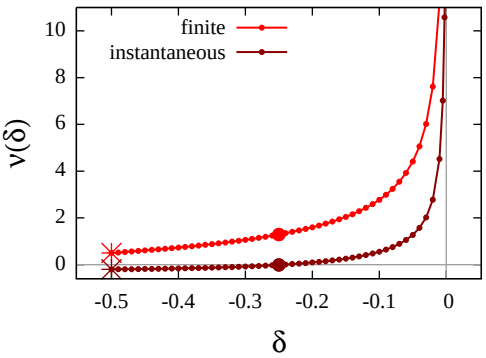

B: tuc | cross	:	7 | 3
N: tuc | neigb. | tot	:	$3 \times 1\,a(1)$ | 7 $\sum = 10$
Free|Dep.|Fix $\mathrm{p}^i_{x,y}$	:	4 | 14 | 2 $\sum = 20$
Set|Free|Dep.|Fix	:	$a^{\parallel}, b^{\parallel}$ | $a^{\perp}, b^{\perp}$|none|none
$\langle \frac{B}{N} \rangle$	:	4.67
$\mathbf{Z}_{\mathbf{Maxwell}}$	:	0
Reference(s)	:	[24], p.67, Fig.12

Auxetic under finite deformation

6.3.21 2-Uniform 16

↓ 0°

$(3.4.3.12; 3.12^2)$ | $p4mm$ (square)

$p4$ (square)

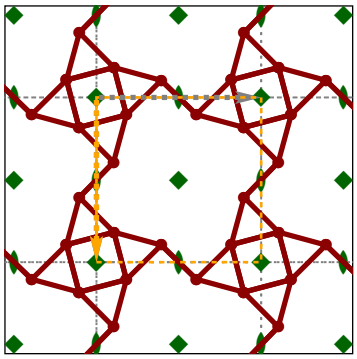

$\delta = -0.10$, $\nu = -1.00$

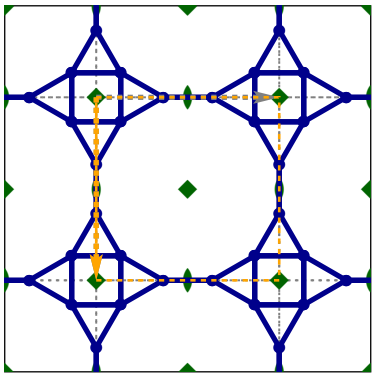

$\delta = 0$, $\boldsymbol{\nu = -1.00}$

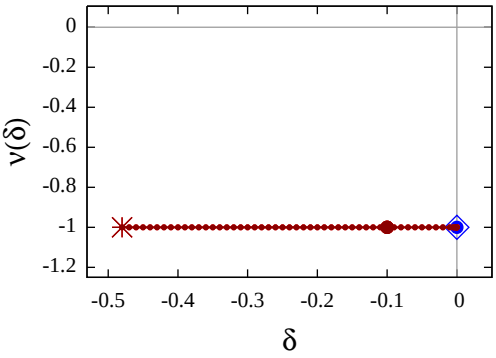

B: tuc | cross	:	14 | 6
N: tuc | neigb. | tot	:	$2 \times 4\, d(1)$ | 12 $\sum = 20$
Free|Dep.|Fix $\mathrm{p}^i_{x,y}$	:	4 | 36 | 0 $\sum = 40$
Set|Free|Dep.|Fix	:	$a^{\parallel}, b^{\parallel}$ | none | $a^{\perp} = -b^{\parallel}$, $b^{\perp} = a^{\parallel}$ | N.A.
$\langle \frac{B}{N} \rangle$	:	3.50
Z_{Maxwell}	:	3
Reference(s)	:	[24], p.67, Fig.12

Auxetic

6.3.22 2-Uniform 17

↓ 0°

$(3.4^2.6; 3.4.6.4)$ | $p6mm$ (hexagonal)

pm_r (rhombus)

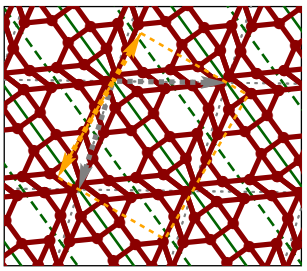

$\delta = -0.15$, $\nu = -0.35$

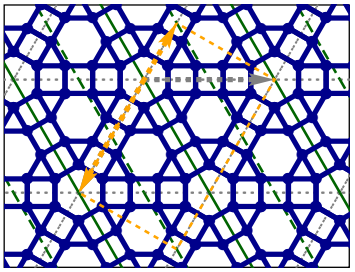

$\delta = 0$, $\boldsymbol{\nu_- = 3.00}$, $\boldsymbol{\nu_+ = -5.00}$

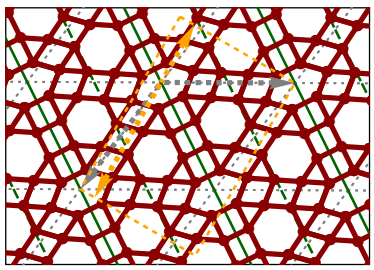

$\delta = 0.018$, $\nu = -\infty$

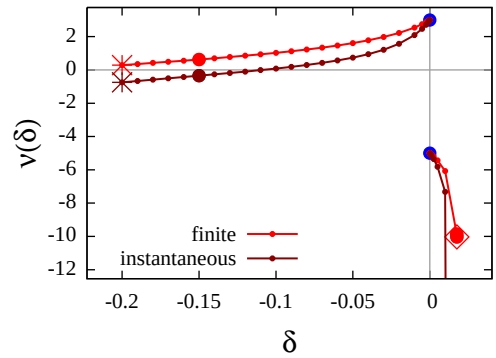

B: tuc | cross	:	36 | 8
N: tuc | neigb. | tot	:	$9 \times 2\, b(1)$ | 16 $\sum = 34$
Free|Dep.|Fix $\mathrm{p}^i_{x,y}$	:	17 | 50 | 1 $\sum = 68$
Set|Free|Dep.|Fix	:	$a^{\parallel}, b^{\parallel}$ | $b^{\perp}$ | $a^{\perp} = f(\delta, b^{\perp})$ | none
$\langle \frac{B}{N} \rangle$	:	4.00
Z_{Maxwell}	:	1
Reference(s)	:	[24], p.67, Fig.12

Auxetic under finite deformation ↓

6.3.23 2-Uniform 18

$(3.4^2.6;3.6.3.6)1$ | $p2mm$ (rectangular)

→ 90°
***p*2 (oblique)**

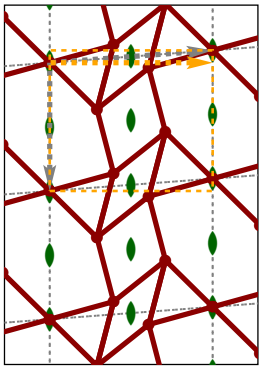

$\delta = -0.10$, $\nu = -0.41$

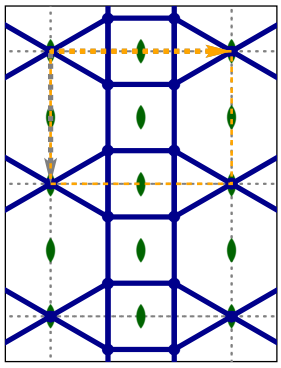

$\delta = 0$, $\boldsymbol{\nu = -0.57}$

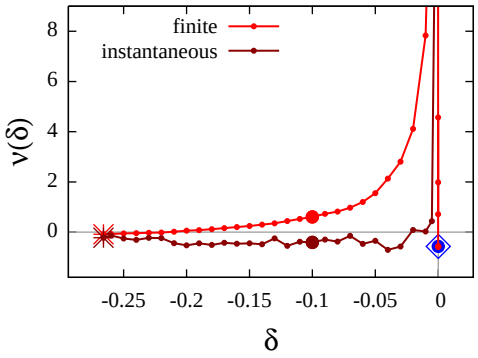

***B*: tuc | cross**	:	10 | 2
***N*: tuc | neigb. | tot**	:	$2\times 2\,e(1), 1\times 1\,a(2)$ | 7 $\sum = 12$
Free|Dep.|Fix $\mathrm{p}^i_{x,y}$	:	4 | 20 | 0 $\sum = 24$
Set|Free|Dep.|Fix	:	$a^{\parallel}, b^{\parallel}$ | $a^{\perp}, b^{\perp}$|none|none
$\langle \frac{B}{N} \rangle$	:	4.00
$\mathbf{Z_{Maxwell}}$	:	1
Reference(s)	:	[24], p.67, Fig.12

Infinitesimally **auxetic**

6.3.24 2-Uniform 19

$(3.4^2.6;3.6.3.6)2$ | $c2mm$ (rectangular)

↘ 45°
***c*2 (oblique)**

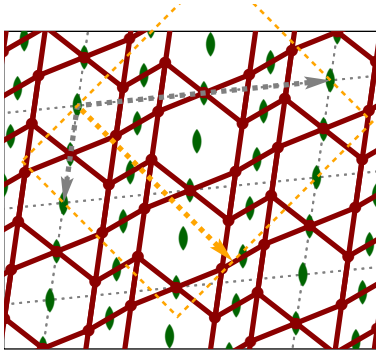

$\delta = -0.15$, $\nu = 0.02$

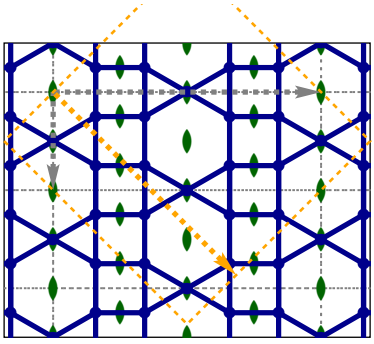

$\delta = 0$, $\boldsymbol{\nu = 1.00}$

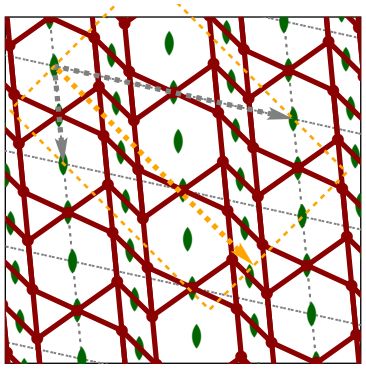

$\delta = 0.089$, $\nu = \infty$

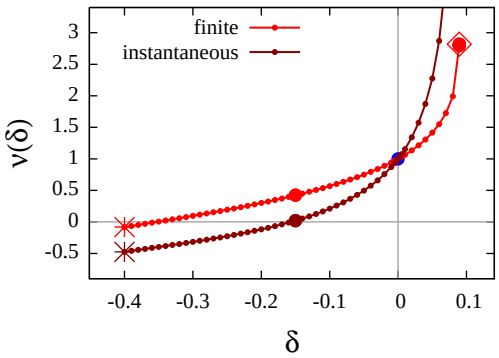

***B*: tuc | cross**	:	20 | 4
***N*: tuc | neigb. | tot**	:	$2\times 4\,d(1), 1\times 2\,b(2)$ | 10 $\sum = 20$
Free|Dep.|Fix $\mathrm{p}^i_{x,y}$	:	4 | 36 | 0 $\sum = 40$
Set|Free|Dep.|Fix	:	$a^{\parallel}, b^{\parallel}$ | $a^{\perp}, b^{\perp}$|none|none
$\langle \frac{B}{N} \rangle$	:	4.00
$\mathbf{Z_{Maxwell}}$	:	1
Reference(s)	:	[24], p.67, Fig.12

Auxetic under finite deformation

6.3.25 2-Uniform 19

$\rightarrow 90^\circ$

$(3.4^2.6;3.6.3.6)2$ | $c2mm$ (rectangular)

$\boldsymbol{c11m}$ **(rectangular)**

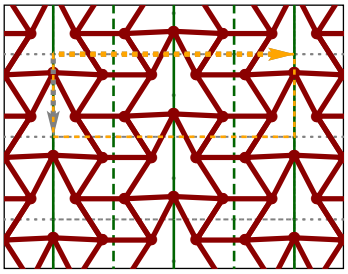

$\delta = -0.10$, $\nu = -1.69$

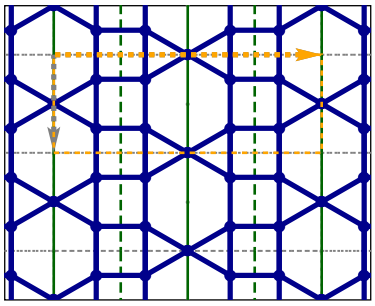

$\delta = 0$, $\boldsymbol{\nu = -1.58}$

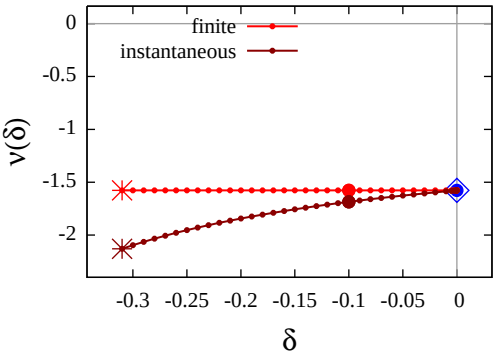

B: tuc | cross	:	20 | 4
N: tuc | neigb. | tot	:	$2\times 4\,b(1), 1\times 2\,a(..m)$ | 10 $\sum = 20$
Free|Dep.|Fix $\mathrm{p}^i_{x,y}$	:	4 | 35 | 1 $\sum = 40$
Set|Free|Dep.|Fix	:	$a^{\parallel}, b^{\parallel}$ | $a^{\perp}$ | $b^{\perp} = -\frac{a^{\parallel}b^{\parallel}}{a^{\perp}}$ | none
$\langle \frac{B}{N} \rangle$	:	4.00
$\mathbf{Z}_{\mathbf{Maxwell}}$	:	1
Reference(s)	:	[24], p.67, Fig.12

Auxetic

6.3.26 2-Uniform 19

$\downarrow 0^\circ$

$(3.4^2.6;3.6.3.6)2$ | $c2mm$ (rectangular)

$\boldsymbol{c11m}$ **(rectangular)**

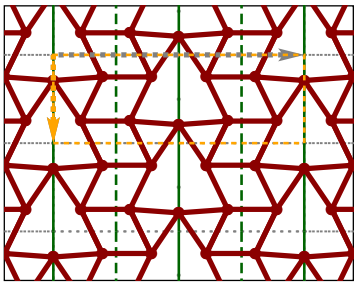

$\delta = -0.10$, $\nu = -0.61$

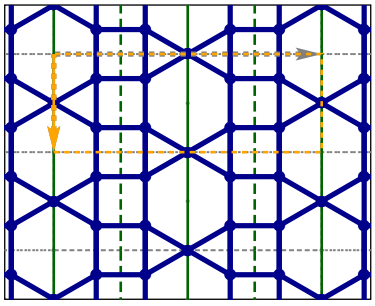

$\delta = 0$, $\boldsymbol{\nu = -0.63}$

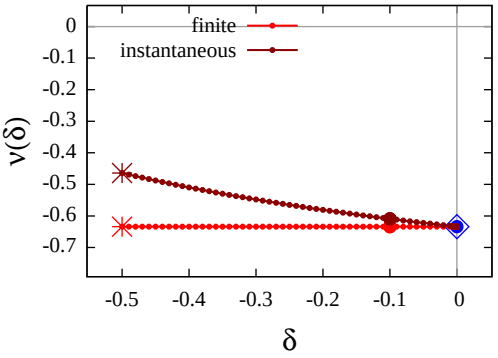

B: tuc | cross	:	20 | 4
N: tuc | neigb. | tot	:	$2\times 4\,b(1), 1\times 2\,a(..m)$ | 10 $\sum = 20$
Free|Dep.|Fix $\mathrm{p}^i_{x,y}$	:	4 | 35 | 1 $\sum = 40$
Set|Free|Dep.|Fix	:	$a^{\parallel}, b^{\parallel}$ | $b^{\perp}$ | $a^{\perp} = -\frac{a^{\parallel}b^{\parallel}}{b^{\perp}}$ | none
$\langle \frac{B}{N} \rangle$	:	4.00
$\mathbf{Z}_{\mathbf{Maxwell}}$	:	1
Reference(s)	:	[24], p.67, Fig.12

Auxetic

6.3.27 2-Uniform 20

↓ 0°

(3.4.6.4; 4.6.12) | *p6mm* (hexagonal)

***p31m* (hexagonal)**

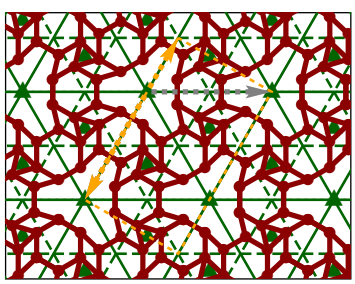

$\delta = -0.10$, $\nu = -1.00$

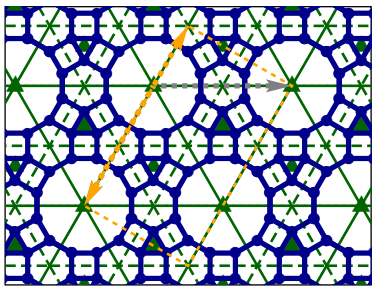

$\delta = 0$, $\boldsymbol{\nu = -1.00}$

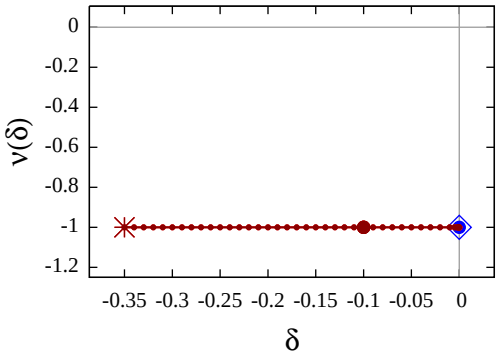

***B*: tuc | cross**	:	30 | 4
***N*: tuc | neigb. | tot**	:	$3 \times 6\, d(1)$ | 8 $\sum = 26$
Free|Dep.|Fix $p^i_{x,y}$	:	6 | 46 | 0 $\sum = 52$
Set|Free|Dep.|Fix	:	$a^{\parallel}, b^{\parallel}$ | none | $a^{\perp} = \frac{a^{\parallel}+2b^{\parallel}}{-\sqrt{3}}$, $b^{\perp} = \frac{2a^{\parallel}+b^{\parallel}}{\sqrt{3}}$ | N.A.
$\langle \frac{B}{N} \rangle$	:	3.33
$\mathbf{Z_{Maxwell}}$	:	7
Reference(s)	:	[24], p.67, Fig.12

Auxetic

Table 6.7: *Infinitesimal deformation behaviour of* star tilings I, *see Table 6.1 for explanation of symbols*

Group	***p6mm***	***p6***	***p31m***	***p3m1***	***p3***	***p4gm***	***p4mm***	***p4***
Lattice Type	hexagonal					square		
Star Tiling I A (*p6*) **1 sym. mode:** 6.4.1	-	**–1**	-	-	U	-	-	-
Star Tiling I B (*p4*) **1 sym. mode:** 6.4.2	-	-	-	-	-	-	-	**–1**
Star Tiling I C (*p6*) **1 sym. mode:** 6.4.3	-	**–1**	-	-	U	-	-	-
Star Tiling I D (*p31m*) **unique:** 6.4.4	-	-	**–1**	-	**–1**	-	-	-

6.4 Star tilings I

Table 6.7 lists the infinitesimal Poisson's ratio of the four uniform tilings consisting of regular polygons and star polygons where all corners are vertices of the tiling (cf. sect. 3.1). *Star tiling I A* and *star tiling I C* have the symmetry group $p6$, *star tiling I D* has $p31m$ as its symmetry and *star tiling I B* belongs to $p4$. So *all four* tilings belong to a hexagonal or square group which constrains the Poisson's ratio to -1 (cf. sect. 3.6). The results show that all have a unique deformation mode in their highest symmetry group and therefore are auxetic in these embeddings. In the groups which do not limit the Poisson's ratio tilings *A, B* and *C* have no unique deformation mechanism. However tiling *D* is fully constrained by the bars to one deformation mode. Thus this is an auxetic periodic skeletal structure. The maximal expansion of *star tiling ID* leads to the *trihexagonal tiling* (compare 6.4.4 and 6.2.17) which is one of the Archimedean tilings and hence this is no further auxetic deformation mechanism.

This is also true for the tilings *A* in $p6$ (6.4.1) and *B* in group $p4$ (6.4.2) which correspond to the Archimedean tilings (3.12^2) (*truncated hexagonal tiling*, 6.2.13) and (4.8^2) (*truncated square tiling*, 6.2.10). And the mechanism of tiling *C* in p6 (6.4.3) equals to the one of the 2-uniform tiling 7. 2-uniform 7 is unique deformable without the symmetry constraints of $p6$ because the rotating hexagons are triangulated. In tiling *C* they are held rigid by the 6-fold symmetry.

Therefore these tilings do not provide new mechanisms. Nevertheless a short description of these mechanisms is given because they share the same fundamental elements which lead to auxetic behaviour. The stars fold or unfold, and the other tiles which are rigid either themselves or due to symmetry constraints rotate simultaneously with the folding process. Therefore these tilings show both of the described features of auxetic behaviour, rotating and reentrant (cf. sect. 5). Tiling *A* is built up of stars with 6 dents and triangles which are intrinsic rigid. During the deformation the triangles rotate and therefore the direction of the dents also rotate (6.4.1). But the most important feature for the auxetic behaviour is the reentrant elements of the stars which allow the expansion or contraction of the lattice lengths in both directions.

Table 6.7: *Infinitesimal deformation behaviour of* star tilings I*, see table 6.1 for explanation of symbols*

c2mm	**p2gg**	**p2mg**	**p2mm**	**cm**	**pg**	**pm**	**p2**	**p1**
rectangular (or rhombus in specific subgroups)							oblique	
-	-	-	-	-	-	-	U	U
-	-	-	-	-	-	-	U	U
-	-	-	-	-	-	-	U	U
-	-	-	-	**-1_{26}**	-	-	**-1**	**-1**

6.4.1 Star Tiling IA

$\downarrow 0°$

$(3.6^{*}_{\alpha}.6^{**}_{\alpha})_{\alpha=30.6°}$ - all corners are vertices | $p6$ (hexagonal)

***p6* (hexagonal)**

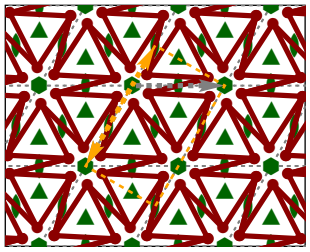

$\delta = -0.20\,, \quad \nu = -1.00$

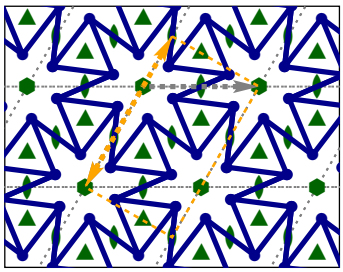

$\delta = 0\,, \quad \boldsymbol{\nu = -1.00}$

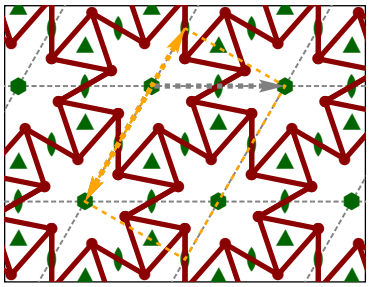

$\delta = 0.15\,, \quad \nu = -1.00$

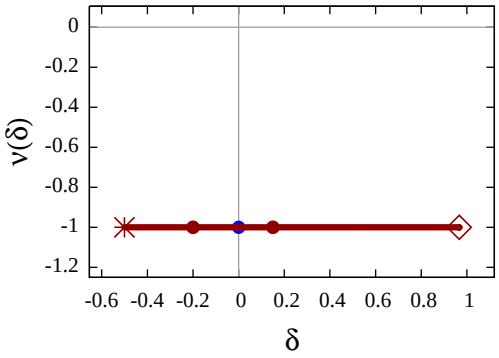

B: tuc | cross	:	9 | 2
N: tuc | neigb. | tot	:	$1 \times 6\, d(1)$ | 4 $\sum = 10$
Free|Dep.|Fix $\mathrm{p}^{i}_{x,y}$	:	2 | 18 | 0 $\sum = 20$
Set|Free|Dep.|Fix	:	$a^{\parallel}, b^{\parallel}$ | none | $a^{\perp} = \frac{a^{\parallel}+2b^{\parallel}}{-\sqrt{3}}$, $b^{\perp} = \frac{2a^{\parallel}+b^{\parallel}}{\sqrt{3}}$ | N.A.
$\langle \frac{B}{N} \rangle$	:	3.00
Z_{Maxwell}	:	4
Reference(s)	:	[24], p.83, Fig.(a)

Auxetic

6.4.2 Star Tiling IB

$\downarrow 0°$

$(4.4^{*}_{\alpha}.4^{**}_{\alpha})_{\alpha=18.5°}$ - all corners are vertices | $p4$ (square)

***p4* (square)**

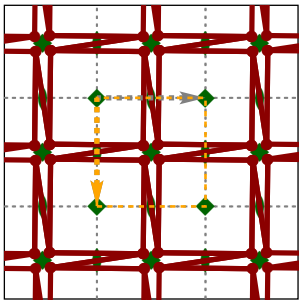

$\delta = -0.12\,, \quad \nu = -1.00$

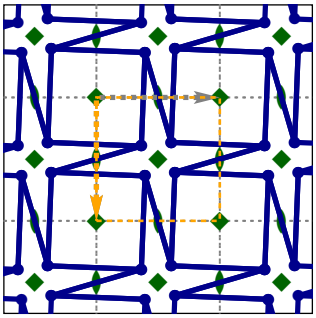

$\delta = 0\,, \quad \boldsymbol{\nu = -1.00}$

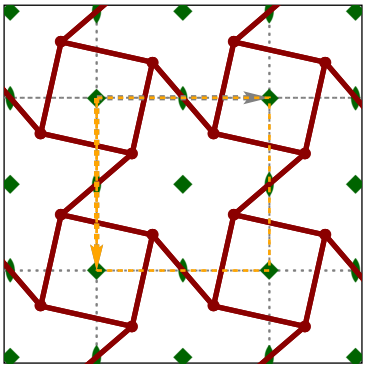

$\delta = 0.4\,, \quad \nu = -1.00$

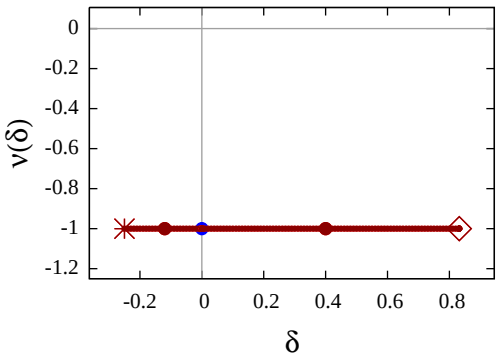

B: tuc | cross	:	6 | 6
N: tuc | neigb. | tot	:	$1 \times 4\, d(1)$ | 8 $\sum = 12$
Free|Dep.|Fix $\mathrm{p}^{i}_{x,y}$	:	2 | 22 | 0 $\sum = 24$
Set|Free|Dep.|Fix	:	$a^{\parallel}, b^{\parallel}$ | none | $a^{\perp} = -b^{\parallel}$, $b^{\perp} = a^{\parallel}$ | N.A.
$\langle \frac{B}{N} \rangle$	:	3.00
Z_{Maxwell}	:	3
Reference(s)	:	[24], p.83 , Fig.(b)

Auxetic

6.4.3 Star Tiling IC

$\downarrow 0°$

$(6.3^{*}_{\alpha}.3^{**}_{\alpha})_{\alpha=25.5°}$ - all corners are vertices | $p6$ (hexagonal)

$p6$ (hexagonal)

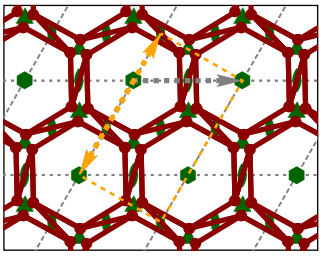

$\delta = -0.06$, $\nu = -1.00$

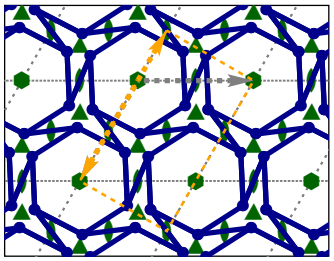

$\delta = 0$, $\boldsymbol{\nu = -1.00}$

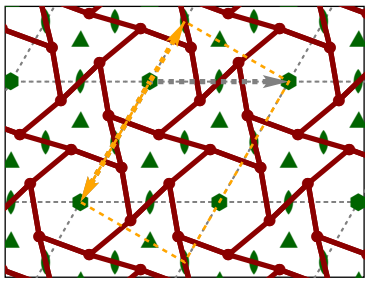

$\delta = 0.2$, $\nu = -1.00$

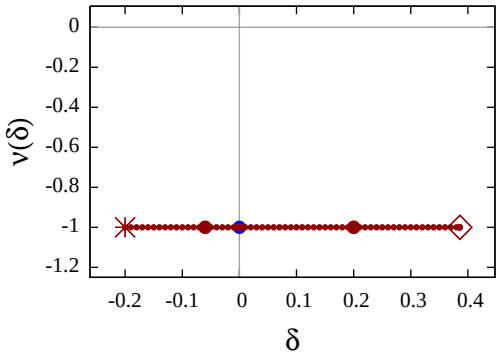

B: tuc | cross : 9 | 6

N: tuc | neigb. | tot : $1 \times 6\, d(1)$ | 8 $\sum = 14$

Free|Dep.|Fix $\mathrm{p}^{i}_{x,y}$: 2 | 26 | 0 $\sum = 28$

Set|Free|Dep.|Fix : $a^{\parallel}, b^{\parallel}$ | none | $a^{\perp} = \frac{a^{\parallel}+2b^{\parallel}}{-\sqrt{3}}$, $b^{\perp} = \frac{2a^{\parallel}+b^{\parallel}}{\sqrt{3}}$ | N.A.

$\langle \frac{B}{N} \rangle$: 3.00

Z_{Maxwell} : 4

Reference(s) : [24], p.83 , Fig.(c)

Auxetic

6.4.4 Star Tiling ID

$\downarrow 0°$

$(3.3^{*}_{\alpha}.3.3^{**}_{\alpha})_{\alpha=23.31°}$ - all corners are vertices | $p31m$ (hexagonal)

$p1$ (oblique)

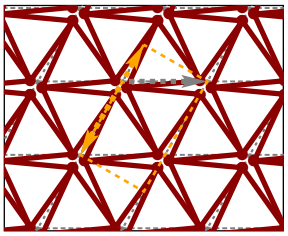

$\delta = -0.13$, $\nu = -1.00$

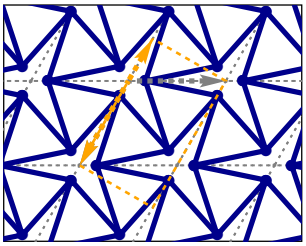

$\delta = 0$, $\boldsymbol{\nu = -1.00}$

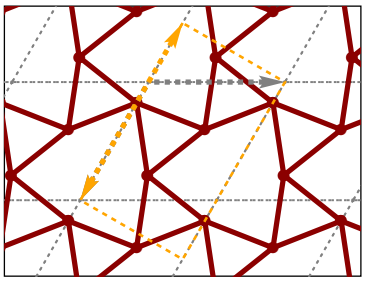

$\delta = 0.4$, $\nu = -1.00$

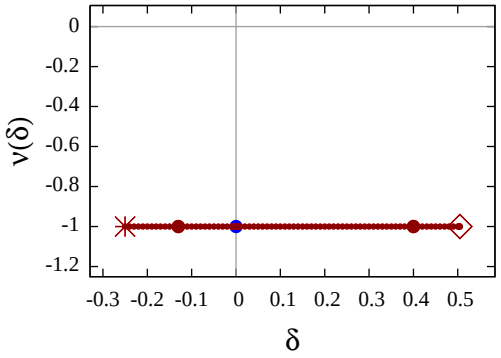

B: tuc | cross : 6 | 0

N: tuc | neigb. | tot : $3 \times 1\, a(1)$ | 2 $\sum = 5$

Free|Dep.|Fix $\mathrm{p}^{i}_{x,y}$: 4 | 4 | 2 $\sum = 10$

Set|Free|Dep.|Fix : $a^{\parallel}, b^{\parallel}$ | $a^{\perp}, b^{\perp}$|none|none

$\langle \frac{B}{N} \rangle$: 4.00

Z_{Maxwell} : 1

Reference(s) : [24], p.83, Fig.(d), [21]

Auxetic

6.5 Star tilings II

The results of the last considered set of tessellations are given in the two Tables 6.8 and 6.9 and Subsections 6.5.1 to 6.5.17. These are the deformations of the 17 uniform tessellations with tiles by regular polygons and regular star polygons that have corners which are not vertices of the tiling (cf. sect. 3.1). Such corners can be identified by the coordination number that is two and in the case of vertices at least three. The strong diversity of different deformation behaviour like in the Archimedean and 2-uniform tilings is not the case. The main features can be summarised for all tilings of this set in a generic description.

Most characteristics are similar to the ones of the star tilings I (Sect. 6.4). None of these

Table 6.8: *Infinitesimal deformation behaviour of* star tilings II A–J*, see Table 6.1 for explanation of symbols*

Group	***p6mm***	***p6***	***p31m***	***p3m1***	***p3***	***p4gm***	***p4mm***	***p4***
Lattice type	hexagonal					square		
Star Tiling II A ($p6mm$) **3 sym. modes:** 6.5.1	R	$\mathbf{-1}^{\ddagger\downarrow}_{(1)}$	$\underline{\mathbf{-1}}^{\ddagger\downarrow}_{(2)}$	R	U	-	-	-
Star Tiling II B ($p4mm$) **3 sym. modes:** 6.5.2	-	-	-	-	-	-	R	$\mathbf{-1}^{\ddagger\downarrow}_{(1)}$
Star Tiling II C ($p4mm$) **1 sym. mode:** 6.5.3	-	-	-	-	-	-	$\underline{\mathbf{-1}}$	U
Star Tiling II D ($p6mm$) **1 sym. mode:** 6.5.4	R	U	$\mathbf{-1}^{\ddagger\downarrow}$	R	U	-	-	-
Star Tiling II E ($p4mm$) **1 sym. mode:** 6.5.5	-	-	-	-	-	-	R	U
Star Tiling II F ($p6mm$) **1 sym. mode:** 6.5.6	$\underline{\mathbf{-1}}$	U	U	$\mathbf{-1}$	U	-	-	-
Star Tiling II G ($p4mm$) **1 sym. mode:** 6.5.7	-	-	-	-	-	-	$\mathbf{-1}$	$\underline{\mathbf{-1}}$
Star Tiling II H ($p6mm$) **1 sym. mode:** 6.5.8	$\mathbf{-1}$	$\mathbf{-1}$	$\mathbf{-1}$	$\mathbf{-1}$	$\underline{\mathbf{-1}}$	-	-	-
Star Tiling II I ($p6mm$) **1 sym. mode:** 6.5.9	$\mathbf{-1}$	$\underline{\mathbf{-1}}$	U	U	U	-	-	-
Star Tiling II J ($p6mm$) **1 sym. mode:** 6.5.10	$\mathbf{-1}$	$\underline{\mathbf{-1}}$	U	U	U	-	-	-

tilings are rigid, all have square or hexagonal groups as their highest symmetry embedding, and all have unique deformations in at least one of the square or hexagonal groups. Nearly all are deformable in the highest symmetry, with four exceptions (*star tilings II A,B,D* and *E*). Nevertheless every tiling has an auxetic mechanism. Note only this set contains tilings which are not rigid in the groups $p6mm, p4mm$ and $p4gm$ (compare tilings *C, F–Q*). These are groups that are not t-subgroups of any other group (cf. Fig. 3.7 on page 31).

Among the star tilings II there is no tessellation with unique mechanism in a non-square group or hexagonal group. Therefore the auxetic behaviour results from the imposed conservation of the symmetries. Of course the skeletal structure must admit a unique deformation mode which is compatible with the symmetry constraints. That differs from tiling to tiling (see e.g. *E* and *G* in $p4mm$).

Table 6.8: *Infinitesimal deformation behaviour of* star tilings II A–J*, see Table 6.1 for explanation of symbols*

c2mm	***p2gg***	***p2mg***	***p2mm***	***cm***	***pg***	***pm***	***p2***	***p1***
rectangular (or rhombus in specific subgroups)							oblique	
$\mathrm{N}_{30}^{0^\circ}$ $1_{30}^{60^\circ}$ (3)	-	-	-	U_{26}, $\mathrm{N}_{27}^{0^\circ}$ $1_{27}^{60^\circ}$ (3)	-	-	U	U
$\infty_{30}^{0^\circ\ddagger\downarrow}$ $1_{30}^{45^\circ}$ (2)	-	-	$1_{(3)}^{0^\circ}$	$\infty_{26}^{0^\circ\ddagger\downarrow}$ $1_{26}^{45^\circ}$ (2)	-	$1_{(3)}^{0^\circ}$	U	U
U_{30}	-	-	U	U_{26}	-	U	U	U
U_{30}	-	-	-	U_{26}, U_{27}	-	-	U	U
U_{30}	-	-	1	U_{26}	-	$\underline{1}$	U	U
U_{30}	-	-	-	U_{26},U_{27}	-	-	U	U
U_{30}	-	-	U	U_{26}	-	U	U	U
U_{30}	-	-	-	U_{26},U_{27}	-	-	U	U
U_{30}	-	-	-	U_{26},U_{27}	-	-	U	U
U_{30}	-	-	-	U_{26},U_{27}	-	-	U	U

Table 6.9: *Infinitesimal deformation behaviour of* star tilings II K–Q.

Group	**p6mm**	**p6**	**p31m**	**p3m1**	**p3**	**p4gm**	**p4mm**	**p4**
Lattice type	hexagonal					square		
Star Tiling II K (p6mm) **1 sym. mode:** 6.5.11	**–1**	U	U	U	U	-	-	-
Star Tiling II L (p4mm) **1 sym. mode:** 6.5.12	-	-	-	-	-	-	**–1**	**–1**
Star Tiling II M (p6mm) **1 sym. mode:** 6.5.13	**–1**	**–1**	U	U	U	-	-	-
Star Tiling II N (p6mm) **1 sym. mode:** 6.5.14	**–1**	**–1**	U	U	U	-	-	-
Star Tiling II O (p4mm) **1 sym. mode:** 6.5.15	-	-	-	-	-	-	**–1**	U
Star Tiling II P (p6mm) **1 sym. mode:** 6.5.16	**–1**	U	U	U	U	-	-	-
Star Tiling II Q (p4gm) **1 sym. mode:** 6.5.17	-	-	-	-	-	**–1**	-	U

The mechanisms of three tilings (*A, B* and *E*) correspond to already given tilings. The equivalents are the *truncated hexagonal*(6.2.13; 6.2.14; 6.2.15, 6.2.16), the *truncated square* (6.2.10; 6.2.11) and the *great rhombitrihexagonal tiling* (6.2.20; 6.2.21). The only differences are additional triangles which are located in the inner of the 8-gon or 12-gon. These lead to an earlier overlap of joints and therefore the plots of the finite deformations show only a part of the equivalents. Due to the equal mechanisms not all results of the finite deformations are given for all mechanisms. The different mechanisms are distinguished in the Table 6.8 by numbers in brackets.

The essential part for the auxetic behaviour is also the re-entrant angles of the stars. The stars fold or unfold during the auxetic deformation mechanism.

A new feature appears in comparison to the star tilings I. For most tilings (with the exception of A,B,D,E) there is no rotation of any element. So only the folding and a pure deformation of tiles occurs. Consider e.g. the star tiling II F (sect. 6.5.6). The triangles located at the 3-fold site symmetry of the group *p*6 keep their orientation. Just the hexagons become smaller or wider and the stars fold or unfold but do not rotate.

Table 6.9: *Infinitesimal deformation behaviour of* star tilings II K–Q.

c2mm	p2gg	p2mg	p2mm	cm	pg	pm	p2	p1
rectangular (or rhombus in specific subgroups)							oblique	
U_{30}	-	-	-	U_{26},U_{27}	-	-	U	U
U_{30}	-	-	U	U_{26}	-	U	U	U
U_{30}	-	-	-	U_{26},U_{27}	-	-	U	U
U_{30}	-	-	-	U_{26},U_{27}	-	-	U	U
U_{30}	-	-	U	U_{26}	-	U	U	U
U_{30}	-	-	-	U_{26},U_{27}	-	-	U	U
U_{31}	U	-	-	U_{28}	U_{23}	-	U	U

6.5.1 Star Tiling II A

$\downarrow \mathbf{0}^\circ$

$(3^3.12^*_{\pi/6}.3^2.12^*_{\pi/6})$ | *p6mm* (hexagonal)

***p31m* (hexagonal)**

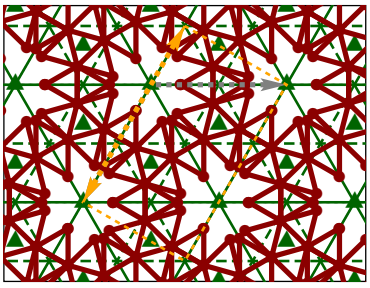

$\delta = -0.02$, $\nu = -1.00$

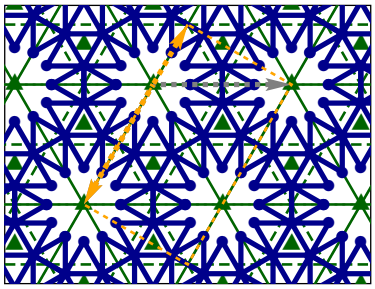

$\delta = 0$, $\boldsymbol{\nu = -1.00}$

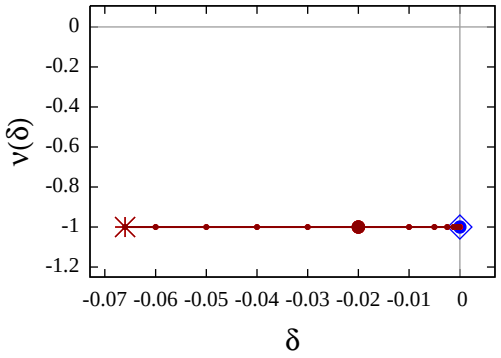

***B*: tuc | cross**	:	33 | 2
***N*: tuc | neigb. | tot**	:	$2\times 6\,d(1), 2\times 3\,c(..m)$ | 8 $\sum = 26$
Free|Dep.|Fix $p^i_{x,y}$	:	6 | 46 | 0 $\sum = 52$
Set|Free|Dep.|Fix	:	$a^{\|\|}, b^{\|\|}$ | none | $a^\perp = \frac{a^{\|\|}+2b^{\|\|}}{-\sqrt{3}}$, $b^\perp = \frac{2a^{\|\|}+b^{\|\|}}{\sqrt{3}}$ | N.A.
$\langle \frac{B}{N} \rangle$	:	3.67
$\mathbf{Z_{Maxwell}}$	:	4
Reference(s)	:	[24] p.84, Fig. (a)

Auxetic

6.5.2 Star Tiling II B

$\downarrow 0°$

$(3^2.8^*_{\pi/12}.3.4.3.8^*_{\pi/12})$ | *p4mm* (square)

pm_r (rhombus)

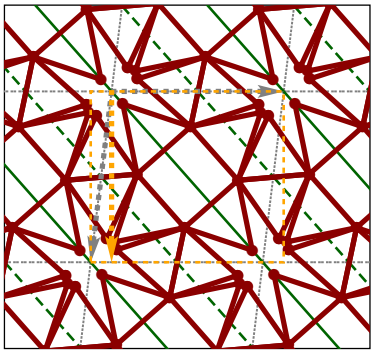

$\delta = -0.01$, $\nu = 5.09$

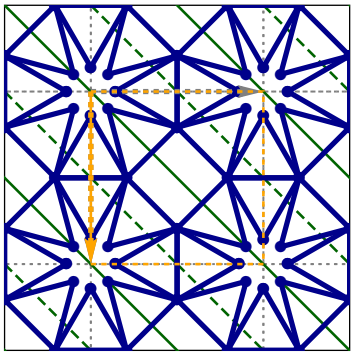

$\delta = 0$, $\boldsymbol{\nu = \infty}$

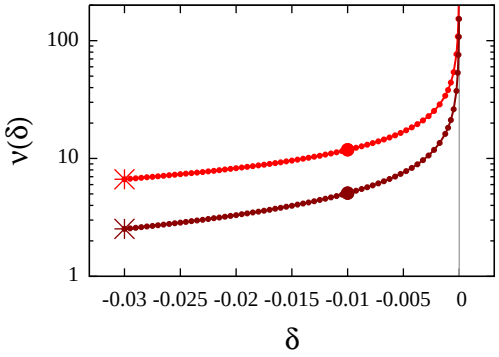

B: tuc | cross	:	22 | 2
N: tuc | neigb. | tot	:	$5\times 2\,b(1), 2\times 1\,a(U)$ | 8 $\sum = 20$
Free|Dep.|Fix $p^i_{x,y}$	:	11 | 28 | 1 $\sum = 40$
Set|Free|Dep.|Fix	:	$a^{\parallel}, b^{\parallel}$ | $b^{\perp}$ | $a^{\perp} = f(\delta, b^{\perp})$ | none
$\langle \frac{B}{N} \rangle$	:	3.67
Z_{Maxwell}	:	3
Reference(s)	:	[24] p.84 , Fig. (b)

Not auxetic

6.5.3 Star Tiling II C

$\downarrow 0°$

$(3^2.8^*_{\pi/12}.4^{**}_{\pi/3}.8^*_{\pi/12})$ | *p4mm* (square)

$p4mm$ (square)

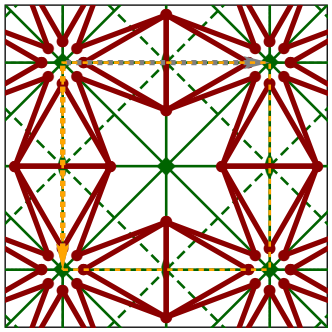

$\delta = -0.10$, $\nu = -1.00$

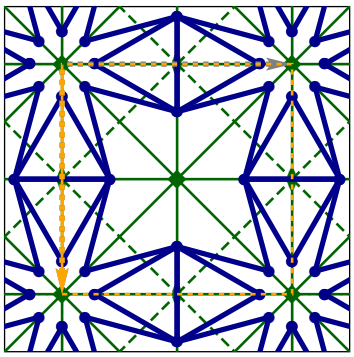

$\delta = 0$, $\boldsymbol{\nu = -1.00}$

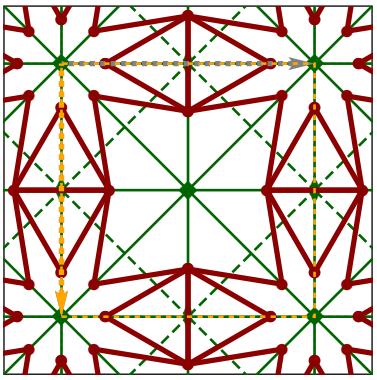

$\delta = 0.1$, $\nu = -1.00$

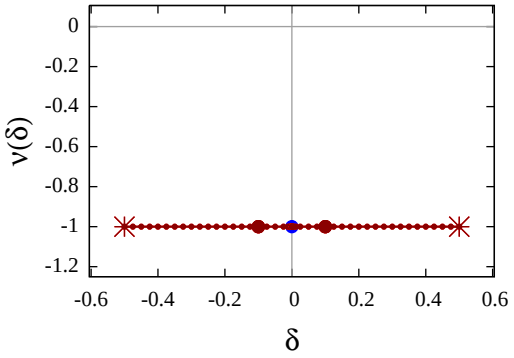

B: tuc | cross	:	18 | 2
N: tuc | neigb. | tot	:	$1\times 4\,f(..m), 1\times 4\,e(.m.), 1\times 4\,d(.m.)$ | 8 $\sum = 20$
Free|Dep.|Fix $p^i_{x,y}$	:	3 | 37 | 0 $\sum = 40$
Set|Free|Dep.|Fix	:	$a^{\parallel}, b^{\parallel}$ | none | $a^{\perp} = -b^{\parallel}$, $b^{\perp} = a^{\parallel}$ | N.A.
$\langle \frac{B}{N} \rangle$	:	3.00
Z_{Maxwell}	:	7
Reference(s)	:	[24] p.84 , Fig. (c)

Auxetic

6.5.4 Star Tiling II D

$\downarrow 0^\circ$

$(3.4.6.3.12^*_{\pi/6})$ | $p6mm$ (hexagonal)

$p6$ (hexagonal)

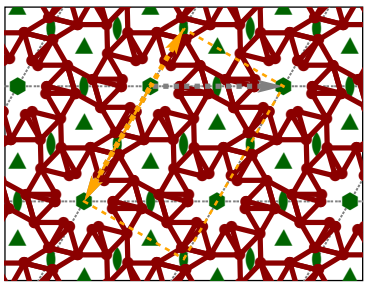

$\delta = -0.04$, $\nu = -1.00$

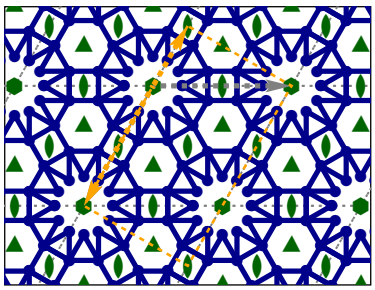

$\delta = 0$, $\boldsymbol{\nu = -1.00}$

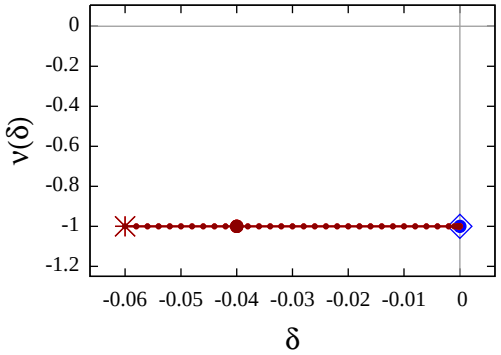

B: tuc | cross	:	42 | 4
N: tuc | neigb. | tot	:	$4 \times 6\, d(1)$ | 12 $\sum = 36$
Free|Dep.|Fix $\mathrm{p}^i_{x,y}$	:	8 | 64 | 0 $\sum = 72$
Set|Free|Dep.|Fix	:	$a^{\parallel}, b^{\parallel}$ | none | $a^{\perp} = \frac{a^{\parallel}+2b^{\parallel}}{-\sqrt{3}}$, $b^{\perp} = \frac{2a^{\parallel}+b^{\parallel}}{\sqrt{3}}$ | N.A.
$\langle \frac{B}{N} \rangle$	:	3.50
$\mathbf{Z}_{\mathrm{Maxwell}}$	:	7
Reference(s)	:	[24], p.85, Fig.(d)

Auxetic

6.5.5 Star Tiling II E

$\downarrow 0^\circ$

$(3.4.8.3.8^*_{\pi/12})$ | $p4mm$ (square)

pm (rectangular)

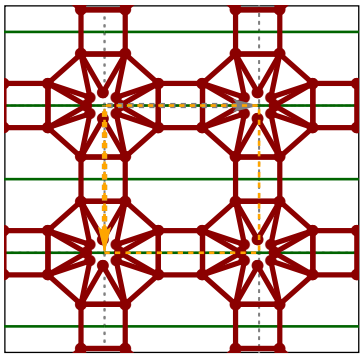

$\delta = -0.03$, $\nu = 0.85$

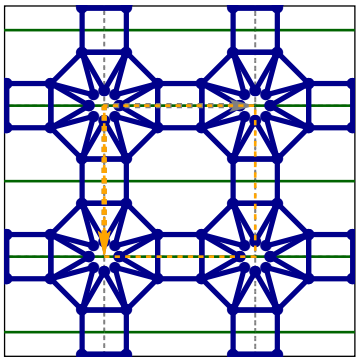

$\delta = 0$, $\boldsymbol{\nu = 1.00}$

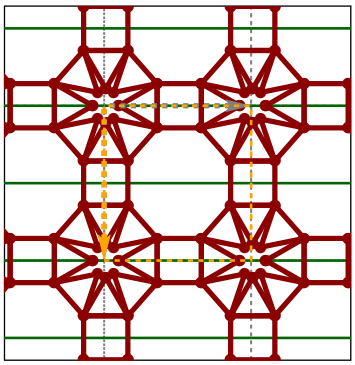

$\delta = 0.025$, $\nu = 1.19$

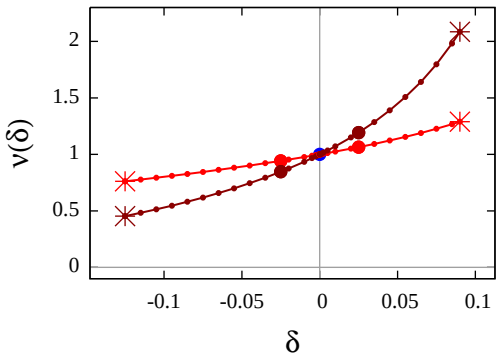

B: tuc | cross	:	28 | 4
N: tuc | neigb. | tot	:	$7 \times 2\, c(1), 2 \times 1\, a(.m.)$ | 12 $\sum = 28$
Free|Dep.|Fix $\mathrm{p}^i_{x,y}$	:	15 | 40 | 1 $\sum = 56$
Set|Free|Dep.|Fix	:	$a^{\parallel}, b^{\parallel}$ | $b^{\perp}$ | $a^{\perp} = -\frac{a^{\parallel}b^{\parallel}}{b^{\perp}}$ | none
$\langle \frac{B}{N} \rangle$	:	3.50
$\mathbf{Z}_{\mathrm{Maxwell}}$	:	5
Reference(s)	:	[24], p.85, Fig.(e)

Not auxetic

6.5.6 Star Tiling II F

$(3.6.6^{*}_{\pi/3}.6)$ | *p6mm* (hexagonal)

↓ 0°

***p*6 (hexagonal)**

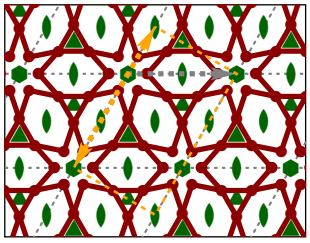

$\delta = -0.10$, $\nu = -1.00$

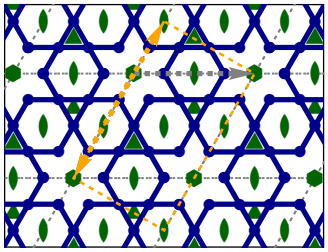

$\delta = 0$, $\boldsymbol{\nu = -1.00}$

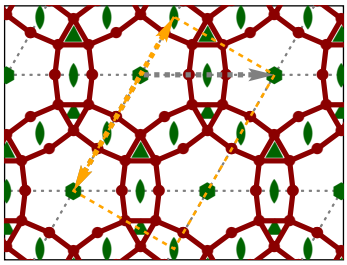

$\delta = 0.11$, $\nu = -1.00$

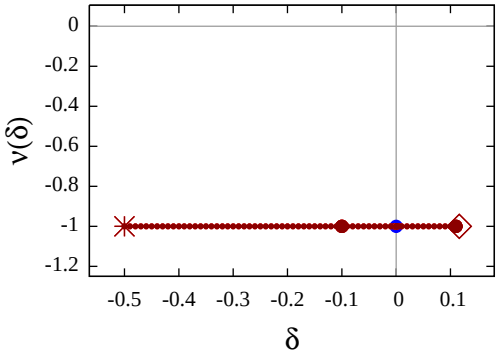

***B*: tuc | cross**	:	18 | 0
***N*: tuc | neigb. | tot**	:	$2 \times 6\, d(1)$ | 4 $\sum = 16$
Free|Dep.|Fix $\mathrm{p}^{i}_{x,y}$	:	4 | 28 | 0 $\sum = 32$
Set|Free|Dep.|Fix	:	$a^{\parallel}, b^{\parallel}$ | none | $a^{\perp} = \frac{a^{\parallel}+2b^{\parallel}}{-\sqrt{3}}$, $b^{\perp} = \frac{2a^{\parallel}+b^{\parallel}}{\sqrt{3}}$ | N.A.
$\langle \frac{B}{N} \rangle$	:	3.00
$\mathbf{Z}_{\mathbf{Maxwell}}$	:	7
Reference(s)	:	[24], p.85, Fig.(f)

Auxetic

6.5.7 Star Tiling II G

$(4.6.4^{*}_{\pi/6}.6)$ | *p4mm* (square)

↓ 0°

***p*4 (square)**

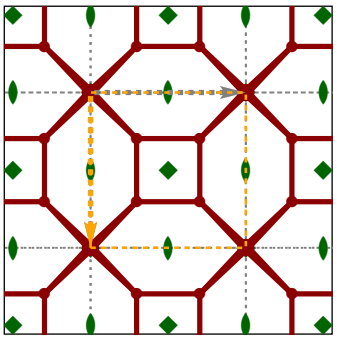

$\delta = -0.10$, $\nu = -1.00$

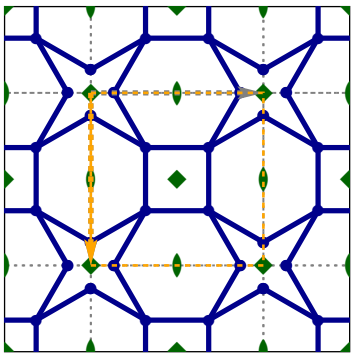

$\delta = 0$, $\boldsymbol{\nu = -1.00}$

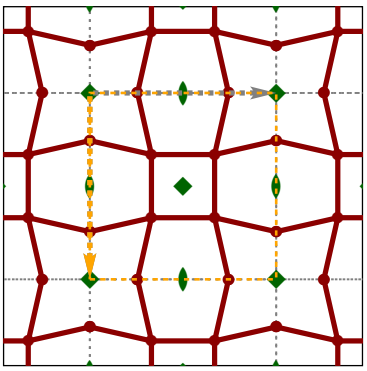

$\delta = 0.08$, $\nu = -1.00$

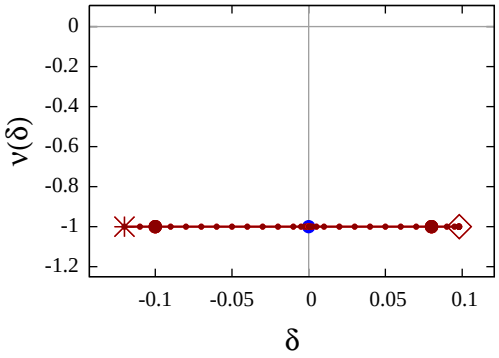

***B*: tuc | cross**	:	12 | 0
***N*: tuc | neigb. | tot**	:	$2 \times 4\, d(1)$ | 4 $\sum = 12$
Free|Dep.|Fix $\mathrm{p}^{i}_{x,y}$	:	4 | 20 | 0 $\sum = 24$
Set|Free|Dep.|Fix	:	$a^{\parallel}, b^{\parallel}$ | none | $a^{\perp} = -b^{\parallel}$, $b^{\perp} = a^{\parallel}$ | N.A.
$\langle \frac{B}{N} \rangle$	:	3.00
$\mathbf{Z}_{\mathbf{Maxwell}}$	:	5
Reference(s)	:	[24], p.84, fig.(g)

Auxetic

6.5.8 Star Tiling II H

$(4.6^{*}_{\pi/6}.4.6^{*}_{\pi/6}.4.6^{*}_{\pi/6})$ | $p6mm$ (hexagonal)

↓ 0°

***p*3 (hexagonal)**

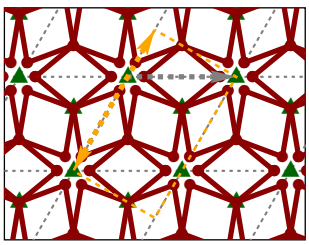

$\delta = -0.10$, $\nu = -1.00$

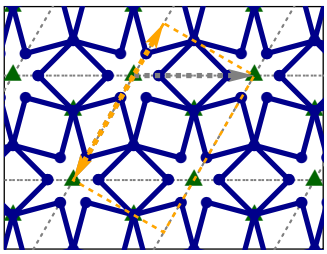

$\delta = 0$, $\boldsymbol{\nu = -1.00}$

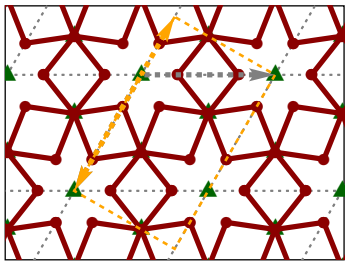

$\delta = 0.11$, $\nu = -1.00$

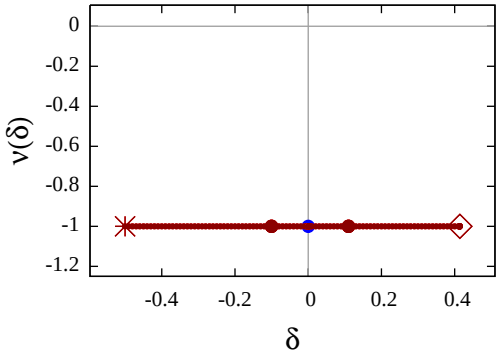

***B*: tuc | cross**	:	12 | 0
***N*: tuc | neigb. | tot**	:	$2\times 3\,d(1), 1\times 1\,c(3..), 1\times 1\,b(3..)$ | 4 $\sum = 12$
Free|Dep.|Fix $\mathrm{p}^{i}_{x,y}$	:	4 | 20 | 0 $\sum = 24$
Set|Free|Dep.|Fix	:	$a^{\parallel}, b^{\parallel}$ | none | $a^{\perp} = \frac{a^{\parallel}+2b^{\parallel}}{-\sqrt{3}}$, $b^{\perp} = \frac{2a^{\parallel}+b^{\parallel}}{\sqrt{3}}$ | N.A.
$\langle \frac{B}{N} \rangle$	:	3.00
$\mathbf{Z}_{\mathbf{Maxwell}}$	:	5
Reference(s)	:	[24] p.84, Fig. Fig. (h)

Auxetic

6.5.9 Star Tiling II I

$(4.6^{*}_{\pi/6}.6^{**}_{\pi/2}.6^{*}_{\pi/6})$ | $p6mm$ (hexagonal)

↓ 0°

***p*6 (hexagonal)**

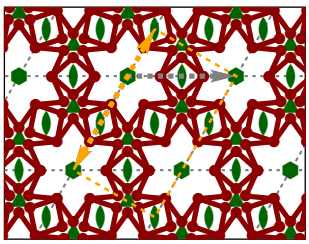

$\delta = -0.10$, $\nu = -1.00$

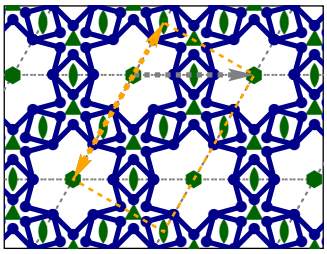

$\delta = 0$, $\boldsymbol{\nu = -1.00}$

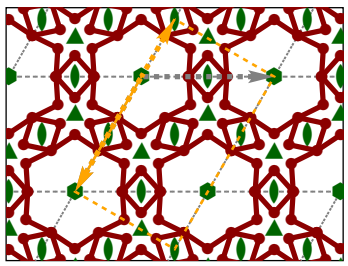

$\delta = 0.1$, $\nu = -1.00$

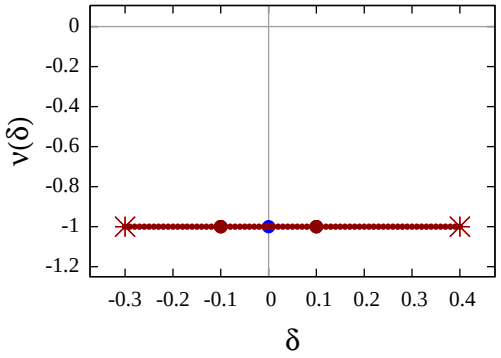

***B*: tuc | cross**	:	24 | 0
***N*: tuc | neigb. | tot**	:	$3\times 6\,d(1)$ | 4 $\sum = 22$
Free|Dep.|Fix $\mathrm{p}^{i}_{x,y}$	:	6 | 38 | 0 $\sum = 44$
Set|Free|Dep.|Fix	:	$a^{\parallel}, b^{\parallel}$ | none | $a^{\perp} = \frac{a^{\parallel}+2b^{\parallel}}{-\sqrt{3}}$, $b^{\perp} = \frac{2a^{\parallel}+b^{\parallel}}{\sqrt{3}}$ | N.A.
$\langle \frac{B}{N} \rangle$	:	2.67
$\mathbf{Z}_{\mathbf{Maxwell}}$	:	13
Reference(s)	:	[24] p.84, Fig. (i)

Auxetic

6.5.10 Star Tiling II J

$(6.6^{*}_{\pi/3}.6.6^{*}_{\pi/3})$ | $p6mm$ (hexagonal)

↓ 0°

***p*6 (hexagonal)**

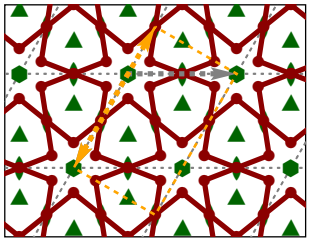

$\delta = -0.10$, $\nu = -1.00$

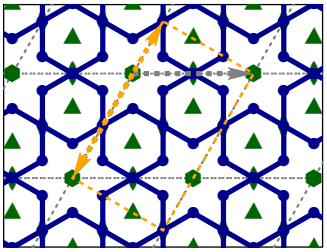

$\delta = 0$, $\boldsymbol{\nu = -1.00}$

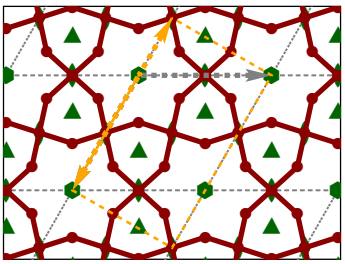

$\delta = 0.1$, $\nu = -1.00$

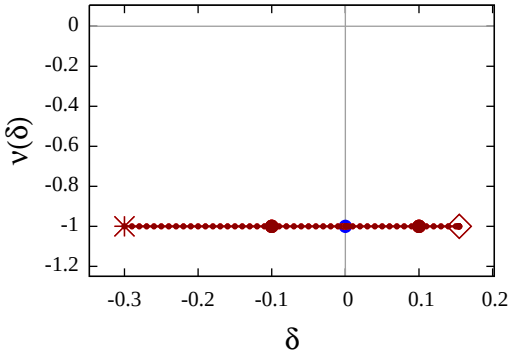

***B*: tuc | cross**	:	12 | 0
***N*: tuc | neigb. | tot**	:	$1\times 6\,d(1), 1\times 3\,c(2..)$ | 2 $\sum = 11$
Free|Dep.|Fix $p^{i}_{x,y}$	:	2 | 20 | 0 $\sum = 22$
Set|Free|Dep.|Fix	:	$a^{\parallel}, b^{\parallel}$ | none | $a^{\perp} = \frac{a^{\parallel}+2b^{\parallel}}{-\sqrt{3}}$, $b^{\perp} = \frac{2a^{\parallel}+b^{\parallel}}{\sqrt{3}}$ | N.A.
$\langle \frac{B}{N} \rangle$	:	2.67
$\mathbf{Z}_{\mathbf{Maxwell}}$	:	7
Reference(s)	:	[24], p.85, Fig.(j)

Auxetic

6.5.11 Star Tiling II K

$(8.3^{*}_{\pi/12}.8.6^{*}_{5\pi/12})$ | $p6mm$ (hexagonal)

↓ 0°

***p6mm* (hexagonal)**

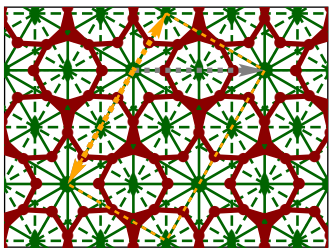

$\delta = -0.10$, $\nu = -1.00$

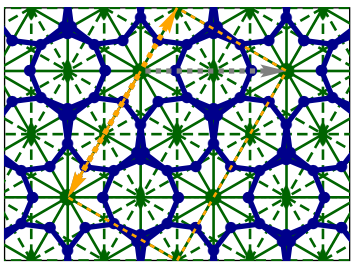

$\delta = 0$, $\boldsymbol{\nu = -1.00}$

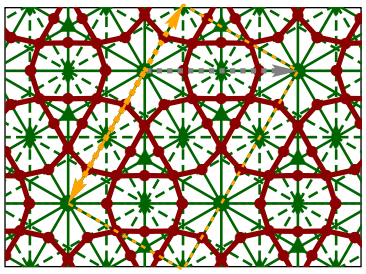

$\delta = 0.05$, $\nu = -1.00$

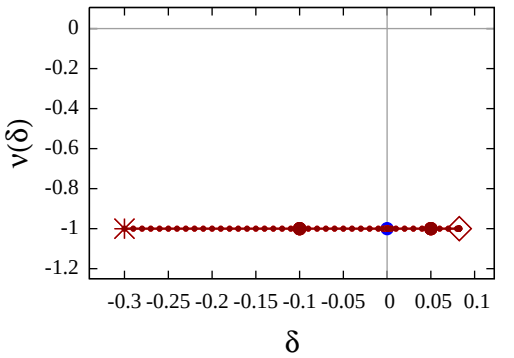

***B*: tuc | cross**	:	24 | 0
***N*: tuc | neigb. | tot**	:	$2\times 6\,e(.m.), 1\times 6\,d(..m)$ | 4 $\sum = 22$
Free|Dep.|Fix $p^{i}_{x,y}$	:	3 | 41 | 0 $\sum = 44$
Set|Free|Dep.|Fix	:	$a^{\parallel}, b^{\parallel}$ | none | $a^{\perp} = \frac{a^{\parallel}+2b^{\parallel}}{-\sqrt{3}}$, $b^{\perp} = \frac{2a^{\parallel}+b^{\parallel}}{\sqrt{3}}$ | N.A.
$\langle \frac{B}{N} \rangle$	:	2.67
$\mathbf{Z}_{\mathbf{Maxwell}}$	:	13
Reference(s)	:	[24], p.85, Fig.(k)

Auxetic

6.5.12 Star Tiling II L

$(8.4^*_{\pi/4}.8.4^*_{\pi/4})$ | $p4mm$ (square)

↓ 0°

***p*4 (square)**

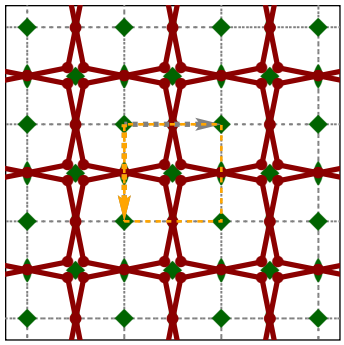

$\delta = -0.10$, $\nu = -1.00$

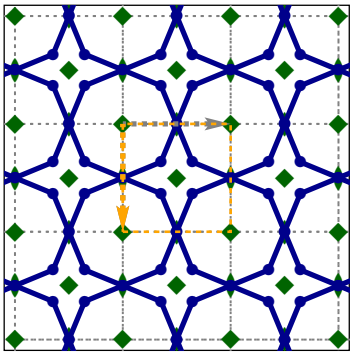

$\delta = 0$, $\boldsymbol{\nu = -1.00}$

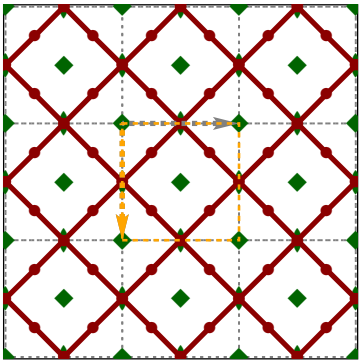

$\delta = 0.083$, $\nu = -1.00$

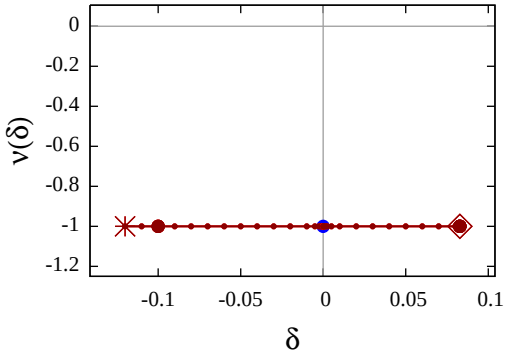

***B*: tuc | cross**	:	8 | 0
***N*: tuc | neigb. | tot**	:	$1\times 4\,d(1), 1\times 2\,c(2..)$ | 2 $\sum = 8$
Free|Dep.|Fix $\mathrm{p}^i_{x,y}$	:	2 | 14 | 0 $\sum = 16$
Set|Free|Dep.|Fix	:	$a^{\parallel}, b^{\parallel}$ | none | $a^{\perp} = -b^{\parallel}$, $b^{\perp} = a^{\parallel}$ | N.A.
$\langle \frac{B}{N} \rangle$	:	2.67
$\mathbf{Z}_{\mathrm{Maxwell}}$	:	5
Reference(s)	:	[24], p.85, Fig.(l)

Auxetic

6.5.13 Star Tiling II M

$(9^2.6^*_{4\pi/9})$ | $p6mm$ (hexagonal)

↓ 0°

***p*6 (hexagonal)**

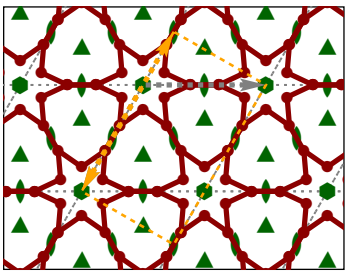

$\delta = -0.10$, $\nu = -1.00$

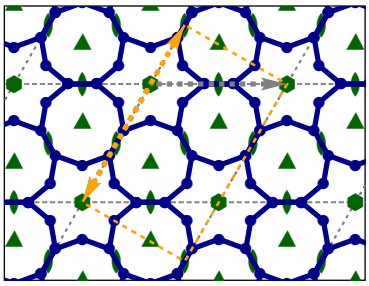

$\delta = 0$, $\boldsymbol{\nu = -1.00}$

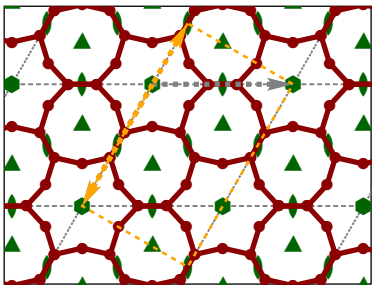

$\delta = 0.03$, $\nu = -1.00$

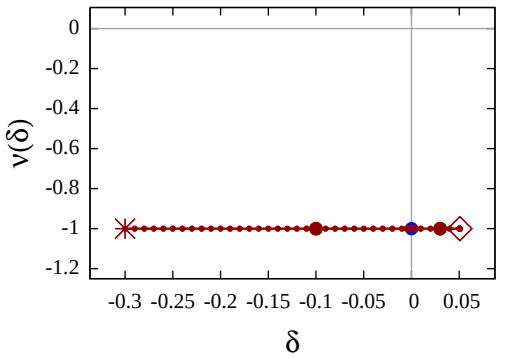

***B*: tuc | cross**	:	15 | 2
***N*: tuc | neigb. | tot**	:	$2\times 6\,d(1)$ | 4 $\sum = 16$
Free|Dep.|Fix $\mathrm{p}^i_{x,y}$	:	4 | 28 | 0 $\sum = 32$
Set|Free|Dep.|Fix	:	$a^{\parallel}, b^{\parallel}$ | none | $a^{\perp} = \frac{a^{\parallel}+2b^{\parallel}}{-\sqrt{3}}$, $b^{\perp} = \frac{2a^{\parallel}+b^{\parallel}}{\sqrt{3}}$ | N.A.
$\langle \frac{B}{N} \rangle$	:	2.50
$\mathbf{Z}_{\mathrm{Maxwell}}$	:	10
Reference(s)	:	[24] p.84, Fig. (m)

Auxetic

6.5.14 Star Tiling II N

$(4.6^*_(pi/6).4.6^*_(pi/6).4.6^*_(pi/6))$ | *p6mm* (hexagonal)

↓ 0°

***p6* (hexagonal)**

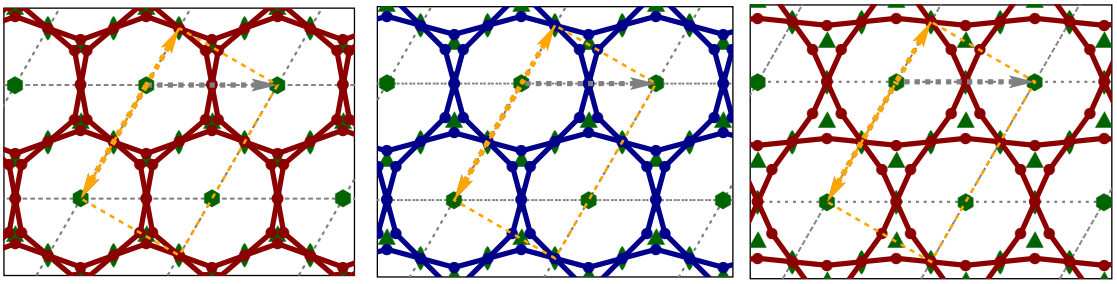

$\delta = -0.03$, $\nu = -1.00$ | $\delta = 0$, $\boldsymbol{\nu = -1.00}$ | $\delta = 0.03$, $\nu = -1.00$

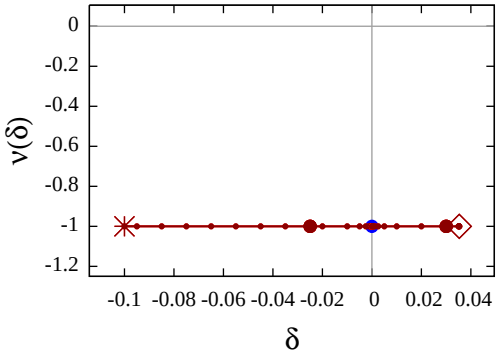

***B*: tuc | cross**	:	12 | 0
***N*: tuc | neigb. | tot**	:	$1\times 6\,d(1), 1\times 3\,c(2..)$ | 2 $\sum = 11$
Free|Dep.|Fix $p^i_{x,y}$	:	2 | 20 | 0 $\sum = 22$
Set|Free|Dep.|Fix	:	$a^{\parallel}, b^{\parallel}$ | none | $a^{\perp} = \frac{a^{\parallel}+2b^{\parallel}}{-\sqrt{3}}$, $b^{\perp} = \frac{2a^{\parallel}+b^{\parallel}}{\sqrt{3}}$ | N.A.
$\langle\frac{B}{N}\rangle$	:	2.67
$\mathbf{Z}_{\mathbf{Maxwell}}$	:	7
Reference(s)	:	[24] p.84, Fig. (n)

Auxetic

6.5.15 Star Tiling II O

$(12^2.4^*_{\pi/3})$ | *p4mm* (square)

↓ 0°

***p4mm* (square)**

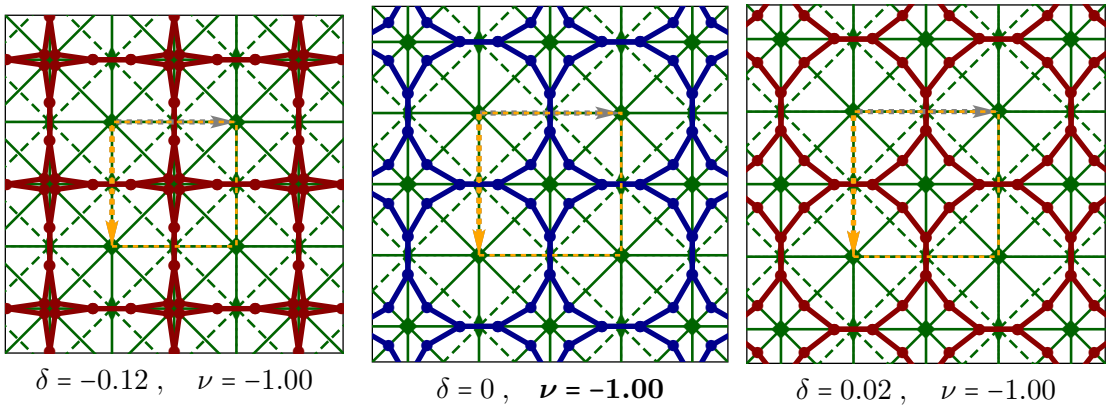

$\delta = -0.12$, $\nu = -1.00$ | $\delta = 0$, $\boldsymbol{\nu = -1.00}$ | $\delta = 0.02$, $\nu = -1.00$

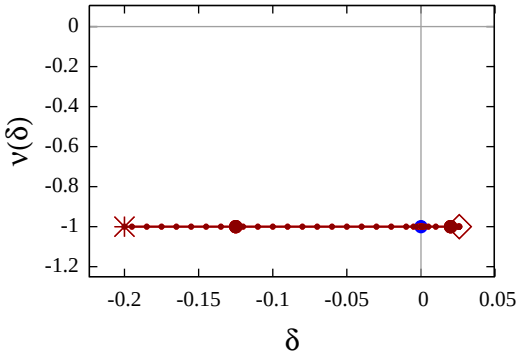

***B*: tuc | cross**	:	10 | 2
***N*: tuc | neigb. | tot**	:	$1\times 4\,f(..m), 1\times 4\,e(.m.)$ | 4 $\sum = 12$
Free|Dep.|Fix $p^i_{x,y}$	:	2 | 22 | 0 $\sum = 24$
Set|Free|Dep.|Fix	:	$a^{\parallel}, b^{\parallel}$ | none | $a^{\perp} = -b^{\parallel}$, $b^{\perp} = a^{\parallel}$ | N.A.
$\langle\frac{B}{N}\rangle$	:	2.50
$\mathbf{Z}_{\mathbf{Maxwell}}$	:	7
Reference(s)	:	[24], p.85, Fig.(o)

Auxetic

6.5.16 Star Tiling II P

$(18^2.3^*_{2\pi/9})$ | *p6mm* (hexagonal)

↓ 0°

***p6mm* (hexagonal)**

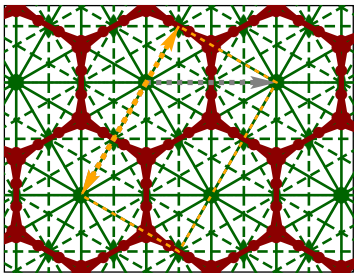

$\delta = -0.03$, $\nu = -1.00$

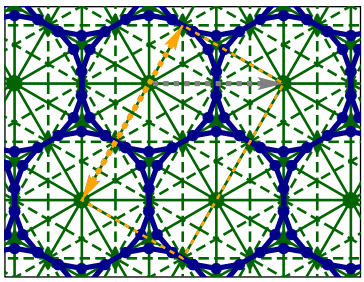

$\delta = 0$, $\boldsymbol{\nu = -1.00}$

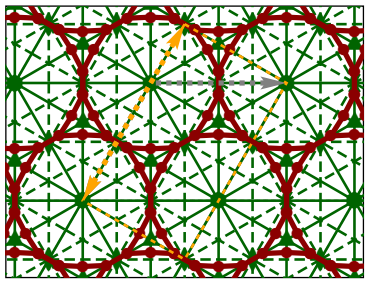

$\delta = 0.01$, $\nu = -1.00$

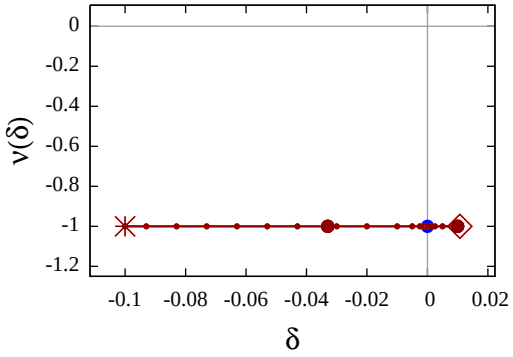

B: tuc | cross	:	15 | 2
N: tuc | neigb. | tot	:	$2\times 6\, e(.m.)$ | 4 $\sum = 16$
Free|Dep.|Fix $\mathrm{p}^i_{x,y}$	:	2 | 30 | 0 $\sum = 32$
Set|Free|Dep.|Fix	:	$a^{\parallel}, b^{\parallel}$ | none | $a^{\perp} = \frac{a^{\parallel}+2b^{\parallel}}{-\sqrt{3}}$, $b^{\perp} = \frac{2a^{\parallel}+b^{\parallel}}{\sqrt{3}}$ | N.A.
$\langle \frac{B}{N} \rangle$	:	2.50
$\mathbf{Z}_{\mathbf{Maxwell}}$	:	10
Reference(s)	:	[24], p.85, Fig.(p)

Auxetic

6.5.17 Star Tiling II Q

$(5^2.4^*_{\pi/10}.5.4^*_{\pi/10})$ | *p4gm* (square)

↓ 0°

***p4gm* (square)**

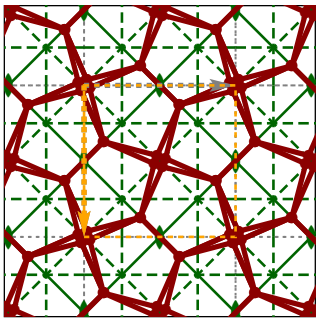

$\delta = -0.05$, $\nu = -1.00$

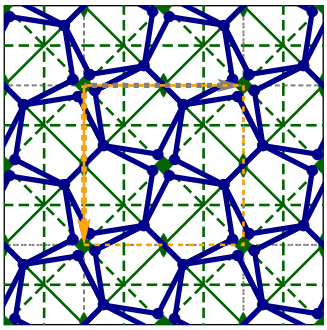

$\delta = 0$, $\boldsymbol{\nu = -1.00}$

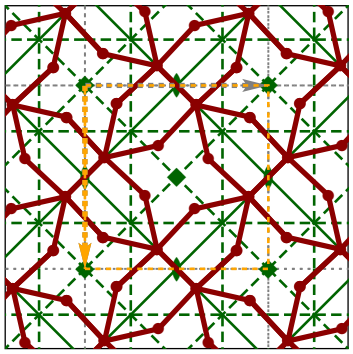

$\delta = 0.15$, $\nu = -1.00$

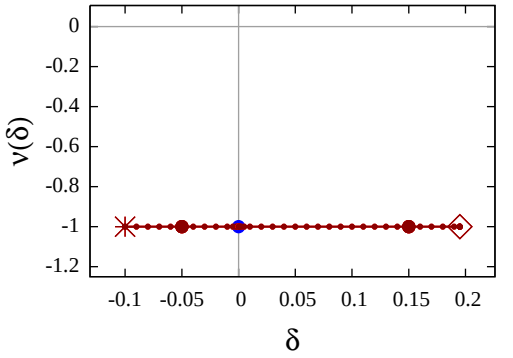

B: tuc | cross	:	18 | 6
N: tuc | neigb. | tot	:	$1\times 8\, d(1), 1\times 4\, c(..m)$ | 8 $\sum = 20$
Free|Dep.|Fix $\mathrm{p}^i_{x,y}$	:	3 | 37 | 0 $\sum = 40$
Set|Free|Dep.|Fix	:	$a^{\parallel}, b^{\parallel}$ | none | $a^{\perp} = -b^{\parallel}$, $b^{\perp} = a^{\parallel}$ | N.A.
$\langle \frac{B}{N} \rangle$	:	3.00
$\mathbf{Z}_{\mathbf{Maxwell}}$	:	7
Reference(s)	:	[24], p.85, Fig.(q)

Auxetic

6.6 Rigid uniform tilings

6.6.1 Triangular Tiling

↓ 0°

(3^6) - Deltille (Conway) | $p6mm$ (hexagonal)

***p*1 (oblique)**

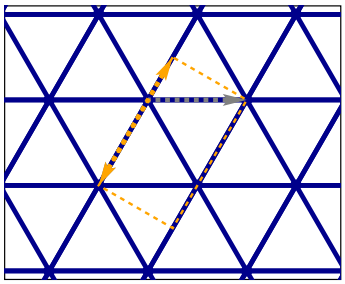

***B*: tuc | cross**	:	3 | 2
***N*: tuc | neigbour | total**	:	$1 \times 1\, a(1)$ | 3 $\sum = 4$
Free|Depend.|Fixed $p^i_{x,y}$	:	0 | 6 | 2 $\sum = 8$
Set|Free|Depend.|Fixed	:	$a^{\parallel}, b^{\parallel}$ | $a^{\perp}, b^{\perp}$|none|none
$\langle \frac{B}{N} \rangle$	:	6.00
$\mathbf{Z}_{\mathbf{Maxwell}}$	:	0
Reference(s)	:	[24], p.63, Fig.1

Rigid

6.6.2 Snub Hexagonal Tiling

↓ 0°

$(3^4.6)$ - Snub Trihexagonal Tiling (Conway) - enantiomorphic | $p6$ (hexagonal)

***p*1 (oblique)**

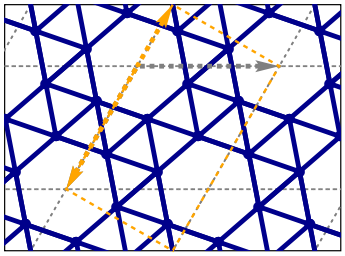

***B*: tuc | cross**	:	15 | 6
***N*: tuc | neigbour | total**	:	$6 \times 1\, a(1)$ | 8 $\sum = 14$
Free|Depend.|Fixed $p^i_{x,y}$	:	10 | 16 | 2 $\sum = 28$
Set|Free|Depend.|Fixed	:	$a^{\parallel}, b^{\parallel}$ | $a^{\perp}, b^{\perp}$|none|none
$\langle \frac{B}{N} \rangle$	:	5.00
$\mathbf{Z}_{\mathbf{Maxwell}}$	:	-2
Reference(s)	:	[24], p.63, Fig.4/5

Rigid

6.6.3 2-Uniform 1

↓ 0°

$(3^6;3^4.6)_1$ | $p6$ (hexagonal)

***p*1 (oblique)**

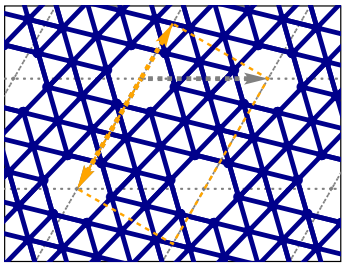

***B*: tuc | cross**	:	33 | 10
***N*: tuc | neigbour | total**	:	$12 \times 1\, a(1)$ | 12 $\sum = 24$
Free|Depend.|Fixed $p^i_{x,y}$	:	22 | 24 | 2 $\sum = 48$
Set|Free|Depend.|Fixed	:	$a^{\parallel}, b^{\parallel}$ | $a^{\perp}, b^{\perp}$|none|none
$\langle \frac{B}{N} \rangle$	:	5.50
$\mathbf{Z}_{\mathbf{Maxwell}}$	:	-8
Reference(s)	:	[24], p.67 , Fig.12

Rigid

6.6.4 2-Uniform 2

↓ 0°

$(3^6;3^4.6)_2$ | $p6mm$ (hexagonal)

***p*1 (oblique)**

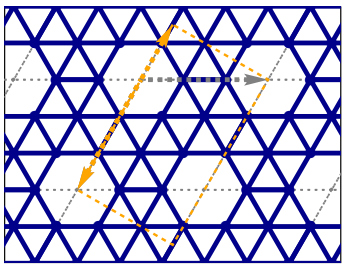

***B*: tuc | cross**	:	21 | 2
***N*: tuc | neigbour | total**	:	$8 \times 1\, a(1)$ | 4 $\sum = 12$
Free|Depend.|Fixed $p^i_{x,y}$	:	14 | 8 | 2 $\sum = 24$
Set|Free|Depend.|Fixed	:	$a^{\parallel}, b^{\parallel}$ | $a^{\perp}, b^{\perp}$|none|none
$\langle \frac{B}{N} \rangle$	:	5.25
$\mathbf{Z}_{\mathbf{Maxwell}}$	:	-4
Reference(s)	:	[24], p.63 , Fig.12

Rigid

7 Conclusion and outlook

This thesis is part of a research field with overriding aim to find a relationship between morphology of a spatial structure and its deformation behaviour. The simple and well-defined model system considered here, skeletal structures, coarsely describe cellular or similar microstructured physical systems and it can be treated numerically. To this purpose this thesis has developed a numerical tool to determine the deformations of skeletal structures. This tool has been used for a quantitative analysis of plane periodic tessellations and their Poisson's ratios, some qualitative corresponding morphology features and auxetic deformation has been observed.

Main results Software to calculate deformations of periodic and symmetric skeletal structures based on plane tessellations has been implemented from scratch. This program computes the response of a skeletal structure to an imposed strain in a given direction and of a given amplitude. It retains the periodicity of the skeletal structure and constrains the deformation to configurations that retain some or all of the symmetries of the original skeletal structure. This software is immediately applicable to any symmetric periodic skeletal structure.

With this program we have analysed finite and infinitesimal Poisson ratios of 55 tilings including Archimedean, 2-uniform and star tilings. This analysis shows that there are a large number of uniform tilings with auxetic behaviour and that there are two common elements of the deformation mode in auxetic skeletal structures: reentrant and rotating elements. We show several examples of auxetic skeletal structures without reentrant elements.

All 55 considered tilings can be categorised in 4 types with respect to the deformation behaviour. *Rigid* tilings that are not deformable (2 Archimedean and 2 2-uniform tilings). Tilings which posses a *unique deformation mode* in $p1$, that means beside the periodicity and the rigidity of the bars there are no more further constraints necessary to reach a one-dimensional solution space. These are of particular interest due to the minimum of further constraints. There are four Archimedean, eight 2-uniform tilings and one star tiling I with this property.
Among these 13 is the trihexagonal tiling already identified as auxetic (that is identical to a deformed version of one of the other 12, see 6.2.17 and 6.4.4), but also two further auxetic structures that have not been identified as such in the literature (see 6.3.6, 6.3.10). Furthermore there are several examples of structures that are not infinitesimally auxetic but become auxetic upon finite, relatively large deformations (see e.g. 6.2.8, 6.3.12 and 6.3.13).

The third type are skeletal structures which can be uniquely deformed if symmetry constraints are enforced. It is possible that the same tiling has different deformation modes when embedded in different symmetry groups, called *unique symmetry mode* in a given group. There are 32 uniform tilings which have 48 unique symmetry modes. Some unique mechanisms of a given tiling yield the same unique mechanism of a different tiling (see e.g. 6.2.18 and 6.3.6).

Finally there are still two tilings which have *no unique deformation modes* in all of their symmetry groups, where the tiling is not rigid (2-uniform 13 and 18).

Relation between infinitesimal and finite deformations The analysis of this thesis includes infinitesimal deformations (that are also the scope of linear rigidity theory [45]) and finite deformations. Our results emphasise that the need to study finite deformations, as we show several examples where the infinitesimal deformation has a positive Poisson's ratio but in contrast under finite deformations the skeletal structure becomes auxetic. We also show several examples where Poisson's ratio is ill-defined, i.e. diverges to ∞ as the strain $\delta \to 0$, for infinitesimal deformations, but where finite deformations are unique and well-behaved. The square is such an example that shows that the infinitesimal result does not allow any conclusions to finite situations. The diverging Poisson's ratio appears only for small δ for finite deformation ν is also finite. A diverging Poisson's ratio at $\delta = 0$ does not allow for a prediction of finite deformations.

More generally speaking, the relationship of the approach and results presented here to linear rigidity theory should be analysed in more detail. Specifically the question if the notion of "rigid" in the sense of rigidity theory and in the sense of our finite deformation at $\delta = 0$ is strictly the same should be addressed, specifically for periodic skeletal structures.

Anisotropy of the deformation problem The numerical approach of this thesis can be applied to studying the anisotropy of the Poisson's ratio, i.e. its dependency on the direction of the applied strain. This aspect of skeletal structure deformation is partially studied already in this thesis (see different deformation directions in the tables in chapter 6, e.g. reentrant honeycomb sects. 6.1.1 and 6.1.2), but a more comprehensive analysis is needed. This relates to a more fundamental problem, namely the definition of the Poisson's ratio for periodic structures for a given strain direction. The particular aspect that needs to be resolved in this context are possibilities to constrain the deformation such that rotations are not possible, which implies further constrains in addition to the symmetry constraints when dealing with non-rectangular symmetry groups, see sect. 2.5. The approach chosen for the results of this thesis allows rotations of the skeletal structure.

A direction-dependent ("anisotropic") analysis is fully implemented in the software. This analysis will be helpful also to gain better insight into the relationship between morphology and deformation.

Ambiguity of the deformation – statistical physics description An important frequently encountered problem in the treatment of deformations of skeletal structures is the lack of unique deformation modes. Often a skeletal structure has more than one deformation mode, i.e. the deformation is not uniquely defined by the applied strain and the system of edge equations has a multi-dimensional solution space. For structures with ambiguous deformations the Poisson's ratio is not immediately defined. In this thesis the problem of ambiguous deformations is approached geometrically, but imposing addition symmetry constraints for the deformed structure. Poisson's ratios are only computed for skeletal structures in symmetry groups where the deformation is unique (see Tables of chapter 6).

A more physical approach to ambiguous deformation modes is provided by ideas from statistical mechanics that may be applicable (with the caveat of possibly very few degrees of freedom). For a structure with a multicontinuous solution space, the resulting Poisson's ratio is determined as an average over all possible configurations (for the given applied strain). If an energy is defined for a given configuration (for example a harmonic spring model for the edge angles at joints, cf. also sect. 2.6), the configurations are weighted by a Boltzmann factor. A definition of a thermodynamically averaged Poisson's ratio then becomes possible, applicable to structures with multi-dimensional solution spaces. With an energy functional defined one may also seek the groundstate deformation, i.e. the deformation that minimizes energy.

The crucial question with regards to the applicability of the presented algorithm is whether or not it allows for a sampling of the configuration space. While evidently the starting configurations can be chosen randomly, the equal sampling of the solution space may be hindered by the minimizing steps in the SVD solution of zeros of the edge equations. It is an open question that should be addressed in the future.

Aperiodic skeletal structures The basic concept of solving a system of bar equations is not limited to consideration of a minimal translational unit cell of periodic plane skeletal structures with periodic boundary conditions. Trivially it is also possible to deform structures that correspond to multiple translational unitcells (note that the algorithm is approximately $\mathcal{O}(B^3)$ in the number of bars B). Evidently, the periodicity of the individual unit cells is then no longer constraint during the deformation. Periodic boundary conditions are also not a conceptional requirement but can be replaced by e.g. pivoting joints at all points where the structure intersects with a given boundary frame. In the same manner non-periodic tilings or skeletal structures can be handled. Of particular interest may be the extension to aperiodic tilings such as the Penrose or spiral tessellations [24] or disordered skeletal structures.

Extension to 3D The presented implementation handles only tessellations of the plane and not of the space. However there is no fundamental reason which limits the approach to the plane. The extension to 3D is of great interest, motivated for example by Lakes' suggestion of an idealised unit cell of his auxetic disordered polymer foam, see Fig. 7.1 [29]. This model is generated by a modification of a 3 dimensional 24-sided polyhedron.

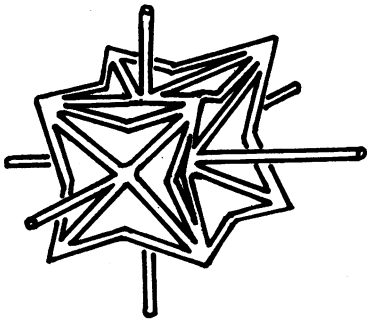

Figure 7.1: *3 dimensional skeletal structure: cell with reentrant elements gained by a symmetrical collapse of a 24-sided polyhedron with cubic symmetry (from [29]). Note not all edges of the limiting faces of the polyhedron are considered as bars.*

The principles of the described approach to deformations of skeletal structures also apply to 3D skeletal structures, with in particular greatly increased number of degrees of freedom (see sect. 2.3) and hence increased computing times. It also seems evident that high-dimensional solution space of the edge equations will be pose more severe problems in 3D.

Nevertheless, the investigation of symmetric 3D tessellations in terms of the deformation behaviour as skeletal structures appears interesting, and resources of spatial tessellations by polyhedra which can tessellate the space are available (see for an introduction of this topic e.g. [11]).

Skeletal structures as models of auxetic physical systems A number of physical systems exhibit auxetic or related behaviour and some of the mechanisms can be interpreted or modelled (at least in a rough approximation) as skeletal structures.

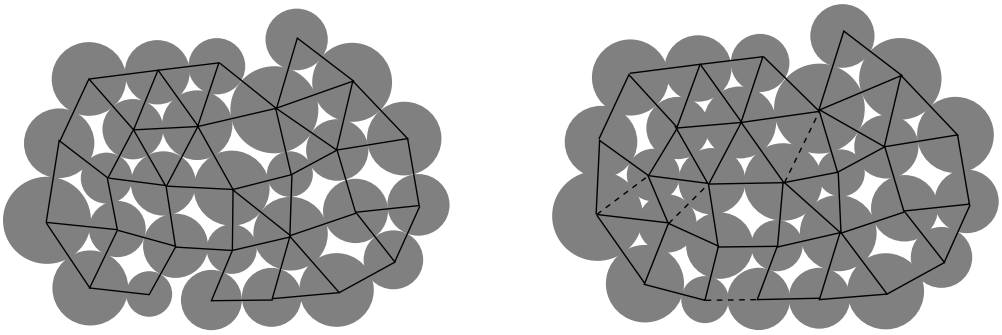

Figure 7.2: *Model of 2d granular matter: particles which are in contact can transmit stresses. The distribution of the stresses can be represented as a contact network of rigid bars linked at joints. This is in general not stable against weak perturbations at leads to other distribution indicated by the right image with dotted lines of new bars.*

In granular matter a phenomenon similar to auxetic behaviour is known as Reynolds dilatancy, meaning granular packings always expand when sheared [39]. Models of granular matter consider an underlying contact network as indicated by the black straight lines in Fig. 7.2 [36]. The contact network illustrates the non-homogenous distribution of stresses of a possible imposed compression. This network changes under weak perturbations which demonstrates that granular matter is actual unstable [36]. This means that dynamically network bars may disappear or emerge. The bars have a sign-constraint that means they carry load only in one direction (compression) – trivial as granular matter is not stable against expansion. Therefore, this model does not correspond immediately to the considered skeletal structure. However if one ensures that two particles that are in contact remain in contact (allowing only sliding of particles) the skeletal structure model applies. This is for example realised by adhesion forces. A concrete physical example is wet sand, where the surface tension of the liquid leads to capillary bridges which links individual grains of the sand [40].

The deformation behaviour of biopolymers is an active field of research, particularly due to the report of so-called *negative normal stress* [28]. A specific toy model for such networks was proposed in [10]: biopolymer filaments are represented by straight segments that may stretch length-wise up to a maximal expansion. If that maximal expansion is reached, the

filaments become bars of a skeletal structure. Fig. 7.3 shows in the left image the initial configuration of the link points of the filaments in a hexagon pattern. The actual filaments are not shown. This shall only illustrate the initial setup. The following images show only those filaments that are maximally expanded and hence represents bars. The last image shows the threshold state, where all filaments are fully expanded. This state represents a skeletal structure, however not necessarily a rigid one. Note the vertices are not plotted, and hence the middle image may contain straight lines consisting of two filaments. This is a system with also a sign-constraint (hindering maximal expansion, hence opposite to the granular media contact network).

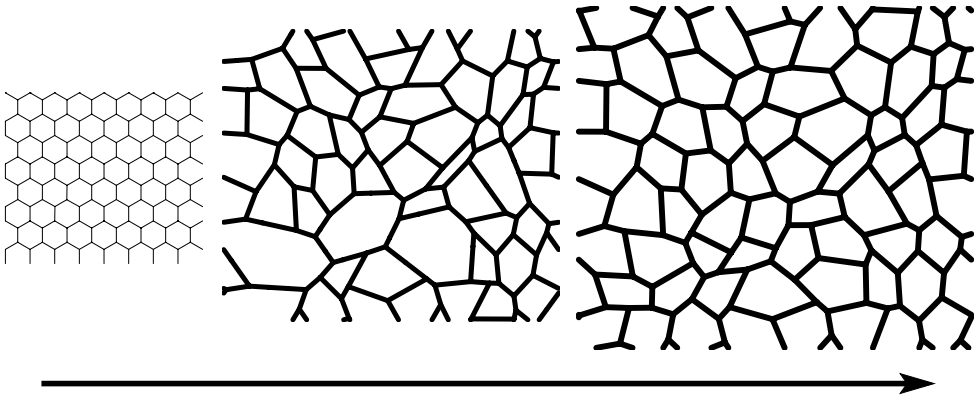

Figure 7.3: *Model of a biopolymer with different lengths of the filaments which will be stretched (from [10]): the left image shows the initial configuration; the lines do not represent the filaments of the polymer, they indicate only the distribution of the vertices where the single filaments are linked. During the stretching different filaments become taut and so a bar of the skeletal structure. These taut filaments are only drawn in the other images. The last image shows the threshold state where all filaments are taut. Although in the case of non-rigidity of the emerged skeletal structure it could be further stretched. This further deformation represents a deformation as considered in this thesis.*

In our skeletal framework model, rotational symmetry constraints can lead to fixed angles between bars linked at a common joint. A physical system with a similar effect is semi-crystalline elastomeric polypropylene (ePP) shown in Fig. 7.4 that was recently found to be locally auxetic [17]. The explanation provided in [17] is that the angle between mother and daughter crystalline lamellae is fixed to $\sim 80°$, because of the epitaxial growth mechanism and is experimentally verified. A fixed angle implies that the structure expands in both perpendicular directions.

Note the similarities to the constraint-symmetry deformations discussed in angle between the substrate plane and the vertically grown crystalline phases. However the length of the crystalline phases is not constant (no "rigid bars") and so it cannot be modelled by a skeletal structure. In order to make the difference clear the proposed model of ePP consists of expandable bars and link points, where the bars are fixed together. The auxetic behaviour occurs only locally and has no reentrant or rotating elements. In contrast our model has rigid bars and joints where the bars can pivot freely and auxetic behaviour has always reentrant or rotating elements.

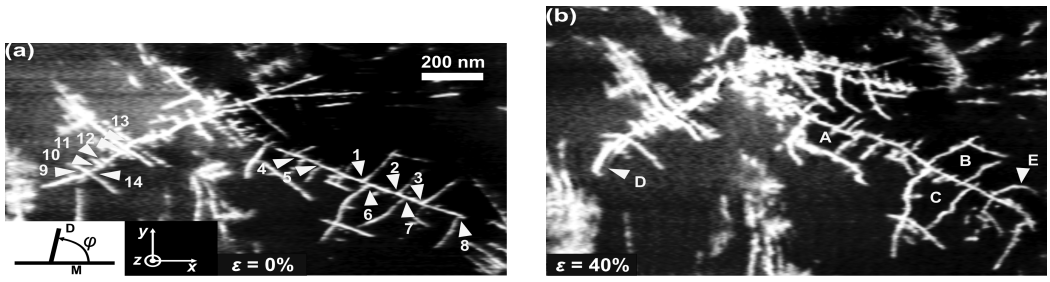

(a) *Undeformed* **(b)** *Deformed*

Figure 7.4: *Elastomeric polypropylene (ePP) - The white lines are the crystalline lamellae and the dark area is the amorphous phase. The deformation is imposed vertically and hence the image of the deformed substrate has a greater height (right image). The white rectangulars are expanded in their length as well as in their height which shows therefore auxetic behaviour. (from [17])*

Deformation and quantitative morphology measures As mentioned above, the eventual goal is to understand how morphology of the initial structure determines the deformation mechanisms. In particular the aim is to identify quantitative morphological measures that relate to Poisson's ratio with simple functional form. As a first step in this direction we intend to analyse if there are correlations between Poisson's ratio and so-called Minkowski functionals [34] or their extensions to (possibly higher-rank) Minkowski tensors [3, 4, 41] which are integral (average) geometric measures. In particular these depend on the curvatures of the structures and may hence be able to distinguish reentrant elements as in the inverted honeycomb pattern or such with stars. These or similar morphology analysis are now possible with the quantitative numerical deformation approach of this thesis.

Appendix A

Subgroups in one-basis representation

As noted in section 3.4 10 of the 17 crystallographic groups have t-subgroups represented in the basis of the original group that differ because of the different basis from the conventional setting proposed in [26].

There are two possibilities. Either the basis of the original group is changed for the subgroup to get the conventional setting or the basis will not be changed and all symmetry operations are done in this basis. In the second case the program `tesselate` needs correct group informations. That are cell type, asymmetric unit, symmetry operations in the correct basis and the description of the different site symmetries denoted by the Wyckoff letter. Only providing the basis transformation is not sufficient for the program `tesselate`. The program `subgroup` must be able to specify the non-conventional subgroups which will be noted in the file which the program `tesselate` reads in. The program `tesselate` can only work correct if the necessary informations to generate the data for the deformation program are available. Additonal group-files are created which describe these isomorphic groups. For instance they contain the symmetry operations represented in the same basis of the original group which are copied from them. Furthermore an appropriate asymmetric unit is denoted by giving vertices of the polygon and wyckoff letters with corresponding sites are listed.

The differences between the conventional representation and the modified can be described by three operations: centered (primitive) unit cell instead of primitive (centered), rotation and translation relation of the basis vectors. These three can occur combined or alone. The table A.1 list all cases of the t-subgroups that occur in different representations.

Table A.1: *t-subgroups of the 17 groups which are represented in a different basis than the conventional ones (#14).*

No.	Used Name	Isomorphic ITC Group	Description	t-subgroup of
18	$c1$	$p1$	centered $p1$	cm, $c2mm$
19	$c2$	$p2$	centered $p2$	$c2mm$
20	$p1m1$	pm	shifted pm	$p2mg$
21	$p11m$	pm	rotated pm	$p2mm$
22	$p11g$	pg	rotated pg	$p2mg$
23	$p1g1$	pg	shifted pg	$p2gg$, $p4gm$
24	$p11gs$	pg	rotated and shifted pg	$p2gg$, $p4gm$
25	$c11m$	cm	rotated cm	$c2mm$
26	pm_r	cm	decentered cm	$p31m$, $p6mm$
27	$p11m_r$	cm	rotated decentered cm	$p4mm$, $p6mm$
28	$p1m1_r$	cm	shifted decentered cm	$p4gm$
29	$p11ms_r$	cm	rotated and shifted decentered cm	$p3m1$, $(p4gm)$
30	$p2mm_r$	$c2mm$	decentered $c2mm$	$p4mm$, $p6mm$
31	$p21ms_r$	$c2mm$	shifted decentered $c2mm$	$p4gm$

A.1 List of the t-subgroups of the 17 conventional plane groups

A.1.1 *p1* (1)

p1 has no t-subgroups. However it is a t-subgroup of all crystallographic groups (unit element of the point group).

A.1.2 *p2* (2)

p2 has as t-subgroup only *p1*. It's a maximal t-subgroup of *p2mm*, *p2mg*, *p2gg* and *p4*.

A.1.3 *pm* (3)

pm is a t-subgroup of p4mm. It's own t-subgroup is only *p1*.

A.1.4 *pg* (4)

Conventional *pg* is not a t-subgroup of any conventional crystallographic group. It's own t-subgroup is only *p1*.

A.1.5 *cm* (5)

t-subgroup of $c2mm$; has as t-subgroup c1;

A.1.6 *p2mm* (6)

Maximal t-subgroup of *p4mm*; but as t-subgroup of *p4mm* no difference in *pm* orientation!

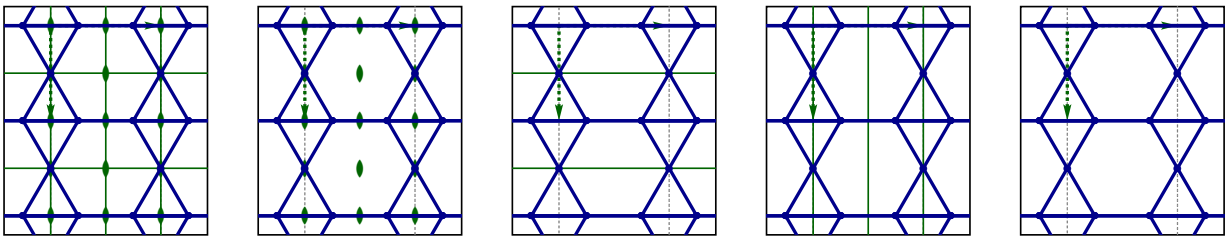

(a) *group: p2mm (6)* **(b)** *subgroup: p2 (2)* **(c)** *subgroup: pm (3)* **(d)** *subgroup: p11m (3, pm)* **(e)** *subgroup: p1 (1)*

Figure A.1: *All t-subgroups of p2mm; shown structure 2-uniform_ 15*

A.1.7 *p2mg* (7)

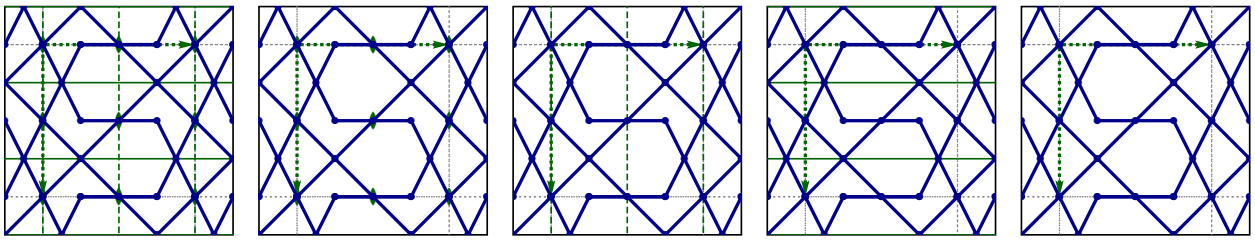

(a) *group: p2mg* **(b)** *subgroup: p2* **(c)** *subgroup: p11g (pg)* **(d)** *subgroup: p1m1 (pg)* **(e)** *subgroup: p1*

Figure A.2: *All t-subgroups of p2mg; a tiling with symmetry group p2mg*

A.1.8 *p2gg* (8)

t-subgroup of p4gm;

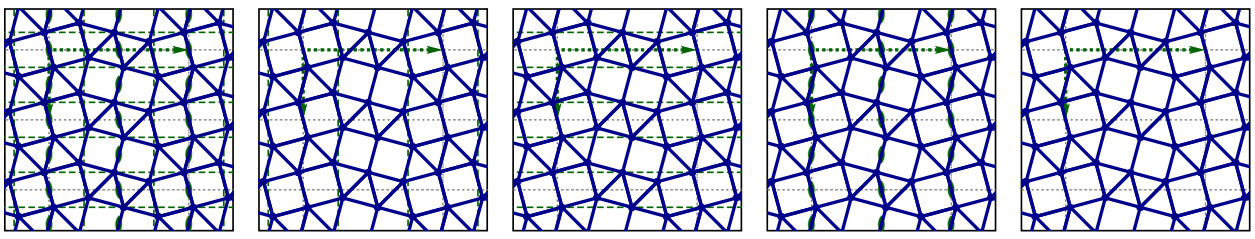

(a) *group: p2gg* **(b)** *subgroup: p11gs (4, pg)* **(c)** *subgroup: p1g1 (4, pg)* **(d)** *subgroup: p2 (2)* **(e)** *subgroup: p1 (2)*

Figure A.3: *All t-subgroups of p2gg; shown structure 2-uniform_ 10*

A.1.9 c2mm (9)

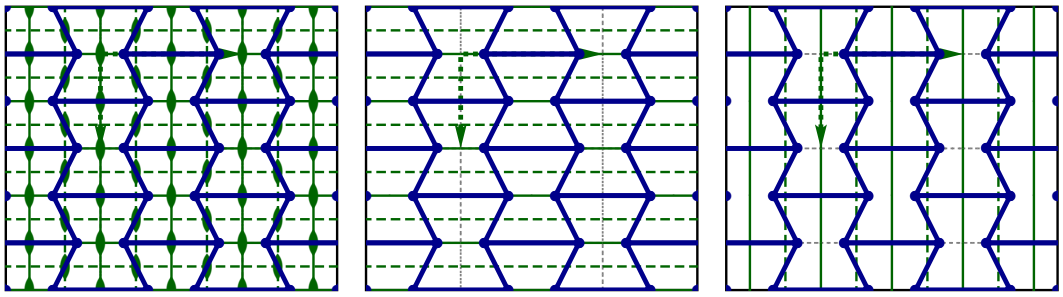

(a) *group: c2mm (9)* **(b)** *subgroup: cm (5)* **(c)** *subgroup: c11m (5, cm)*

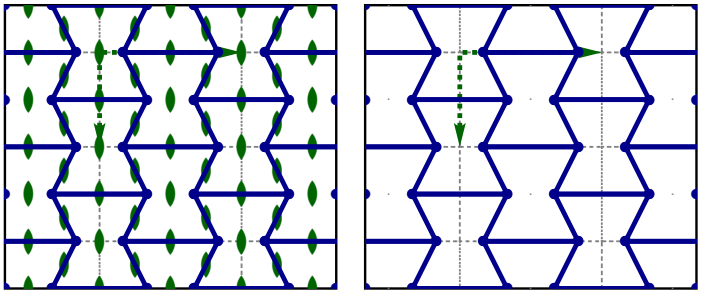

(d) *subgroup: c2 (2, p2)* **(e)** *subgroup: c1 (1, p1)*

Figure A.4: *All t-subgroups of c2mm; shown structure re-entrant honeycomb*

A.1.10 p4 (10)

maximal t-subgroup of *p4mm*, *p4gm*;

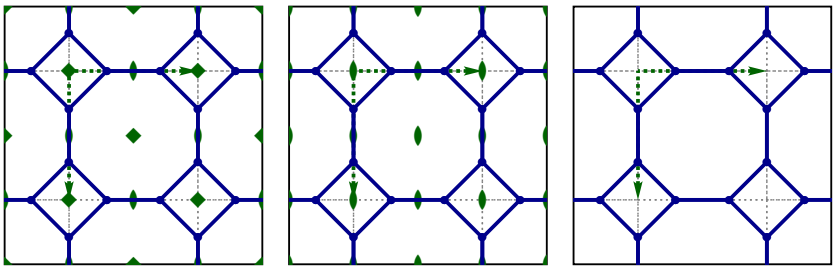

(a) *group: p4 (10)* **(b)** *subgroup: p2 (2)* **(c)** *subgroup: p1 (1)*

Figure A.5: *Maximal t-subgroup p4 of p4mm with all its t-subgroups (truncated square tiling)*

A.1.11 p4mm (11)

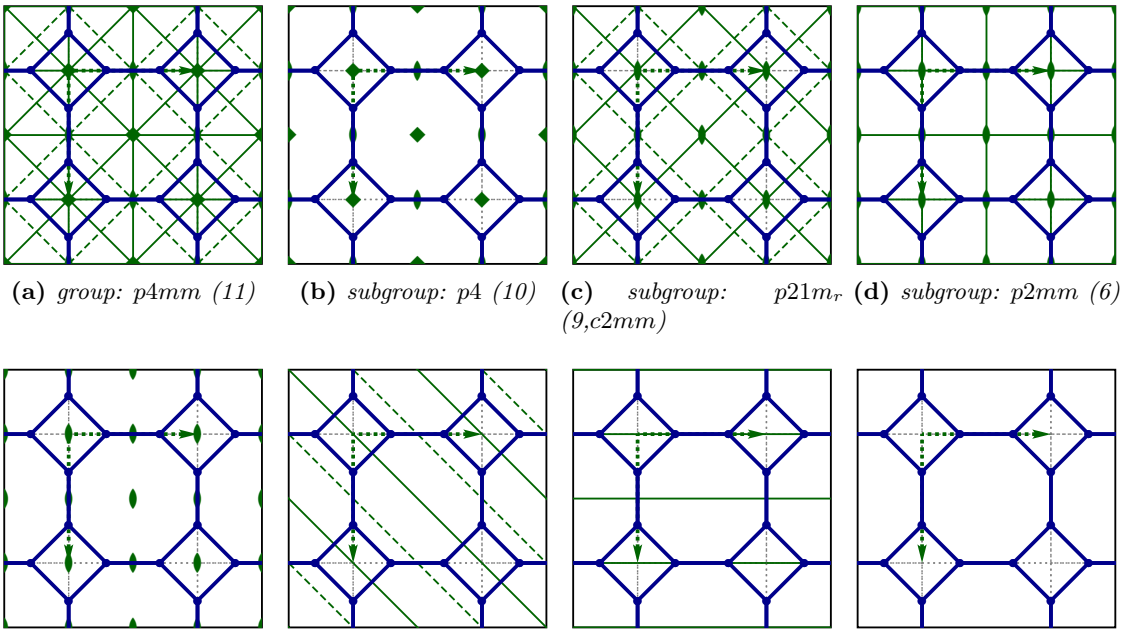

(a) *group: p4mm (11)* **(b)** *subgroup: p4 (10)* **(c)** *subgroup: $p21m_r$ (9,c2mm)* **(d)** *subgroup: p2mm (6)*

(e) *subgroup: p2 (2)* **(f)** *subgroup: pm_r (5, cm)* **(g)** *subgroup: pm (3)* **(h)** *subgroup: p1 (1)*

Figure A.6: *All t-subgroups of p4mm(11) (truncated square tiling)*

A.1.12 p4gm (12)

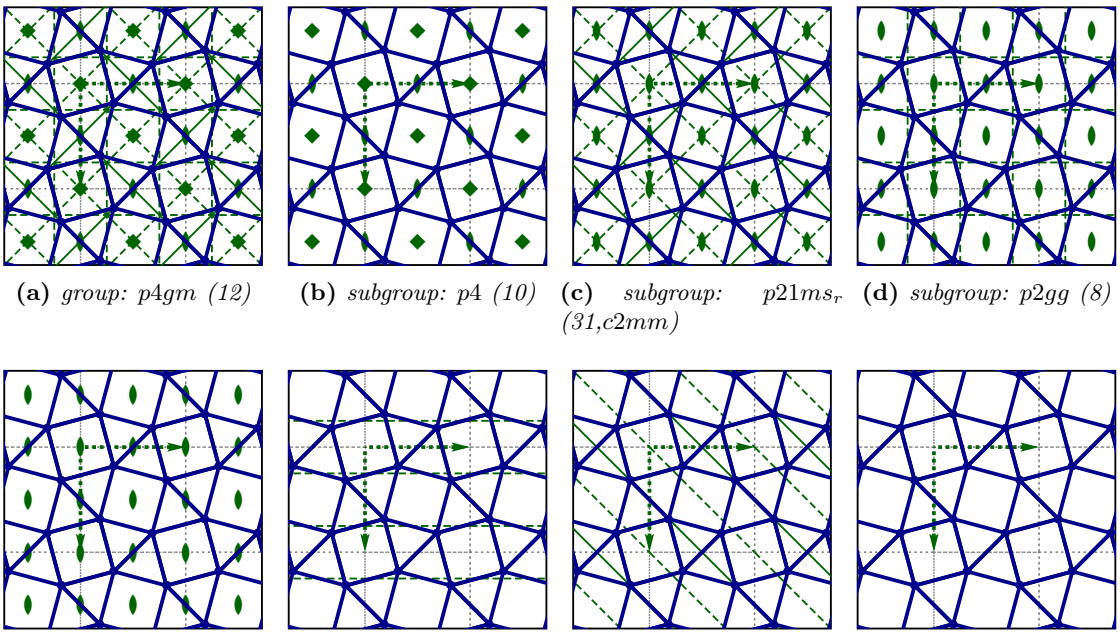

(a) *group: p4gm (12)* **(b)** *subgroup: p4 (10)* **(c)** *subgroup: $p21ms_r$ (31,c2mm)* **(d)** *subgroup: p2gg (8)*

(e) *subgroup: p2 (2)* **(f)** *subgroup: p1g1 (4,pg)* **(g)** *subgroup: $p1m1_r$ (5,cm)* **(h)** *subgroup: p1 (1)*

Figure A.7: *All t-subgroups of p4gm (12); shown structure Archimedean tiling* $(3^2.4.3.4)$

A.1.13 p3 (13)

$p3$ has only $p1$ as a t-subgroup and is a maximal t-subgroup of $p6$.

A.1.14 p3m1 (14)

$p3m1$ is a maximal t-subgroup of $p6mm$. All t-subgroups of $p3m1$ are shown in Fig. A.8.

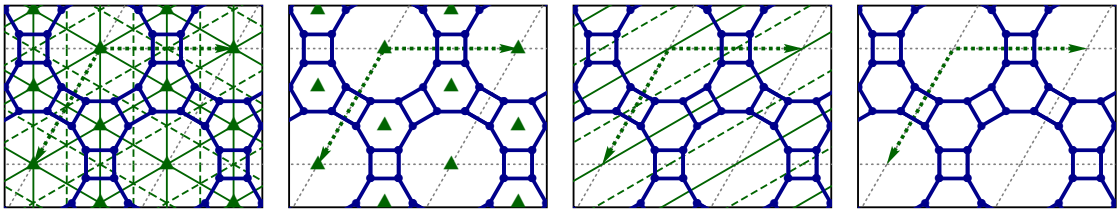

(a) *group: p3m1 (14)* **(b)** *subgroup: p3 (13)* **(c)** *subgroup: p11ms_r (5, cm)* **(d)** *subgroup: p1 (1)*

Figure A.8: *All t-subgroups of p3m1 (14)*

A.1.15 p31m (15)

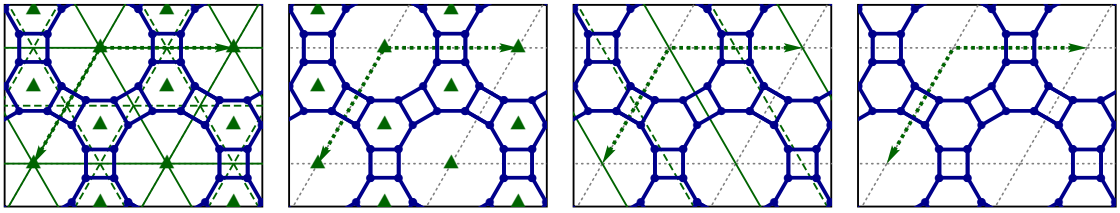

(a) *group: p31m (15)* **(b)** *subgroup: p3 (13)* **(c)** *subgroup: pm$_r$ (5, cm)* **(d)** *subgroup: p1 (1)*

Figure A.9: *All t-subgroups of p31m; shown the maximal t-subgroup p6 with its t-subgroups*

A.1.16 p6 (16)

maximal t-subgroup of $p6mm$.

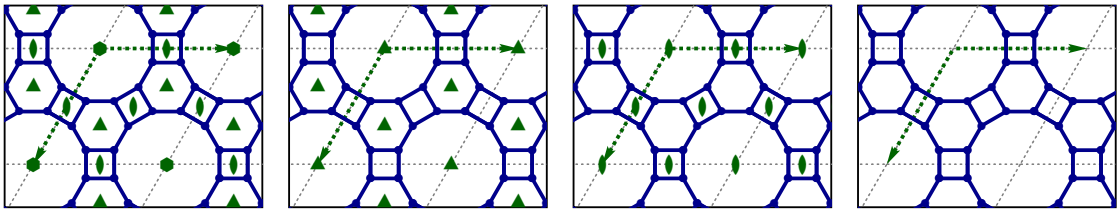

(a) *group: p6 (4)* **(b)** *subgroup: p3 (3)* **(c)** *subgroup: p2 (2)* **(d)** *subgroup: p1 (1)*

Figure A.10: *All t-subgroups of p6 (16); shown the maximal t-subgroup p6 with its t-subgroup*

A.1.17 p6mm (17)

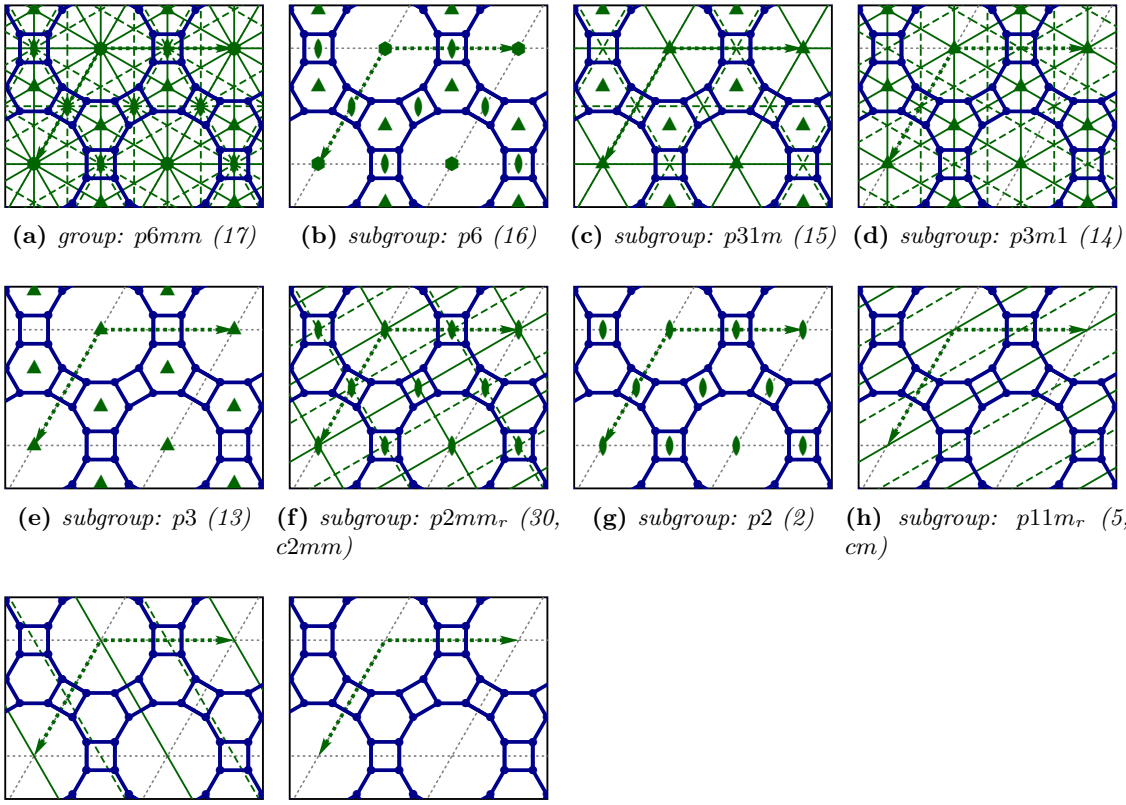

(a) *group: p6mm (17)* **(b)** *subgroup: p6 (16)* **(c)** *subgroup: p31m (15)* **(d)** *subgroup: p3m1 (14)*

(e) *subgroup: p3 (13)* **(f)** *subgroup: p2mm$_r$ (30, c2mm)* **(g)** *subgroup: p2 (2)* **(h)** *subgroup: p11m$_r$ (5, cm)*

(i) *subgroup: pm$_r$ (5, cm)* **(j)** *subgroup: p1 (1)*

Figure A.11: *All t-subgroups of p6mm; (great rhombitrihexagonal tiling)*

List of Figures

Bibliography

[1] R. f. Almgren. An isotropic three-dimensional structure with poisson's ratio =-1. *Journal of Elasticity*, 15(4):427–430, 1985.

[2] K. Ando and H. Onda. Mechanism for deformation of wood as a honeycomb structure i: Effect of anatomy on the initial deformation process during radial compression. *Journal of Wood Science*, 45(2):120–126, 04 1999.

[3] C. Beisbart, R. Dahlke, K. Mecke, and H. Wagner. Vector- and tensor-valued descriptors for spatial patterns. *Morphology of Condensed Matter*, pages 238–260, 2002.

[4] B. Breidenbach. *Scalar and tensor-valued Minkowski functionals of spatially complex structures*. PhD thesis, Naturwissenchaftliche Fakultäten der Universität Erlangen-Nürnberg, 2007.

[5] H. Burzlaff and H. Zimmermann. *Kristallsymmetrie, Kristallstruktur*. Merkel, Erlangen, 1986.

[6] T. J. Chung and T. J. Chung. *General continuum mechanics*. Cambridge University Press, Cambridge, 2nd edition, 2007.

[7] R. Connelly and H. Servatius. Higher-order rigidity-what is the proper definition? *Discrete and Computational Geometry*, 11(1):193–200, 1994.

[8] D. A. Cox, J. B. Little, and D. O'Shea. *Ideals, varieties, and algorithms: an introduction to computational algebraic geometry and commutative algebra*. Springer-Verlag, New York, 1992.

[9] H. S. M. Coxeter. *Introduction to geometry*. Wiley, New York, 2nd edition, 1969.

[10] G. W. Delaney, D. Weaire, and S. Hutzler. Onset of rigidity for stretched string networks. *EPL (Europhysics Letters)*, 72(6):990–996, 2005.

[11] O. Delgado-Friedrichs. Gepflasterte materie. *Spektrum der Wissenschaft*, August 2008.

[12] V. S. Deshpande, M. F. Ashby, and N. A. Fleck. Foam topology: bending versus stretching dominated architectures. *Acta Materialia*, 49(6):1035–1040, 4 2001.

[13] K. Evans and A. Alderson. Auxetic materials: Functional materials and structures from lateral thinking! *Advanced Materials*, 12(9):617–628, 2000.

[14] K. E. Evans. Auxetic polymers: a new range of materials. *Endeavour*, 15(4):170–174, 1991.

[15] K. E. Evans, M. A. Nkansah, I. J. Hutchinson, and S. C. Rogers. Molecular network design. *Nature*, 353(6340):124, 1991.

[16] R. P. Feynman, R. B. Leighton, and M. L. Sands. *The Feynman lectures on physics*. Addison-Wesley, Reading, Mass., 1964.

[17] M. Franke and R. Magerle. Auxetic behavior of elastomeric polypropylene on the 100-nm length scale. *unpublished*, 2009.

[18] B. L. Galebach. n-uniform tilings. `http://probabilitysports.com/tilings.html`, 1999.

[19] L. J. Gibson and M. F. Ashby. *Cellular solids: structure and properties*. Cambridge University Press, Cambridge, 2nd ed edition, 1997.

[20] G. H. Golub and C. F. Van Loan. *Matrix computations*. Johns Hopkins University Press, Baltimore, 3rd ed edition, 1996.

[21] J. N. Grima and K. E. Evans. Self expanding molecular networks. *Chemical Communications*, (16):1531–1532, 2000.

[22] J. N. Grima, R. Jackson, A. Alderson, and K. E. Evans. Do zeolites have negative poisson's ratios? *Advanced Materials*, 12(24):1912–1918, 2000.

[23] J. N. Grima, R. Gatt, N. Ravirala, A. Alderson, and K. E. Evans. Negative poisson's ratios in cellular foam materials. *Materials Science and Engineering A*, 423(1-2): 214–218, 2006.

[24] B. Grünbaum and G. C. Shephard. *Tilings and patterns*. W.H. Freeman, New York, 1987.

[25] S. D. Guest and J. W. Hutchinson. On the determinacy of repetitive structures. *Journal of the Mechanics and Physics of Solids*, 51(3):383 – 391, 2003. ISSN 0022-5096.

[26] T. Hahn, U. Shmueli, and A. J. C. Wilson. *International tables for crystallography*. D. Reidel Pub. Co., Dordrecht, Holland, 2005.

[27] R. Hutchinson and N. Fleck. The structural performance of the periodic truss. *Journal of the Mechanics and Physics of Solids*, 54(4):756 – 782, 2006.

[28] P. A. Janmey, M. E. McCormick, S. Rammensee, J. L. Leight, P. C. Georges, and F. C. MacKintosh. Negative normal stress in semiflexible biopolymer gels. *Nat Mater*, 6(1):48–51, 01 2007.

[29] R. Lakes. Foam structures with a negative poisson's ratio. *Science*, 235(4792):1038–1040, 1987.

[30] G. Laman. On graphs and rigidity of plane skeletal structures. *Journal of Engineering Mathematics*, 4(4):331–340, 10 1970.

[31] L. D. Landau, H.-G. Schöpf, and E. M. Lifshitz. *Elastizitätstheorie*, volume 7 of *Lehrbuch der theoretischen Physik*. Akademie-Verlag, Berlin, 4th edition, 1975.

[32] A. E. H. Love. *A treatise on the mathematical theory of elasticity*. Dover Publications, New York, 4th edition, 1944.

[33] J. C. Maxwell. On the calculation of the equilibrium and stiffness of frames. *The London And Edinburgh Philosohpical Magazine and Journal of Science*, 27:294–299, 1864.

[34] K. Mecke. Additivity, convexity, and beyond: Applications of minkowski functionals in statistical physics. *Statistical Physics and Spatial Statistics*, pages 111–184, 2000.

[35] G. W. Milton. *The theory of composites*, volume 6. Cambridge University Press, Cambridge, 2002.

[36] C. F. Moukarzel. Granular matter instabiltiy: A structural rigidity point of view. In M. Thorpe and P. Duxbury, editors, *Rigidity theory and applications*, 1999.

[37] H. Müller. Truss bridge made by fischer technik. `http://www.ftcommunity.de/details.php?image_id=13633`, Februar 2008.

[38] W. H. Press. *Numerical recipes: the art of scientific computing*. Cambridge University Press, Cambridge, UK, 3rd edition, 2007.

[39] O. Reynolds. On the dilatancy of media composed of rigid particles in contact, with experimental illustrations. *The London, Edinburgh and Dublin philosophical magazine and journal of science*, 20(5):469–481, December 1885.

[40] M. Scheel, R. Seemann, M. Brinkmann, M. Di Michiel, A. Sheppard, B. Breidenbach, and S. Herminghaus. Morphological clues to wet granular pile stability. *Nat Mater*, 7(3):189–193, 03 2008.

[41] G. E. Schröder-Turk, S. Kapfer, B. Breidenbach, C. Beisbart, and K. Mecke. Tensorial minkowski functionals and anisotropy measures for planar patterns. 2009.

[42] B. Servatius and H. Servatius. Generic and abstract rigidity. In M. Thorpe and P. Duxbury, editors, *Rigidity theory and applications*, 1999.

[43] C. W. Smith, J. N. Grima, and K. E. Evans. A novel mechanism for generating auxetic behavior in reticulated foams: Missing rib foam model. *Acta Mater.*, (48): 3439–4356, 2000.

[44] J. Stoer and R. Bulirsch. *Introduction to numerical analysis*, volume 12. Springer-Verlag, New York, 2nd edition, 1993.

[45] M. F. Thorpe and P. M. Duxbury. *Rigidity theory and applications: edited by M.F. Thorpe and P.M. Duxbury*. Kluwer Academic/Plenum Publishers, New York, 1999.

[46] W. Yang, Z. . Li, W. Shi, B. . Xie, and M. . Yang. On auxetic materials. *Journal of Materials Science*, 39(10):3269–3279, 2004.

Acknowledgements

I would like to thank Dr. Gerd E. Schröder-Turk for his great support in all issues as my tutor during the whole diploma thesis time, Prof. Dr. Klaus Mecke giving me the opportunity for this diploma thesis, Prof. Dr. Helmuth Zimmermann for the profitable discussions about symmetry groups, the whole group at Lehrstuhl für Statistische Physik for their familiar terms and my parents to give me the possibility to study and for their encouragement.

Erklärung der Selbstständigkeit

Hiermit versichere ich, die vorliegende Arbeit selbstständig verfasst und keine anderen als die angegebenen Quellen und Hilfsmittel benutzt sowie die Zitate deutlich kenntlich gemacht zu haben.

Erlangen, den 17.08.2009

Holger Mitschke